**Title**

Skeletomuscular morphology and evolution in millipede genitalia



**Author**

Zahnle, Xavier Jacob

**Publication Date**

2023

Peer reviewed|Thesis/dissertation

Skeletomuscular Morphology and Evolution in Millipede Genitalia

By

XAVIER J. ZAHNLE

DISSERTATION

Submitted in partial satisfaction of the requirements for the degree of

DOCTOR OF PHILOSOPHY

in

Entomology

in the

OFFICE OF GRADUATE STUDIES

of the

UNIVERSITY OF CALIFORNIA

DAVIS

Approved:

Jason Bond, Chair

Philip Ward

Lynn Kimsey

Committee in Charge

2023

**Abstract**

Mate choice, copulation, genital morphology, and sperm storage are not very well understood in millipedes. In particular, the morphology of millipede male genitalia, called gonopods, is critical for genus and species diagnosis in most taxa. However, the external form and function of gonopods vary drastically at the family and ordinal level, complicating morphological comparison across taxa. Three-dimensional x-ray computed tomography (μCT) has provided unprecedented access to internal morphological data, including chitinous sclerites and membranes, muscles, glands, oviducts, and sperm conduits. This work uses μCT data to investigate functional, evolutionary, and developmental aspects of millipede genitalia. First is presented a complete integrated account of morphology and function in the female genital organs (vulvae) in the family Polydesmidae (Diplopoda: Polydesmida), alongside a description of the functional morphology of copulatory interface in the genus *Pseudopolydesmus* Attems, 1898. This is followed by a comparison of the walking legs and gonopods in *Pseudopolydesmus* in order to identify homologous elements shared among each type of appendage. Skeletal elements were homologized, but muscle homologies were limited by the dissimilarity of muscle attachment sites between appendage types and by images of juvenile males showing that appendage musculature is totally obliterated once gonopod development begins. Finally, comparative anatomical study of appendage skeletomusculature was extended across a broad swathe of representative millipede taxa. This work included the application of Anatomical Network Analysis to compare the organization of millipede gonopods and walking legs among and within each studied taxon.

**Acknowledgements**

I am indebted to numerous mentors, collaborators, friends, and family members, without whom this work would not have come to be. First, I must thank Jason Bond, who provided me the freedom to explore my own research interests as well as the organismal expertise to guide that exploration. I am incredibly grateful to Petra Sierwald for the opportunity to research myriapods at the Field Museum of Natural History and for flying me around the world to collect them. I am also very appreciative of the mentorship of several professors at the University of California, Davis. Geoffrey Attardo, Lynn Kimsey, Philip Ward, Peter Wainwright, and Harris Lewin were generous with their time and knowledge both as committee members and as unofficial mentors. The Bond Lab postdoctoral researchers Vera Opatova, James Starrett, and Lisa Chamberland were replete with technical knowledge and personal wisdom, which I thank them for sharing.

I am fortunate to have been accompanied through my academic journey by supportive and insightful fellow travelers, each of whom I regard as a close friend. I am grateful to have had Patrick Dean as a roommate, confidant, and fast friend during my time at Auburn University. In the Bond Lab, I was surrounded by colleagues whose work I admire and whose friendship and counsel were critical. As my academic seniors, Rebecca Godwin and Lacie Newton made me feel welcome into the Bond Lab and thankfully dragged me along to many a social event, making Xavier less of a dull boy. Emma Jochim and Iris Quayle joined the lab after me, but I am inspired by their brilliance in research as well as in life at large. I am also immensely appreciative of Jill Oberski, Taylor Kelly, Adelicia Johnson, Elizabeth Davis, and all the other residents and friends of Bug House, who provided a supportive and vibrant community. I would also be remiss in omitting Brendon Boudinot, Lindsey Mack, Zachary Griebenow, or Ziv

Lieberman, all of whose friendship and intellect enriched my time at Davis. I must also include Megan Ma, Kaitai Liu, and Elisa Zelaya, who shared the time-consuming task of 3D image segmentation with me. Their curiosity and excitement were energizing, and I suspect that they taught me at least as much as I taught them.

Finally, my family is the firm foundation of my career. My parents, Kenneth and Gayle Zahnle, have always encouraged my interests in the arts and sciences, no matter how eclectic or esoteric. Most importantly, my fiancée and best friend Abigail Shearrow made this work possible. Despite six years and one world pandemic apart while pursuing our respective doctorates, she has been steadfastly supportive. She has participated in no fewer than three transcontinental road trips to transport all my worldly possessions. Thank you for everything.

**Genital morphology and the mechanics of copulation in the millipede genus *Pseudopolydesmus* (Diplopoda: Polydesmida: Polydesmidae)**

This chapter was originally published in January 2020, in volume 54 of the journal Arthropod Structure & Development.

**Authors**

Xavier J. Zahnle, Petra Sierwald, Stephanie Ware, Jason E. Bond

**Highlights**

• 2D and 3D imaging are used to investigate millipede genitalic functional anatomy.

• Females evert their vulvae outside of their bodies for copulation and oviposition.

• Male genitalia contain a looped duct that delivers seminal fluid to the vulvae.

• Vulvae require matching male genitalia for mechanical coupling.

• Seminal fluid is stored in female spermathecae, completely separate from oviducts.

**Abstract**

Mate choice, copulation, genital morphology, and sperm storage are not very well understood in millipedes. The use of three-dimensional x-ray computed tomography (μCT) provides new morphological data regarding millipede reproductive systems in both the female and male, including chitinous sclerites and membranes, muscles, glands, oviducts, and sperm conduits. Here we present a complete integrated account of the morphology and function of the female genital organs in the family Polydesmidae (Diplopoda: Polydesmida) using μCT, UV fluorescence imaging, and scanning electron microscopy. These data allow us to consider competing hypotheses regarding millipede vulva formation. We additionally present the morphology of copulatory interface in *Pseudopolydesmus* Attems, 1898 using images of a mating pair *in copula* and by simulating the interface of the organs using 3D models from μCT, allowing us to tentatively identify a lock-and-key-like mechanism. Finally, we use μCT to reveal the topology of the seminal canal in the gonopod of male *Pseudopolydesmus*, a topic that has remained unresolved for nearly 80 years.

**Keywords**

Diplopoda; Female Genitalia; Reproductive Anatomy; Sexual Selection; Ultraviolet Fluorescence; X-ray Tomography

# 1 Introduction

Zoologists have long been fascinated by the staggering diversity of copulatory organs across the animal kingdom. Genitalia are often observed to vary between related species, implying that they are evolving rapidly and divergently at the species level (Eberhard, 1985). Central to the discussion of genital variation are the evolutionary mechanisms that drive it. Three of the most often posited explanations are a lock-and-key mechanism, sexual selection by female choice, and antagonistic coevolution between sexes (Kraus, 1968; Eberhard, 1985; Shapiro and Porter, 1989; Hosken and Stockley, 2004). Both the lock-and-key and sexual selection by female choice hypotheses may produce patterns of correlated variation (similarity resulting in "better fit") between male and female genitalia.

Lock-and-key and mechanical female choice are therefore difficult to disentangle. For a lock-and-key hypothesis, correlated variation is necessary. However, female choice could result in patterns of greater or lesser morphological correlation depending on whether females exert selective pressure on males for their stimulatory ability or their mechanical fit. Under female choice, male reproductive success passes through the selective filter of female preference. However, female reproductive success also passes through the female choice filter, albeit indirectly, via the reproductive success of the female's sons – the female is incentivized to choose a male that will sire successful offspring. Therefore, female choice might drive both male and female reproductive morphology. Female choice based only on male stimulatory ability should drive behavioral selection on females. In contrast, female choice based on mechanical fit should select for morphological correlation between males and females (Eberhard, 1985).

Few lock-and-key mechanisms have been described in millipedes. Examples of taxa with proposed lock-and-key mechanisms include two families of flat-backed millipedes (Polydesmida): Paradoxosomatidae (Wojcieszek *et al.*, 2012; Wojciescek and Simmons, 2013) and Xystodesmidae (Tanabe and Sota, 2008). Existing research suggests that body size is more effective in maintaining genetic isolation between sympatric species than genital morphology (Bond and Sierwald, 2002; Tanabe and Sota, 2008). However, it must be kept in mind that many taxonomic works have focused primarily on male genitalia, sometimes to the exclusion of all other morphology (see discussions in Bond *et al.*, 2003;

Sierwald *et al.*, 2019). This may be due to the difficulty in observing the invaginated or eversible female genitalia, a perceived lack of divergence in the female genitalia compared to the male genitalia, a cultural bias magnifying the significance placed on male anatomy for sexual selection, or a combination of the above (Ah-King *et al.*, 2014). Several studies explicitly investigating species-level variation in female genitalia have been unable to find any in the millipede orders Spirostreptida (Kraus, 1966; 1968) and Chordeumatida (Shear, 1972; 1976; 1981). On the other hand, female genitalia have been used for species diagnosis in representatives of the orders Julida (Voigtländer *et al.*, 2017) and Polydesmida (Demange, 1968; Withrow, 1988; Tadler and Thaler, 1993). Additionally, Kurnik and Thaler (1985; also Kurnik, 1988; 1990) reported species-level variation in the vulvae of chordeumatids from the eastern alpine region in Austria based on SEM imaging, and Schubart (1934: 58) asserted that chordeumatid vulval structure aligns with generic taxonomic structure. These findings confirm that female genitalia do evolve divergently, at least in some groups.

In addition to the morphological diversity in male genitalia, the sexual selection hypothesis is strengthened by behavioral observations of millipede courtship and copulation. Preliminary intromission, defined as copulatory intromission in which the gonopods are not yet charged with seminal fluid, has been recorded in the millipede order Julida (Haacker and Fuchs, 1970; Tadler, 1996) and the families Xystodesmidae (Tanabe and Sota, 2008) and Platyrhacidae (Eberhard, 1985: 161) in the order Polydesmida. Preliminary intromission may motivate female choice. Sexual selection might also act on somatic characters; in *Scytonotus* Koch, 1847 (family Polydesmidae), mate recognition may be based on presence or absence of paranota in females and of leg tubercles in males (Shelley, 1993).

Past studies characterizing female millipede genital morphology have been stymied by their often small and internally complex nature, including highly sclerotized plates alternating with thin, soft membranes. To overcome this hurdle, we employ three-dimensional x-ray computed tomography (µCT) to resolve the reproductive anatomy of the flat-backed millipede genus *Pseudopolydesmus* Attems, 1898. µCT morphological data has been evaluated in a variety of millipede groups (Wojciescek *et al.*, 2012; Blanke and Wesener, 2014; Akkari *et al.*, 2015; Liu *et al.*, 2017; Moritz *et al.*, 2018; Stoev *et al.*, 2019;

Moritz and Wesener, 2019; Wesener, 2019; Naumann *et al.*, 2019). Notably, although the use of μCT seems to be accelerating, this is the first publication using it to study female genital function in millipedes.

The increasingly widespread use of three-dimensional imaging technologies has tremendous potential to improve anatomical research. An animal can be scanned, digitally segmented into morphological elements, and then exported into a fully interactive 3D rendering that conveys vastly more information per pixel than a standard two-dimensional image. In particular, reconstructed μCT data allow "virtual dissection" of complex and very small internal anatomy without the need to destructively dissect specimens or section them using histology. For example, μCT scans contributed to the discovery of nervous tissue in the male copulatory palps in two spider families (Lipke *et al.*, 2015; Sentenská *et al.*, 2017). Another novel use of segmented μCT data is to digitally manipulate morphological elements to determine the limit of motion between articulated elements (Kamp *et al.*, 2014) or to assess the interface between corresponding elements.

In this paper, we present the reproductive morphology of the North American millipede genus *Pseudopolydesmus*, with a focus on the anatomy and function of the female vulva. A hinged plate formed from fused coxae, which seals the vulvae inside the body ring, is described and illustrated. The variable orientation of the vulva for copulation and oviposition is fully illustrated for the first time, using schematic diagrams and an animated 3D model. The cuticular elements, oviducts, and glands of the vulvae are described and illustrated, along with their associated connective membranes. Furthermore, the previously unresolved internal anatomy of the male gonopod is revealed and the copulatory interface of the gonopod with the vulva is demonstrated from an *in copula* mating pair and a simulated mating using 3D models. The origins of vulval and gonopodal elements are discussed, with data provided to evaluate existing hypotheses regarding vulvae formation.

## 2 Materials and Methods

### 2.1 Museum Specimens and Dissection

All specimens imaged are vouchered in the Field Museum of Natural History's Insect Collection (FMNHINS), with specimen data provided in Table 1. Lot FMNHINS 3120685 contained a complete adult female *Pseudopolydesmus erasus* (Loomis, 1943) with withdrawn vulvae, from which body ring 3 was dissected to enable *in situ* 2D imaging of the vulvae. Both vulvae were subsequently dissected from body ring 3 to enable scanning electron microscope (SEM) imaging and digested in trypsin to remove non-cuticular tissue.

Lot FMNHINS 7344 contained an adult mating pair of *Pseudopolydesmus serratus* (Say, 1821) *in copula*, providing the unique opportunity to study the copulatory interface. The joined pair was first imaged as found in the vial. The legs surrounding the genitalia were then carefully dissected away to allow unobstructed imaging of the genitalia. Finally, the joined pair was carefully separated to reveal the distribution of glandular secretions on the genitalia. Unfortunately, the pair was separated before work on 3D µCT imaging began, so the opportunity to use 3D imaging to view the copulatory interface was lost. All other specimens were imaged as found and remain as intact as possible.

### 2.2 Light, UV, and SEM Imaging

High depth of field images were acquired following the methods of Sierwald *et al.* (2019), using the same Microptics system (Dun Inc., Richmond, VA). UV autofluorescence was employed as described in the same paper.

Scanning electron micrographs were acquired using the same methods and equipment as in Sierwald *et al.* (2019), with the following exception: body ring 3 (and its vulvae) was prepared for scanning electron micrography using critical point drying (Shively and Miller, 2009) in addition to the ethanol dehydration series used for other SEM preparations.

### 2.3 3D µCT Imaging

All specimens imaged using µCT were dehydrated successively in a series of 80%, 85%, 90%, and finally 95% ethanol (unless already stored in 95% ethanol) with at least 2 hours in each stage.

Specimens were stained for 24-48 hours in a 1% solution of iodine in 100% ethanol (after Metscher, 2009). The iodine stains soft tissues (Gignac *et al.*, 2016), increasing their contrast under x-ray imaging. After imaging, the iodine stain was neutralized in the specimens using a 5% solution of sodium thiosulfate, returning the specimens to their original color as preserved in ethanol (Gignac *et al.*, 2016).

Specimens were mounted in 95% ethanol in either a 0.5 mL or 1.0 mL microfuge tube depending on their size. Intact full body specimens were mounted head-first and gently wedged in place (to prevent movement during imaging) using a small layer of cotton. Body ring fragments were mounted between two cotton layers.

3D image acquisition was performed using an XRadia microXCT-200 housed in the Center for Molecular and Genomic Imaging at the University of California, Davis. Images were acquired using detectors with 4x or 10x magnification (producing images with 4.5 µm and 2.0 µm voxel resolution, respectively). Specifications for each scan are provided in Table S1. The 3D images were reconstructed as .txm files and are available online at Dryad.

### 2.4 3D Segmentation and Presentation

Morphological elements of interest, such as sclerites and prominent membranes, were isolated from the original 3D images in a process called segmentation. The original XRadia .txm files were cropped and converted to Metaimage (.mhd) format using default settings in Drishti Import 2.6.4 (Limaye, 2012). The Drishti package was used only for this step. The .mhd files were automatically segmented in ITK-SNAP 3.8.0 (Yushkevich *et al.*, 2006) using the "Thresholding" algorithm (also called "Region Competition" or "Intensity Regions" in older versions of ITK-SNAP). This algorithm isolates morphological elements based on the relative intensity of their constituent voxels. Threshold levels can be adjusted to only incorporate voxels within a particular intensity range. The exact threshold levels used to generate labels for each morphological element are listed in Table S1. The user must initialize the algorithm by placing a series of spheres, or "bubbles," throughout the morphological element of interest. The algorithm then expands the selection of voxels from the initial bubbles until the entire morphological

element is selected. A desktop tablet with pressure-sensitive pen (Wacom Cintiq 22HD) was used to place bubbles and to manually touch up automatically segmented labels using the "Paintbrush" tool. Labels were exported as .stl meshes, which are available online at MorphoSource.

Meshes generated from ITK-SNAP were subsequently imported into the 3D animation program Blender, available free from blender.org. Because .stl mesh files each contain only one segmented morphological element, meshes belonging to the same organ (*e.g.* the sclerites and membrane of a vulva) were batch imported into Blender to preserve their relative positions to each other. This can be done simply by shift-clicking each desired mesh file in the import menu. The scale function was used to reduce the meshes to an appropriate size, and the meshes were subsequently translated and rotated into the desired position and orientation. Color was added to each mesh by adding a new material under the "Material" tab (sphere icon) and selecting the desired color for that material from the "Diffuse" color palette. The telopodite material in Fig. 13 was made translucent by checking the box at the top of the "Transparency" menu and reducing the "Alpha" option to 0.1 (10% opacity). Lighting was provided by the default "Point" lamp placed near the camera. Figures were created using the "Animation" function (filming clapperboard icon) under the "Render" tab (camera icon) and output as .tif files. A single image was exported by setting "End Frame" to 1 under the "Dimensions" menu (otherwise additional identical images will be exported in series). The background color was selected using the "Horizon Color" palette under the "World" tab (Earth icon). The "Render" button (camera icon) allows the user to preview the exported image from the camera's perspective.

### 2.4.1 Optimizing ITK-SNAP Segmentation Procedure [this should be a text box]

Even with automated assistance from an algorithm, 3D image segmentation is very time intensive. Even small optimizations can save hours, while improving the quality of the final product. The following techniques were used to optimize the segmentation process in ITK-SNAP for the morphological elements presented in this paper:

- During “Initialization” (Presegmentation Step 2), the Enter key adds a bubble at the current position of the crosshair as selected by the “Crosshair Mode” tool. When using a desktop tablet, configure one of its buttons or one of the buttons on the pen as the Enter key to drastically reduce time spent on the Initialization step.
- Distribute bubbles evenly throughout the region of interest to reduce the number of iterations necessary during the “Evolution” stage (Presegmentation Step 3). This reduces the computation time and may also reduce the amount of undesired bleeding into nearby morphological elements if thresholding is inadequate to entirely separate elements.
- ITK-SNAP’s Thresholding algorithm often struggles to capture thin (≤3 voxel-thick) flanges and projections. After automated segmentation, be sure to check any thin sections of the morphological element to see if they need to be manually labelled.
- Casting: In some cases, it may be simpler to assign the background to a label before assigning any morphological elements in order to protect these voxels from being assigned to another label. For example, in this paper we made a “cast” while segmenting the gonopod telopodite of *Ps. serratus* (FMNHINS 1513). By setting an upper threshold (in Presegmentation Step 1) we were able to assign all the low-intensity voxels to the cast label, including the voxels inside the telopodite pertaining to the seminal chamber and seminal canal. After segmenting the telopodite using a lower threshold limit, we simply reassigned these voxels to the “Seminal Chamber” and “Seminal Canal” labels.

### 2.5 Animation

Figures 3 and 16 were animated in Blender using the “Timeline” window pane (clock icon). The resulting animations are presented as Video 1 and Video 2, respectively. The meshes representing the coxae and sternite were united into one object using the “Join” function in order to ensure they move as one unit, as were the various sclerites of the vulvae. Animation was then programmed by selecting the desired frame in the “Timeline” window pane, then altering the “Location” coordinates and/or “Rotation”

under the “Object” tab (orange cube icon), and finally right-clicking the coordinates and/or rotation and selecting the “Replace Keyframes” option. This causes the object to adopt the specified position and orientation at the specified frame on the timeline. Motion between specified keyframes is smoothly interpolated by default. The objects can also be translated and rotated in the main “3D View” windowpane (white cube icon) to find the next desired keyframes by trial and error. This is how Videos 1 and 2 were animated.

Animating the rotation of the coxal plate in Video 1 along its hinged joint with body ring 3 required a more complex technique. The midpoint of the coxal plate’s axis of rotation was found by average the coordinates of the two points representing the tips of the apophyses of the hinge joint. The origin of the coxal plate was moved to the midpoint coordinates. To animate the swinging motion of the coxal plate, a new empty object was added to function as a “handle” for coxal plate rotation. A “Locked Object” constraint was then added to the coxal plate object under the “Constraints” tab (chain links icon), with the empty handle object selected under the “Target” pull-down menu. This makes the coxal plate rotate along the axis through its origin (midpoint between the apophyses) in response to translation of the handle. Therefore, the handle’s coordinates were used as the animation keyframes for the coxal plate.

The animation videos were captured by using the “Animation” function under the “Render” tab in a process similar to capturing still images. To capture video in the .mp4 format, the format in the “Output” menu was changed from “TIFF” to “FFmpeg video”. Using the “Presets” drop-down menu under the “Encoding” menu, the “h264 in MP4” preset was selected. Finally, clicking the “Animation” button (filming clapperboard icon) begins the rendering and export of the animated video.

## 3 Results

The results are divided into the following four sections: (1) A very brief introduction to generalized millipede reproductive anatomy. (2) Description of the morphology of the female vulvae and sexual characteristics of the third body ring of *Pseudopolydesmus* in depth. We also include notes on female genital morphology of members of the genus *Polydesmus* Latreille, 1802 because research on the

vulvae of Polydesmidae has historically been conducted on *Polydesmus*. (3) An account of the internal anatomy of the gonopods of male *Pseudopolydesmus*, focusing on the route of seminal fluid through the telopodite. (4) Description the copulatory interface between the gonopod and vulva using a mated pair preserved *in copula* and by virtually simulating a copulatory interface. Throughout, we have sought to synthesize our findings with the work of previous authors; therefore, alternative names for morphological features from the literature are provided whenever available. For terms that were adopted in numerous publications, only the original publication describing the term is cited. For well-known anglicized variants of terms adopted from non-English publications (*e.g.* "telopodite" from *"Telopodit"*) no citation is provided.

### 3.1 Brief Introduction to Millipede Reproductive Anatomy

In millipedes, the reproductive tract splits cephalad into two paramedian ducts that open on the ventral side of the third body ring (Fig. 1: br3). These are called the vasa deferentia and oviducts in males and females, respectively. In both males and females the gonopores are located at body ring 3, opening on or behind the coxae of the second leg pair. In males of the diverse millipede clade Helminthomorpha (including Polydesmida) the seminal fluid from the vasa deferentia must be transferred to the copulatory gonopods of the seventh body ring. The transfer of seminal fluid from the gonopore to the gonopods was observed first by Fabre (1855, in Polydesmida and Julida); Verhoeff (1928: 179) summarized the observations of von Rath (1891) and his own in Chordeumatida (Verhoeff, 1910). In females the oviducts open directly onto the copulatory vulvae of body ring 3 (Minelli and Michalik, 2015). It has long been known that the vulvae of *Polydesmus* can be withdrawn within BR3 or everted outside of the body (Verhoeff, 1928: 742), as can the vulvae of the related genus *Pseudopolydesmus* (Withrow, 1988: 69). When fully everted, the vulvae of *Pseudopolydesmus* extend caudally from BR3 (Fig. 1).

### 3.2 Female Sexual Morphology

#### 3.2.1 Body Ring Modifications

The third body ring (BR3) and its legs (leg pair 2, LP2) are heavily modified compared to a typical body ring (Fig. 2B: cx2, pf2). The main functional modification to BR3 is a large indentation at its anterior ventral margin to accommodate vulval eversion (Figs. 1C, 2A: am). In *Polydesmus inconstans* Latzel, 1883 and *Po. complanatus* (Linnaeus, 1761) there is a large tubercle extending ventrally from the ventral margin of BR3 (Blower, 1985: fig. 64B; Withrow, 1988: fig. 65; Tadler and Thaler, 1993: fig. 4), but it is always absent in *Pseudopolydesmus*. Whether or not a median tubercle is present, the ventro-lateral surface of BR3 bears various tubercles, pits, or rugose patches (Fig. 2A: eg; Blower, 1985: fig. 61G-L) that are useful for species diagnosis in some taxa. Collectively, these features have been called the epigyne (Blower, 1985).

The indented margin of BR3 is a near perfect fit for the movable flattened coxal plate of LP2 ("syncoxosternum": Withrow, 1988). In *Pseudopolydesmus* the indented margin of BR3 is moderately concave (Figs. 1C, 2A: am), though apparently the interface between BR3 and the coxal plate can instead adopt a complex interlocking shape, as in *Polydesmus angustus* Latzel, 1884 (Demange, 1968: 280, fig. 5). The coxal plate comprises the two broad, flattened coxae of LP2 and a small, triangular, median sternite between them, in addition to the connective tissue joining these three sclerites (Figs. 2B, 3A: cx2, st). The sternite consists of a subtriangular anterior plate connected to a convex posterior plate by a thin stalk (Fig. 3B: sta, stp). In its overall appearance, the coxal plate of *Pseudopolydesmus* is convex and roughly semicircular. It is laterally hinged, articulating against apophyses on BR3 located at approximately half the height of the body ring (Fig. 2C: hi). This hinge allows the coxal plate to extend up to ~90° antero-dorsally from its closed position (Video 1; Figs. 3C, 4B: cx2, st). The coxal plate is extended by a pair of muscles that originate at the tracheal apodeme of leg pair 1 and insert onto the lateral corners of the sternite.

The prefemur of LP2 is also modified. Its proximal dorsal surface is strongly concave. Furthermore, it is unusual in being longer than the femur of LP2 (Fig. 2B: pf2); in *Pseudopolydesmus* and *Polydesmus*, the femur is typically longer than the prefemur of the same leg (Sierwald *et al.*, 2019: fig. 6).

The elongated prefemora may compensate for the modified coxae, whose prefemoral articulations are displaced medially compared to typical walking legs.

### 3.2.2 Vulval Orientation and Relation to Body Ring 3

The vulvae are paired reproductive structures of the adult female millipede that, in *Pseudopolydesmus*, are withdrawn inside of BR3 before copulation and oviposition (Video 1; Figs. 3A, 4A, 5-6). Because the vulvae alter their orientation with respect to the main body axes when they are everted, it is necessary to define a standard anatomical position for reference (Fig. 4). Brölemann and Lichtenstein (1919) described the generalized anatomy (*"esquisse schématique"*) of the vulvae in Diplopoda as consisting of two unequal parts divided by the oviduct: a large posterior bursa (*"Coxit"*: Verhoeff, 1928) and a small anterior operculum (*"Vaginalklappe"* or *"Telopodit"*: Verhoeff, 1928). Brölemann and Lichtenstein were apparently unaware of the withdrawn position, listing the vulvae of *Polydesmus* among those *"placée en surface"* in contrast to *"vulves invaginées"*. Schubart (1934: 11) assumed that eversion of the vulvae was the result of preservation. When fully everted into the ovipositing position, the vulvae of *Pseudopolydesmus* match the orientation described by Brölemann and Lichtenstein (Video 1; Figs. 3D, 4C). Therefore, we propose that the fully everted position of the vulvae represents the standard anatomical position in *Pseudopolydesmus* and other Polydesmida in which the vulvae can be withdrawn. Therefore, when withdrawn, the anteriormost part of the vulvae (the operculum) will be the furthest toward the animal's posterior (Figs. 3A, 4A).

The vulvae are connected to the animal's body by a medial mass of connective tissue surrounding the oviducts and haemocoel conduits (Fig. 7: mj, mn, ov). It is likely impossible for the animal to evert one vulva and not the other because of their shared basal connective tissue; we have never observed a female with just one everted vulva. This mass of connective tissue must be extended a substantial length during vulval eversion. In fact, while the vulvae remain withdrawn, the oviducts are folded into an S-shape (Fig. 7: ov) that is straightened out when the vulvae are everted. As each oviduct passes between the operculum and bursa, it widens medio-laterally into a slot-like vagina that opens on the ventral side of

the vulva (Fig. 7: va). The bulk of the bursa lies posterior from the vagina and is only attached proximally. The bursa interior is continuous with the ventral perineural sinus of the haemocoel (perineural sinus illustrated in Wirkner and Xylander, 2015: fig. 7.2E). When the vulvae are fully everted, the continuity of each bursa to the perineural sinus is reduced to a narrow conduit posterior to the oviduct (Fig. 4C).

When the vulvae are in the withdrawn position, the oviducts insert ventrally between the operculum and the proximal extremity of the bursa (the dorsal side of the vulva; Fig. 4; Fig. 7: va). Of the female specimens imaged using μCT, one was gravid with fully everted vulvae and the other was non-gravid with withdrawn vulvae. In the gravid female (FMNHINS 1451), the oviducts can be traced posteriorly from their insertion into the vulvae as the vaginae until they fuse medially into the central ovary. The lumen of the oviduct is distinctly crenellated, unlike that of the ovary. The ovary lies directly between the perineural sinus ventrally and the gastrointestinal tract dorsally. In the non-gravid female (FMNHINS 1513) the oviducts proceed ventrally from the bursa as discussed above (Fig. 7: ov). However, instead of immediately converging into a medial ovary, they individually curl dorsally over the vulvae to extend anteriorly. Finally, they turn postero-medially and fuse into a dorso-ventrally flattened median ovary. Immature oocytes are visible inside the anterior portion of the ovary lumen.

The vulvae themselves are contained within a membranous pouch while withdrawn (Figs. 5-7: mj, mn; *"sac vulvaire":* Demange, 1968; *"Vulventaschen":* Tadler and Thaler, 1993). When the vulvae are everted, the membranes comprising this pouch invert to face outside of the body in the same manner as a pants pocket. Because the vulvae rotate as they evert, the ventral surface (dorsal side when vulvae are withdrawn) of the vulvae necessarily traces a longer arc than the dorsal surface. Consequently, the membrane covering the ventral surface must be longer than that covering the dorsal surface. We call these the major membrane and minor membrane, respectively, based on their size (Figs. 3, 7: mj, mn). The major membrane originates along the posterior dorsal rim of the coxal plate of LP2 (*"tablier syncoxosternal":* Demange, 1968), extending posteriorly to blanket the vulvae when they are withdrawn, and finally inserts along the dorsal rims of the valves and operculum (on the ventral side when vulvae are

withdrawn). This leaves a gap through which the oviducts and haemocoel conduit pass (Fig. 6: gap). The minor membrane originates from the internal apodematic phragma of BR3 before splitting into anterior and posterior sections (Fig. 6C: mn). The anterior section medially inserts into the anterior rim of the gorgets, while laterally it unites with the major membrane. The posterior section of the minor membrane spans body rings 3 and 4, inserting onto the internal apodematic phragma of body ring 4 (Figs. 4, 7: br4). Demange (1968: fig. 1; *cf.* Fig. 5) based his vulval anatomy on anterior dissections of BR3 in which he removed LP2. Accordingly, he recognized the origin of the major membrane at the coxae of LP2 and that of the minor membrane at the ventral phragma (*"lame infra-sternale interne"*) of BR3. However, he did not describe their points of insertion onto the vulvae.

As a final note on the vulval pouch, the major membrane encloses a fluid-filled cavity beneath its surface (Fig. 7: cav). The cavity is contained entirely between two layers of the major membrane and is non-continuous with any other body cavity. It forms a layer that roughly matches the contours of the vulval pouch while the vulvae are withdrawn but changes shape and location during eversion, being gathered into the ventral end of BR3 and in the aperture between BR3 and the coxal plate.

### 3.2.3 Vulval Sclerites

The bursa comprises three sclerites with connective membranes (Figs. 8-10). The main structure is provided by two large convex sclerites called the valves. Each vulva has a medial and lateral valve. The valves of *Pseudopolydesmus* are curved, with an approximately reniform silhouette, although the acuteness of the curve varies between species. The lateral valves (Figs. 8A, 9A, 10A: lv) tend to be more convex than the medial valves (Figs. 8B, 9B, 10B: mv), the latter of which are flattened so that they fit together compactly when the vulvae are withdrawn (Figs. 5A, B). Each valve bears from ~30-60 postero-ventrally directed setae concentrated at the anterior end of the bursa (Fig. 8A, B). In *Pseudopolydesmus*, the medial valve bears a thin distal flange from its posterior edge ("cyphopod plate": Withrow, 1988) that partially or entirely surrounds the posterior end of the bursa medially and dorsally (Fig. 11: df). The shape of the distal flange is variable between species and may be diagnostic. For example, the distal flange of

*Ps. pinetorum* (Bollman, 1888) is angled dorso-laterally, giving the vulva a distinctly skewed appearance from a posterior view (Fig. 11D; Withrow, 1988: fig. 111), whereas that of *Ps. serratus* wraps dorsally around the bursa, nearly touching the lateral valve (Figs. 9A, 11B).

The bursa is supported on its dorsal surface by a sclerite called the gorget (Figs. 6A, 8B, 9C: go; *"gorgerin":* Brölemann and Lichtenstein, 1919; *"Sternit der Cyphopoden":* Verhoeff, 1928; *"Basalsklerit":* Tadler and Thaler, 1993; possibly "receptacle": Withrow, 1988, see 4.2 below). The name gorget is derived from the piece of medieval armor worn over the collar to protect the throat (Brölemann, 1917); likewise, the gorget of the vulva is a sclerite that partially covers the dorsal connective tissue of the vulva (Figs. 7, 8B). The rims of the gorget are turned ventrally to form a concave area under the gorget surface that houses glandular tissue (Fig. 7: glg).

The operculum in *Pseudopolydesmus* is a small door-like sclerite, hinged proximally with a distal free end (Figs. 8B, 12: op). It functions as a hatch, opening to allow eggs to pass through the vagina during oviposition (Figs. 4C, 7: va). It is nearly symmetrical and contains two closely associated sclerites. The outer sclerite is a very slightly convex discoid, medially indented at its distal edge (Fig. 12A, B: opd). In the observed specimens, it bears ~12 sensory setae, all of which are angled ventrally. The inner sclerite takes the form of an arch, with each arm running along the medial and lateral edges of the operculum, respectively (Fig. 12C: opa). The dorsal half of each arm is medially folded, forming apodematic flanges that receive muscles from the anterior ends of the lateral and medial valves (ofl). The arms of the inner sclerite fuse disto-medially to form a bridge that completes the arch, while also extending distally into a pair of prongs on each side of the bridge. The inner and outer sclerites join together where the bridge of the inner sclerite and the distal indentation of the outer sclerite meet, although they are not fully fused (Fig. 9C).

### 3.2.4 Ventral Membrane and Spermatheca

A thickened ventral membrane spans the valves (Figs. 8C, 9: vm; *"cimier":* Brölemann and Lichtenstein, 1919; *"Zentralbereich":* Tadler and Thaler, 1993). It passes longitudinally along the ventral

surface of the vulva, posteriorly extending past the valves to form a convex bulge (*"crête du cimier":* Brölemann and Lichtenstein, 1919; *"Terminalbereich":* Tadler and Thaler, 1993) that dorsally inserts onto the distal flange of the medial valve and the posterior margin of the medial valve (Figs. 8B, 9A). In some species the surface of the ventral membrane slopes gently dorsally (Fig. 9), whereas in others it abruptly angles dorsally (Fig. 8). Anteriorly it terminates in an arch that forms the posterior mouth of the vagina, complementing the shape of the operculum. Laterally and medially the ventral membrane overlies the margins of the lateral and medial valves, respectively, gradually tapering to a thin membranous layer (Fig. 9A, B). The cuticle of the ventral membrane is substantially thickened compared to the connective membranes throughout the rest of the vulva (Fig. 7) and appears to be rigid.

The lateral and medial margins of the ventral membrane each bear a longitudinal row of posteriorly directed bristles (Figs. 7-9: ms). Although most of these bristles are apparently fused onto the ventral membrane itself, the anteriormost bristles in each row are distinctly socketed (Fig. 9D), thus most likely representing modified setae. The morphology of the modified setae varies substantially between species, with those of *Ps. serratus* being chisel-shaped (Fig. 9) while those of *Ps. erasus* are thick and arcuate with irregularly twisted tips (Fig. 8).

The ventral membrane is bisected by a longitudinal seam (Fig. 8C). As it curves postero-dorsally, the seam opens into a longitudinal crevice – the vulval aperture into which seminal fluid is deposited during copulation (Figs. 1, 8C, 9E: ap). Curiously, previous authors do not seem to have taken note of this feature, despite Brölemann and Lichtenstein's accurate illustration of the vulval aperture from lateral and ventral views (1919: 178, figs. II, III). The lips of the vulval aperture close anteriorly into a fused seam (*"Coxitgrube"* of the vulva: Verhoeff, 1928) that is flanked by two rows of flattened "scale-like" projections (Fig. 8C: sspt; *"schuppenartige Skulpturelemente":* Tadler and Thaler, 1993). These "scales" create an impression of transverse stitching that inspired Tadler and Thaler's (1993) name for the seam: *"Naht"*. Like the modified setae, they are directed slightly posteriorly, causing the projections within each row to overlap like roof shingles. The "scales" on each side of the seam are offset from each other and

occasionally interdigitate. Posteriorly, the “scales” gradually broaden and fuse into a continuous sheet, while anteriorly they become progressively narrower.

Although the “scales” mostly cover the longitudinal seam, there are narrow gaps between them through which we believe the vulval glands open onto the ventral membrane. In this case, copulatory secretions would be extruded through these gaps before agglomerating onto the external surface of the ventral membrane and the modified setae. When the copulatory secretions are extruded, they adhere mainly to the ventral surface of the bursa; in the specimens we observed the vulval aperture (site of insemination) and operculum (opening of genital tract) were not covered (Fig. 1C: ap). We report three substantial glandular masses in the bursa (Fig. 7: glb, glf, glg): a large subspherical gland just posterior to the vagina, a smaller subspherical gland nestled into the curled distal flange of the medial valve, and a lobate gland on the inner surface of the gorget. These respectively correspond to the *“gland de la bourse,” “glandes valvaires,”* and *“glandes du gorgerin”* of Brölemann and Lichtenstein (1919: fig. IV). The functions and destinations of secretory products from each gland are currently unknown (see 4.5 below).

The longitudinal seam is the superficial manifestation of the spermatheca. Beneath the surface of the ventral membrane lies a “sinuous canal” (*“canal sinueux”:* Brölemann and Lichtenstein, 1919) whose walls are continuous with the longitudinal seam. This is the lumen of the spermatheca. When viewed from the ventral surface, the spermatheca lumen has an approximately sinusoidal shape, with the amplitude and “wavelength” varying throughout its length (Fig. 9C, D: spt). In general, the amplitude increases anteriorly, reaching its maximum at approximately one quarter the length of the bursa from the vagina. The medial and lateral walls containing the lumen are continuous with the longitudinal seam and project deep into the interior of the bursa. The projection depth of the spermatheca into the bursa sinus also increases anteriorly. Furthermore, the upper and lower limits of the sinusoidal amplitude in the spermatheca project even deeper into the bursa sinus and serve as apodemes. These are the insertion points for sheets of muscles that extend ventrally from the interior of the lateral and medial valves (Fig. 7: spt; Brölemann and Lichtenstein, 1919: figs. IV-VIII). Contrary to Brölemann and Lichtenstein's (1919)

assertions, these walls do not open into a ventral slit (*"fente du cimier"*) along the length of longitudinal seam (Fig. 8C). The function of this structure as a spermatheca, or sperm storage container, was first recognized by Voges (1878), with Brölemann and Lichtenstein (1919: figs. IV-VIII) identifying *"spermatozoïdes"* (spermatozoa) inside the sinuous lumen of the spermatheca. Verhoeff (1928: 700) confirmed this interpretation, describing *"hutförmige… Samenkörper"* (hat-shaped spermatozoa) in the receptacular structures in vulvae of Julida and in the vasa deferentia of millipede males (see Minelli & Michalik, 2015 for diplopod sperm sturcture).

### 3.3 Gonopod Functional Anatomy

The gonopod of *Pseudopolydesmus* consists of the coxa, telopodite, and cannula (see Sierwald *et al.*, 2019: figs. 8, 10). In Polydesmidae the coxa and telopodite in the adult male respectively develop from the coxa and prefemur in the juvenile, whereas the femur and all other distal podomeres are lost during a pre-adult stadium. The cannula develops from a hooked lobe that divides from the coxa in the final two stadia (Petit, 1976). Both the telopodite and cannula articulate against the coxa and are controlled using muscles that originate in the sternite and coxa. The cannula's tapered tip inserts into the proximal opening of the telopodite seminal canal.

The seminal canal is divided into two sections – a superficial groove on the surface of the telopodite, and an invaginated section within it. The superficial groove originates at the telopodite "prefemur" (the proximal part of the telopodite, which is bulb-shaped and setose), whose medial surface bears a furrow (*"Schenkelgrube":* Attems, 1894; *"Präfemurgrube":* Verhoeff, 1928; *"Spermagrube":* Verhoeff, 1931) that narrows and deepens distally (Fig. 13A, 14A: fu). Eventually the walls of the furrow narrow to the extent that they join together over the furrow but do not fuse, creating an externally visible suture (Sierwald *et al.*, 2019: fig. 12). This encloses the superficial groove (Fig. 13: ca, Figs. 14B-E: cag; *"Spermacanal":* Verhoeff, 1892; *"Samenrinne":* Attems, 1894; *"Spermarinne":* Verhoeff, 1928; "sperm canal" and "sperm/seminal groove" of various authors) formed from the joining of the furrow walls extends distally along the antero-medial surface. As it nears the pulvillus, the seminal canal curves

laterally, crosses over to the lateral surface of the telopodite, and continues its curve until it is orientated proximally (Fig. 14F: ca).

At this point, the seminal canal is just proximo-lateral of the pulvillus (pu). Contrary to the assertions of previous authors (Verhoeff, 1931; Carl, 1941; Sierwald *et al.*, 2019), the seminal canal does not open here. Rather, it continues proximally (Fig. 14E: cai), its sclerotized walls pinching off from the surface of the telopodite into the haemocoel of the telopodite (Fig. 14D). The internal, invaginated portion of the seminal canal (portion of *"Spermaschlauch"* contained by its *"äußere Wand":* Carl, 1941; "deeply invaginated groove": Hoffman, 1974) continues proximally into the "prefemur" of the telopodite, finally discharging into an internal bursa, the seminal chamber (Fig. 14C).

Within the seminal chamber (Figs. 13, 14B: ch; *"Samenblase":* Attems, 1894; *"Spermahöhle":* Verhoeff, 1931; portion of *"Spermaschlauch"* between its *"innere Wand"* and *"äußere Wand":* Carl, 1941; "seminal vesicle": Withrow, 1988) seminal fluid proceeds distally via the crescent-shaped lumen of the seminal chamber (Fig. 14D). The seminal chamber is fused to the wall of the invaginated section of the seminal canal for most of its length inside the telopodite; its crescent shape is the result of its adjacency with the seminal canal, which it surrounds on three sides. Carl (1941) emphasized that the cuticular wall of the seminal canal (*"innere Wand des Samenschlauches"*) is much thicker than that of the seminal chamber (*"äußere Wand des Samenschlauches"*). The two passages are adjacent and antiparallel, with seminal fluid flowing proximally through the seminal canal into the seminal chamber, then distally through the seminal chamber, finally splitting from the seminal canal (Fig. 14F) to exit the telopodite through a pore at the base of the pulvillus (Fig. 14G: pu). The pulvillus consists of a trowel-shaped process (Carl, 1941, described the process as *"hufreisenförmig"*: horseshoe-shaped) from which a dense field of hair-like protrusions extends on the proximal side. The seminal fluid presumably emerges into this field.

### 3.4 Copulatory Interface

Based on observations of preserved specimens, adult females of *Pseudopolydesmus* can have their vulvae in one of three positions: withdrawn, partially everted, and fully everted (Figs. 3-4). The first and third positions have been amply illustrated in the previous sections because female specimens are usually found with their vulvae in one or the other. The intermediate position is only found in copulating females. During copulation, the coxal plate is extended to its maximal position, more or less 90° from its fully closed position (Figs. 3C, 4B). The vulvae are also ~90° from their withdrawn position and anteriorly displaced to clear the sternum of BR3 (see animated version of Fig. 3). By positioning the long axis of the vulvae at ~90° from the long axis of her body, the female makes the bursa available to the male's gonopod when the mating pair is in its copulating position (Fig. 15). At some point after copulation the female everts her vulvae to their fullest extent, revealing the opercula at the anterior end (Figs. 3D, 4C). With the vulvae fully everted, the coxal plate is shut most of the way. The long axes of the vulvae and the body are now aligned, albeit in the opposite orientation from when the vulvae were withdrawn.

When a mating pair is *in copula*, the male telopodite interfaces with the female bursa in its partially everted position (Figs. 15, 16, Video 2). Based on the *Ps. serratus* mating pair preserved *in copula* (FMNHINS 7344), the sites of sperm transfer were determined to be the pulvillus in the male and the vulval aperture at the posterior end of the ventral membrane in the female (Fig. 15B: pu). During copulation, the pulvillus is inserted into the genital aperture of the female's vulva. Furthermore, it appears that the first medial process (*m1*, see Sierwald *et al.*, 2019) is also inserted into the vulval aperture (Fig. 16: m1). The distally oriented pulvillus process and the proximally oriented *m1* process may function together to hold open the vulval aperture. The remaining distal length of the telopodite arcs over much of the ventral membrane of the vulval bursa (Figs. 15, 16). The exact interface of the telopodite over the ventral membrane is discussed below (4.6).

# 4 Discussion

## 4.1 Mechanics of Vulval Eversion and Retraction

The fact that the vulvae must be everted for copulation and oviposition raises the question of whether vulval eversion is reversible. In this context we deliberately use the word “withdrawn” to describe the position of the vulvae and “retract” to describe repositioning the vulvae from an everted position to the withdrawn position. If there is a delay between copulatory insemination and oviposition it would probably be beneficial for the vulvae to be protectively retracted until oviposition occurs. We expect there to be such a delay because there would be no need for a sperm-storing spermatheca if fertilization occurred immediately after insemination. Alternatively, the vulvae could be fully everted immediately after copulation without subsequently being retracted. It might even be impossible for mated females to retract the increased bulk of the vulvae after they are covered in copulatory secretions. Among specimens we dissected or imaged using μCT, FMNHINS 3120685 and 1513 had their vulvae withdrawn and lacked mature eggs in their ovaries whereas FMNHINS 1451 had her vulvae fully everted and was gravid. This establishes a correlation between vulval eversion and the presence of mature eggs, but the evidence is circumstantial and based on very few specimens. Furthermore, we cannot know if the vulvae of FMNHINS 1451 were voluntarily everted before the time of death, because collecting the specimen in ethanol sometimes induces vulval eversion (Schubart, 1934: 11). More data will be required to resolve this question.

In our animation simulating vulval eversion (Fig. 3), parts of the vulval sclerites overlap the coxal plate as they are everted. Therefore, it is possible that the coxal plate needs to be flexed outward to accommodate vulval eversion. This could be facilitated by the composition of the coxal plate: three sclerites attached by connective tissue. The connective membranes would allow flexibility between the sclerites. Furthermore, the anterior and posterior plates of the sternite are connected by a thin stalk (Fig. 3B: sta, stp). The stalk may be flexible, allowing the anterior and posterior plates to compress together to accommodate the vulvae.

The gorgets may provide protection to the dorsal connective tissue during vulval eversion. The smooth, hard outer surfaces of the gorgets are perfectly positioned to slide across the indentation of BR3 during eversion to the copulatory position. Furthermore, when the vulvae are completely everted to the

ovipositing position, the gorgets align neatly into the external ventral groove between the anterior and posterior ventral margins of BR3 (Fig. 3D).

4.2 Comparative Morphology and Formation of the Vulva

Many authors have noted the potential utility of female genitalia for taxonomic diagnosis (*e.g.*, Wesener & Sierwald, 2005, Enghoff, 2011), and several taxonomic works that sought to integrate vulval or epigynal morphology into the taxonomy of Polydesmidae have been published (Demange, 1968; Blower, 1985; Withrow, 1988; Tadler and Thaler, 1993). The utility of these results for species diagnosis is variable, with the most useful features often being epigynal rather than vulval. *Pseudopolydesmus*, however, generally lacks major epigynal modification (Fig. 2A: eg). Our results reveal new potential for species diagnosis by using the distinct variation in the distal flange of the medial valve and the modified setae of the ventral membrane. Withrow (1988), the only other author to have published on the vulval morphology of *Pseudopolydesmus*, described species-level variation in the former but not the latter.

Verhoeff (1909; 1928: 718) advocated the Cyphopod Hypothesis of vulva formation in Diplopoda. In Verhoeff's hypothesis components of the vulvae (= cyphopods *sensu* Verhoeff) represent the modified or degenerate podomeres of a pair of walking legs, similar to the male gonopods. This would correspond to either a posterior leg pair of BR3 or an anterior leg pair of BR4 (Verhoeff, 1909). There is no evidence to suggest that the vulvae are derived from modified walking legs; unlike the male gonopods, they do not arise from previously formed walking legs, but from the distal openings of the oviducts. Furthermore, there is no evidence of BR3 bearing two leg pairs in any known millipede group.

Although we reject the Cyphopod Hypothesis, we have presented it here to alleviate confusion stemming from Verhoeff's naming conventions. Like Brölemann and Lichtenstein (1919), Verhoeff divided the vulva into two components. He used the term *"Coxit"* for the bursa and *"Telopodit"* for the operculum. Using the Cyphopod Hypothesis, Verhoeff called the gorget of *Polydesmus* the *"Sternit der Cyphopoden"* or the *"Sternithälfte"* (literally "half sternite"), inferring that the two gorgets represent the medially divided sternite of the cyphopod leg pair.

In contrast, Brölemann and Lichtenstein (1919) forwarded a hypothesis of *de novo* vulva formation. Instead of being the transformed residues of leg podomeres, the sclerotized valves formed *de novo* from the part of the intersegmental membrane surrounding the orifice of the oviduct. The ventral intersegmental membrane became the invaginated vulval pouch. Our results support Brölemann and Lichtenstein's *de novo* hypothesis, especially our finding that the vulvae are embedded in the continuous membrane connecting LP2 to the sternum of BR3 (Figs. 4, 6C, 7: mj, mn). If the vulvae represented the residues of walking legs, we would expect the vulvae to be connected to a sternum of BR3 rather than being "free floating".

Unlike the valves and operculum, the gorget is not a universal feature in millipede vulvae. Brölemann (1917) inferred that the gorget represents a lobe of one of the valves that subsequently separated. It is also possible that the gorget shares a similar evolutionary origin with the receptacle of Euryuridae (Hoffman, 1978). Like the gorget of Polydesmidae (Fig. 9C), the receptacle of Euryuridae is approximately dorsal to the valves and remarkably glabrous compared to the valves, which are setose in both groups (Jorgensen, 2013: fig. 6.5). The terms receptacle and *receptaculum seminis* should not be confused, the latter being an alternative name for the spermatheca.

As an aside, Withrow (1988) described a "receptacle" in the vulvae of *Polydesmus, Scytonotus, Utadesmus* Chamberlin and Hoffman, 1950, and *Bidentogon* Buckett and Gardner, 1968, all members of the family Polydesmidae. The receptacle described by Withrow may be the gorget, although he claimed it is absent in *Pseudopolydesmus*. He never identified the receptacle in an illustration, so it is unclear if he was in fact referring to the same sclerite we call the gorget.

### 4.3 Origin of the Seminal Chamber

Both Verhoeff (1931) and Carl (1941) recognized the elongated *"schlauchförmige*" seminal chamber in *Pseudopolydesmus*, but disagreed on its topological relationship to the seminal canal. Verhoeff described a superficial seminal canal that opens externally via a small gap at the lateral base of the pulvillus and simultaneously flows basally into the internal seminal tube, without recognizing the

invaginated part of the seminal canal. Carl (1941) also described a superficial seminal canal opening at the base of the pulvillus, but did not connect it to the seminal chamber at all. instead showing the invaginated seminal canal as a blind duct emptying into the seminal chamber. Our results show no gap at all at the lateral base of the pulvillus (Figs. 13, 14F). Instead, the superficial groove of the seminal canal transitions directly into the invaginated section without an intrinsic demarcation. Only Hoffman's (1974) diagnosis of the genus *Pseudopolydesmus* accurately describes the topology of the seminal canal and seminal chamber. Verhoeff (1931) and Carl (1941) described the seminal chamber as opening externally via a large pore basal to the pulvillus, and on this point we agree with both authors.

As outlandish as the elongated loop of the seminal tract in *Pseudopolydesmus* gonopods seems, its topology is comparable to related members of other polydesmid taxa. Attems (1894) noted that in *Polydesmus* and *Brachydesmus* Heller, 1858 the seminal canal terminates in a bladder-like chamber (*"Samenblase"*) in which he hypothesized seminal fluid was stored. It seems likely that the seminal chamber of *Pseudopolydesmus* is an elongated form of the seminal bladder that has become deeply invaginated into the telopodite. Unlike the bladder-shaped chamber, the tubular seminal chamber of *Pseudopolydesmus* requires a long invaginated seminal canal to maintain flow of seminal fluid. If the seminal canal terminated into the distal end of the seminal chamber, older seminal fluid would become trapped at the basal end. This would be especially untenable if accessory seminal products are secreted into the seminal chamber, the accessory products being trapped in the basal end of the seminal chamber. In this scenario, it seems necessary for the seminal canal to extend internally to deliver seminal fluid to the basal end of the seminal chamber.

### 4.4 Bristles and Sensory Setae

The valves and operculum in female *Pseudopolydesmus* all bear numerous long setae (Figs. 1B, 8, 9, 12). In segmented 3D models of the valves and operculum the setae are indirectly detectable as apparent circular pores in the sclerites (Figs. 9, 11A, 12B). These gaps actually represent the non-sclerotized attachment points of the setae. It seems likely that these socketed setae have a sensory

function; the gaps would allow nerve access. The vulvae are covered in these long setae, with over 90 visible in our SEM images of a *Ps. erasus* vulva (FMNHINS 3120685, Figs. 8A-B, 12A). The setae are concentrated on the anterior side of the bursa and on the operculum, away from the vulval aperture, so it appears unlikely that they function to detect the male gonopods by touch. It is plausible, however, that they are used for proprioception during vulval eversion, for sensing the substrate during oviposition, or for both purposes.

Although most of the bristles lining the margins of the ventral membrane are not socketed, sockets are visible in a few of the anteriormost bristles. The presence of socketed marginal setae is evidence that the non-socketed marginal bristles are modified from sensory setae for specialization in the retention of secreted glandular discharge.

The gonopod coxa in male *Pseudopolydesmus* bears two very long, socketed setae directed ventromedially (see Sierwald *et al*., 2019: Figs 20, 25, 31). Like the setae of the vulval sclerites, the sockets of the two coxal setae are visible in the μCT dataset as circular gaps in the sclerite. The location of these setae suggests they could detect the movement of the telopodite if it is flexed dorsally. Therefore, we suspect they are used for proprioception of the telopodites, although they might be used to sense the location of the female vulvae to ensure they are correctly mated to the telopodites.

### 4.5 Glandular Secretions

The functions and destinations of secretory products from each gland (Fig. 7: glb, glf, glg) are unknown to us, but two likely secretory products are the copulatory secretions and secretions for preserving sperm in the lumen of the spermatheca. The bursal gland (glb) is the largest, and near the spermatheca, making it potentially a good candidate for production of the copulatory secretions. The flange gland (glf) is near the site of insemination, making it a good candidate for secretions for preserving sperm. The gorget glands (glg) might assist either of these functions.

The function of the bursal muscle sheets is probably inextricably connected to the bursal secretions. Because they attach the valves to the ventral membrane, their contraction would reduce the

volume of the bursa by pulling the valves together and flexing the ventral membrane dorsally. A possible result of this contraction could be the expulsion and extrusion of secretory products from the bursa during copulation.

Verhoeff (1928) reported a glandular duct in the gonopod coxa that passes into the telopodite through the joint between the two sclerites, discharging into the setose furrow at the basal end of the seminal canal. We did not detect this duct or its associated gland using μCT imaging, nor did we detect any other glandular tissue in the gonopod.

### 4.6 Genital Interface

The shape of the posterior convex bulge in the ventral membrane of the vulva may be significant for sexual selection and species recognition. Among ventral membranes of vulvae we have studied in detail, those of *Ps. erasus* (Fig. 8) and *Ps. canadensis* (Newport, 1844) (Fig. 1C) angle sharply antero-dorsally, whereas that of *Ps. serratus* (Figs. 1B, 9, 16) slopes gently dorsally posterior to the vulval aperture. The ventral membrane in *Ps. pinetorum* is also gently curved, but the vulval aperture is near the posterior extremity of the ventral membrane. This is consistent with Withrow's illustrations of the vulvae (1988: figs. 67 and 106-109). The variable morphology of the ventral membrane correlates with the gonopod telopodite. For example, the short curving distal part of the telopodite of *Ps. pinetorum* (Sierwald *et al.*, 2019: figs. 18-20) matches the vulval aperture on the curved posterior part of the ventral membrane, and the long nearly straight central part of the telopodite of *Ps. canadensis* allows the pulvillus to align with vulval aperture on the ventral surface (Figs. 15, 16).

After transmission to the vulva aperture, sperm must travel through the sinuous spermatheca toward the operculum. It is possible that the long spermatheca provides a venue for sperm competition. Male-male intrasexual competition has been studied in millipedes of the order Spirostreptida (Telford and Dangerfield, 1996). However, male-male competition cannot explain species-level variation in the female vulvae. We favor mechanisms of intersexual selection – female choice and lock-and-key mechanisms – as the main explanation.

One argument often given against the lock-and-key mechanism as a general hypothesis to explain genitalic variation is that female genitalia do not vary enough at the species level to be a corresponding match to the highly variable male genitalia (Eberhard, 1985; Shapiro and Porter, 1989). However, female genital morphology in animals has not been investigated to the same extent as male genital morphology. When investigated, it has often shown to vary at the species and population level (Ah-King *et al.*, 2014). Our results, although not focused on species diagnosis, show that variation in female genital morphology in *Pseudopolydesmus* corresponds closely to that in male genitalia at the species. However, this correlated morphology could also be a result of female choice for mechanical fit.

Lock-and-key and/or mechanical female choice cannot entirely explain the variation in gonopod morphology distal from the pulvillus. Species of *Pseudopolydesmus* are diagnosable primarily by the number and shape of distal cuticular processes (Sierwald *et al.*, 2019). Unlike the overall shape of the telopodite and the position of the pulvillus, the number and shape of distal processes does not have an observable counterpart in the vulva. It is possible that the distal processes serve a stimulatory function in female choice, with a female rejecting males that have an incorrect morphology. This would be consistent with observations of preliminary intromission in some other millipede groups (Haacker and Fuchs, 1970; Tanabe and Sota, 2008), but in contrast to the strict lock-and-key mechanism described in Paradoxosomatidae (Wojcieszek *et al.*, 2012; Wojciescek and Simmons, 2013). Because genital morphology in *Pseudopolydesmus* varies both at the copulatory interface and in adjacent regions not necessary for copulation, we suggest that lock-and-key interactions or mechanical female choice on the one hand, and stimulatory female choice on the other, each represent possible selective filters to male reproductive success in *Pseudopolydesmus*.

## 5 Conclusions

The use of μCT imaging has enabled the discovery of a potential lock-and-key relationship between male and female genitalia in the genus *Pseudopolydesmus* by demonstrating species-level variation in the female genitalia and by digitally simulating the copulatory interface between male and

female genitalia. Furthermore, it has allowed us to confidently describe the anatomy of the seminal canal and seminal chamber in the male gonopod, which had remained unresolved for nearly 80 years using traditional microscopy methods. The overall curve of the telopodite and the position of the pulvillus along the curve appear to be the most important factors determining the lock-and-key fit of the gonopods to the female vulvae, whereas the number and shape of distal processes likely play a role in sexual selection by female choice.

## Author Contributions

XJZ, PS, and JEB designed the study. XJZ and PS dissected specimens and acquired SEM images. SW acquired digital light microscope images, including enhancing existing protocols for imaging under ultraviolet illumination. XJZ acquired μCT images and carried out label segmentation. XJZ wrote the original draft and designed the figures. All authors revised the manuscript and read and approved the final version.

## Acknowledgements

We would like to thank the following persons and institutions: Douglas Rowland provided critical assistance to XJZ for μCT image acquisition at the Center for Molecular and Genomic Imaging (CMGI) at University of California, Davis (UCD). Betty Strack assisted XJZ and PS with SEM imaging at the Field Museum. Lisa Kanellos (Field Museum) illustrated Fig. 4 on behalf of PS. Julia Snyder shipped specimens from the Field Museum to UCD. μCT imaging for this project was supported by a pilot grant from the CMGI at UCD (https://cmgi.ucdavis.edu) to XJZ and JEB. The remaining research for this project was funded by National Science Foundation grants DEB 1256150 to PS and DEB 1256139 to JEB and the Evert and Marion Schlinger Foundation (UCD). XJZ would like to thank Geoffrey Attardo, Zachary Griebenow, Brendon Boudinot, and Jill Oberski of UCD for their various roles in supporting this project.

References

Ah-King, M., Barron, A.B., Herberstein, M.E., 2014. Genital evolution: Why are females still understudied? PLOS Biology 12, e1001851.

Akkari, N., Enghoff, H., Metscher, B.D., 2015. A new dimension in documenting new species: High-detail imaging for myriapod taxonomy and first 3D cybertype of a new millipede species (Diplopoda, Julida, Julidae). PLOS ONE 10, e0135243.

Attems, C.M.T., 1894. Die Copulationsfüsse der Polydesmiden. Sitzungberichte der Kaiserlichen Akademie der Wissenschaften, Mathematisch-Naturwissenschaftliche Classe, Abteilung I 103, 39–54.

Blanke, A., Wesener, T., 2014. Revival of forgotten characters and modern imaging techniques help to produce a robust phylogeny of the Diplopoda (Arthropoda, Myriapoda). Arthropod Structure & Development 43, 63–75.

Blower, J.G., 1985. Millipedes. Synopses of the British Fauna, n.s. 35, 1–242.

Bond, J.E., Beamer, D.A., Hedin, M.C., Sierwald, P., 2003. Gradual evolution of male genitalia in a sibling species complex of millipedes (Diplopoda : Spirobolida : Rhinocricidae : *Anadenobolus*). Invertebrate Systematics 17, 711.

Bond, J.E., Sierwald, P., 2002. Cryptic speciation in the *Anadenobolus excisus* millipede species complex on the island of Jamaica. Evolution 56, 1123–1135.

Brölemann, H.W., 1917. Les vulves des Polydesmiens (Myriapodes) note préliminaire. Bulletin de la Société Entomologique de France 1917, 60–62.

Brölemann, H.W., Lichtenstein, J.L., 1919. Les vulves des Diplopodes, mémoire préliminaire. Archives de Zoologie Expérimentale et Générale 58, 173–218.

Carl, J., 1941. Diplopodenstudien V. Zoologischer Anzeiger 133, 285–295.

Demange, J.-M., 1968. Étude des femelles appartenant aux genres *Polydesmus* et *Brachydesmus* pour servir a une faune des myriapodes de France. Bulletin de la Société d'Histoire Naturelle de Toulouse 104, 276–305.

Eberhard, W.G., 1985. Sexual Selection and Animal Genitalia. Harvard University Press, Cambridge, Massachusetts.

Enghoff, H., 2011. East African giant millipedes of the tribe Pachybolini (Diplopoda, Spirobolida, Pachybolidae). Zootaxa 2753, 1–41.

Fabre, A.-C., 1855. Recherches sur l'anatomie des organes reproducteurs et sur le développement des Myriapodes. Annales des Sciences Naturelles, 4 3, 257–316.

Gignac, P.M., Kley, N.J., Clarke, J.A., Colbert, M.W., Morhardt, A.C., Cerio, D., Cost, I.N., Cox, P.G., Daza, J.D., Early, C.M., Echols, M.S., Henkelman, R.M., Herdina, A.N., Holliday, C.M., Li, Z., Mahlow, K., Merchant, S., Müller, J., Orsbon, C.P., Paluh, D.J., Thies, M.L., Tsai, H.P., Witmer, L.M., 2016. Diffusible iodine-based contrast-enhanced computed tomography (diceCT): An emerging tool for rapid, high-resolution, 3-D imaging of metazoan soft tissues. Journal of Anatomy 228, 889–909.

Haacker, U., Fuchs, S., 1970. Das Paarungsverhalten von *Cylindroiulus punctatus* Leach. Zeitschrift für Tierpsychologie 27, 641–648.

Hoffman, R.L., 1974. A new polydesmid milliped from the southern Appalachians, with remarks on the status of *Dixidesmus* and a proposed terminology for polydesmid gonopods. Proceedings of the Biological Society of Washington 87, 345–350.

Hoffman, R.L., 1978. North American millipeds of the genus *Euryurus* (Polydesmida: Platyrhacidae). Transactions of the American Entomological Society 104, 37–68.

Hosken, D.J., Stockley, P., 2004. Sexual selection and genital evolution. Trends in Ecology & Evolution 19, 87–93.

Jorgensen, M.C., 2013. Systematic studies of polydesmidan millipedes (Diplopoda, Polydesmida) (PhD Thesis). University of Illinois, Chicago, Chicago.

Kamp, T. van de, dos Santos Rolo, T., Vagovič, P., Baumbach, T., Riedel, A., 2014. Three-dimensional reconstructions come to life – Interactive 3D PDF animations in functional morphology. PLOS ONE 9, e102355.

Kraus, O., 1966. Phylogenie, Chorologie und Systematik der Odontopygoideen. Abhandlungen der Senckenbergischen Naturforschenden Gesellschaft 152, 1–143.

Kraus, O., 1968. Isolationsmechanismen und Genitalstrukturen bei wirbellosen Tieren. Zoologischer Anzeiger 181, 22–38.

Kurnik, I., 1988. Zur Taxonomie ostalpiner Chordeumatida: Vulvenmorphologie und Identifikation der Weibchen. Zoologische Jahrbücher, Abteilung für Systematik, Ökologie und Geographie der Tiere 115, 229–302.

Kurnik, I., 1990. Vulval structures and their bearing on the taxonomy of the Chordeumatida (Diplopoda). In: Proceedings of the 7th International Congress of Myriapodology. Brill, Leiden, pp. 25–26.

Kurnik, I., Thaler, K., 1985. Die Vulven der Chordeumatida: Merkmale von taxonomischer Bedeutung (Diplopoda; Helminthomorpha). Contributions to Zoology 55, 116–124.

Limaye, A., 2012. Drishti: A volume exploration and presentation tool. Proceedings of SPIE 8506, 85060X.

Lipke, E., Hammel, J.U., Michalik, P., 2015. First evidence of neurons in the male copulatory organ of a spider (Arachnida, Araneae). Biology Letters 11, 20150465.

Liu, W., Rühr, P.T., Wesener, T., 2017. A look with μCT technology into a treasure trove of fossils: The first two fossils of the millipede order Siphoniulida discovered in Cretaceous Burmese amber (Myriapoda, Diplopoda). Cretaceous Research 74, 100–108.

Metscher, B.D., 2009. MicroCT for comparative morphology: Simple staining methods allow high-contrast 3D imaging of diverse non-mineralized animal tissues. BMC Physiology 9, 11.

Minelli, A., Michalik, P., 2015. Diplopoda, reproductive system. In: Minelli, A. (Ed.), The Myriapoda Volume 2. Brill, Leiden, pp. 237–265.

Moritz, L., Wesener, T., 2019. The first known fossils of the Platydesmida—An extant American genus in Cretaceous amber from Myanmar (Diplopoda: Platydesmida: Andrognathidae). Org Divers Evol 19, 423–433.

Moritz, L., Wesener, T., Koch, M., 2018. An apparently non-swinging tentorium in the Diplopoda (Myriapoda): Comparative morphology of the tentorial complex in giant pill-millipedes (Sphaerotheriida). ZooKeys 741, 77–91.

Naumann, B., Reip, H.S., Akkari, N., Neubert, D., Hammel, J.U., 2019. Inside the head of a cybertype – Three-dimensional reconstruction of the head muscles of *Ommatoiulus avatar* (Diplopoda: Juliformia: Julidae) reveals insights into the feeding movements of Juliformia. Zoological Journal of the Linnean Society zlz109.

Petit, G., 1976. Developpements compares des appendices copulateurs (gonopodes) chez *Polydesmus angustus* Latzel et *Brachydesmus superus* Latzel (Diplopodes : Polydesmidae). International Journal of Insect Morphology and Embryology 5, 261–272.

Rath, O. vom, 1891. Ueber die Fortpflanzung der Diplopoden (Chilognathen). Berichte der Naturforschenden Gesellschaft zu Freiburg i. B. 5, 1–28.

Schubart, O., 1934. Die Tierwelt Deutschlands und der angrenzenden Meeresteile nach ihren Merkmalen und nach ihrer Lebensweise, 28. Teil: Tausendfüßler oder Myriapoda, I: Diplopoda. Gustav Fischer Verlag, Jena.

Sentenská, L., Müller, C.H.G., Pekár, S., Uhl, G., 2017. Neurons and a sensory organ in the pedipalps of male spiders reveal that it is not a numb structure. Scientific Reports 7, 12209.

Shapiro, A.M., Porter, A.H., 1989. The lock-and-key hypothesis: Evolutionary and biosystematic interpretation of insect genitalia. Annual Review of Entomology 34, 231–245.

Shear, W.A., 1972. Studies in the milliped order Chordeumida (Diplopoda): A revision of the family Cleidogonidae and a reclassification of the order Chordeumida in the New World. Bulletin of the Museum of Comparative Zoology 144, 151–352.

Shear, W.A., 1976. The milliped family Conotylidae (Diplopoda, Chordeumida) revision of the genus *Taiyutyla*, with notes on recently proposed taxa. American Museum Novitates 2600, 1–22.

Shear, W.A., 1981. The milliped family Tingupidae (Diplopoda, Chordeumatida, Brannerioidea). American Museum Novitates 2715, 1–20.

Shelley, R.M., 1993. Revision of the milliped genus *Scytonotus* Koch (Polydesmida: Polydesmidae). Brimleyana 19, 1–60.

Shively, S., Miller, W.R., 2009. The use of HMDS (hexamethyldisilazane) to replace critical point drying (CPD) in the preparation of tardigrades for SEM (scanning electron microscope) imaging. Transactions of the Kansas Academy of Science 112, 198–200.

Sierwald, P., Hennen, D.A., Zahnle, X.J., Ware, S., Marek, P.E., 2019. Taxonomic synthesis of the eastern North American millipede genus *Pseudopolydesmus* (Diplopoda: Polydesmida: Polydesmidae), utilizing high-detail ultraviolet fluorescence imaging. Zoological Journal of the Linnean Society 187, 117–142.

Stoev, P., Moritz, L., Wesener, T., 2019. Dwarfs under dinosaur legs: A new millipede of the order Callipodida (Diplopoda) from Cretaceous amber of Burma. ZooKeys 841, 79–96.

Tadler, A., 1996. Functional morphology of genitalia of four species of julidan milllipedes (Diplopoda: Nemasomatidae; Julidae). Zoological Journal of the Linnean Society 118, 83–97.

Tadler, A., Thaler, K., 1993. Genitalmorphologie, Taxonomie und geographische Verbreitung ostalpiner Polydesmida (Diplopoda, Helminthomorpha). Zoologische Jahrbücher, Abteilung für Systematik, Ökologie und Geographie der Tiere 120, 71–128.

Tanabe, T., Sota, T., 2008. Complex copulatory behavior and the proximate effect of genital and body size differences on mechanical reproductive isolation in the millipede genus *Parafontaria*. The American Naturalist 171, 692–699.

Telford, S.R., Dangerfield, J.M., 1996. Sexual selection in savanna millipedes: Products, Patterns and Processes. Mémoires du Muséum National d'Histoire Naturelle 169, 565–576.

Verhoeff, K.W., 1892. Neue Diplopoden der paläarktischen Region. Zoologischer Anzeiger 15, 377–387.

Verhoeff, K.W., 1909. Über die Vulven der Ascospermophora, das Cyphopodensegment und Spermatophoren als Begattungszeichen, eine vorläufige Mitteilung. Sitzungsberichte der Gesellschaft Naturforschender Freunde zu Berlin 1909, 219–225.

Verhoeff, K.W., 1910. Ueber Diplopoden. 19. (39.) Aufsatz: Iuliden und Ascospermophora. Jahreshefte des Vereins für vaterländische Naturkunde in Württemberg 66, 337–398.

Verhoeff, K.W., 1928. Klassen und Ordnungen des Tierreichs, Band 5, Abteilung II, Buch 2: Klasse Diplopoda. Akademische Verlagsgesellschaft, Leipzig.

Verhoeff, K.W., 1931. *Pseudopolydesmus* "im Wechsel der Zeiten", 122. Diplopoden-Aufsatz. Zoologischer Anzeiger 94, 305–318.

Voges, E., 1878. Beiträge zur Kenntniss der Juliden. Zeitschrift für Wissenschaftliche Zooologie 31, 127–194.

Voigtländer, K., Naumann, B., Lang, B., Reip, H.S., 2017. The taxonomic value of the vulvae in millipedes of the family Julidae (Diplopoda). Tropical Natural History Supplement 5, 63.

Wesener, T., 2019. The oldest pill millipede fossil: A species of the Asiatic pill millipede genus *Hyleoglomeris* in Baltic amber (Diplopoda: Glomerida: Glomeridae). Zoologischer Anzeiger 283, 40–45.

Wesener, T., Sierwald, P., 2005. The giant pill-millipedes of Madagascar: Revision of the genus *Sphaeromimus*, with a review of the morphological terminology (Diplopoda, Sphaerotheriida, Sphaerotheriidae). Proceedings of the California Academy of Sciences, 4 56, 557–599.

Wirkner, C.S., Xylander, W.E.R., 2015. Diplopoda, circulatory system. In: Minelli, A. (Ed.), The Myriapoda Volume 2. Brill, Leiden, pp. 153–160.

Withrow, C.P., 1988. Revision of the genus *Pseudopolydesmus* Attems, 1898 and its relationships to the North American genera of the family Polydesmidae Leach, 1815 (PhD Thesis). Ohio State University, Columbus, Ohio.

Wojcieszek, J.M., Austin, P., Harvey, M.S., Simmons, L.W., 2012. Micro-CT scanning provides insight into the functional morphology of millipede genitalia: Functional morphology of millipede genitalia. Journal of Zoology 287, 91–95.

Wojcieszek, J.M., Simmons, L.W., 2013. Divergence in genital morphology may contribute to mechanical reproductive isolation in a millipede. Ecology and Evolution 3, 334–343.

Yushkevich, P.A., Piven, J., Hazlett, H.C., Smith, R.G., Ho, S., Gee, J.C., Gerig, G., 2006. User-guided 3D active contour segmentation of anatomical structures: significantly improved efficiency and reliability. NeuroImage 31, 1116–1128.

**Table 1.** List of specimens illustrated in this paper. All specimens collected in the United States. Abbreviations: Co. – county; F – female; F+M – mating pair; M – male; SEM – scanning electron micrograph; UV – ultraviolet autofluorescence image; W – west; µCT – micro-computed tomography (4x and 10x refer to detector lens used). US states identified by standard 2-letter postal abbreviations.

| FMNHINS | Species | Sex | Collection Locality | Collection Date | Imaging Modalities |
|---|---|---|---|---|---|
| 1451 | *Ps. pinetorum* | F | IL, Union Co.: Wolf Lake, Pine Hills | 22-Sep-1975 | µCT: 4x |
| 1513 | *Ps. serratus* | F | IN, Parke Co.: Hajji Hollow, 4 mi W of Rockville | 28-Jun-1958 | µCT: 4x, 10x |
| 1513 | *Ps. serratus* | M | IN, Parke Co.: Hajji Hollow, 4 mi W of Rockville | 28-Jun-1958 | µCT: 10x |
| 2817 | *Ps. serratus* | F | IL, Lake Co.: Spring Bluff | 9-Jun-1999 | UV |
| 6934 | *Ps. canadensis* | F | TN, Sevier Co.: Great Smoky Mountains National Park, Le Conte quadrant, W from Grotto Falls Parking Lot | 17-Jun-1999 | UV |
| 7344 | *Ps. serratus* | F+M | WI, Ozaukee Co.: Cedarberg Bog, Cedar Swamp | 19-Jun-2003 | Light, UV |
| 3120685 | *Ps. erasus* | F | NC, Macon Co.: Highlands, Cliffside Lake Recreation Area, 35.0815° N, 83.2368° W | 1-Jun-2015 | Light, UV, SEM |

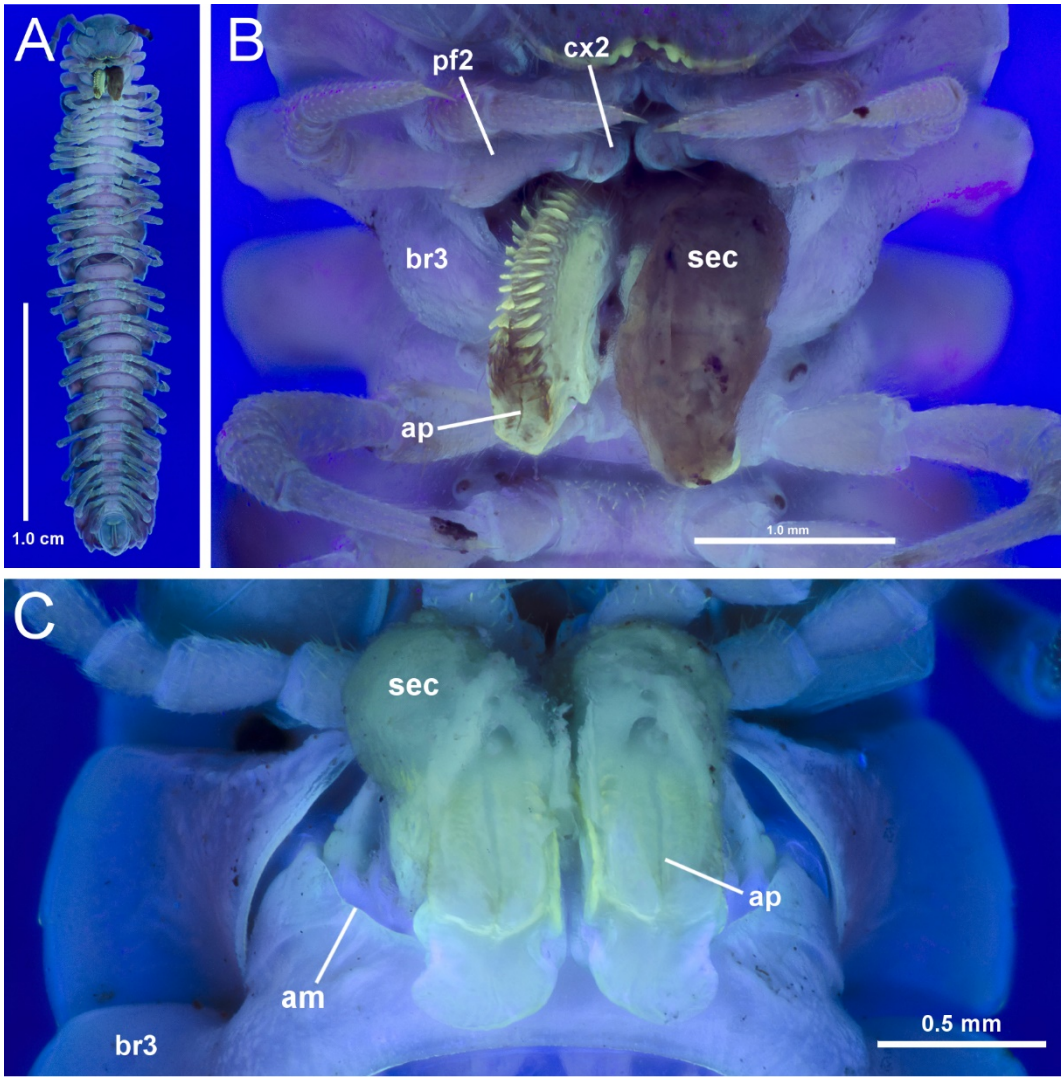


**Figure 1.** Overview of adult female *Pseudopolydesmus*. (A) Female *Ps. serratus* with vulvae everted, *habitus*, ventral view (FMNHINS 2817, UV-enhanced image). (B) Enlargement of everted vulvae of the same. Left vulva is encrusted with glandular secretions, right vulva is not. (C) Female *Ps. canadensis*, enlargement of everted vulvae, ventral view (FMNHINS 6934, UV-enhanced image). Abbreviations: am – indented anterior margin of body ring 3; ap – vulval aperture; br3 – body ring 3; cx2, pf2 – coxa and prefemur of second leg pair, respectively; sec – copulatory secretions.

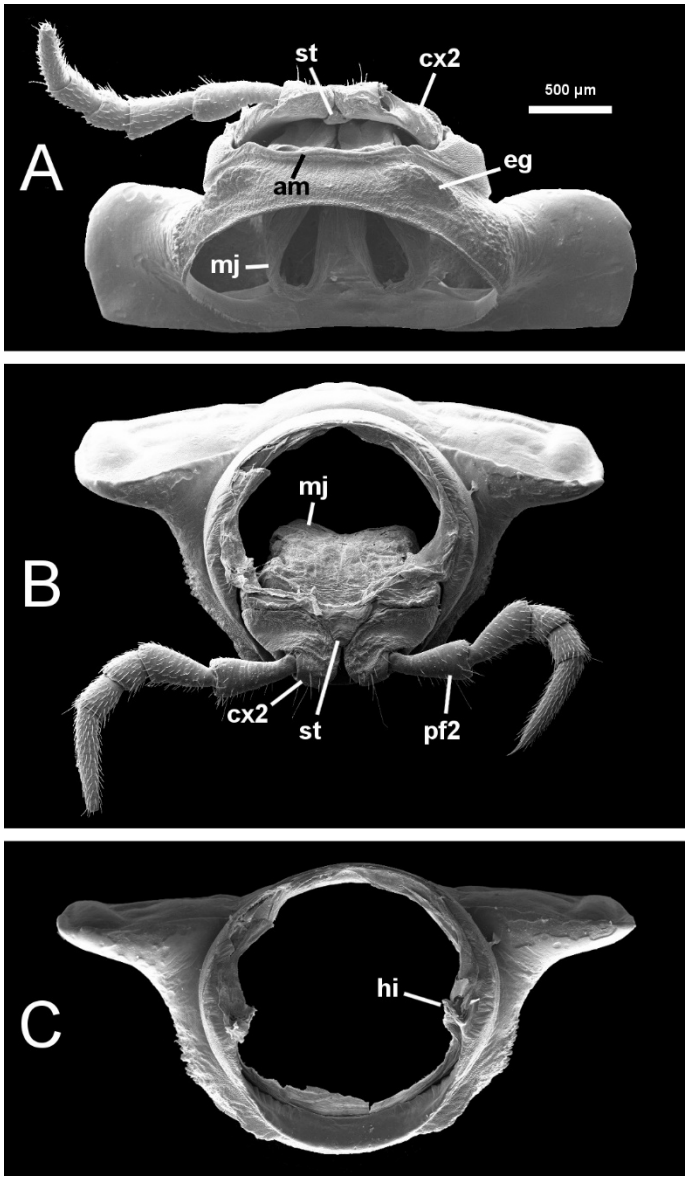


**Figure 2.** Body ring 3 of *Pseudopolydesmus erasus* (FMNHINS 3120685, SEM images), showing female sexual characteristics. (A) Ventral view with coxal plate partly open revealing distal extremity of bursa. Left leg 2 removed, except the coxa. (B) Anterior view showing coxal plate, with vulvae withdrawn behind major membrane. (C) Anterior view with leg pair 2 and vulvae removed, laterally showing apophyses of coxal plate articulation. Abbreviations: am – indented anterior margin of body ring; cx2 – coxa of second leg pair; eg – epigynal tubercles; hi – hinged apophysis; mj – major vulval membrane; pf2 – prefemur of second leg pair; st – sternite of coxal plate.

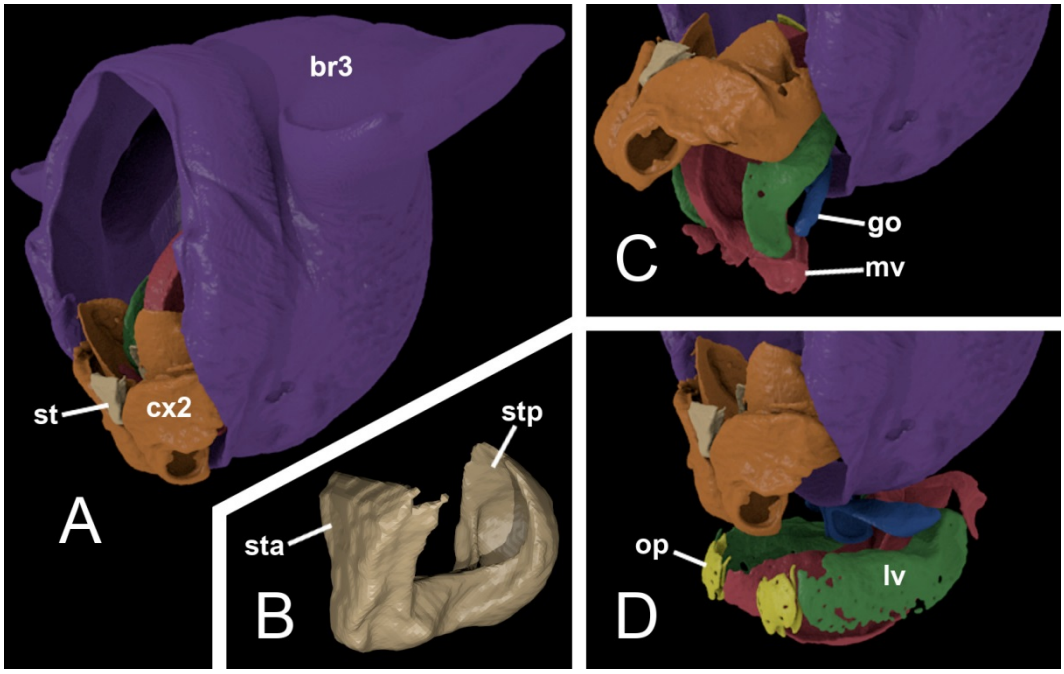


**Figure 3.** Virtually dissected sclerites of body ring 3 in female *Pseudopolydesmus serratus* (FMNHINS 1513). (A) Vulvae withdrawn within body ring 3, coxal plate in closed position. (B) Virtually dissected sternite, magnified to show anterior and posterior plates connected by longitudinal stalk. (C) Coxal plate extended ~90° antero-dorsally, with vulvae partially everted for copulation. (D) Vulvae fully everted, with opercula exposed for oviposition. The coxal plate is flexed to nearly its closed position (compare with A), but remains partially extended to accommodate passage of eggs through the extended oviducts. Abbreviations: br3 – body ring 3; cx2 – flattened coxae of leg pair 2; go – gorget; lv, mv – lateral and medial valves, respectively; op – operculum; st – sternite of coxal plate; sta, stp – anterior and posterior plates of sternite, respectively.

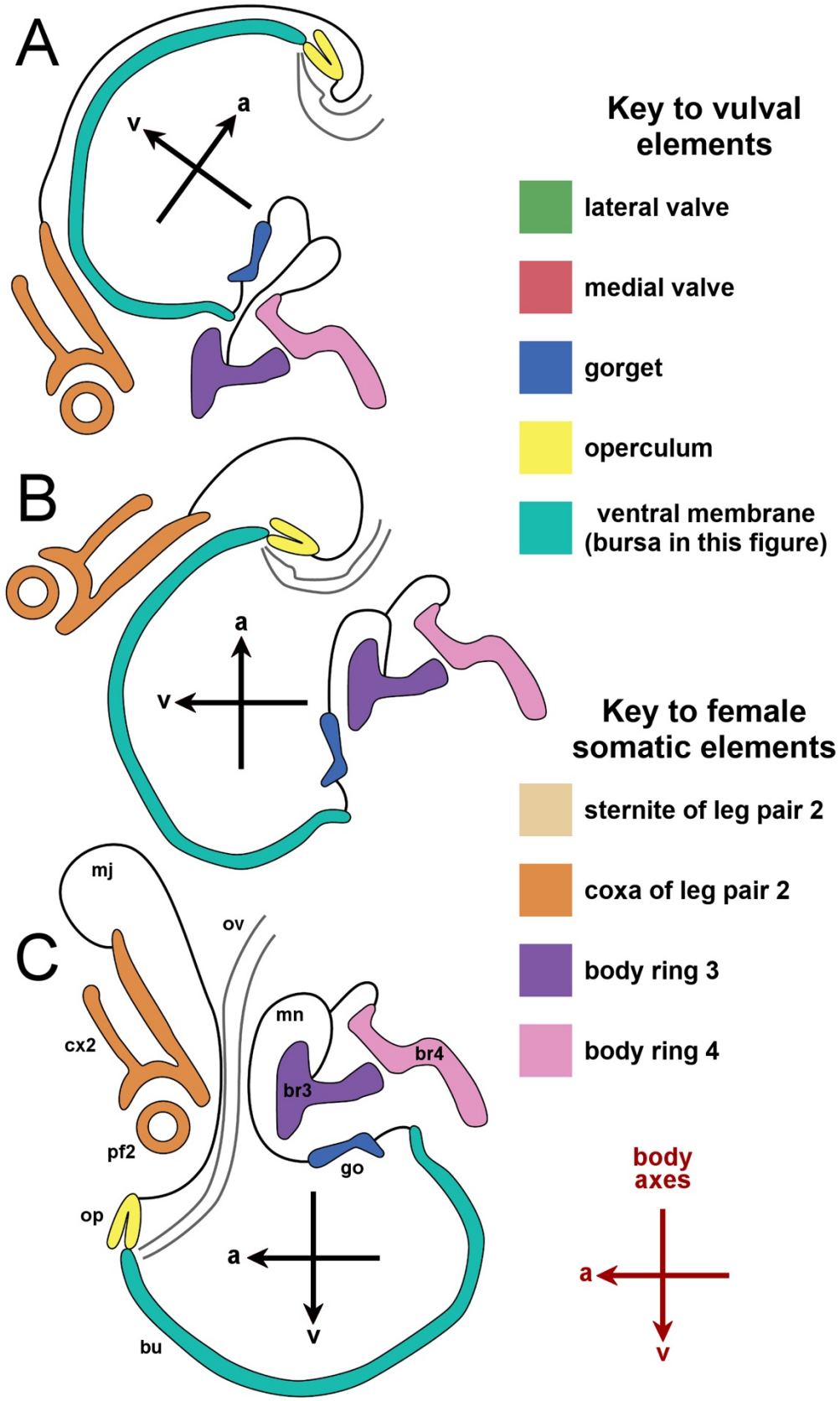
A
v
a
B
a
v
C
mj
ov
cx2
mn
br4
br3
pf2
go
op
a
v
bu
Key to vulval elements
lateral valve
medial valve
gorget
operculum
ventral membrane (bursa in this figure)
Key to female somatic elements
sternite of leg pair 2
coxa of leg pair 2
body ring 3
body ring 4
body axes
a
v

**Figure 4.** Schematic line drawings showing a parasagittal section through a vulva. (A) Vulva withdrawn. (B) Vulva everted to copulatory position. (C) Vulva fully everted to ovipositing position (standard anatomical position). Sclerites color coded, membranes depicted with thick black stroke, walls of oviduct and vagina depicted with thick gray stroke. For simplicity, the ventral membrane color (teal) is used to represent the entire bursa, including ventral membrane and valves. The color keys apply to all colorized figures in this paper. Vulval axes are shown for each orientation, with body axes provided for reference. Abbreviations: a – anterior axis polarity; br3, br4 – ventral portions of body rings 3 and 4, respectively; bu – bursa (including valves and ventral membrane); cx2 – coxa of second leg pair; go – gorget; mj, mn – major and minor vulval membranes, respectively; op – operculum; ov – oviduct; pf2 – prefemur of second leg pair; v – ventral axis polarity.

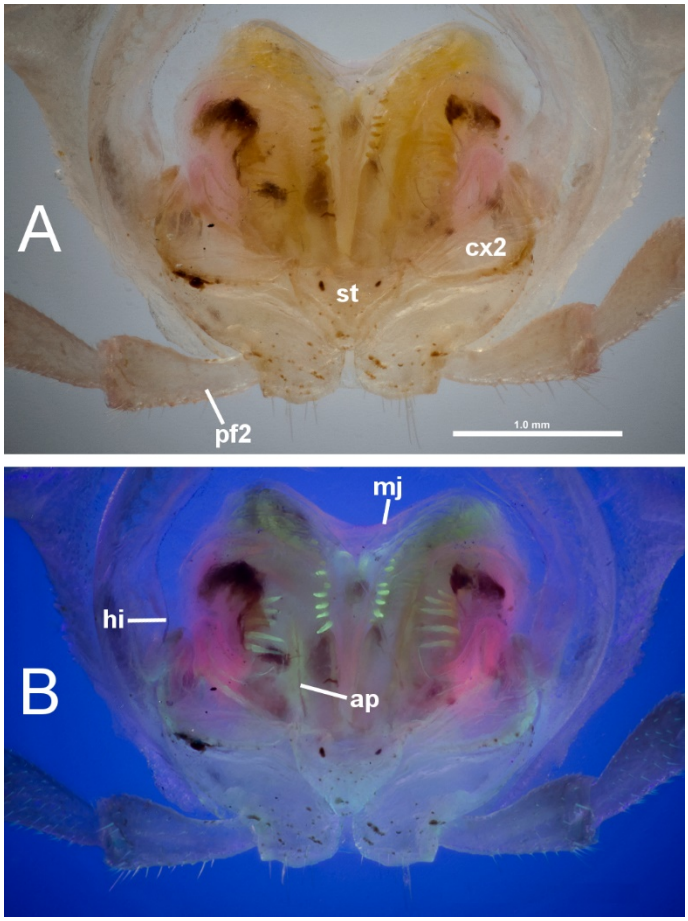


**Figure 5.** Dissected body ring 3 of female *Pseudopolydesmus erasus* showing withdrawn vulvae *in situ*, anterior view (FMNHINS 3120685). Vulvae are visible through the translucent major membrane. (A) White light image. (B) UV-enhanced image. Abbreviations: ap – vulval aperture; cx2 – coxa of second leg pair; hi – hinged apophysis; mj – major vulval membrane; pf2 – prefemur of second leg pair; st – sternite of coxal plate.

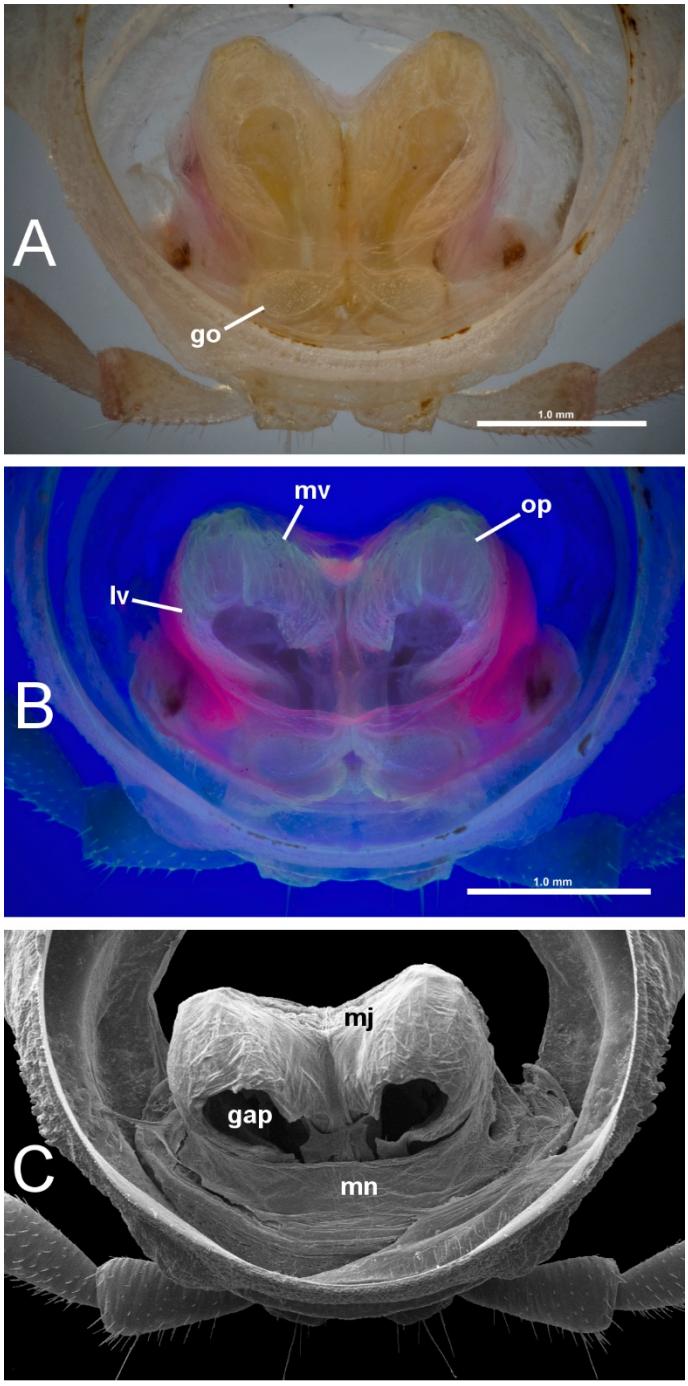


**Figure 6.** Dissected body ring 3 of female *Pseudopolydesmus erasus* showing withdrawn vulvae *in situ*, posterior view (FMNHINS 3120685). Vulvae are visible through the translucent major and minor membranes. (A) White light image. (B) UV-enhanced image. (C) SEM image. Abbreviations: gap – vulval gap for oviduct and haemocoel conduit; go – gorget; lv – lateral valve of bursa; mj, mn – major and minor vulval membranes, respectively; mv –medial valve of bursa; op – operculum.

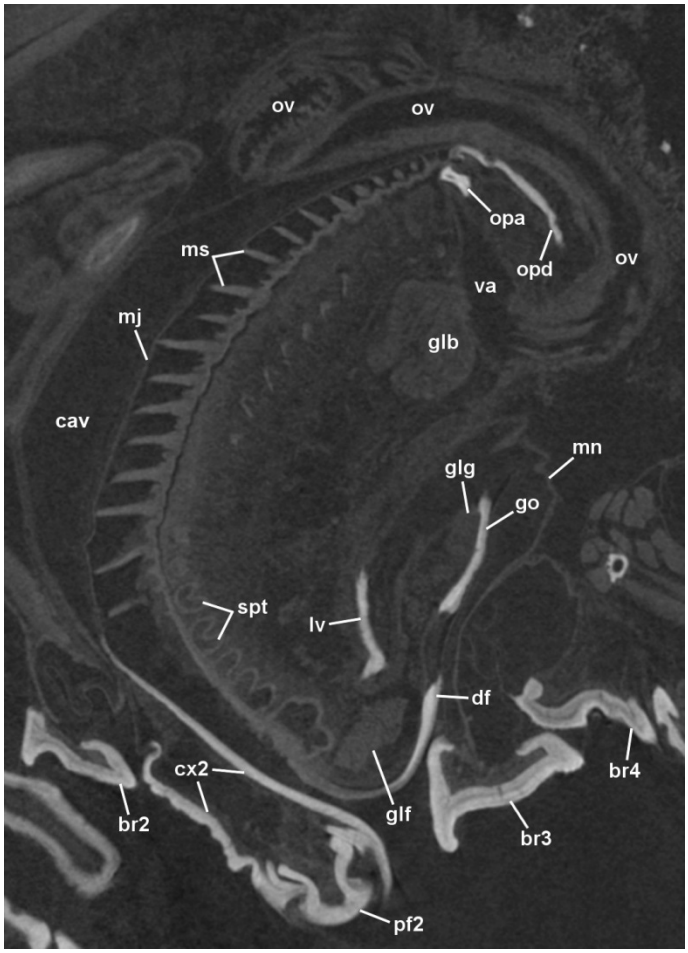


**Figure 7.** Parasagittal section of *Pseudopolydesmus serratus* female, showing withdrawn left vulva and internal anatomy from µCT image (FMNHINS 1513, 2.1 µm resolution, sagittal slice #602). Compare to Fig. 4A. Abbreviations: br2, br3, br4 – ventral portions of body rings 2, 3, and 4, respectively; cav – cavity of vulval pouch; cx2 – coxa of second leg pair; df – distal flange of medial valve; glb – bursal gland; glf – gland of distal flange; glg – gorget gland; go – gorget; lv – edge of lateral valve; mj, mn – major and minor vulval membranes, respectively; ms – modified setae; opa – arched sclerite of operculum, distal extremity (*cf.* Fig. 12C); opd – discoid sclerite of operculum (*cf.* Fig. 12A, B); ov – oviduct; pf2 – prefemur of second leg pair; spt – spermatheca, sagittal sections; va – vagina.

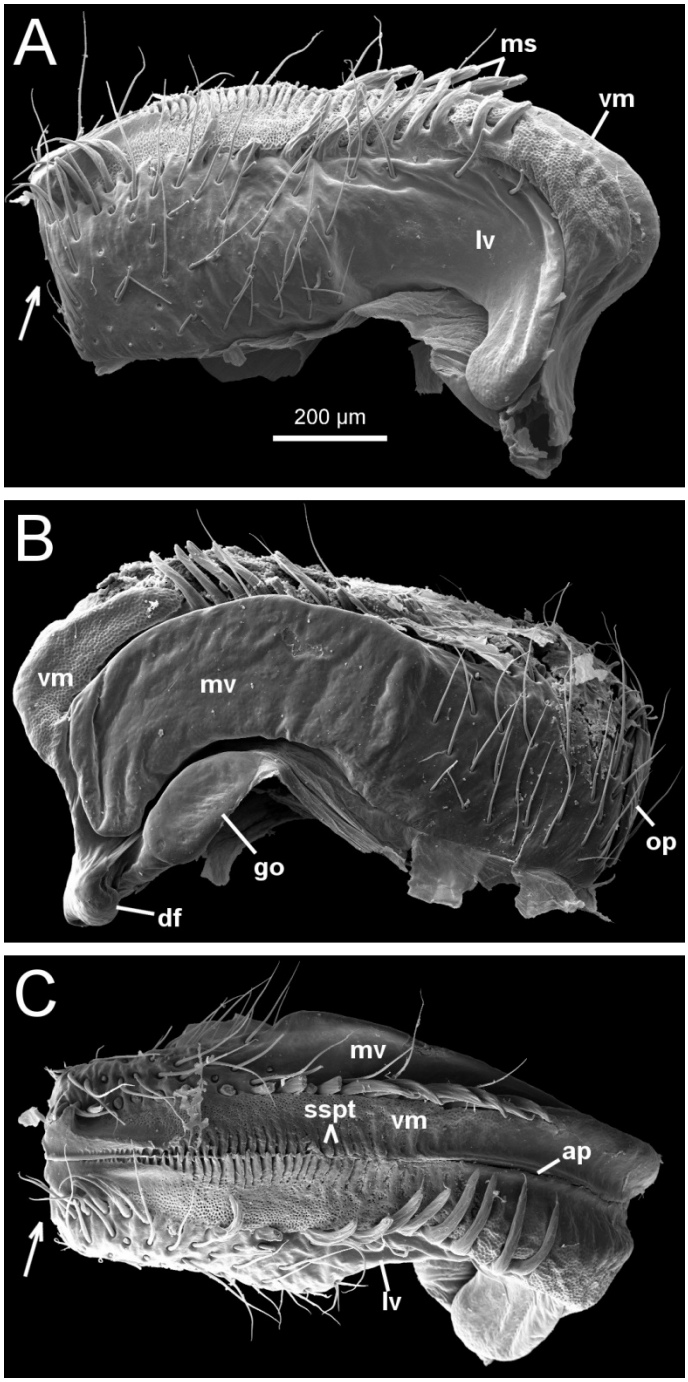


**Figure 8.** Bursa of *Pseudopolydesmus erasus* (FMNHINS 3120685), SEM. Images oriented to appear as if bursa is rotated 90° along a longitudinal axis between each image. (A) Left bursa, lateral view, operculum removed. Image flipped to appear as right bursa. (B) Right bursa, medial view. (C) Left bursa, ventral view, operculum removed. Image flipped to appear as right bursa. Arrows in A and C indicate where operculum was removed. Abbreviations: ap – vulval aperture; df – distal flange of medial valve; go

– gorget; lv – lateral valve; ms – modified setae; mv – medial valve; op – operculum; sspt – overlapping "scales" covering the spermatheca; vm – ventral membrane of bursa.

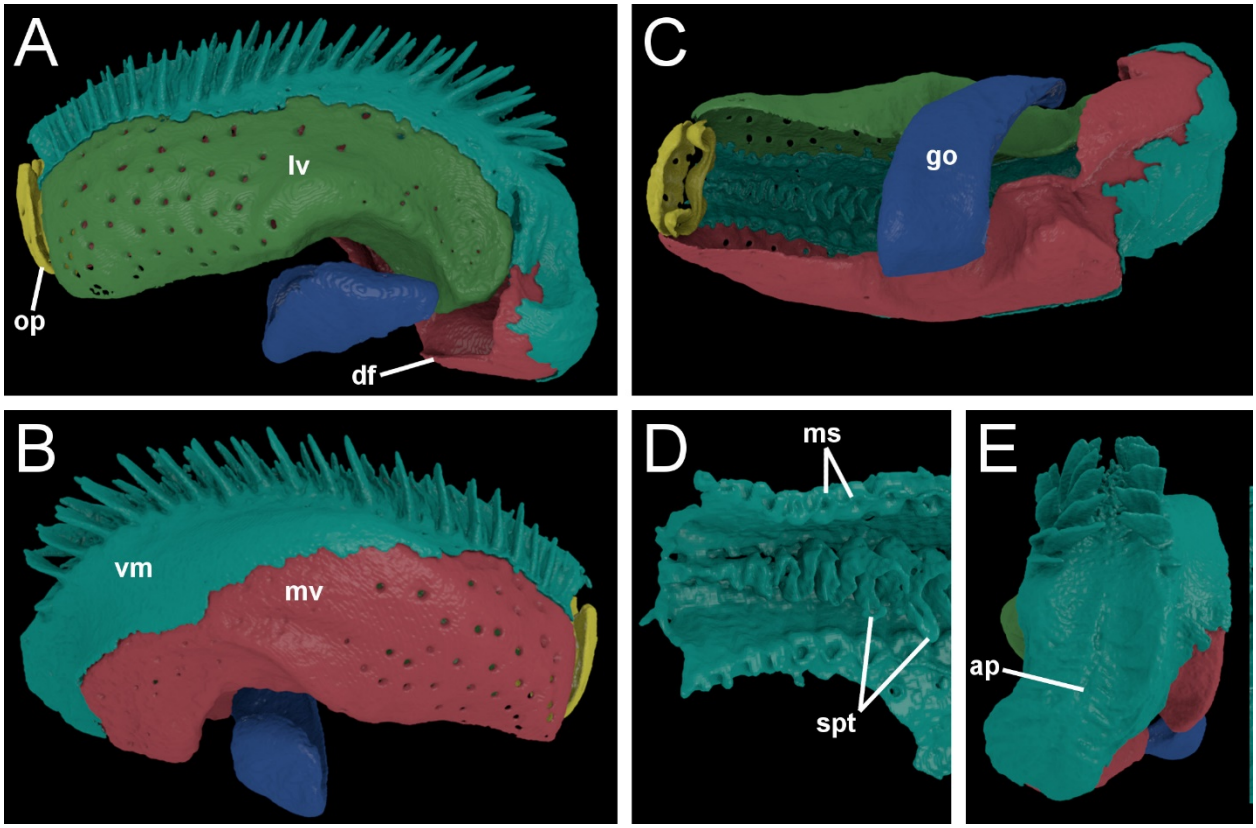


**Figure 9.** Vulval sclerites and ventral membrane of female *Pseudopolydesmus serratus* (FMNHINS 1513), right vulva. Segmented µCT image, 2.1 µm resolution. The ventral membrane partially covers the adjacent margins of the valves laterally and medially, gradually attenuating. Furthermore, it is dorsally continuous to membranes surrounding the oviducts and haemocoel conduit. Therefore, these three boundaries as displayed here are arbitrary. (A) Lateral view. (B) Medial view. (C) Dorsal view. (D) Enlarged view of dorsal (internal) surface of ventral membrane. "Sinuous canal" and apodematic projections of spermatheca are visible. (E) Posterior view of vulva. Vulval aperture visible. Abbreviations: ap – vulval aperture; df – distal flange of medial valve; go – gorget; lv – lateral valve; ms – insertion points of modified setae; mv – medial valve; op –operculum; spt – apodematic projections of spermatheca; vm – ventral membrane of bursa.

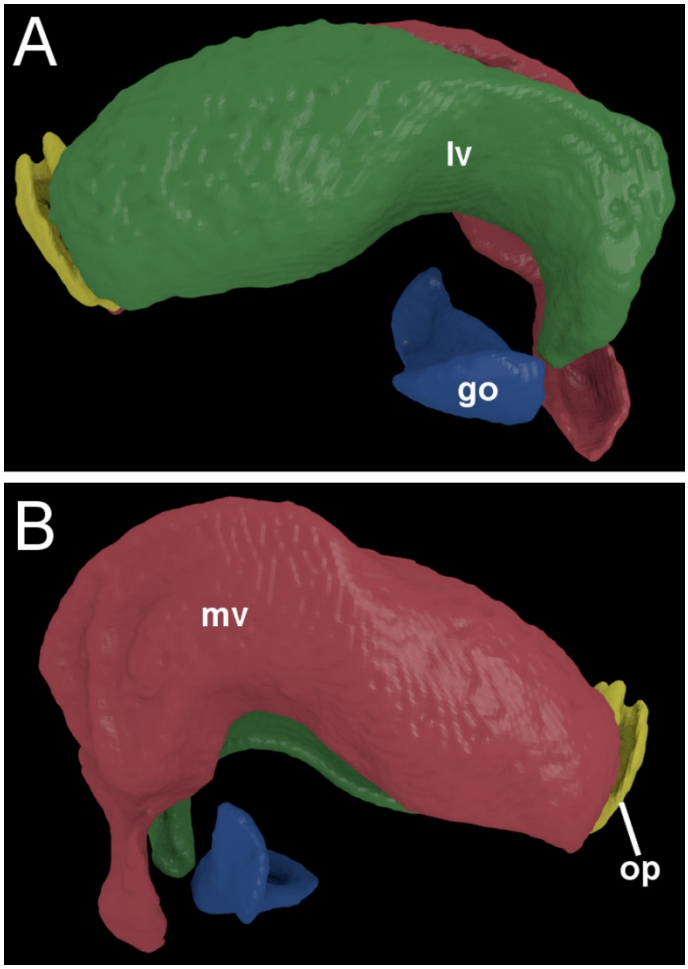


**Figure 10.** Vulval sclerites of female *Pseudopolydesmus pinetorum* (FMNHINS 1451), right vulva. Ventral membrane not shown. Segmented µCT image, 4.5 µm resolution. (A) Lateral view. (B) Medial view. Gaps for setae (numerous circular pores) are not shown because they were not distinguishable in the 4.5 µm resolution image used. Abbreviations as in Fig. 9.

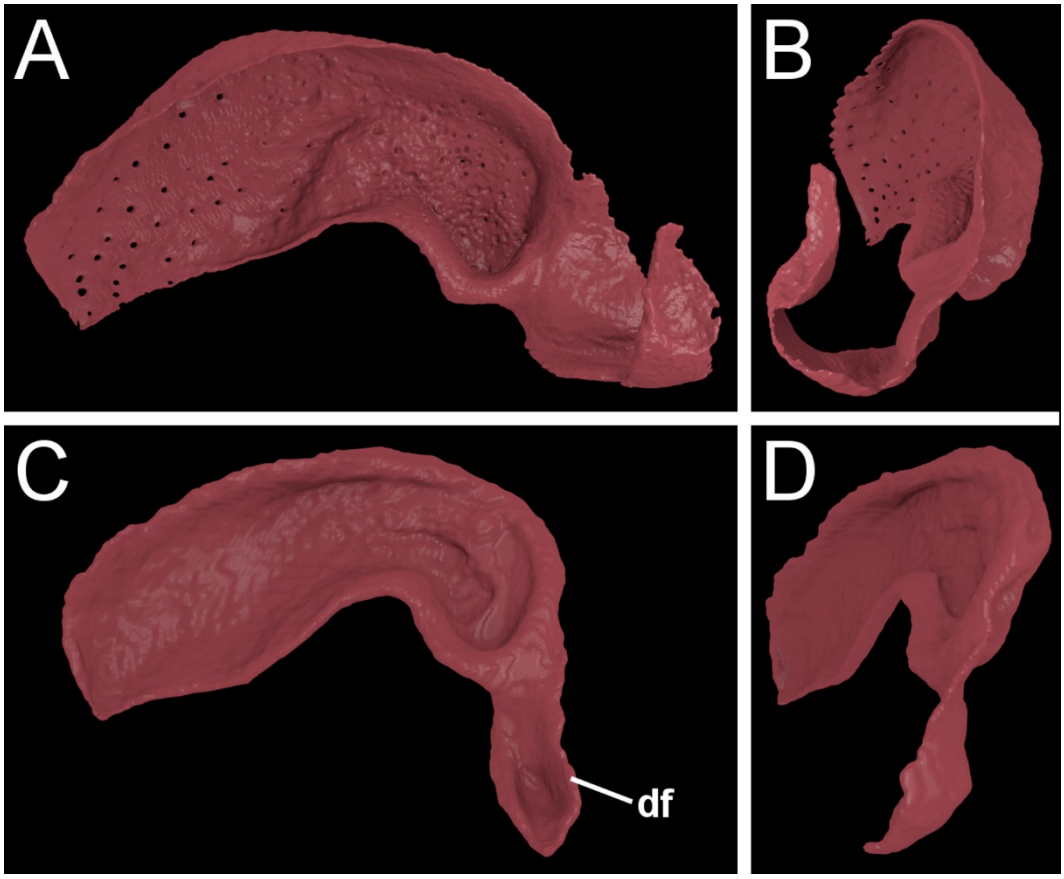


**Figure 11.** Comparison of medial valves in two *Pseudopolydesmus* species. (A) Medial valve of *Ps. serratus* (FMNHINS 1513), lateral view – i.e., view from inside the bursa. Segmented µCT image, 2.1 µm resolution. (B) Same as the immediately preceding, foreshortened posterior view showing shape of the long distal flange (df) that wraps dorsally around the bursa. (C) Medial valve of *Ps. pinetorum* (FMNHINS 1451), lateral view. Segmented µCT image, 4.5 µm resolution. (D) Same as the immediately preceding, foreshortened posterior view showing shape of the short but twisted distal flange. Gaps for setae (numerous circular pores) are not shown in Figs. 9C and 9D because they were not distinguishable in the 4.5 µm resolution image.

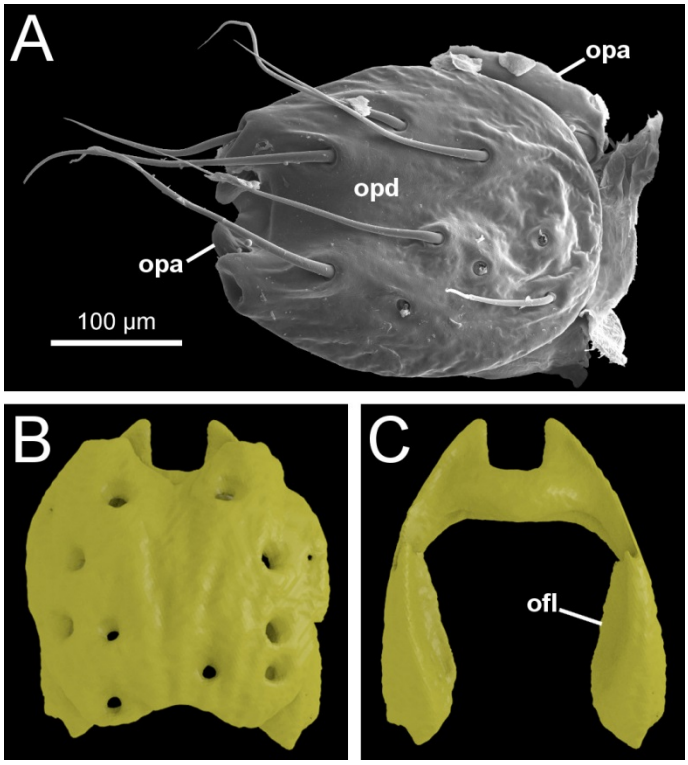


**Figure 12.** Opercula of *Pseudopolydesmus*. (A) Left operculum of *Ps. erasus* (FMNHINS 3120685, SEM). Arched sclerite (opa) partially visible basally and apically beneath discoid sclerite (opd). (B) Right operculum of *Ps. serratus* (FMNHINS 1513). Segmented µCT image, 2.1 µm resolution. (C) Same as above, with discoid sclerite removed via virtual dissection so that the arched sclerite is fully visible. Apodematic flanges are visible (ofl).

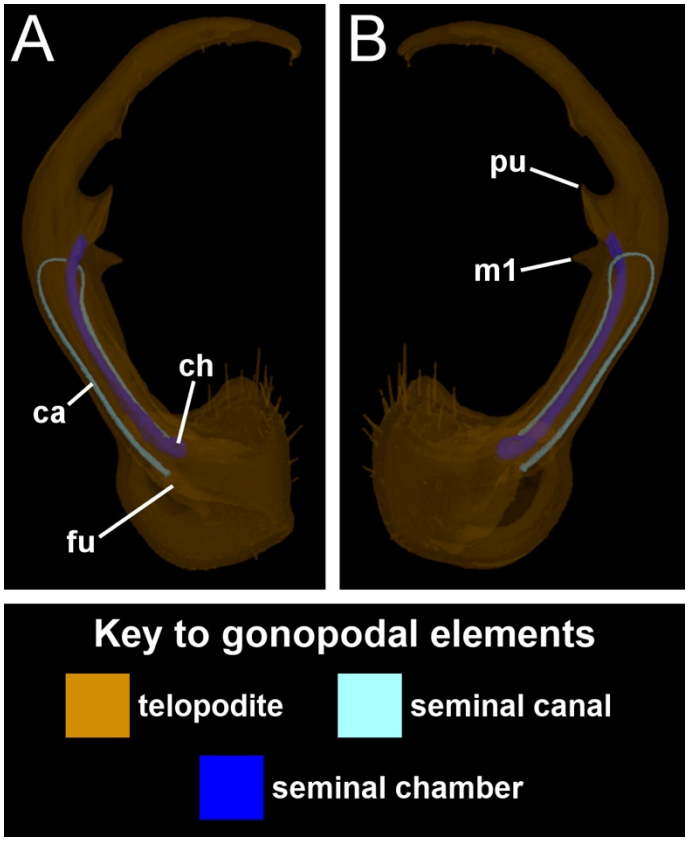


**Figure 13.** Right gonopod of *Pseudopolydesmus serratus* (FMNHINS 1513). Telopodite translucent to show internal morphology, with lumen of seminal canal and seminal chamber colored cyan and blue, respectively. Segmented µCT image, 2.1 µm resolution. *Cf.* Sierwald *et al.*, 2019: fig. 33. (A) Medial view. (B) Lateral View. Abbreviations: ca – seminal canal; ch – seminal chamber; fu – medial furrow of telopodite; m1 – medial process 1 (*cf.* Sierwald *et al.*, 2019); pu – pulvillus.

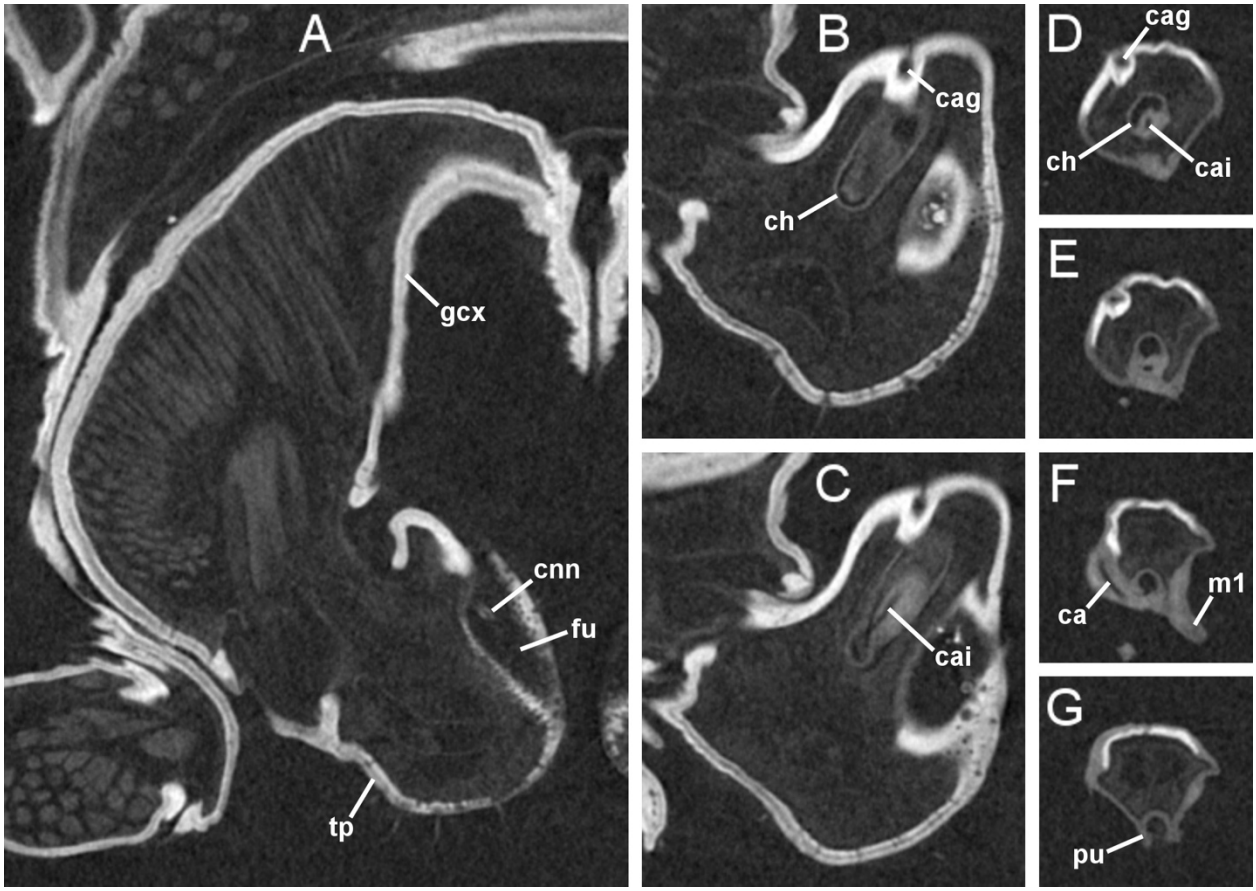


**Figure 14.** Cross-sections of right gonopod telopodite of *Pseudopolydesmus serratus* from µCT image (FMNHINS 1513, 2.1 µm resolution, axial slices) from proximal to distal showing salient features of the seminal duct. Slices listed in coronal plane. (A) Medial furrow at telopodite base with tip of cannula inserted (slice #590). (B) Proximal limit of seminal chamber in telopodite; the seminal chamber is partially fused to the cuticle of the seminal canal's superficial groove (slice #545). (C) Seminal chamber and proximal extremity of seminal canal's invaginated section (slice #537). (D) Seminal chamber (crescent-shaped lumen) and invaginated section of seminal canal (circular lumen) showing antiparallel configuration; not yet fused to telopodite outer cuticle (slice #459). (E) Seminal chamber and invaginated section of seminal canal; now fused to telopodite outer cuticle (slice #425). (F) Apogee of the seminal canal loop (slice #404). (G) External pore of seminal chamber at base of pulvillus (slice #380). Abbreviations: ca – apogee of seminal canal where superficial and invaginated sections join; cag, cai – superficial groove and invaginated section of seminal canal, respectively; ch – seminal chamber; cnn – tip

of cannula; fu – medial furrow of telopodite; gcx – gonopod coxa; m1 – medial process 1 (*cf.* Sierwald *et al.*, 2019); pu – pulvillus; tp – gonopod telopodite.

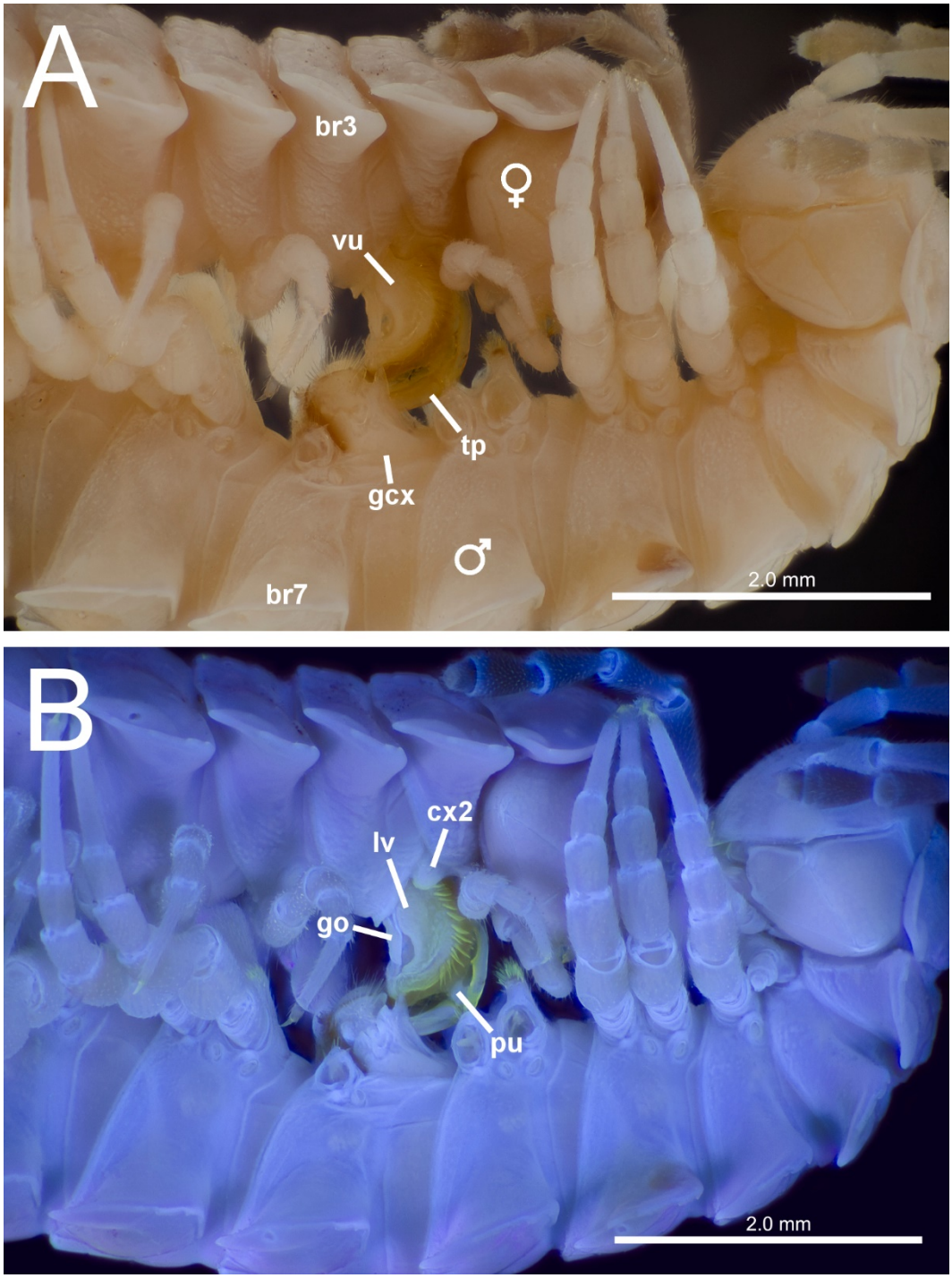


**Figure 15.** *Pseudopolydesmus serratus* mating pair preserved *in copula* (FMNHINS 7344). Female above, male below. Leg pairs 6, 7, and 9 removed from the male. (A) Light microscope image. (B) UV-enhanced microscope image. Abbreviations: br3 – body ring 3 of female; br7 – body ring 7 of male; cx2 –

coxal plate (female leg pair 2); gcx – gonopod coxa; go – vulva gorget; lv – vulva lateral valve; pu – pulvillus of telopodite; tp – gonopod telopodite; vu – vulva.

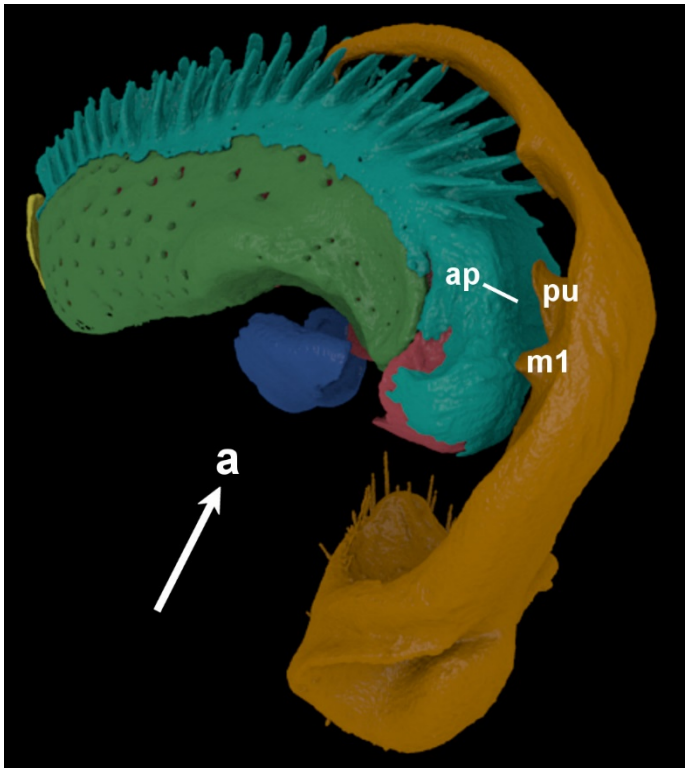


**Figure 16.** Vulva and complementary gonopod telopodite of *Pseudopolydesmus serratus*, showing copulatory interface (FMNHINS 1513, male and female). Note the position of the pulvillus and *m1* process of the telopodite. Arrow depicts approximate anterior body axis of copulating pair. Abbreviations: ap – vulval aperture; m1 – medial process 1 of gonopod; pu – gonopod pulvillus.

**Video 1.** Video version of Figure 3A, C, D. Virtually dissected sclerites of body ring 3 in female *Pseudopolydesmus serratus* (FMNHINS 1513). At the start of the video, the vulvae are withdrawn within body ring 3. The coxal plate is extended ~90° antero-dorsally, after which the vulvae are partially everted for copulation. The vulvae are fully everted after a brief pause, with the opercula becoming exposed for oviposition. Finally, the coxal plate is flexed to nearly its closed position, but remains partially extended to accommodate passage of eggs through the extended oviducts.

**Video 2.** Video version of Figure 16. Vulva and complementary gonopod telopodite of *Pseudopolydesmus serratus*, showing copulatory interface (FMNHINS 1513, male and female). Vulva and telopodite begin separate, then the telopodite moves toward the vulva until it is in its complementary position for copulation. Note the position of the pulvillus and *m1* process of the telopodite.

**Skeletomuscular atlas and deep homology of a metamorphosing genitalic appendage in a flat-backed millipede (Polydesmida: Polydesmidae: *Pseudopolydesmus*)**

This chapter was originally published in July 2022, in volume 6 of the journal Insect Systematics and Diversity.

**Authors**

Xavier J. Zahnle, Megan Ma, Jason E. Bond

**Abstract**

In millipedes, gonopods are male copulatory genitalia derived from walking legs that metamorphose during postembryonic development. The morphology of gonopods is critical for genus and species diagnosis in most taxa. However, the form and function of gonopods vary drastically at the family and ordinal level, making intricate morphological comparison practically impossible. Internal morphology could provide the basis for homologizing morphological elements present in the walking legs and gonopods. Therefore, we used x-ray computed tomography to produce 3D segmentations of *Pseudopolydesmus* Attems, 1898 millipedes incorporating two types of morphological elements: skeletal elements and muscles. In addition to imaging the trunk and appendages of an adult male, we imaged the developing gonopod across a series of juvenile male stadia in order to trace the identities of morphological elements. Skeletal elements were homologized, but muscle homologies were limited by the dissimilarity of muscle attachment sites between the walking leg and gonopod. Furthermore, images of juvenile males showed that appendage musculature is totally obliterated once gonopod development begins in the fourth stadium. Due to these limitations, we believe it may be more tractable to homologize

gonopod musculature of various millipede taxa to each other than to that of the walking legs. Because distinct genetic developmental networks responsible for walking leg and gonopod patterning have been evolving separately since the common ancestor of gonopod-bearing millipedes (a case of paramorphy), skeletomusculature among gonopods of unrelated millipede taxa is expected to be more similar than that of the gonopod and walking leg within a given millipede lineage.

**Keywords**

Development, Life History; Morphology; Reproduction

**Introduction**

Millipedes (class Diplopoda) are a diverse group of arthropods, comprising some 13,000 named species (Sierwald *et al.*, 2022). Of these, the bulk of extant species belongs to the infraclass Helminthomorpha, the gonopod-bearing millipedes. In millipedes, gonopods are a unique type of paired appendage present only adult males that replace one or two pairs of walking legs near the anterior end of the body during postembryonic development. Helminthomorph species diagnosis is frequently based on features of the adult gonopods (Brewer & Bond, 2013). Gonopods are used for intromittent copulation, which requires seminal fluid to be externally transferred from the male's paired primary genital orifices (gonopores) to a reservoir or groove on the gonopod. Seminal fluid is then transmitted to the paired female genital orifices (vulvae) via copulatory interface (Haacker & Fuchs, 1970; Tadler, 1996a; Tanabe & Sota, 2008; Wojcieszek *et al.*, 2012; Zahnle *et al.*, 2020).

Although the gonopod's overall homology to the walking leg is well established, the homologies of its constituent morphological elements (MEs) are not. Primary MEs of interest are the muscles and the sclerotized skeletal elements. The developmental continuity from walking leg pair to adult gonopod pair implies that at least some of these MEs are serial homologs between the two types of appendages. Consequently, putative homologies have been used to justify gonopod anatomy terms such as "coxa" (="gonocoxa"), "femorite", and "tibiotarsus" (see, *e.g.*, Keeton, 1960; Shear, 1972; Shelley, 1993). In practice, the highly derived condition of the gonopod MEs in many taxa makes it very difficult to compare the elements in a gonopod to those of a walking leg, let alone comparisons across different orders (Demange, 1967; Brewer *et al.*, 2012).

The challenging problem of gonopod ME homology has been approached by several past researchers. Petit (1973; 1976) convincingly demonstrated that in the family Polydesmidae, the

two articulating gonopod segments are derived from the appendicular coxa and prefemur, with the more distal podomeres being unnecessary for gonopod formation. However, this work was limited to externally visible anatomy. More recently, Drago *et al.* (2011) contributed to the understanding of sub-cuticular gonopod development by studying the gonopod's transition between the sub-adult and adult stadia. The adult gonopod takes its shape during this transition by inflating inside the dome or balloon-shaped sub-adult cuticle. Furthermore, there have been multiple works examining gonopod musculature across various helminthomorph taxa (West, 1953; Demange, 1967; Wilson, 2002; Drago *et al.,* 2011). Although Silvestri (1903) and Manton (1954; 1958; 1961) substantially contributed to the understanding of appendicular musculature, neither author examined the gonopods in substantive detail. Demange (1967) was the first to present a survey of gonopod musculature across the helminthomorphs, but did not attempt to homologize the muscles and sclerites as he did with the walking legs.

The helminthomorph order Polydesmida (flat-backed millipedes) is an ideal candidate for investigating the skeletomusculature of the gonopod. The gonopod anatomy in this order is relatively simple, with only one pair of walking legs at the eighth leg pair position (LP8) modified into gonopods (Fig. 1A). The gonopod comprises the basal coxa with two distal branches articulating from it (Fig. 1B). The telopodite is larger, carries the seminal canal, and interfaces with the female vulva during copulation. The cannula is apparently involved in charging the telopodite with seminal fluid (Zahnle *et al.*, 2020). In immature male stadia, the developing gonopod primordia are readily recognizable as a pair of externally visible domes at LP8 (Petit, 1973). Another advantage offered by polydesmidans is that their postembryonic development is teloanamorphic (Enghoff *et al.*, 1993) and each sequential stadium has a defined number of body rings (Youngsteadt, 2009; Drago *et al.*, 2011), meaning it is possible to unambiguously identify the stadium of any individual specimen.

Here we partially homologize the walking leg skeletomusculature in the flat-backed millipede genus *Pseudopolydesmus* Attems, 1898 (Polydesmida: Polydesmidae) to that of its gonopods. We used

µCT x-ray imaging of an adult male *Pseudpolydesmus serratus* (Say, 1821) to study and illustrate the trunk and appendage skeletomusculature in both the gonopod-bearing body ring and an adjacent, gonopod-lacking ring. Two types of morphological elements (ME) were considered: skeletal elements and muscles. We hypothesized that it would be possible to homologize skeletal elements between the walking leg and gonopod using their common positions relative to other skeletal elements and any unique landmarks that were available. For muscles, points of origin and insertion onto the skeletal elements were used for homology inference.

To acquire additional evidence, we imaged an ontogenetic series of *Pseudopolydesmus* juveniles of progressive stadia to visualize the postembryonic development of LP8 from walking legs, to gonopod primordia, and finally to fully developed adult gonopods. This approach takes advantage of the developmental continuity of LP8 while its morphology transitions from walking legs to gonopods. We hypothesized that skeletal elements and muscles present in the walking leg can be traced through postembryonic development to determine the corresponding homologous element in the gonopod. This is the first instance of non-destructive 3D scanning being used to visualize the developing gonopod in a millipede. A limitation of this approach is that it relies on persistence of MEs throughout postembryonic development.

## Material and Methods

### *Specimen acquisition and identification*

We obtained ethanol preserved *Pseudopolydesmus* specimens from both the Field Museum of Natural History Insects Collection (FMNHINS) and the Auburn University Museum of Natural History (AUMS). Specimens are listed in Table 1. To differentiate between stadia, we counted the number of rings and leg pairs (Youngsteadt, 2009: table 1). Stadia I and II lack appendages in the LP8 position, with walking legs appearing at LP8 in stadium III. Gonopod development begins in stadium IV and proceeds to completion in stadium VIII (adult stadium). We specifically chose to scan stadium III as the only male

stadium with walking legs in the LP8 position. Because males and females appear identical in stadia I-III, we were unable to determine the sex of the imaged stadium III juvenile. We chose to refer to the juveniles by stadia rather than instars because none of the specimens appeared to be undergoing apolysis (Klowden, 2013: 95).

Although juveniles could not be definitively identified to the species level, we are confident that (1) the structural organization of the appendages and (2) the developmental sequence of the male gonopods does not vary between species of *Pseudopolydesmus*. We feel the first assumption is justified because the more distantly related polydesmid genus *Scytonotus* Koch, 1847 shares MEs with identical relationships to those in adult *Ps. serratus* despite being very distinct in its somatic morphology (West, 1953; see below). To justify our second assumption, polydesmidans as distantly related as *Polydesmus angustus* Latzel, 1884 and *Oxidus gracilis* (Koch, 1847) show the same pattern in the developmental sequence of stadia and the status of gonopod development as *Pseudopolydesmus* do (Petit, 1973; Drago *et al.*, 2011). Based on the localities where the specimens were collected, the possible species represented in our μCT imaged specimens are likely restricted to *Ps. serratus, Ps. canadensis* (Newport, 1844), and *Ps. erasus* (Loomis, 1943).

*μCT imaging and segmentation*

We followed established methods (Zahnle *et al.*, 2020) for three-dimensiona μCT imaging and image segmentation. In brief, we used an XRadia MicroXCT-200 at the Center for Molecular and Genomic Imaging at the University of California, Davis to acquire 3D images. Specimens were stained with 1% $I_2$ in a 99% ethanol solution for 48 hours, then imaged in a medium of 95% ethanol. 3D images were centered at the gonopodal region.

Our segmentations are derived from six 3D images (available from Dryad). We first segmented trunk musculature from the sixth and seventh body rings in a lower resolution (4x lens) 3D image of an adult male *Ps. serratus* (FMNHINS 1513), as well as the body rings themselves. This established whether trunk musculature was modified in the gonopod-bearing body ring and helped us isolate the appendicular

muscles from the trunk muscles during subsequent segmentations. We subsequently segmented muscles and skeletal elements in the gonopods and in the sixth walking leg pair (LP6) of this individual. For juveniles, we acquired a series of five images spanning stadia III through VII at a higher resolution (10x lens). In stadia IV-VII we segmented the developing gonopod primordium along with the surrounding sternite of the seventh body ring (BR7). In stadium VII, we additionally segmented any distinguishable internal morphological features related to gonopod development.

Segmentation of the images was carried out to isolate MEs for 3D visualization. Therefore, segmentation is a necessary part of data collection in order to accurately delimit the physical structures as represented by an array of 3D cubes (voxels). Simultaneously, it was a critical part of our analysis process as we sought to identify biologically meaningful MEs. Segmentation was carried out using ITK-SNAP (Yushkevich *et al.*, 2006) following the semi-automated process described by Zahnle *et al.* (2020). Final figures were rendered within the ITK-SNAP 3D view.

Segmentation was carried out on three main types of tissue: (1) sclerotized cuticle, (2) muscles, and (3) developing tissue which is not yet fully differentiated. Segmented objects in the adult stadium are considered MEs, whereas segmented objects in the juvenile stadia were selected for convenient 3D visualization without attempting to capture MEs. Using ITK-SNAP's semi-automated segmentation tool, upper and lower voxel intensity thresholds can be assigned to prevent the "bleeding" of the in-process segmentation beyond the boundaries of the object intended for segmentation. Segmentation of muscle and cuticle was straightforward, requiring upper and lower thresholds in the former case, and only a lower threshold in the latter case. Developing undifferentiated tissue was also segmented using upper and lower thresholds, but required substantial manual segmentation. Table 1 lists the relevant thresholds used to segment the various ME.

*Definitions of morphological elements (ME)*

The two types of MEs segmented were the skeletal elements and muscles. MEs can be either adjoining or disjointed from each other on the macroscopic level, and either intrinsically or extrinsically identifiable from each other on the histological and/or cellular levels (Young, 1993).

Using this framework, each sclerite was intrinsically differentiated from other types of MEs by being composed of hardened cuticle and macroscopically differentiated from each other sclerite due to being disjoint (connected only with non-hardened cuticular membrane). Due to the fusion and splitting of sclerites through gonopod ontogeny, it was necessary to define skeletal elements as distinct from sclerites. In any given stadium, two or more skeletal elements may be fused together into a single sclerite or a skeletal element may comprise a single sclerite. Skeletal elements can be differentiated because each is macroscopically disjoint from adjoining skeletal elements at some stadium during ontogeny, even if there is not one single stadium in which it is an independent sclerite. In our segmentations, this was exemplified by the tracheal apodeme, a skeletal element which is fused to the body ring in stadia III but is instead fused to the coxa in stadium VIII. The tracheal apodeme is therefore disjoint from the coxa early in juvenile development and disjoint from the body ring in adulthood.

Each muscle was intrinsically differentiated from other types of MEs by being composed of parallel and/or converging muscle fibers and macroscopically differentiated as disjoint from each other muscle. Furthermore, it is useful for functional and comparative anatomy to classify muscles based on their sites of attachment to sclerites. An attachment site on a sclerite that remains stationary during muscle contraction is defined as an **origin**, whereas the attachment site on the movable sclerite is defined as the **insertion** (Kent, 1983: 273). For the purposes of this paper, a muscle is defined as all the muscle fibers that share a single insertion site. Under this definition it is possible for fibers that converge onto a single insertion from multiple origins to collectively comprise a single muscle. In the text below, origin and insertion sites are indicated using the abbreviations **(O)** and **(I)**, respectively.

Finally, the developing tissue in the subadult male is disjoint and intrinsically differentiated from each other ME.

**Results and Comparative Discussion**

Our results are organized into five sections. (1) Trunk muscles in the sixth and seventh body rings of an adult male are presented and described. (2) The muscles and skeletal elements of a walking leg pair (LP6) from the same individual are presented and described. (3) A brief discussion of walking leg skeletomuscular asymmetry is presented. (4) The muscles and skeletal elements of the gonopod pair from the same individual are presented and described. (5) The developing gonopod primordia from a series of juveniles (stadia IV-VII) are presented and described.

*Trunk musculature*

There were seven pairs of trunk muscles distinguishable in the adult male *P. serratus* specimen (Fig. 2). Polydesmidan trunk muscles have already been well characterized (Silvestri, 1903; Seifert, 1932; West, 1953; Manton, 1961), so we restrict the current treatment to comparisons with the existing literature. We use Manton's (1961) naming scheme, and correspondence between published muscle names is shown in Table 2. Demange (1967) also recognized the *levator apophysis posticae* as the *"muscle trachéo-dorsal postérieur"* which we have not included in Table 2.

We were unable to distinguish two of the ventral longitudinal muscles. These were labelled by West (1953) as the *retractor membranosus* and *intersegmentalis* (*"retractor ventralis"* of Manton, 1961). We believe that the $I_2$ stain was inadequate to show these threadlike muscles in the 3D image. The only other discrepancy with published data was the lack of distinct *flexor internus dorsalis* and *flexor externus dorsalis* muscles. Our segmentation shows only a single *"flexor dorsalis"* muscle that lies dorsal and lateral to the *retractor dorsalis*. This corresponds to the spatial positions of both the *flexor internus dorsalis* and *flexor externus dorsalis* combined. West's illustrations (1953: figs. 22-24) show the posterior arthrodial membrane stretched to its fullest extent along with both muscles, whereas our digital dissection

shows the muscle(s) contracted. Considering the presence of two distinct muscles in both *Po. angustus* and *Scytonotus virginicus* (Loomis, 1943) it seems likely that separate muscles are present but compactly contracted (West, 1953; Manton, 1961).

*Walking leg musculature*

All muscles that insert onto the coxa or prefemur of walking leg pair six (LP6, the anterior leg pair of BR6) are presented (Fig. 3, Table 3). Muscles inserting onto more distal podomeres were omitted because podomeres distal from the prefemur have no role in gonopod development (Petit, 1973; 1976). The coxae, prefemora, and tracheal apodemes associated with LP6 are also presented. Of the seven muscles segmented, four insert onto the coxa and three insert onto the prefemur. Six are extrinsic to the walking leg (originating at a site on the body ring or tracheal apodeme, rather than inside the leg), with only the *depressor brevis prefemoris* originating inside the coxa. One additional muscle, the *fenestralis,* was illustrated by West (1953) but cannot be distinguished in our 3D image.

Coxal and prefemoral muscles are functionally divided into four categories. Contraction of the **(1)** *promotores coxarum* rotates the coxa to the anterior, whereas contraction of the **(2)** *remotores coxarum* rotates the coxa to the posterior. In addition, contraction of the **(3)** *depressores prefemorum* rotates the prefemur ventrally and the **(4)** *levator prefemoris* rotates the prefemur dorsally. In this paper we follow Manton's (1954; originally derived from Silvestri, 1903) nomenclature for the prefemoral muscles and adapt West's (1953) names for the coxal muscles. We believe this combination of nomenclature best represents the prevailing antagonistic motions contributed by each set of muscles. Even so, we agree with Demange (1967) that the best criteria for identifying muscle homology are consistent points of origin and insertion, not muscle function.

**(1)** ***Promotores coxarum:*** Two muscles that are responsible for rotating the distal end of the coxa, and therefore the entire leg, anteriorly. The *promotor longus coxae* (Fig. 3B: ProLCx) is the anteriormost muscle of the walking leg pair. It is a nearly cylindrical muscle with densely-packed fibers originating from the anterior ventral portion of the trachea **(O)**. These paired muscles cross over each

other as they proceed ventrally across the body, inserting onto the anterior dorsal portion of the opposite coxa **(I)**. The actual sclerite insertion is at the end of a long tendon that is not visible in our illustrations (*cf.* West, 1953: figs. 25, 28-31). The *promotor brevis coxae* (Fig. 3C: ProBCx) consists of a flat block of muscle that originates along the lateral arc of the tracheal pouch **(O)** and inserts ventrolaterally into the anterior dorsal portion of the coxa **(I)**. This muscle sits posterior and ventral to the *promotor longus coxae*, and anterior to the *remotor brevis coxae*.

**(2) *Remotores coxarum:*** Two muscles that rotate the distal end the coxa (and the entire leg with it) posteriorly. The *remotor brevis coxae* (Fig. 3F: RemBCx) is a fan-shaped muscle with loosely-packed fibers extending ventrolaterally from the arc of the tracheal apodeme **(O)** that insert onto the posterior dorsal portion of coxa **(I)**. It is posterior to the *promotor brevis coxae* and anterior to the *remotor longus coxae*. The *remotor longus coxae* (Fig. 3E: RemLCx) is a massive, uniformly dense block of muscle fibers whose origin envelops the posterior base of the tracheal apodeme **(O)**. Like the *promotor longus coxae*, the muscles of the *remotor longus coxae* cross over the body's midline to insert onto the opposite coxae. The insertion is at the dorsal posterior portion of the coxa **(I)**, at the end of a long and thick tendon that is not visible in our illustrations (*cf.* West, 1953: fig. 26). The muscle sits dorsal and posterior to the *remotor brevis coxae*.

**(3) *Depressores prefemorum:*** Two muscles that rotate the prefemur ventrally when contracted. The *depressor longus prefemoris* (Fig. 3E-F: DepLPf) is a subcylindrical muscle that originates at the distal tip of the tracheal apodeme **(O)** and proceeds ventrolaterally through the coxa to insert onto the ventral base of the prefemur **(I)**. This is an extrinsic muscle because it passes through the coxa. The *depressor brevis prefemoris* (Fig. 3B-C: DepBPf) is a dense fan-shaped muscle with fibers radiating from the anterior, medial, and basal rim of the coxa **(O)** into a concentrated point in the ventral rim of the prefemur **(I)**. It is superficially wrapped around the distal portions of the *depressor longus prefemoris* and the *levator prefemoris*. The *depressor brevis prefemoris* is intrinsic to the walking legs because it originates inside the coxa. West (1953: fig. 27) interpreted the *depressor brevis prefemoris* as two separate antagonistic muscles and divided it into anterior and posterior portions.

**(4) *Levator prefemoris:*** The *levator prefemoris* (Fig. 3B-C: LevPf) incorporates the slim, finger-like bundles of muscle fibers that originate variously on the inner surface of the sternite and near the distal tip of the tracheal apodeme **(O)**. These fibers converge laterally to a shared origin at the dorsal base of the prefemur **(I)**. Along with the *depressor longus prefemoris,* it is ventral and superficial to all the other extrinsic muscles described above. West (1953: figs. 25, 27) identified this as two separate muscles based on the distinct origin sites, whereas Manton (1954: fig. 3e) seems to have omitted the fibers originating on the sternite entirely. Seifert (1932: fig. 21) labels a separate levator muscle that inserts onto the dorsal portion of the trochanter in *Strongylosoma stigmatosum* (Eichwald, 1830) (=*Strongylosoma pallipes* of Seifert), but there is no separate trochanter in our specimen.

*Asymmetry in the walking legs*

Asymmetry in the walking legs manifests as both crossing-over of extrinsic leg muscles and as uneven tracheal apodeme length. There are two pairs of chiasmatic (crossed-over) walking leg muscles in *Pseudopolydesmus* and *Scytonotus: promotor longus coxae* and *remotor longus coxae* (Table 3; West, 1953). These are both large walking leg muscles responsible for rotating the leg forward and backward during locomotion, with the *remotor longus coxae* being the most massive walking leg muscle.

The tracheal apodemes are the primary origin site for extrinsic muscles inserting onto the coxae and prefemora in the walking legs. Both apodemes project posteroventrally into the body cavity (hemocoel) but as they converge medially one apodeme is truncated. The other apodeme continues posteriorly, broadening into a midsagittal flange occupying the medial centerline of the body axis. This midsagittal flange is the exclusive origin site for the *depressor longus prefemoris* and one of the origin sites for the *remotor brevis coxae* and *levator prefemoris* muscles (Fig. 3C,F). West (1953) clearly shows this same apodeme asymmetry in *Scytonotus* (figs. 25-26 and 28-31).

*Gonopod musculature*

In adult male Polydesmida, the gonopods are the anterior appendage pair of BR7 (LP8; refer to Fig. 1). This makes them directly comparable to the anterior walking leg pair of BR6 (LP6), discussed above. We present all gonopodial muscles as well as the gonopod sclerites: coxa, telopodite, and cannula (Fig. 4, Table 4). Like the walking leg muscles, the gonopodial muscles can be divided into two groups based on their origins. Muscles originating from within the gonopod coxal sclerite are considered intrinsic muscles. In contrast, muscles originating from the inner walls of the body ring or from the tracheal apodeme are considered extrinsic muscles. The only muscle without an origin is the gonopod abductor, which transversely spans the gonopod coxae, with symmetrical insertion sites on either coxa. In this section we follow West's (1953) names for the gonopodial muscles. Homologies between muscles of the walking legs and gonopods are treated in the Discussion section below.

**Intrinsic gonopod muscles:** These consist of three muscles originating from the coxal sclerite and inserting onto the more distal sclerites, along with a single unpaired muscle that transversely spans the two coxal sclerites. Telopodite (=prefemur) movement is controlled by two intrinsic muscles: the *flexor telopoditis* and the *extensor telopoditis,* which rotate the telopodite dorsally towards and ventrally away from the sternite of BR7, respectively (Fig. 4C-D: *DepBPf and *LevPf). The muscle fibers of the *flexor telopoditis* originate, fanlike, from the lateral and anterior internal surfaces of the coxa **(O)** and the muscle inserts onto the anterior base of the telopodite **(I)**. The *extensor telopoditis* instead originates from the lateral section of the gonopod's tracheal apodeme **(O)**, extending posteroventrally to insert at the posterior base of the telopodite **(I)**. As the *extensor telopoditis* passes through the coxa, it is surrounded laterally and anteriorly by the *flexor telopoditis*.

The final paired intrinsic gonopod muscle, the *adductor cornui* (Fig. 4C-D: AddCo) originates from the medial section of the gonopod's tracheal apodeme **(O)** before passing posteroventrally through the coxa to the base of the medial base of the cannula **(I)**. It is medial to the *extensor telopoditis,* and the two muscles run roughly parallel to each other. The *adductor cornui* is the only muscle motivating the cannula.

The *intercoxae* muscle (Fig. 4A-C: IntCx) spans the gonopod coxae transversely, with attachment sites at the two opposite dorsolateral corners of the coxae **(I/O)**. The *intercoxae* is somewhat dorsoventrally flattened. Contraction of this muscle rotates both coxae ventrolaterally, which alters the transverse distance between the two telopodites distal to the coxae.

**Extrinsic gonopod muscles:** The extrinsic gonopod muscles can be functionally divided into two categories. The *protractores coxarum* draw the coxae ventrally out of BR7, whereas the *retractores coxarum* retract the coxae dorsally into BR7.

There are two *protractores coxarum* to the anterior and posterior of the gonopod. The *protractor coxae anterior* (Fig. 4A-B: ProCxA) originates from the ventrolateral surface of the BR7 prozonite and the posterior wall of the BR7 prophragma **(O)**. It extends dorsally to insert near apex of gonopod tracheal apodeme, on its anteroventral surface **(I)**. The *protractor coxae posterior* (Fig. 4A-B: ProCxP) originates from the anterodorsal surface of the tracheal apodeme of leg pair nine **(O)**; leg pair nine is the posterior appendage pair of BR7. The *protractor coxae posterior* extends anterodorsally from its origin and inserts onto the posterior surface of the gonopod tracheal apodeme at its apex **(I)**.

The *retractores coxarum* comprise two closely associated blocks of muscle fibers (Fig. 4A-B: RCxSup and RCxInf). They can therefore be considered either a single muscle or subdivided into two separate muscles. We label both muscle blocks as separate muscles in this paper. Both muscles originate from the lateral wall of the BR7 prozonite **(O)** and proceed ventromedially, inserting along the dorsolateral rim of the coxa **(I)**. The *retractor coxae superior* is dorsal to the *retractor coxae inferior.* However, the muscle fibers of the *retractor coxae superior* insert posteriorly to the muscle fibers of the *retractor coxae inferior*. Additionally, the substantial gap between visibly segmented *retractor coxae superior* muscle tissue and the gonopod coxa suggests that a large tendon connects this muscle to its insertion point.

*Gonopod Developmental Morphology*

The morphology of LP8 is summarized at each stadium of juvenile development, beginning with stadium III (Fig. 5). This is the first and final stadium in which walking legs are present in the LP8 position (Youngsteadt, 2009). In the immediately following stadium IV, this pair of walking legs is replaced by a pair of dome-shaped gonopod primordia, which persist until localized metamorphosis is completed in stadium VIII (Petit, 1973; Youngsteadt, 2009; Drago *et al.*, 2011).

**Stadium III:** Typical walking leg pair. Skeletomusculature of LP8 is essentially identical to that shown in leg pair six of the adult millipede.

**Stadium IV:** On the ventral surface of BR7, LP8 has been superficially replaced with a pair of dome-shaped structures (Fig. 5A). These domes and the unorganized tissue underneath comprise the developing gonopod primordium. Distinguishable appendicular muscles have been totally obliterated. The cuticle of the primordium is sub-cylindrical and extends ventrolaterally. Its posterior surface is closely appressed to the ventral surface of BR7. Any extrinsic demarcation between the sternite, coxa, and prefemur has been obliterated. Therefore, we consider the sternite of BR7 to be fused with the coxa and prefemur of LP8. In addition to the loss of the walking legs, the anterior stigma pair of the BR7 (associated with LP8) has disappeared, with slight external concavities where the stigmata would normally be. The internal tracheal apodeme is retained (Fig. 5B). Based on cross-sections of the 3D image, we determined that the tracheal apodeme is hollow with no muscles attached. The apodeme has shortened, projecting less far into the hemocoel. Gas exchange cannot occur because the stigmata are sealed. We were not able to identify any discrete muscles or muscle fibers, but there was an amorphous mass of tissue deep to the cuticle.

**Stadium V:** The external dome of the gonopod primordium is smaller in size relative to BR7 compared to the previous stadium, despite the fact that it is larger in absolute size due to the overall growth of the millipede between stadia (Fig. 5C). The apodeme, which projected posteromedially into the hemocoel in the previous two stadia, is now reoriented anterolaterally, though it remains fused with the rest of the gonopod primordium (Fig. 5D). There are no distinguishable appendicular muscles.

**Stadium VI:** The external cuticle of the two gonopod primordia appears more compact, with the two domes now in medial contact with each other (Fig. 5E). Internally, the tracheal apodeme is enlarged (Fig. 5F). There are no distinguishable appendicular muscles.

**Stadium VII:** Cuticle of the gonopod primordia similar to stadium VI. Tissue of future stadium VIII gonopod cuticle is nascent (Fig. 6). Surprisingly, this nascent gonopod tissue is spatially continuous with the soft tissue comprising the developing genital tract. This is an unexpected finding, given the adult gonopods are not connected to the genital tract, nor are the walking legs of BR7 connected to the genital tract at any point during development. The tissue of the nascent genital tract is identifiable due to its paramedian position on either side of the ventral nerve cord, and by its absence in stadium VI. The roughly tubular paramedian folds of the nascent genital tract form an identifiable lumen that passes longitudinally through BR7 and the adjacent body rings. These tubes approximate the genital tract and occupy the same space in the hemocoel that the genital tract does in the adult (Fig. 6E,F).

In the region dorsal to the gonopod primordium, a branch of these tubular folds continuously merges ventrally with tissue of the nascent gonopod telopodite. This branch proceeds medially to the integumentary wall of the stadium VII gonopod primordium. This relatively amorphous folded tissue constricts medially and connects contiguously with a well-defined dome-shaped tissue. Together, this well-defined dome and amorphous involuted tube seem to comprise the stadium VIII gonopod telopodite.

Dorsal to the dome-shaped basal section of the telopodite lies the future stadium VIII coxa. Its shape closely resembles that of the mature gonopod coxa, incorporating the fused tracheal apodeme and showing the distinctive ventrolateral plates present in the adult (Fig. 6D; *cf.* Sierwald *et al.*, 2019: fig. 33A). The cannula is not yet formed, and is only represented by a small subconical protrusion from the anteromedial edge of the future gonopod coxa. There are no distinguishable appendicular muscles.

**General Discussion**

Although it is certain that the walking leg is the ontogenetic precursor to the gonopod, it is challenging to establish homologies between skeletomuscular MEs of the two appendage types. In the case of muscles, it is practically impossible. This is due to the fusing together of skeletal elements and obliteration of muscles that occurs at the beginning of gonopod development. Because this localized metamorphosis can be traced back to the common ancestor of gonopod-bearing millipedes, we argue that appendage evolution will be satisfactorily explained only by comparative anatomy across the entire diplopod Tree of Life. These results provide a novel context for future multi-ordinal level comparative studies across diplopods and potential insight into the underlying genomics of limb and genitalic development. In addition, we offer brief commentary on two topics related to appendage evolution and ontology: skeletomuscular asymmetry in polydesmidans and our novel discovery of an apparent ontogenetic link between the gonopod and genital tract.

*Appendage Skeletal Element Homology Hypotheses*

We were able to corroborate the existing homology hypotheses of the skeletal elements in gonopods of Polydesmidae. There are three separately articulated sclerites in the gonopod of *Pseudopolydesmus* (Fig. 7). Based on existing knowledge of integumentary development (Petit, 1973; 1976), we *a priori* considered the coxa and telopodite of the gonopod to be homologs of the coxa and prefemur of the walking legs, respectively. The third and final articulated sclerite, the cannula, forms a second branch from the coxa and has no apparent homolog in the unbranched walking leg. This suggests that it either evolved as a duplication of the limb axis distal to the coxa (duplicated prefemur) or *de novo* from co-option of other limb-patterning processes.

The coxal sclerite of the gonopod incorporates a large flange along its anterior margin that projects dorsally into the body cavity (hemocoel). Therefore, the approximately frontal plane of the arthrodial membrane that spans BR7 and the gonopod coxae is transversely intersected by the coxal sclerite. This flange or lamella is a common feature of eugnathan gonopods (Demange, 1967) and has long been hypothesized to be serially homologous to the tracheal apodeme of the walking legs (Voges,

1878; Brölemann, 1914). The line along which the sclerite and arthrodial membrane intersect forms a convenient intrinsic demarcation between the coxal skeletal element that projects distally from the body axis and the tracheal apodematic skeletal element that projects deep to the integument.

Investigation of the internal morphology of the tracheal apodeme through postembryonic development has yielded valuable evidence supporting the hypothesis that the tracheal apodeme in the walking legs is homologous with the gonopod coxal sclerite's internal flange. This skeletal element's developmental continuity is clearly traced in stadia III-VIII (Figs. 5, 7), as the tracheal apodeme fuses with the gonopod primordium, reorients itself laterally (in the walking legs it projects medially), and finally separates from the other sclerites as an integrated part of the coxal sclerite. Additional support for this interpretation comes from the fact that the residual tracheal apodeme remains hollow in the stadium IV male.

*Appendage Muscle Homology Hypotheses*

Direct comparison of adult walking legs and gonopods yielded limited results due to the extremely derived condition of the gonopods. Ultimately, it was possible to propose compelling serial homology hypotheses for only two of the gonopod muscles. These muscles are the *levator prefemoris* and *depressor brevis prefemoris* (labelled *LevPr and *DepBPr, respectively, to indicate their hypothesized homologous identities). In both appendage types, the *levator prefemoris* (=*extensor telopoditis*) is a subcylindrical muscle that originates from the tracheal apodeme, passes through the coxa, and inserts onto the prefemur. In the walking leg, the *levator prefemoris* is surrounded on its anterior, medial, and posterior sides by the *depressor brevis prefemoris* (Fig. 3B-C), whereas in the gonopod it is surrounded on its anterior and lateral sides. However, this discrepancy is explained by the reorientation of the coxa from its approximately lateral orientation in the walking leg to its ventral orientation in the gonopod.

The final intrinsic gonopod muscle, the *adductor cornui* (Fig. 4C-D: AddCo), might be homologous to the *depressor longus prefemoris* (Fig. 3E-F: DepLPr). This hypothesis requires a *de novo* origin of the cannula followed by migration of the muscle's insertion point to the base of the cannula.

This is supported by the muscle's origin on the tracheal apodeme and the fact that it passes through the coxa to insert onto a more distal sclerite. However, the uncertain homology of the cannula may invalidate this hypothesis.

Compelling homology hypotheses could not be proposed for the remaining gonopod muscles. Most of these are extrinsic muscles that originate from various sites across BR7 and the tracheal apodeme of leg pair nine before inserting onto the gonopod's coxa and tracheal apodeme. These muscles' coxal attachment sites may have migrated to the BR7 sclerite, and thence to their various current origin sites (see Deep Homology of Diplopod Appendages below for further discussion). The *intercoxae* muscle, which transversely spans the two gonopod coxae, has no apparent counterpart in the walking legs.

Unlike with the skeletal elements, the internal morphology of juvenile males conclusively demonstrates that there is no developmental continuity between the muscles of LP8 in stadium III and those of the gonopods. In the gonopod primorida of stadium IV the muscles are entirely obliterated, and no new muscle is formed from stadia IV to VII. Therefore, the gonopod muscles must develop in their entirety during stadium VII. This complete lack of developmental continuity is consistent with the interpretation that gonopod development is a form of localized metamorphosis (Drago *et al.*, 2008).

*Gonopod Homologies and Development in Order Polydesmida*

Our descriptions of the adult gonopod musculature in *P. serratus* exactly match previous work in another member of the family Polydesmidae (West, 1953: *S. virginicus*) and in the distantly related polydesmidan family Paradoxosomatidae (Drago *et al.*, 2011: *O. gracilis*). Instead of a cannula, the gonopod of *O. gracilis* has a "solenomerite" sclerite that articulates on the medial side of the coxa and has a single muscle ("solenomerite abductor"). Unlike the polydesmid cannula, this "solenomerite" is apparently mid-distally surrounded by cuticle of the telopodite (=prefemur) with its distal flagelliform tip emerging on the solenophore branch of the telopodite. Regardless, we consider this sclerite to be homologous to the cannula due to the fact that it articulates on the medial side of the coxa and is the insertion point for a muscle that originates at the tracheal apodeme.

Compared to *Pseudopolydesmus*, the juvenile postembryonic development in *O. gracilis* appears to be less sudden between stadia. The stadium IV gonopod primordium in *O. gracilis* retains external stigmata associated with the 8th leg pair (Drago *et al.*, 2011) unlike in *Pseudopolydesmus*. Additionally, gonopod muscle development begins earlier in the gonopod primordium of *O. gracilis*. Stadia VI and VII in *O. gracilis* have a single defined muscle with an origin at the tracheal apodeme that proceeds posteroventrally and spans the apparently non-articulated gonopod primordium (Drago *et al.*, 2011: fig. 13D). The function of this muscle is unclear – perhaps it is related to the differentiation of the cannula (=solenomerite) from the remaining tissue of the gonopod primordium.

It may be useful to compare internal skeletomuscular development between polydesmid males with 20 body rings as adults (*e.g. Pseudopolydesmus*) against those with 19 body rings (*e.g. Scytonotus, Brachydesmus* Heller, 1858). *Brachydesmus superus* Latzel, 1884 is known to reach adulthood at stadium VII (Petit, 1976), which must affect the timing of gonopod development.

*Deep Homology of Diplopod Appendages*

Gonopods associated with BR7 (and occasionally also body ring eight) are a characteristic feature of the millipede infraclass Helminthomorpha, although metamorphosing male genitalia have evolved at least twice in millipedes. In Pentazonia, the legs just before the anus metamorphose into telopods, whereas in Colobognatha and Eugnatha legs near the front of the body metamorphose into gonopods. Within Helminthomorpha, there is a marked divide between the simple, clearly segmented gonopods of Colobognatha and the fantastically modified gonopods of Eugnatha. The colobognath gonopod has been interpreted as either (i) a primitive version of the gonopod shared with Eugnatha that more closely resembles their shared ancestor (two novelty genitalia hypothesis, see Fig. 8A; Demange, 1967; Hoffman, 1979); or (ii) a separate novel derivation of gonopods (three novelty hypothesis, Fig. 8B; Gardner, 1974).

Each evolutionary derivation of metamorphosing genitalia likely represents a duplication and subsequent divergence in genetic character identity networks (ChIN) resulting in paramorphic appendages (*sensu* Wagner, 2014). Within this context, the evolutionary precursor to the gonopod of

*Pseudopolydesmus* is not the walking leg, which is merely its developmental precursor. Rather, the genetic ancestry of the gonopod ChIN can be traced back to the ancestral origin of gonopods – either at the ancestor of Eugnatha (three genitalia novelty hypothesis) or the helminthomorph ancestor of Eugnatha + Colobognatha (two genitalia novelty hypothesis). This perspective is congruent with previous assertions that ontogenetic heterochrony between the walking leg and gonopod enables evolutionary independence between the two appendage types (Tadler, 1996b; Akkari *et al.*, 2014). The potential existence of a gene product "earmarking" BR7 for metamorphosis during early ontogeny would provide the mechanism for a localized switch between the two specified ChINs (Akkari *et al.*, 2014).

In either the two origin or three origin genitalia hypotheses, it will likely be more illuminating to examine the comparative anatomy of metamorphosing male genitalia (gonopods and telopods) in order to identify homologous skeletal elements and muscles. Using this approach, the ancestral gonopod(s) and telopod can be posited, at which point the homologies between the walking leg and genitalic paramorphs could be identified.

*Future Research on Appendage Homology*

In the absence of clear serial and developmental homologies between the muscles of the walking legs and gonopods in *Pseudopolydesmus*, alternative approaches must be explored. One underexplored option is evolutionary developmental biology. The increasing availability of high-quality genomes will allow developmental experimental methods to be applied to many previously non-model organisms. Gene knockout experiments have recently revealed a salient unified hypothesis of deep homology among the body walls and appendage segments across Pancrustacea (Coulcher *et al.*, 2015; Bruce & Patel, 2020). Despite the variety in form and function in pancrustacean appendages, eight ancestral leg segments have been identified, of which one or more basal segments have fused to the body wall in various pancrustacean lineages. These gene products are expressed regardless of whether an appendage or outgrowth is present, suggesting that a universal series of gene expression fields defines arthropod

appendage formation (Bruce & Patel, 2020). Similar research in millipedes has the potential to identify homologous MEs of the sternite, tracheal apodeme, and leg articles in the gonopod.

A broad comparative morphological approach will also be necessary to understand the evolutionary histories of gonopod skeletal elements and muscles. A cursory comparison between the gonopods of Polydesmidae and those of its close relatives in the clade Juliformia (orders Julida, Spirostreptida, and Spirobolida) yields mixed results. The gonopod muscular anatomy of Julida (Drago *et al.*, 2011) superficially resembles that of Polydesmida (West, 1953; Drago *et al.*, 2011; and this paper). Both orders share a general pattern of extrinsic gonopod protractor and retractor muscles inserting onto the gonopod apodeme(s) from various origins on the adjacent walking leg tracheal apodemes and body rings. However, julidans have two pairs of gonopods, so the muscles in Julida that have functional counterparts in Polydesmida are split between the two gonopod pairs. The gonopod coxa may additionally be spanned by a transverse intercoxal muscle ("gonopod abductor"), although it is apparently absent in gonopods with medially fused coxae. Although the muscle origin sites do not exactly match between taxa, these sites could migrate in response to functional needs through the process of sexual selection.

On the other hand, it is more difficult to posit muscle homologies between these two orders and Spirostreptida. As currently understood, the gonopod tracheal apodeme in Spirostreptidea (one of the two suborders of Spirostreptida) is divided into two independently articulating sclerites, one of which is fused with the coxa and telopodite (Demange, 1967; Wilson, 2002). This articulating apodeme forms an elbowed arm which allows the large gonopod to swing anteroventrally out from its retracted position. The remarkable modification of this gonopod deserves further evaluation within a comparative anatomical context. In particular, the fact that the gonopod skeletomusculature of Cambalidae (a family in the spirostreptidan suborder Cambalidea) is more similar to that of Julida (Demange, 1967) suggests that the condition in Spirostreptidea is derived. Unfortunately, the phylogenetic relationships among spirostreptidan taxa are not yet adequately understood to sufficiently test this hypothesis (Mauriès, 1992; Enghoff *et al.*, 2015: 434; Iniesta *et al.*, 2020).

Another important detail is that the tracheal apodeme is often not fused to the gonopod coxa in Spirostreptida and Spirobolida (Demange, 1967; Wesener *et al.*, 2008; Pitz & Sierwald, 2010). Detailed comparative morphology of the skeletomusculature in the Eugnatha will doubtlessly yield many more discrepancies and potential homologies.

*Appendage Skeletomuscular Asymmetry*

Tracheal apodeme asymmetry allows consolidation of left and right extrinsic leg muscle insertions onto a single, more robust apodeme. In the imaged adult male *Ps. serratus* (FMNHINS 1513: Table 5), the apodemes for LP7 and LP9 are equal in length without forming a flange. In both cases, the muscles which normally originate from the flange instead originate from the tip of the tracheal apodeme corresponding to their respective sides of the body. The tracheal apodemes in LP9 are unique in that they do not project medially to the centerline of the body, remaining laterally distant from each other. This is most likely due to the substantial lateral displacement of the coxae of LP9 caused by the very large gonopod coxae (LP8).

The absence of muscle asymmetry in the gonopod of Polydesmida could be due to a lack of chiasmatic muscles in the walking leg of the last common ancestor of gonopod-bearing millipedes. If polydesmidan gonopods were modified from walking legs, we would expect to see at least one set of chiasmatic muscles, perhaps originating at the tracheal apodeme and inserting onto the opposite prefemur (=telopodite). However, the millipede groups with chiasmatic walking leg muscles are scattered across the millipede Tree of Life (Koch, 2015: 102), so it is unclear whether the ancestral gonopod-bearing millipede, and therefore the nascent gonopod paramorph, possessed chiasmatic muscles.

It must be stressed that our interpretation is based on limited available data for each of the sampled species (Table 5). In particular, we cannot infer whether patterns of asymmetric handedness are consistent within each species, although we suspect they are not.

*Integrated Development of Diplopod Reproductive System?*

It was surprising to find a possible developmental linkage between gonopod and genital tract development. In stadium VII, the gonopod primordium contains the soft, nascent tissue of the future gonopod (Fig. 6). This is consistent with previous observations of the pharate final instar inflating the stadium VIII gonopod while it is protected within the expanded cuticle of stadium VII (Drago *et al.*, 2011). In contrast, our observation that the tissue of the developing genital tract is spatially continuous with the soft tissue of the developing adult gonopod is totally new. This is an unexpected finding, given that the adult gonopods are not connected to the genital tract, nor are the walking legs of body ring 7 connected to the genital tract at any point during earlier development. In the imaged stadium VII male, the medial constriction between the presumed future coxa and telopodite defines a gap (Fig. 6B). We speculate that the involuted tube would need to pass through this gap when it everts to become the distal part of the mature telopodite.

The developmental connection between the gonopods and genital tract is only present in stadium VII. Therefore, in our scenario the future telopodite would need to separate from the future genital tract before or during eversion of the telopodite.. If the sexual development of these two organs is indeed coordinated, it would emphasize the ontogenetic and functional aspects of the paramorphic split between walking legs and gonopods. This aspect of millipede development requires better sampling and taxonomic representation before firm conclusions can be drawn.

**Conclusions**

Ultimately, we were able to homologize a limited set of skeletomuscular MEs between the serially homologous walking leg and gonopod appendage types. The use of 3D μCT imaging provided new evidence demonstrating the identity of the gonopod coxal sclerite's dorsal flange as the homolog of the tracheal apodeme from the walking leg. The presence of only a few conserved muscle attachment sites between the appendage types limited the available evidence for muscle homologies. Investigation of the developing gonopod in the juvenile stadia leading up to sexual maturity revealed the complete obliteration

of walking leg musculature prior to gonopod formation, resulting in no developmental continuity between walking leg and gonopod muscles. If metamorphosing male genitalia, including the gonopod and telopod, are in fact deeply diverging paramorphs of the walking leg, then future work on millipede appendage homology will require a broader comparative perspective that incorporates the deep ancestral nodes at which these appendages originated.

**Acknowledgements**

We would like to thank the following persons and institutions: Douglas Rowland provided critical assistance to XJZ for μCT image acquisition at the Center for Molecular and Genomic Imaging (CMGI) at University of California, Davis (UCD). Melissa Callahan at the Auburn University Museum of Natural History and Julia Snyder at the Field Museum of Natural History (FMNH) graciously loaned the imaged specimens from their institutions. The images in Fig. 1 were derived from images produced by Stephanie Ware and Petra Sierwald at FMNH. James Starrett, Iris Bright, Lacie G. Newton, & Emma E. Jochim provided invaluable feedback during editing and revision. μCT imaging for this project was supported by a pilot grant from the CMGI at UCD (https://cmgi.ucdavis.edu) to XJZ and JEB. Additional project support was funded by National Science Foundation grant IOS 1556165 to JEB and the Evert and Marion Schlinger Foundation (UCD).

**Author Contribution Statement**

XJZ: Conceptualization; Funding acquisition; Investigation; Writing – original draft. MM: Conceptualization; Investigation; Writing – original draft. JEB: Conceptualization; Funding acquisition; Writing – review & editing.

**References**

Akkari, N., H. Enghoff, and A. Minelli. 2014. Segmentation of the millipede trunk as suggested by a homeotic mutant with six extra pairs of gonopods. Front. Zool. 11: 6.

Brewer, M. S., and J. E. Bond. 2013. Ordinal-level phylogenomics of the arthropod class Diplopoda (millipedes) based on an analysis of 221 nuclear protein-coding loci generated using next-generation sequence analyses. PLoS One. 8: e79935.

Brewer, M. S., P. Sierwald, and J. E. Bond. 2012. Millipede taxonomy after 250 years: classification and taxonomic practices in a mega-diverse yet understudied arthropod group. PLoS One. 7: e37240.

Brölemann, H. W. 1914. Étude sur les Spirobolides (Myriapodes). Ann. Soc. Entomol. Fr. 83: 1–38.

Bruce, H. S., and N. H. Patel. 2020. Knockout of crustacean leg patterning genes suggests that insect wings and body walls evolved from ancient leg segments. Nat. Ecol. Evol. 4: 1703–1712.

Coulcher, J. F., G. D. Edgecombe, and M. J. Telford. 2015. Molecular developmental evidence for a subcoxal origin of pleurites in insects and identity of the subcoxa in the gnathal appendages. Sci. Rep. 5: 15757.

Demange, J.-M. 1967. Recherches sur la segmentation du tronc des Chilopodes et des Diplopodes Chilognathes (Myriapodes). Mém. Mus. Natl. Hist. Nat., n.s. 44: 1–188.

Drago, L., G. Fusco, E. Garollo, and A. Minelli. 2011. Structural aspects of leg-to-gonopod metamorphosis in male helminthomorph millipedes (Diplopoda). Front. Zool. 8: 1–16.

Drago, L., G. Fusco, and A. Minelli. 2008. Non-systemic metamorphosis in male millipede appendages: long delayed, reversible effect of an early localized positional marker? Front. Zool. 5: 1–4.

Enghoff, H., W. Dohle, and J. G. Blower. 1993. Anamorphosis in millipedes (Diplopoda)—the present state of knowledge with some developmental and phylogenetic considerations. Zool. J. Linn. Soc. 109: 103–234.

Enghoff, H., S. I. Golovatch, M. Short, P. Stoev, and T. Wesener. 2015. Diplopoda – taxonomic overview, pp. 363–453. In Minelli, A. (ed.), The Myriapoda Volume 2. Brill, Leiden.

Gardner, M. R. 1974. Revision of the millipede family Andrognathidae in the Nearctic region. Mem. Pac. Coast Entomol. Soc. 5: 1–61.

Haacker, U., and S. Fuchs. 1970. Das Paarungsverhalten von *Cylindroiulus punctatus* Leach. Z. Tierpsychol. 27: 641–648.

Hoffman, R. L. 1979. Classification of the Diplopoda. Muséum d'Histoire Naturelle de Genève, Geneva.

Iniesta, L. F. M., H. Enghoff, A. D. Brescovit, and R. S. Bouzan. 2020. Phylogenetic placement of the monotypic genus *Holopodostreptus* Carl, 1913 and notes on the systematics of Pseudonannolenidae (Spirostreptida : Cambalidea). Invertebr. Syst. 34: 661–677.

Keeton, W. T. 1960. A taxonomic study of the milliped family Spirobolidae (Diplopoda: Spirobolida). Mem. Am. Entomol. Soc. 17: 1–146.

Kent, G. C. 1983. Comparative Anatomy of the Vertebrates, 5th ed. C. V. Mosby Company, St. Louis.

Klowden, M. J. 2013. Physiological Systems in Insects, 3rd ed. Elsevier, Amsterdam.

Koch, M. 2015. Diplopoda – skeletomuscular system and locomotion, pp. 101–107. In Minelli, A. (ed.), The Myriapoda Volume 2. Brill, Leiden.

Manton, S. M. 1954. The evolution of arthropodan locomotory mechanisms. Part 4. The structure, habits and evolution of the Diplopoda. Zool. J. Linn. Soc. 42: 299–368.

Manton, S. M. 1958. The evolution of arthropodan locomotory mechanisms. Part 6. Habits and evolution of the Lysiopetaloidea [Diplopoda], some principles of leg design in Diplopoda and Chilopoda, and limb structure of Diplopoda. Zool. J. Linn. Soc. 43: 487–556.

Manton, S. M. 1961. The evolution of arthropodan locomotory mechanisms. Part 7. Functional requirements and body design in Colobognatha (Diplopoda), together with a comparative account of diplopod burrowing techniques, trunk musculature and segmentation. Zool. J. Linn. Soc. 44: 383–462.

Mauriès, J.-P. 1992. Sur la vraie place du genre *Protosilvestria* Handschin dans las classification des Diplopodes Iuliformes (Iuliformia, Iulida, Cambalidea). Ber. Naturwiss.-med. Ver. Innsb. Suppl. 10: 23–31.

Petit, G. 1973. Étude morphologique et expérimentale de la métamorphose d'un appendice ambulatoire en gonopode chez le diplopode *Polydesmus angustus* Latz. Ann. Embryol. Morphogen. 6: 137–149.

Petit, G. 1976. Developpements compares des appendices copulateurs (gonopodes) chez *Polydesmus angustus* Latzel et *Brachydesmus superus* Latzel (Diplopodes : Polydesmidae). Int. J. Insect Morphol. Embryol. 5: 261–272.

Pitz, K. M., and P. Sierwald. 2010. Phylogeny of the millipede order Spirobolida (Arthropoda: Diplopoda: Helminthomorpha). Cladistics 26: 497–525.

Rodriguez, J., T. H. Jones, P. Sierwald, P. E. Marek, W. A. Shear, M. S. Brewer, K. M. Kocot, and J. E. Bond. 2018. Step-wise evolution of complex chemical defenses in millipedes: a phylogenomic approach. Sci. Rep. 8: 3209.

Seifert, B. 1932. Anatomie und Biologie des Diplopoden *Strongylosoma pallipes* Oliv. Z. Morph. Ökol. Tiere 25: 362–507.

Shear, W. A. 1972. Studies in the milliped order Chordeumida (Diplopoda): A revision of the family Cleidogonidae and a reclassification of the order Chordeumida in the New World. Bull. Mus. Comp. Zool. 144: 151–352.

Shelley, R. M. 1993. Revision of the milliped genus *Scytonotus* Koch (Polydesmida: Polydesmidae). Brimleyana 19: 1–60.

Sierwald, P., D. A. Hennen, X. J. Zahnle, S. Ware, and P. E. Marek. 2019. Taxonomic synthesis of the eastern North American millipede genus *Pseudopolydesmus* (Diplopoda: Polydesmida: Polydesmidae), utilizing high-detail ultraviolet fluorescence imaging. Zool. J. Linn. Soc. 187: 117–142.

Sierwald, P., and J. Spelda. 2022. MilliBase. Accessed at https://www.millibase.org on 2022-04-01. doi:10.14284/370

Silvestri, F. 1903. Acari, Myriopoda et Scorpiones Hucusque in Italia Reperta. Classis Diplopoda. Vol. 1. Anatome. Pars 1a. Segmenta, Tegumentum, Musculi. Antonio Berlese, Portici.

Tadler, A. 1996a. Functional morphology of genitalia of four species of julidan milllipedes (Diplopoda: Nemasomatidae; Julidae). Zool. J. Linn. Soc. 118: 83–97.

Tadler, A. 1996b. Functional morphology and evolution of the genitalia of Diplopoda - Helminthomorpha. Mém. Mus. Natl. Hist. Nat., n.s. 169: 327–330.

Tanabe, T., and T. Sota. 2008. Complex copulatory behavior and the proximate effect of genital and body size differences on mechanical reproductive isolation in the millipede genus *Parafontaria*. Am. Nat. 171: 692–699.

Voges, E. 1878. Beiträge zur Kenntniss der Juliden. Z. Wiss. Zool. 31: 127–194.

Wagner, G. P. 2014. Homology, Genes, and Evolutionary Innovation. Princeton University Press, Princeton.

Wesener, T., H. Enghoff, and J.-W. Wägele. 2008. Pachybolini - a tribe of giant Afrotropical millipedes: arguments for monophyly and the description of a new genus from Madagascar (Diplopoda:Spirobolida:Pachybolidae). Invertebr. Syst. 22: 37–53.

West, W. R. Jr. 1953. An anatomical study of the male reproductive system of a Virginia millipede. J. Morphol. 93: 123–175.

Wilson, H. M. 2002. Muscular anatomy of the millipede *Phyllogonostreptus nigrolabiatus* (Diplopoda: Spirostreptida) and its bearing on the millipede "thorax." J. Morphol. 251: 256–275.

Wojcieszek, J. M., P. Austin, M. S. Harvey, and L. W. Simmons. 2012. Micro-CT scanning provides insight into the functional morphology of millipede genitalia: Functional morphology of millipede genitalia. J. Zool. 287: 91–95.

Young, B. A. 1993. On the necessity of an archetypal concept in morphology: with special reference to the concepts of "structure" and "homology." Biol. Philos. 8: 225–248.

Youngsteadt, N. W. 2009. Laboratory observations on the natural history of *Pseudopolydesmus pinetorum* (Diplopoda, Polydesmida, Polydesmidae) with emphasis on reproduction and growth. Trans. Kans. Acad. Sci. 112: 67.

Yushkevich, P. A., J. Piven, H. C. Hazlett, R. G. Smith, S. Ho, J. C. Gee, and G. Gerig. 2006. User-guided 3D active contour segmentation of anatomical structures: significantly improved efficiency and reliability. NeuroImage. 31: 1116–1128.

Zahnle, X. J., P. Sierwald, S. Ware, and J. E. Bond. 2020. Genital morphology and the mechanics of copulation in the millipede genus *Pseudopolydesmus* (Diplopoda: Polydesmida: Polydesmidae). Arthropod Struct. Dev. 54: 1–19.

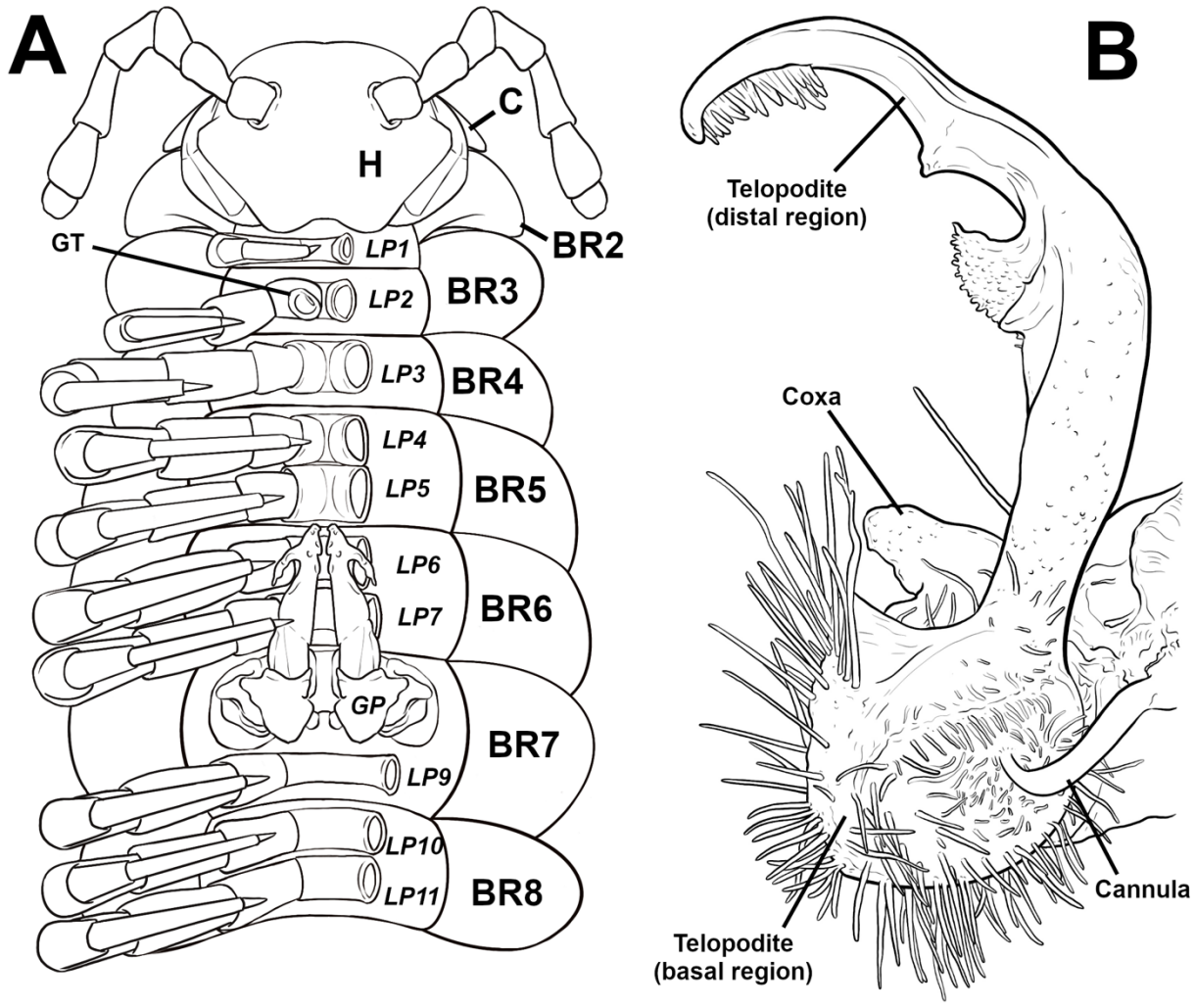


**Figure 1.** Line drawings of male *Pseudopolydesmus* anatomy. (A) Anterior end of *Ps. canadensis* viewed ventrally. Walking legs on the left side the body are removed. All body rings and leg pairs labelled for ease of reference. (B) Gonopod of *Ps. serratus* from medial view. Abbreviations: BR – body ring; C: collum (=body ring 1); GP – gonopod pair (=leg pair 8); GT – gonopore (opening of genital tract); H – head; LP – walking leg pair.

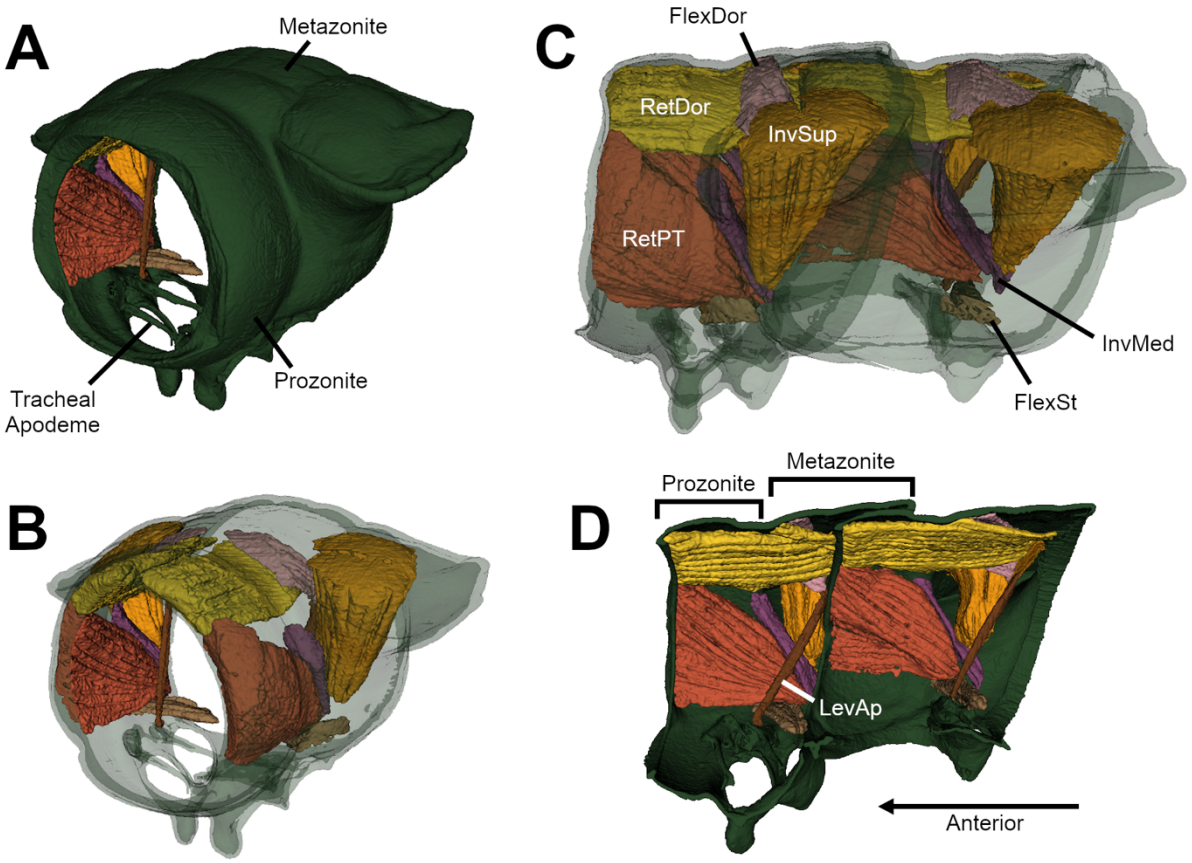


**Figure 2.** Trunk musculature in male *Ps. serratus.* Body rings six and seven illustrated. (A) Oblique anterior view of BR6 and its trunk musculature, with BR6 translucent. (B) Oblique anterior view of BR6 and its trunk musculature, with BR6 opaque. (C) Left lateral view of BR6 and BR7 with trunk musculature, with body rings translucent. (D) Midsagittal view of BR6 and BR7 with trunk musculature of right side, with left half of body removed. Arrow shows the orientation of body rings in panels C and D. Abbreviations: FlexDor – *flexor dorsalis* muscle; FlexSt – *flexor sternalis* m.; InvMed – *involvens medius* m.; InvSup – *involvens superus* m.; LevAp – *levator apophysis* m.; RetDor – *retractor dorsalis* m.; RetPT – *retractor paratergalis* m.

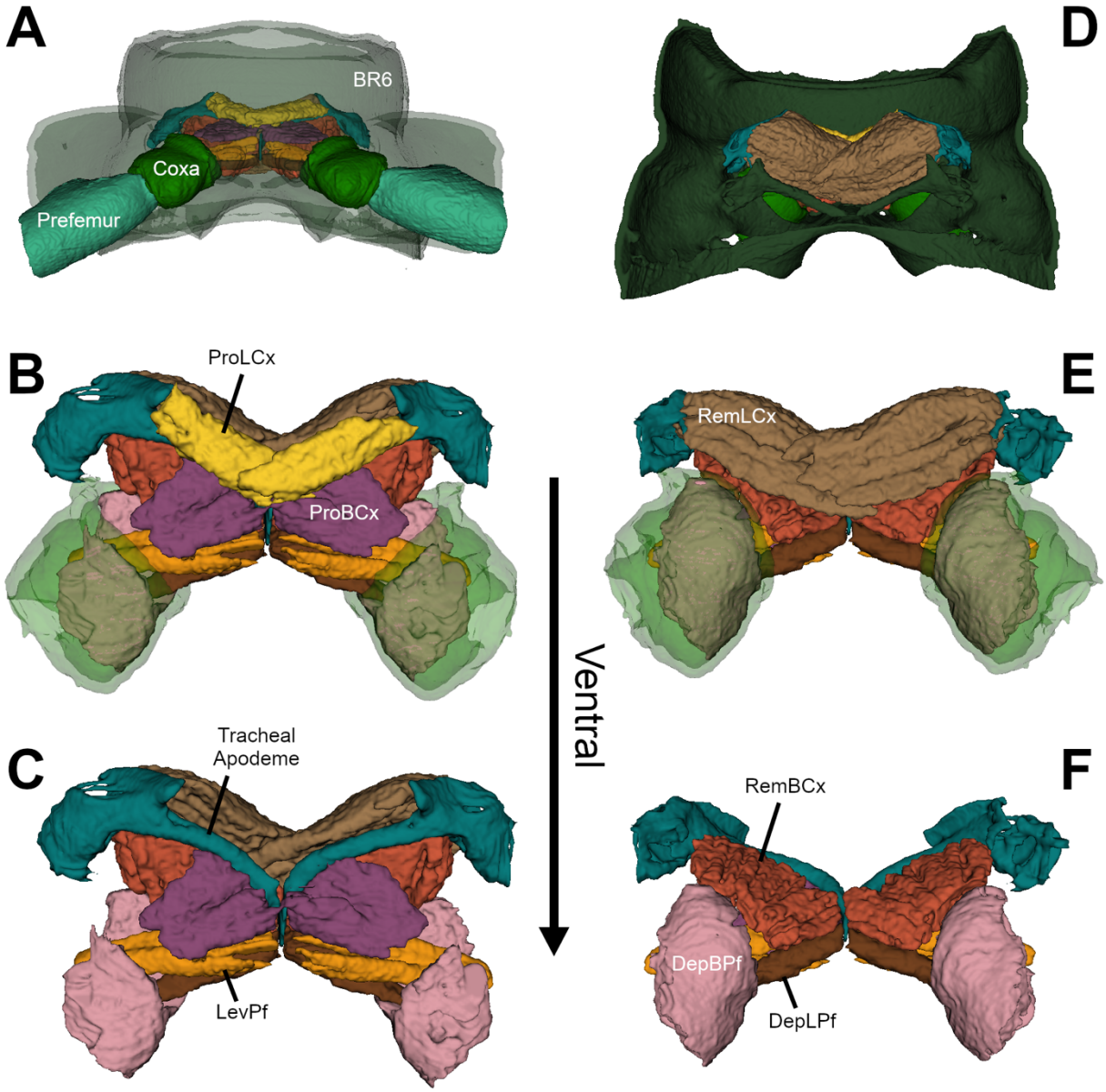


**Figure 3.** Walking leg skeletomusculature in male *Ps. serratus.* Leg pair six (anterior pair on body ring six) illustrated. (A) Ventral view of BR6 showing skeletal elements and muscles of LP6, with BR6 translucent. (B) Anteroventral view of LP6 skeletal elements and muscles, with coxa translucent. (C) Anteroventral view of LP6 skeletal elements and muscles, with *promotor longus coxae* and coxa removed. (D) Dorsal view of BR6 showing skeletal elements and muscles of LP6, with tergite of BR6 removed. (E) Posterodorsal view of LP6 skeletal elements and muscles, with coxa translucent. (F)

Posterodorsal view of LP6 skeletal elements and muscles, with *remotor longus coxae* and coxa removed. Arrow shows the orientation of walking leg skeletomusculature in panels B, C, E, and F. Abbreviations: DepBPf – *depressor brevis prefemoris* muscle; DepLPf – *depressor longus prefemoris* m.; LevPf – *levator prefemoris* m.; ProBCx – *promotor brevis coxae* m.; ProLCx – *promotor longus coxae* m.; RemBCx – *remotor brevis coxae* m.; RemLCx – *remotor longus coxae* m.

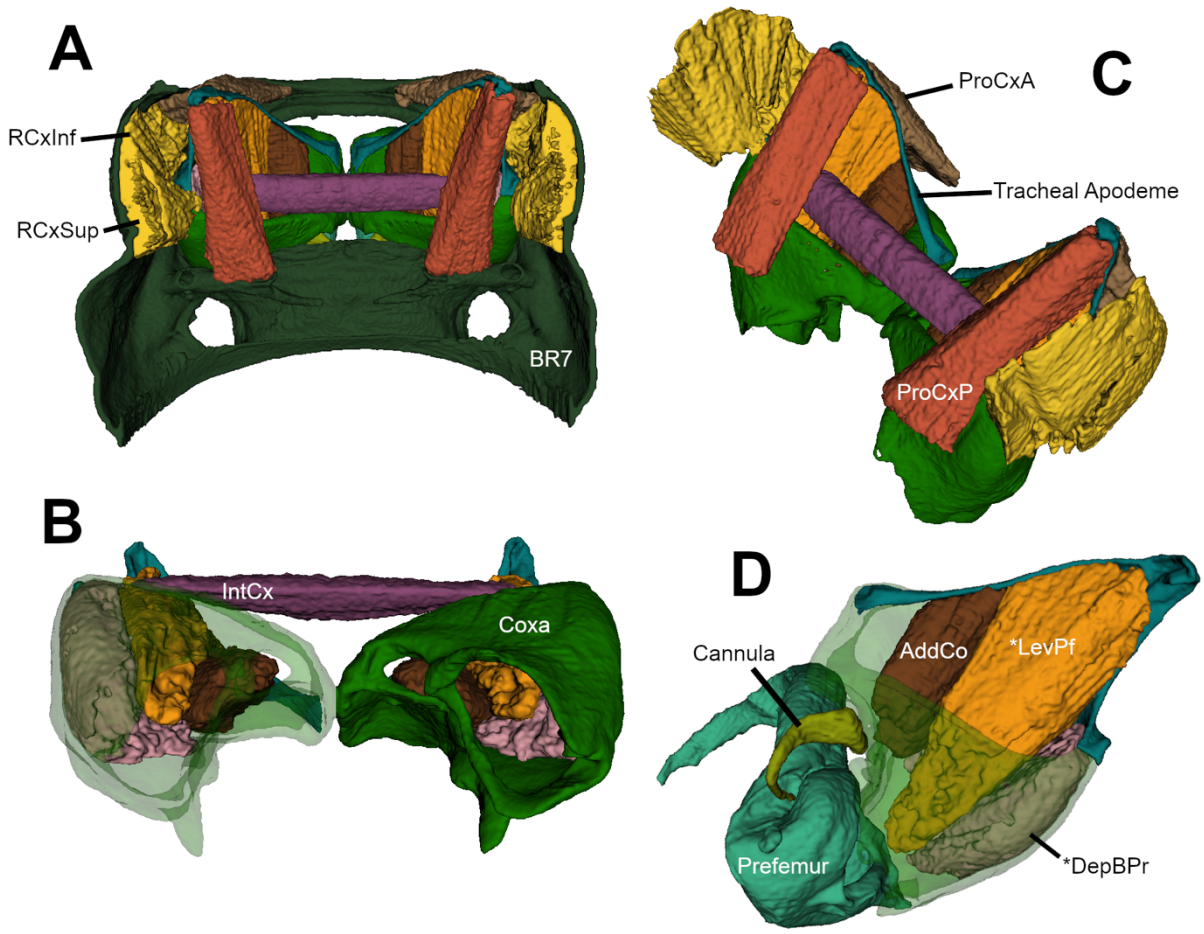


**Figure 4.** Gonopod skeletomusculature in male *Ps. serratus*. (A) Dorsal view of body ring seven showing skeletal elements and muscles of the gonopod, with tergite of BR7 removed. (B) Oblique posterior view of gonopod skeletal elements and muscles. (C) Posterior view of gonopod coxa, tracheal apodeme, and intrinsic muscles. Left coxa translucent and right coxa opaque. (D) Posterior view of skeletal elements and intrinsic muscles of the left gonopod, with coxa translucent. Abbreviations: AddCo – *adductor cornui* muscle; *DepPf – *depressor prefemoris* m. (=*flexor telopoditis* of West, 1953); IntCx – *intercoxae* m.; *LevPf – *levator preefemoris* m. (=*extensor telopoditis* of West, 1953); ProCxA – *protractor coxae anterior* m.; ProCxP – *protractor coxae posterior* m.; RCxInf – *retractor coxae inferus* m.; RCxSup – *retractor coxae superus* m.

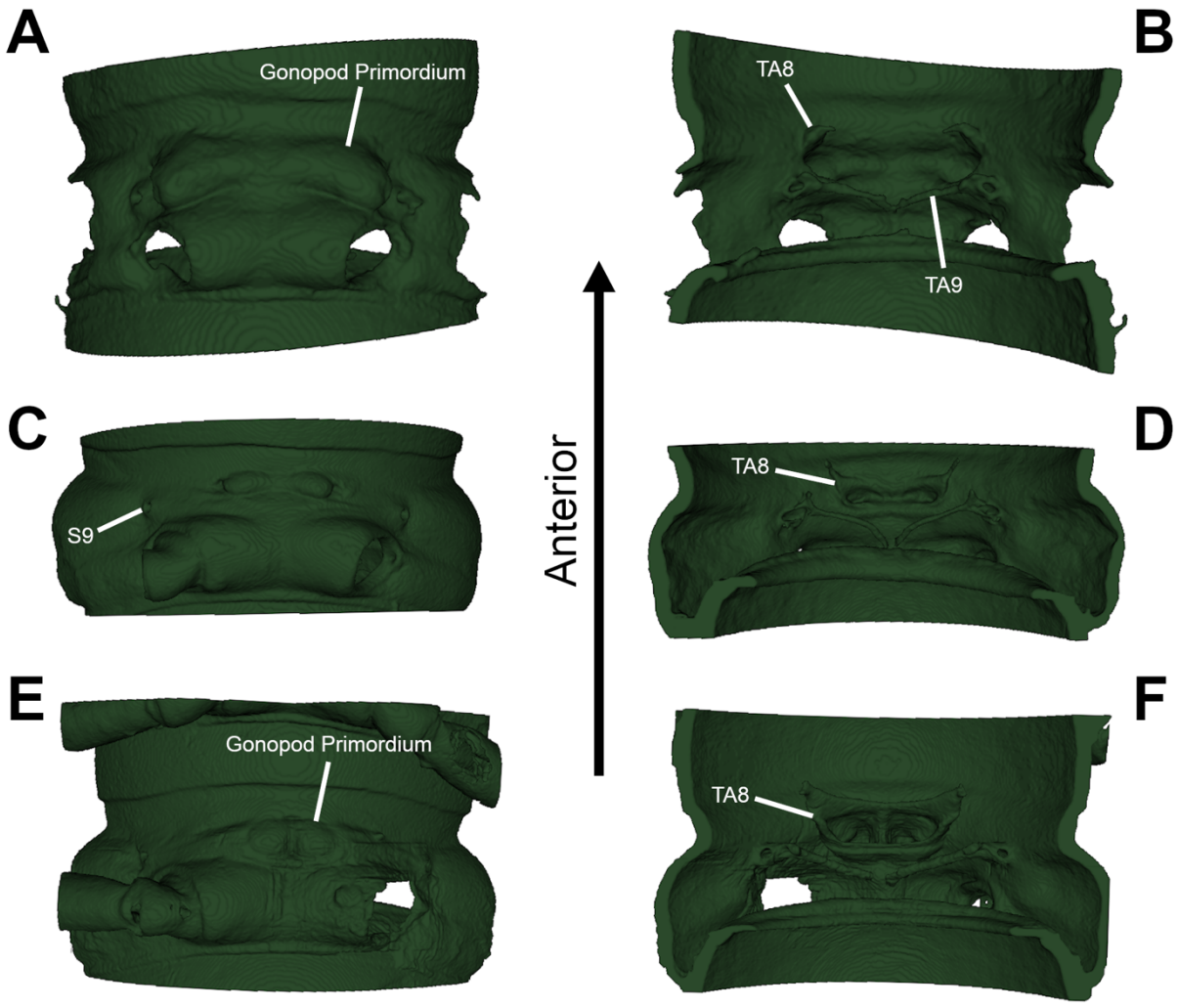


**Figure 5.** Cuticle of gonopod primordium in juvenile male *Pseudopolydesmus* spp. Stadia IV through VI shown. (A-B) Stadium IV. (C-D) Stadium V. (E-F) Stadium VI. (A, C, E) Ventral view showing exterior cuticle. (B, D, F) Dorsal view with pleurotergite removed showing interior cuticle. Arrow shows the orientation of body rings in all panels. Abbreviations: S9 – stigma of ninth walking leg pair; TA8 – tracheal apodeme of the eighth appendage pair (fused with gonopod primordium); TA9 – tracheal apodeme of the ninth appendage pair (walking leg pair).

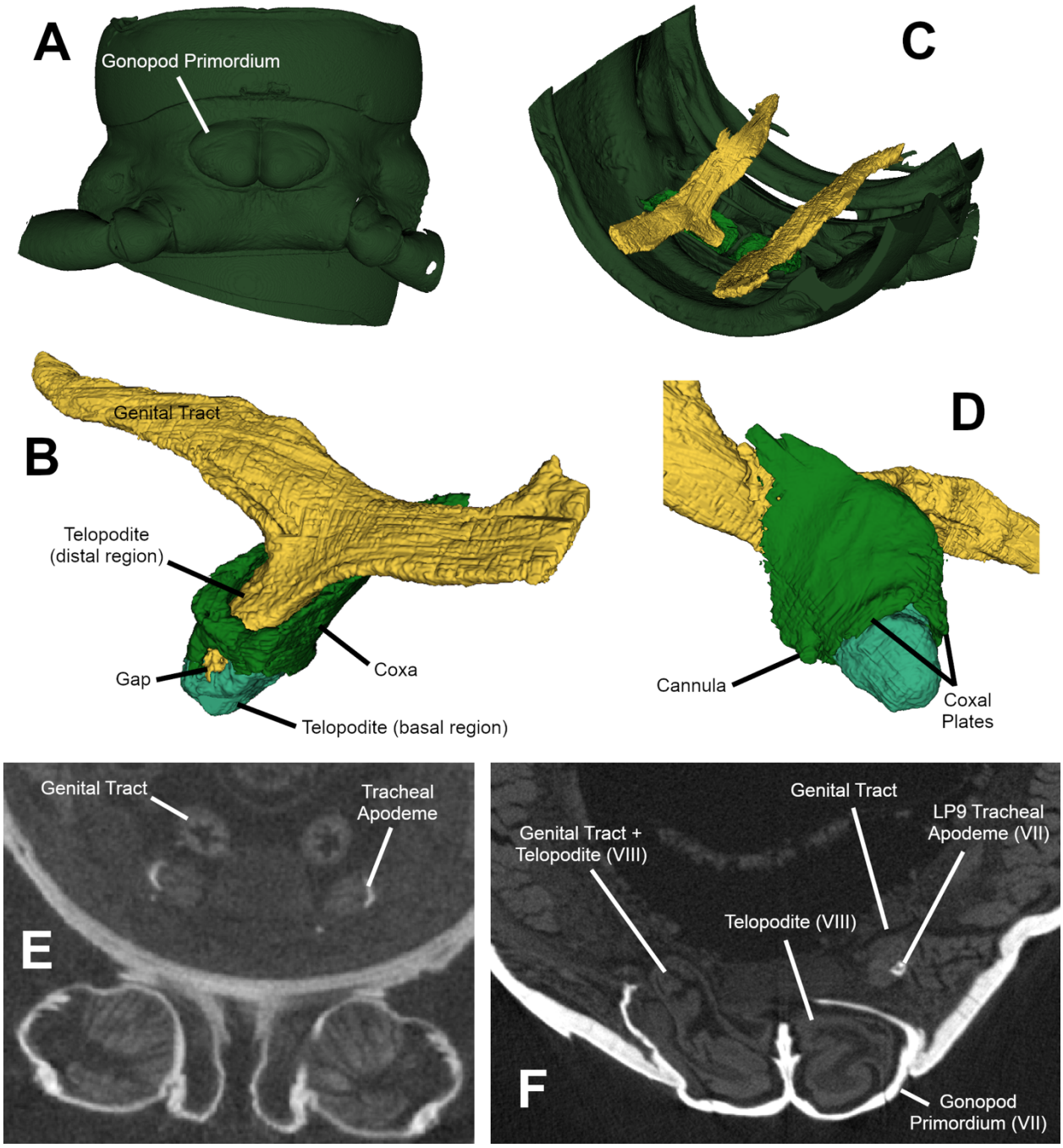


**Figure 6.** Internal reproductive structures in stadium VII juvenile male *Pseudopolydesmus* sp. (A) Ventral view showing external cuticle. (B) Oblique view showing developing reproductive tissues *in situ*. (C) Medial view of developing reproductive tissue. Continuity of genital tract tissue with distal region of the telopodite is visible, along with the medial gap which the distal region possibly everts through. (D)

Lateral view of developing reproductive tissue, showing coxal plates and non-differentiated cannula. (E) Transverse section of adult male *Ps. serratus* at the anterior leg pair of the sixth body ring (leg pair 6). Paired paramedian genital tract is positioned directly dorsal to tracheal apodemes of leg pair 6. It is circular in cross-section, with a star-shaped lumen. (F) Transverse section of stadium VII male *Pseudopolydesmus* sp. at the gonopod primordium. Section is slightly oblique, so that the genital tract and future stadium VIII telopodite are separated on one side but shown as continuously connected on the other side. Although the genital tract is dorsoventrally flattened, it is positioned directly dorsal to the tracheal apodeme (leg pair 9 in this case) as it is in the adult.

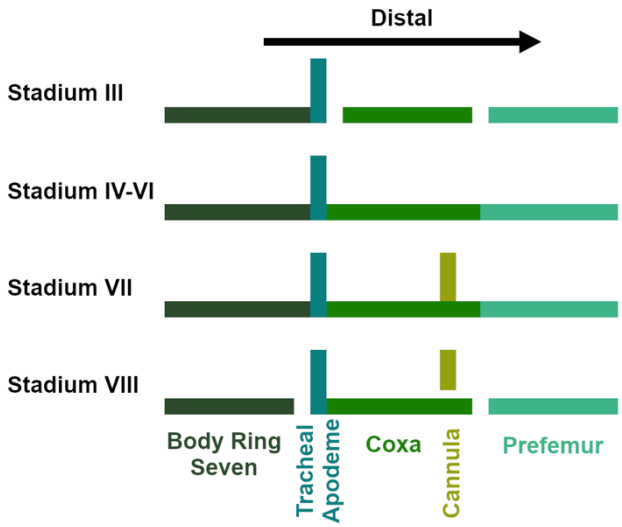


**Figure 7.** Schematic illustration of the appendicular skeletal elements showing gonopod development during each male stadium. Gaps between adjacent skeletal elements indicate articulations with sclerites connected by arthrodial membranes. Skeletal elements connected without gaps are fused into a single sclerite. Arrow shows the relative position of skeletal elements along the basal-distal axis.

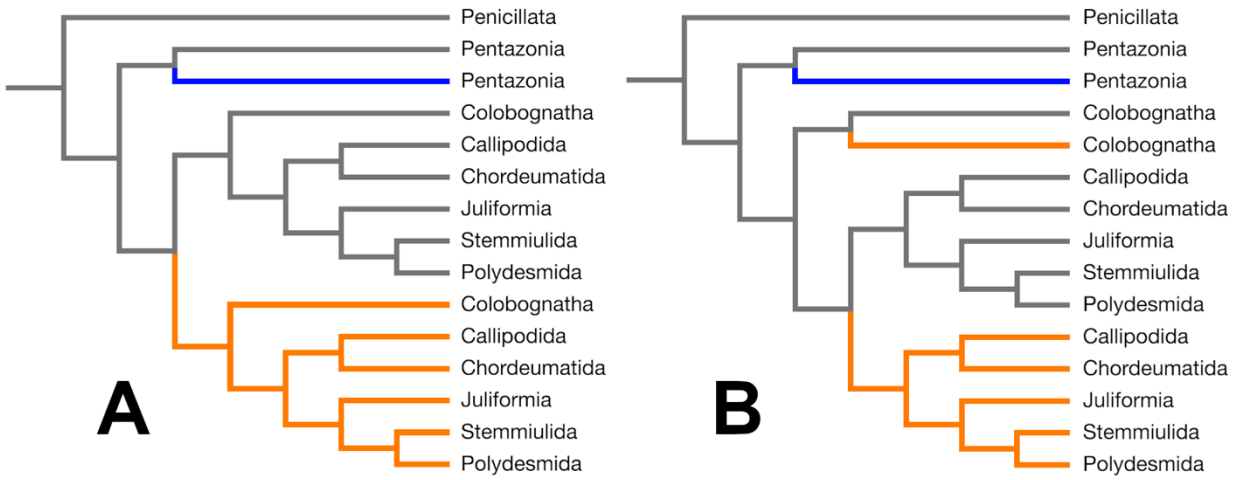


**Figure 8.** Two alternative paramorph trees depicting the evolution of metamorphosing male genitalia from the ancestral millipede walking leg. Appendage identity is depicted as branch color, with color change along a branch represent evolution of a novel appendage type. Black represents the ancestral walking leg paramorph, blue represents a telopod appendage paramorph, and orange represents a gonopod paramorph. (A) Two novelty hypothesis, in which novel gonopods arose once in the common ancestor of all gonopod-bearing millipedes. (B) Three novelty hypothesis, in which novel gonopods arose in the ancestor of all extant Colobognatha and independently in the common ancestor of all extant Eugnatha. Tree topology derived from the Millipede Tree of Life (Rodriguez *et al.*, 2018) and simplified for illustrative purposes.

**Table 1.** Museum specimens illustrated in this paper. Thresholds refer to voxel intensity thresholds used during semi-automated ITK-SNAP segmentation for the specified types of tissue. Cuticle segmentations were conducted without an upper bound.

| Specimen ID | Locality | Preservation | Stadium | Sex | Species | Thresholds (lower, upper) |
|---|---|---|---|---|---|---|
| AUMS 6063 | GA, Pickens Co. | 80% EtOH | III | unknown | *Pseudopolydesmus* sp. | N/A |
| AUMS 6063 | GA, Pickens Co. | 80% EtOH | IV | male | *Pseudopolydesmus* sp. | Cuticle (12413, N/A) |
| AUMS 15703 | TN, Van Buren Co. | 95% EtOH | V | male | *Pseudopolydesmus* sp. | Cuticle (21993, N/A) |
| AUMS 15259 | FL, Jackson Co. | 70% EtOH | VI | male | *Pseudopolydesmus* sp. | Cuticle (6380, N/A) |
| AUMS 7129 | GA, Dawson Co. | 80% EtOH | VII | male | *Pseudopolydesmus erasus* | Cuticle (22709, N/A);<br>Soft tissue (12531, 30070) |
| FMNHINS 1513 | IN, Parke Co. | 70% EtOH | VIII | male | *Pseudopolydesmus serratus* | Cuticle (14101, N/A);<br>Soft tissue (18730, 65535) |

**Table 2.** Identities of polydesmidan trunk muscles according to literature records, with the figures from those papers used to compile the table listed. Left column lists abbreviations used by figures in this paper. The "–" symbol indicates that the specified muscle was not identified in the corresponding paper.

| **Abbr.** | **Silvestri, 1903 (figs. 311, 316)** | **Seifert, 1932 (figs. 13-15)** | **West, 1953 (figs. 22-24)** | **Manton, 1961 (fig. 24)** |
|---|---|---|---|---|
| RetDor | *retractor dorsalis* | *retractor dorsalis* | *retractor dorsalis* | *retractor dorsalis* |
| FlexDor | *flexor internus dorsalis* | *flexor internus dorsalis* | *flexor internus dorsalis* | *flexor internus dorsalis* |
| | *flexor externus dorsalis* | *flexor externus dorsalis* | *flexor externus dorsalis* | *flexor externus dorsalis* |
| InvSup | *involvens* | *torquens* | *torquens major* | *involvens superus* |
| InvMed | | *involvens* | *involvens brevis* | *involvens medius* |
| RetPT | *retractor paratergalis* | | *involvens* | *flexor inferus longus-retractor paratergalis* |
| LevAp | *levator apophysis posticae* | – | *torquens minor* | *levator apophysis posticae* |
| FlexSt | *flexor sternalis* | – | *flexor ventralis* | *flexor sternalis* |
| – | – | – | *intersegmentalis* | *retractor ventralis* |
| – | – | – | *retractor membranosus* | – |

**Table 3.** Identities of polydesmidan walking leg muscles according to literature records, with the figures from those papers used to compile the table listed. Rows of the table are organized by muscle functional groups listed in the "Walking Leg Musculature" section of Results. The second column from left lists abbreviations used by figures in this paper. The "–" symbol indicates that the specified muscle was not identified in the corresponding paper. German language terms used by Seifert (1932) are not italicized on the basis that these are not foreign language terms within the context of the original paper, in contrast to the Latin language terms.

| | **Abbr.** | **Silvestri, 1903 (figs. 329, 337-339, 342-343)** | **Seifert, 1932 (figs. 21, 58)** | **West, 1953 (figs. 25-31)** | **Manton, 1954 (fig. 3e-f)** |
|---|---|---|---|---|---|
| **(1)** | ProLCx | *retractor longus subcoxae* | – | *promotor coxae longus* | *retractor longus coxae* |
| | ProBCx | *protractor brevis subcoxae* | unterer Hüftmuskel | *promotor coxae brevis* | *protractor brevis coxae* |
| **(2)** | RemLCx | *protractor longus subcoxae* | sich kreuzende Taschenmuskeln | *remotor coxae longus* | *protractor longus coxae* |
| | RemBCx | – | oberer Hüftmuskel | *remotor coxae brevis* | *retractor brevis coxae* |
| **(3)** | DepLPf | – | – | *depressor 1-trochanteris* | – |
| | DepBPf | *depressor coxae* | *depressor praefemoris* | *promotor 1-trochanteris* & *remotor 1-trochanteris* | *depressor prefemoris* |
| **(4)** | LevPf | *levator coxae* | *levator anelli komplementaris* & *levator praefemoris* | *levator 1-trochanteris anterior* & *levator 1-trochanteris posterior* | *levator prefemoris* |
| | – | – | – | *fenestralis* | – |

**Table 4.** Identities of polydesmidan gonopod muscles according to literature records, with the figures from those papers used to compile the table listed. Left column lists abbreviations used by figures in this paper. An asterisk "*" is added to abbreviations that assert a homology hypothesis between muscles of the walking leg and gonopod. A dash "–" indicates that the specified muscle was shown in figures in the corresponding paper but not identified or labelled.

| **Abbr.** | **West, 1953 (fig. 23)** | **Drago *et al.*, 2011 (figs. 13, 15)** |
|---|---|---|
| ProCxA | *protractor coxae anterior* | gonopod retractor |
| ProCxP | *protractor coxae posterior* | gonopod protractor |
| RCxSup | *retractor coxae* | – [shown but not labelled] |
| RCxInf | | |
| IntCx | *intercoxae* | gonopod abductor |
| AddCo | *adductor cornui* | solenomerite abductor |
| *LevPf | *extensor telopoditis* | prefemur flexor [not shown] |
| *DepBPf | *flexor telopoditis* | prefemur extensor |

**Table 5.** Available data on handedness of the midsagittal flange of the tracheal apodeme in Polydesmidae. Images of female specimens FMNHINS 1513 and FMNHINS 1451 are from previously published data (Zahnle *et al.*, 2020). "L" and "R" represent extension of the left or right tracheal apodeme, respectively. "=" indicates that there is no midsagittal flange, with both apodemes being equal in length. "*" indicates that the tracheal apodemes do not extend medially to the midline of the body ring. "GP" indicates the gonopod or gonopod primordium. Blank cells represent a lack of available data.

| Specimen | Sex | Species | BR4 | BR5 | | BR6 | | BR7 | | BR8 | | BR9 | |
|---|---|---|---|---|---|---|---|---|---|---|---|---|---|
| | | | LP3 | LP4 | LP5 | LP6 | LP7 | LP8 | LP9 | LP10 | LP11 | LP12 | LP13 |
| FMNHINS 1513 | Male, adult | *Ps. serratus* | | L | R | L | = | GP | =* | L | L | L | L |
| West, 1953 | Male, adult | *S. virginicus* | | | | L | L | GP | R | R | L | | |
| AUMS 7129 | Male, subadult | *Ps. erasus* | | | | | | GP | L | L | L | R | L |
| FMNHINS 1513 | Female, adult | *Ps. serratus* | R | R | L | L | L | | | | | | |
| FMNHINS 1451 | Female, adult | *Ps. pinetorum* | L | L | R | L | L | | | | | | |

**Anatomical Network Analysis of Gonopod Macroevolution in Millipedes**

**Table of Contents**

## Introduction

The majority of millipede species belong to the infraclass Helminthomorpha (~12,000 out of 13,000 according to Sierwald & Spelda, 2023), in which sexual reproduction is accomplished through external copulatory organs (Fig. 1). The male copulatory organs, called gonopods, are secondary genitalia that develop from normal walking legs. During a juvenile male's postembryonic development, one or two pairs of legs are replaced by paired nub-shaped primordia which mature into gonopods in the adult male stadium (Petit, 1973; 1976; Drago *et al.,* 2011). On this basis, each gonopod appendage pair is considered to be a serial homolog of the walking leg pairs. In millipede taxa that have them, gonopods are often used as the primary source of morphological characters for defining and identifying species (Sierwald & Bond, 2007; Mwabvu *et al.,* 2013). An understanding of gonopod developmental anatomy and walking leg homology is imperative for the comparative study of gonopods across species.

However, the radically transformed anatomical organization of the gonopods in many species presents a challenge when attempting to homologize gonopod parts to walking leg parts. Early authors proposed various homology schemes for the gonopod segments (Attems, 1926; Verhoeff, 1928; Brölemann, 1935), but such schemes were largely speculative. Developmental research shows that distal walking leg segments tend to be dismantled during gonopod transformation, with only the most proximal parts being retained (Demange, 1964; 1972; Petit, 1973; 1976; Drago *et al.,* 2011; Zahnle *et al.,* 2022).

Additional factors complicate the interpretation of gonopod homology between higher level millipede taxa at the ordinal and subordinal levels. These complications can be summarized as three anatomical comparative "factors": (1) number and positions of gonopod appendage pairs; (2) position of sperm transferring structure (solenomere); (3) degree of similarity of gonopods to walking legs.

In this paper, factors (1) and (2) are collectively referred to as gonopod configuration. In all gonopod-bearing millipedes (infraclass Helminthomorpha) the gonopod complex is made up of either one or two pairs of gonopod appendages (Fig. 2). Depending on the millipede order in question, these appendage pairs can occupy the anterior or posterior positions of the seventh body ring (BR7) or the anterior position of the eighth body ring (BR8). There are usually two gonopod pairs, but in some taxa

there is only a single pair. Regardless of the number of gonopods, only one pair carries the solenomere, which is the structure used to transfer sperm from the gonopods to the female vulvae (Koch, 2015). In taxa with two gonopod pairs, the solenomere can be carried on either pair (possible configurations shown in Fig. 2).

There is also a marked contrast between the organization of gonopods in the sister subterclasses Eugnatha and Colobognatha (factor 3). In Colobognatha the gonopods contain multiple serial segments that resemble those of the walking legs, whereas the gonopods of Eugnatha usually contain only a few proximal segments and do not resemble the walking legs (Fig. 1). The dissimilarity of colobognath and eugnath gonopods has been used as evidence that gonopods were derived independently in the two lineages (Gardner, 1974), although this hypothesis is controversial (Demange, 1967; Hoffman, 1979).

One additional challenge to studying the evolutionary history of millipede gonopods is the paucity of fossil evidence during their origin. The divergence of gonopod-bearing millipedes is tentatively dated between 285-420 Mya and the diversification of the eugnathan crown group is dated between 265-374 Mya (Rodriguez *et al.,* 2018). However, millipedes with preserved gonopods are not available during this time range (Shear & Edgecombe, 2010). Preserved gonopods appear in the fossil record ~100 Mya in Burmese amber, but by this time the modern millipede orders are already recognizable and the organization of their gonopods closely resembles the extant fauna (Liu *et al.,* 2017; Wesener & Moritz, 2018; Jiang *et al.,* 2019; Stoev *et al.,* 2019; Moritz & Wesener, 2019; 2021). For this reason, it is not possible to study the intermediate forms of gonopods during their most formative period of evolution. Instead, alternative approaches are required for comparing the often dissimilar extant forms of gonopods.

Anatomical network analysis (AnNA) is one such alternative approach, enabling quantitative anatomical comparisons that do not rely entirely on the identification of homologies (Rasskin-Gutman & Esteve-Altava, 2014). Discretizing the morphologically complex appendages into their constituent components allows us model them as networks. These components are called morphemes, and are encoded as discrete nodes. The physical relationships among morphemes are encoded as network edges. Once a network is encoded, a battery of quantitative measurements can quickly be extracted from it

(Molnar *et al.,* 2017; Esteve-Altava *et al.,* 2018). Measurements derived from different networks can subsequently be used as the basis for comparative phylogenetic analyses. AnNA offers a complementary approach to comparative anatomy based on descriptive morphology. Although it cannot offer insights into the homologies of the constituent parts of millipede appendages, it does allow direct comparisons of their overall anatomical organization.

We conducted AnNA on the gonopods and walking legs of ten millipede taxa. To our knowledge, this is one of the first applications of AnNA to an arthropod system (Ostachuk, 2019; 2021), and the first in Myriapoda. The chosen taxa provide a broad but shallow representation of gonopod organizational diversity at the ordinal level. Colobognatha was expected to have limited gonopod variability, so only two of its four orders were included. The only eugnath order excluded was Siphoniulida. Both suborders of Spirostreptida were represented (Spirostreptidea and Cambalidea), due to their distinctive gonopod organization. We used a combination of new 3D μCT images and existing published data (Manton, 1954; 1956; 1958; 1961; Demange, 1967; Wilson, 2002; Akkari *et al.,* 2015; Zahnle *et al.,* 2022) as our sources for anatomical data. For each of the newly imaged gonopods as well as the gonopods of *Ommatoiulus avatar* Akkari & Enghoff, 2015, we provide descriptions of the skeletomuscular anatomy.

For each included taxon, we generated four anatomical networks. One network modeling skeletal organization was generated for each appendage type (gonopod complex or walking legs). In addition, a network modelling muscle organization was generated for each appendage type. A variety of network measurements were calculated for each network, and were interpreted as proxies for biological complexity, integration, anisomerism, and modularity in the anatomy of millipede appendages (Rasskin-Gutman & Esteve-Altava, 2014; Molnar *et al.,* 2017; Arnold *et al.,* 2017; Esteve-Altava *et al.,* 2018). These network measurements were mapped onto the tips of the most recent existing millipede phylogeny (Rodriguez *et al.,* 2018) and used as the basis for continuous ancestral character estimation.

Using AnNA, we address the following questions. (1) Do gonopods in more closely related taxa share similar organization (phylogenetic signal)? (2) Are there substantial developmental constraints limiting evolvability of gonopods? (3) Can copulatory function be linked to specific changes in gonopod

organization? Specifically, are particular gonopod configurations associated with changes in gonopod organization?

## Materials & Methods

*Taxon Selection*

In total, ten millipede taxa were selected for AnNA (Table S1). Our goal in selecting taxa for imaging and anatomical network analysis was to represent the macroevolutionary diversity in gonopod-bearing millipedes (Helminthomorpha). We chose the order as the taxonomic level of study. This is due to the deep evolutionary divergences between orders (Shear & Edgecombe, 2010; Rodriguez *et al*., 2018) and the relative morphological stasis within orders (Liu *et al.,* 2017; Wesener & Moritz, 2018; Jiang *et al.,* 2019; Stoev *et al.,* 2019; Moritz & Wesener, 2019; 2021). We were able to include representatives of every helminthomorph order except Platydesmida and Siphoniulida. The gonopods of Platydesmida are similar in organization to those of Polyzoniida and so were not prioritized. The skeletomusculature of Siphoniulida would have been a valuable inclusion, but was ultimately excluded due to inadequate 3D imaging resolution owing to its very small size. Nine helminthomorph orders were included in our AnNA. The order Spirostreptida was represented by two taxa, the suborders Spirostreptidea and Cambalidea. Therefore, the total count of included taxa is ten.

The existing literature was consulted in order to include AnNA of walking legs for these ten taxa. Morphological data from multiple sources (Manton, 1954; 1956; 1958; 1961; Demange, 1967; Wilson, 2002; Zahnle *et al.,* 2022) was compiled and used to construct networks for AnNA (Table S1).

*Identifying Body Rings and Appendage Pairs*

The anteriormost body ring in millipedes is immediately posterior to the head. It consists of a tergite called the collum and a sternite called the gula, with each isolated from the other. When identifying the body rings of millipedes, it is common practice to label this anteriormost body ring (BR) as body ring 1 (BR1) and assign each succeeding body ring a number in sequence. Because BR1 is legless, the anteriormost leg pair (LP) is associated with BR2, with BR3 and BR4 each bearing one associated LP. Beginning with BR5, each BR bears two LP, including the gonopod-bearing rings BR7 and BR8.

In this paper, we use a LP identification scheme based on the position of the LPs within the BRs. For example, the anterior LP of BR6 is identified as LP6-1 and its posterior LP is identified as LP6-2. We will also use this scheme when referring to the positional identity of gonopods or other appendages modified from the leg pairs, even though such appendages are not leg pairs from a functional perspective. This scheme facilitates easy morphological comparison.

*Morphemes*

Morphemes are the smallest fundamental unit used for describing skeletomusculature in this paper (*sensu* Richter & Wirkner, 2014). We used morphemes as an organizational tool to discretize the component skeletal and muscular parts of appendages and describe the organizational relationships between these parts (referred to as "morphological element" by Zahnle *et al.,* 2022 with the same meaning as "morpheme"). Organismal anatomy can be conceptualized on multiple spatial and temporal scales, so the appropriate scale for morphemes used in any given study depends on the scale of interest in that study (Richter & Wirkner, 2014). In this paper we investigate the skeletomuscular organization of millipede appendages at the macroevolutionary level. At this scale, the smallest morphological units of interest are compositionally homogenous (or nearly so) and are either spatially disjunct from other morphemes that share the same composition or can be extrinsically identified based on a distinct evolutionary history. In this paper we identify two types of morphemes: the skeletal element (SE) and the muscle. SEs are composed of hardened cuticle, whereas muscles are composed of muscle fibers.

Young (1993) presented a scheme for identifying morphological elements (=morphemes) on a purely descriptive basis. In this scheme, a morphological element is classified as either disjointed or adjoining based on its proximity other elements, and additionally classified as either intrinsically or extrinsically identifiable from other elements based on material composition (Table 1). Any muscle is intrinsically identifiable from any SE based on their contrasting material compositions, regardless of whether the muscle and SE are in close spatial proximity (adjoining) or separated (disjointed). Any two muscles that come into contact (*e.g.* at a closely shared attachment site) are adjoining and extrinsically

identified. If they were not in contact, they would be disjointed and extrinsically identified. Finally, any two SE are likewise extrinsically identified and can be either disjoint or adjoining. Adjoining, extrinsically identified SEs take the form of a single continuous sclerite.

In the cases of adjoining extrinsically identified morphemes (*i.e.* two adjoining SEs or two adjoining muscles), clear consistent criteria for extrinsic identification are required. In the case of adjoining SEs, evidence of a distinct evolutionary history can be used for extrinsic identification. That is to say, an SE may be fused with another SE (combined into a single sclerite) and still be considered extrinsically identifiable if it is not fused to that same SE in another taxon or appendage type. For example, the tracheal apodeme is fused to the sternite in millipede walking legs, but is instead fused to the coxa in some gonopods. Even though we have not found any instance of a freely independent (disjointed, extrinsically identified) tracheal apodeme sclerite, the fact that the tracheal apodeme is fused with a different SE in different appendages establishes its distinct evolutionary history. The justification for identifying homologous SEs in different taxa and appendage types is provided below.

In cases of two adjoining muscles, extrinsic identification relies on their attachment sites of muscles' constituent muscle fibers. Each muscle fiber runs between two skeletal attachment sites, and the collection of all the muscle fibers that share both attachment sites is considered a single muscle. In practice, extrinsic identification is needed when two muscles share one of their two attachment sites, with densely adjoining muscle fibers. The muscle fibers can be traced from their opposite attachment sites as they converge onto the shared attachment site, allowing the adjoining muscle fibers to be identified as belonging to one or the other muscle. In some cases, we describe multiple extrinsically identified muscle morphemes as a single muscle, and describe the extrinsically identified morphemes as subunits of the larger muscle. When constructing networks, each subunit is always encoded as a separate node.

In the morphological descriptions of gonopods, we used several terms that describe inferred muscle function. Attachment sites were classified as origin or insertion based on their functional polarity. That is to say, the origin site is on the stationary sclerite whereas the insertion is on the sclerite which is moved by muscle contraction. This distinction requires a functional judgement as to which sclerite is

stationary during muscle contraction. It cannot be applied for muscles in which neither sclerite remains stationary, for example in transverse muscles that span symmetrical sclerites across the body midline. We only distinguish between origin and insertion sites in text descriptions of muscles; attachment site polarity is not encoded into our anatomical networks.

Morphological descriptions also include classification of muscle function based on the position of their origin sites relative to the appendage motivated by the muscle. If a muscle originates from one of the SEs comprising the moveable appendage (see below), it is considered intrinsic to that appendage. Otherwise, the muscle is considered extrinsic to the appendage because it originates from outside the appendage.

*Homology Comparisons*

The comparison of homologous appendages is fundamental to AnNA. If some networks exclude a morpheme whose homologs are included in other networks (*i.e.*, if a gonopod network includes the tracheal apodeme homolog but a walking leg network excludes the tracheal apodeme) then analysis of the resulting networks is not meaningful.

We identified the most proximal morphemes present in all appendages to ensure homologous comparisons among appendages. In the walking legs as well as in colobognath gonopopds, the most proximal SE of the moveable appendage is the coxa. However, we found that in eugnath gonopods the tracheal apodeme and sternite are often well integrated into the gonopod complex and move with it (see next paragraph). In these cases, the most proximal SEs are the tracheal apodeme and sternite. We therefore determined that the sternite and tracheal apodeme needed to be included into the SE networks for all taxa and appendage types.

This interpretation is justified by the anatomy of the imaged millipede appendages. Although the homologies of many morphemes are unclear between appendage types or across taxa, the identities of the sternite and tracheal apodeme have been established with reasonable confidence (Zahnle *et al.,* 2022). Our confidence is bolstered by the tendency of proximal parts of appendages to be better preserved over

evolutionary and developmental timescales due to the developmental dependence of more distal parts on them (Esteve-Altava *et al.,* 2018).

The sternites and tracheal apodemes were the only homologous SEs that could be identified in both the gonopods and walking legs of all taxa. Because the sternites and tracheal apodemes are the proximalmost SEs of all appendages, we were able to treat all compared appendages as serial or evolutionary homologs of each other.

We used the first and second of Remane's main homology criteria (1952) to infer these homologies. The second criterion states that special qualities shared among structures can be taken as evidence for homology of those structures. In the millipede walking legs, the tracheal apodemes are hollow, elongate endoskeletal structures that serve dual functions. The hollow inside of the tracheal apodeme contains a tracheal trunk that allows gases to pass between the external stigma and smaller tracheal branches that stem from the trunk (Hilken *et al.,* 2015). Simultaneously, the sclerotized outer surface provides attachment sites for skeletal muscles. In the gonopods, tracheal apodemes may either retain their internal tracheation or lose it entirely. However, even when the tracheation is lost, a residual hollowness is retained. This special quality allowed us to identify tracheal apodemes in all investigated appendages.

Remane's first main homology criterion states that the positional relationships of body parts in comparable structural systems can be used to infer their homology. In millipede walking legs, the relationship between the sternite and tracheal apodemes is consistent: one sternite is fused to a pair of tracheal apodemes, each of whose hollow regions open externally at the sites of fusion, which are just lateral to the corresponding leg coxae (Fig. 3A; Manton, 1956).

However, the sternite and tracheal apodemes are often no longer fused in the gonopods. Regardless, their positional relationships in the walking legs inform our expectations of their positions in the gonopods. Even when separated from the sternite, 3D image data have shown that tracheal apodemes are invariably hollow in cross-section, implying that the separated tracheal apodeme is entirely internal to the millipede's body because there is no spiracle present. Similarly, the sternite is inferred to have both an

internal and an external surface, because in walking legs the spiracles need to perforate through the sternite's external surface to reach the tracheal apodemes. Therefore, even highly modified gonopod tracheal apodemes and sternites can be identified because the former is always hollow and completely enclosed in the body, and because the latter has at least part of its surface exposed externally. This is even true in gonopods that entirely lack spiracles (Fig. 3B) and therefore lack any respiratory function.

*Morpheme Labeling Scheme*

Whereas sternites and tracheal apodemes were identifiable throughout the gonopods included in this paper, this was not true of most other morphemes, especially in the highly modified eugnathan gonopods. For this reason, we developed an alphanumeric labeling scheme for gonopod morphemes that is not informed by each morpheme's evolutionary or developmental history.

Each paired or single SE in a eugnathan gonopods was assigned an alphanumeric label (*e.g.,* A1, A2, etc.). Gonopod SEs were grouped based on which appendage pair they belong to. Group A comprises SEs present in the anterior appendage pair of the gonopod complex, whereas group P comprises SEs from the posterior pair. SEs in millipede taxa with gonopods derived from only a single pair of appendages belong to group A.

The letter is followed by an arbitrarily assigned number. The tracheal apodeme and sternite are always assigned unique labels regardless of whether they are fused to other SEs because we can be certain of their identities. For all remaining SEs, we assign a unique label to each sclerite. Although this approach risks overlooking distinct SEs that are fused together in the distal sections of the gonopods, it was deemed necessary in order to avoid including purely speculative SE. For taxa in which the pleurotergite is fused to the sternite (*i.e.,* Polydesmida & Juliformia) the sternite is still treated as a separate SE.

In Polydesmida there is no suture or other intrinsic demarcation between the anterior and posterior sternites of each body ring, nor is there a demarcation between the sternites and the pleurotergite. We therefore used an intuitive definition in which the sternites of Polydesmida comprise the ventral quarter of each body ring (Fig. 4A). The demarcation between anterior and posterior sternites was

defined laterally as the posterior edge of the anterior coxa and medially as the transverse furrow between sternal bulges (Fig. 4B; Manton's "ventral dilations of the pedigerous lamina", 1954). This definition accounts for the anterior position of the posterior leg pair's spiracle, halfway between the anterior and posterior coxae. According to this definition of the sternite, the ventral quarter of the prozonite is part of the anterior sternite, including the anterior ventral band of BR7 just anterior to the gonopod.

Unlike in eugnathan gonopods, the homologies of colobognathan gonopod SEs to walking leg SEs were easily established. The walking leg SE names are used when referring to colobognathan SEs, so the alphanumeric scheme is unnecessary.

Each paired or single muscle was assigned an alphanumeric label similar to those given to SEs (*e.g.,* E1, E2, etc.). Paired muscles were grouped based on their origin and insertion sites relative to the gonopod complex appendage pairs. Groups E and F contain muscles that originate from SEs outside the gonopod complex (extrinsic to gonopod), with insertions onto SEs of the anterior gonopod appendage pair (group E) or onto SEs of the posterior pair (group F). Muscles in groups I and J originate from SEs that belong to the gonopod complex. Group I muscles are intrinsic to the anterior gonopod appendage pair and group J muscles are intrinsic to the posterior pair. Group K contains muscles with an attachment site on one SE from each gonopod appendage pair, which could be considered as either intrinsic to the gonopod complex as a whole or as extrinsic to both appendage pairs.

The muscles within each group are assigned an arbitrary number. In colobognath gonopods, some of the muscles were also identified as serial homologs of walking leg muscles. In such cases, this is stated explicitly in the muscle description.

Any transverse muscle is given the label T (there were no instances of a gonopod complex with multiple transverse muscles).

Note that defining the sternites and tracheal apodemes as part of the gonopod complex results in muscles that originate from either a sternite or tracheal apodeme being labelled as intrinsic muscles. This definition is counterintuitive when applied to walking legs or colobognathan gonopods, in which the sternite and its accompanying tracheal apodemes are typically considered as part of the body ring.

For purposes of muscle attachment sites, the pleurite and tergite are always treated as a single SE, even for taxa in which they are not fused (*i.e.,* Polyzoniida & Siphonophorida; Fig. 4C). This avoids the need to define separate attachment sites for taxa in which the pleurite and tergite are fused with no intrinsic differentiation.

*Network Construction*

We used the identified morphemes to construct forty networks for AnNA. The morphemes identified through the process described above were used as the nodes for these networks. For each of the ten taxa included in our analyses (see Table S1 for list of taxa), we constructed four networks. These four networks were differentiated by appendage type (walking legs or gonopod complex) and by node type (SE or muscle). Our broad taxonomic selection includes representatives of most gonopod-bearing millipede orders, allowing our downstream AnNA to show macroevolutionary trends. Furthermore, our choice of network types facilitates comparisons between gonopods and walking legs as well as between skeletal and muscular anatomy.

The process used to construct the networks follows the methods of Esteve-Altava *et al.* (2018). Loosely speaking, this involves construction of two different network types: skeletal networks and muscular networks. In a skeletal network, nodes represent skeletal components (defined in this paper as SEs) and edges represent articulations or other close physical associations of the nodes. In a muscular network, nodes represent muscles and edges represent attachment sites shared by linked muscles (Fig. 5).

In some of the networks we encoded, only one pair of appendages was represented. In the SE and muscle networks for the gonopods of the orders Callipodida and Polydesmida this was due to the gonopod complex only occupying LP7-1, with LP7-2 being a normal walking leg pair. In these four networks, the values of N and K were doubled for AnNA to approximate the values as if there were two gonopod appendage pairs. The same correction was applied to the walking leg muscle networks the orders Spirobolida, Julida, and Polydesmida because the lack of connectivity between muscles of the anterior

and posterior leg pairs led to multiple non-connected networks being modeled. In all three networks, the largest single network was retained with any other networks being excluded from AnNA.

*Network Analyses and Ancestral State Reconstruction*

Seven network measurements were generated for AnNA (Tables 2-3). These are number of nodes (N), number of edges (K), density of edges per node (D), local clustering coefficient (C), longest path length (L), node degree heterogeneity (H), and parcellation (P). The calculation for P requires the nodes be divided up into modules, which was done by running the spinglass algorithm for 500 spins in the igraph package for R. Each measurement was tested for phylogenetic signal (Table 4) and mapped onto the millipede phylogeny (Figs. 6-7, S1-4).

Because any two muscles can share both attachment sites, it is possible for nodes in a muscle network to be connected by two edges, resulting in a weighted network. When calculating network measurements for each muscle network, we used an unweighted version of the network. The weighted version was only used for determining the number of modules via the spinglass algorithm (this follows the methods of Esteve-Altava *et al.,* 2018).

We used a modified version of the most up to date millipede phylogeny (Rodriguez *et al.,* 2018). The original tree was pruned and converted into an ultrametric tree using chronopl in the R package ape (Paradis *et al.,* 2004). Ten terminal taxa were retained corresponding to the ten taxa that we modelled as networks. For each combination of appendage type (gonopod or walking leg), network type (SE or muscle), network measurement, we performed the Blomberg's K test (Münkemüller *et al.,* 2012) and mapped ancestral character state using the R package phytools (Revell, 2012).

Some appendage type/network type/network measurement combinations were excluded from AnNA for practical reasons. N from walking leg SE networks was excluded because all such networks had the same number of SE nodes (38 in all taxa). C from all SE networks was excluded because three SE networks (gonopods of Siphonophorida & Spirobolida, walking legs of Polyzoniida) produce meaningless C values of zero.

The network measurements from each appendage type and network type were visualized by mapping them onto the pruned ultrametric millipede phylogeny. Continuous ancestral character estimation was performed using the contMap function in phytools (Figs S1-S4). The continuous character states were also mapped using the phenogram function in phytools, with ancestral state values being estimated using maximum likelihood (Figs. 6-7). In these trees, the tips are colored according to gonopod configuration. There are four configurations observed in the gonopod-bearing millipedes: (1) gonopod complex comprises LP7-2 and LP8-1, with sperm transfer at LP7-2; (2) gonopod complex comprises LP7-1 and LP7-2, with sperm transfer at LP7-2; (3) gonopod complex comprises LP7-1 and LP7-2, with sperm transfer at LP7-1; (4) gonopod comprises LP7-1. Closely related millipede orders do not necessarily share the same gonopod configuration. Shared gonopod configuration may indicate developmental or functional similarities among distantly related taxa. Phenograms are presented so as to facilitate comparison among taxa, gonopod configurations, appendage types, and network measurements.

**Results**

*Gonopod Skeletomusculature Descriptions*

Siphonophorida: Siphonophoridae: *Siphonophora* sp. (Figs. S5-S6)

• Skeletal elements

Each appendage pair in *Siphonophora* is essentially similar in organization. Each leg pair and gonopod pair consists of a ventral sternite fused to paired tracheal apodemes, with the distal podomeres emerging ventrally from the sternite.

Each sternite is a fully separate sclerite, connected to the preceding and succeeding sternites with a membranous sheet as well as to the flanking pleurites. The sternite forms an arch along the ventral quarter of the body, with two coxae emerging from transversely ovoid gaps. The coxae do not contact each other, being separated by a median strip of the sternite. The edges of the sternite extends dorsally in the form of a transversely oblong rectangle, more than twice as wide as it is long.

As in the walking legs, the gonopod tracheal apodemes in *Siphonophora* are fused to the sternite. The tracheal apodemes are basally fused to external stigmata, which form at the posterolateral corners of the sternite. Within the body cavity, the tracheal apodemes extend dorsomedially and slightly anteriorly. Distally, each tracheal apodeme expands along the anterior-posterior axis into a dorsoventrally flattened lamella. The lamellae are fused anteriorly and posteriorly onto the respective dorsal rims of the sternite, as well as being fused medially to each other. The distal lamellae dorsally enclose the boxlike sternite, and are well supported with three rigid attachment points to the sternite. The tracheal apodemes are internally hollow except at the distal extremities of their lamellae, and presumably retain full tracheal function in the gonopods.

In the gonopod appendage pairs, the anterior gonopod (LP7-2) is smaller than the posterior gonopod. The anterior gonopod coxa is around half the thickness of the posterior gonopod coxa along the anterior-posterior axis. Neither gonopod appears to have any remnant of the trochanter, but all other podomeres from the coxa to the tibia are present. The anterior gonopod additionally has a tarsus distal to the tibia. In overall shape, both gonopod pairs arc posteroventrally. The curve of the anterior gonopod is

more acute, such that the tarsus extends nearly posteriorly and slots into longitudinal grooves along the ventromedial surface of the posterior gonopod tibia. Each podomere forms a full ring between the podomeres directly basal and distal to itself, aside from the terminal podomeres (tarsus of anterior gonopod and tibia of posterior gonopod) which are subconical.

• Extrinsic muscles inserting onto sternites and tracheal apodemes

There are two paired ventral longitudinal muscles linking successive appendage pairs, which are unmodified in the gonopod appendage pairs. The first is identified as E1 between the anterior and posterior sternites of BR7 (LP7-1 & LP7-2), as K1 between the gonopod sternites (LP7-2 & LP8-1), and as F1 between the anterior and posterior sternites of BR8 (LP8-1 & LP8-2). E1, K1, and F1 are oriented longitudinally with fibers that attach along the anterolateral projections of the sternites ("sternite apodemes" of Manton, 1961). The other ventral longitudinal muscle pair is identified as E2, K2, and F2 and connects each sternite to the tracheal apodeme pair of the succeeding sternite. The sternal attachment site is medial of the E1/K1/F1 attachment site. For example, K2 attaches to the posterior surface of the anterior gonopod sternite (LP7-2) just medial to K1 and passes posteriorly to attach onto the anterior surfaces of the posterior gonopod tracheal apodemes (LP8-1).

Four pairs of muscles originate from the BR7 and BR8 tergites and pass ventrally to the gonopod sternites and are unmodified from the corresponding muscles present in the walking legs. Muscles E3 and F3 are closely associated, both originating halfway along the length of the BR7 tergite and passing ventromedially to their respective insertion sites. E3 inserts onto the posterolateral corner of the anterior gonopod sternite (LP7-2) and F3 inserts onto the anterolateral corner of the posterior gonopod sternite (LP8-1). Muscles E4 and F4 originate from near the anterior rim of the BR8 tergite, just behind its prophragma. E4 passes ventromedially and slightly anteriorly to its insertion at the posterolateral corner of the anterior gonopod sternite, whereas F4 passes ventromedially and slightly posteriorly to its insertion at the posterolateral corner of the posterior gonopod sternite.

An additional three pairs of muscles originate from the BR7 and BR8 pleurites and pass more or less dorsally to the gonopod sternites. Corresponding muscles insert onto the sternites of the walking legs. Muscles E5 originates near the anterior rim of the BR7 pleurite and passes posteromedially to its insertion at the lateral rim of the posterior gonopod sternite (LP7-2). The muscle fibers that comprise F5 converge from their dispersed origin sites near the posterior rim of the BR7 pleurite and pass dorsally to their insertion at the anterolateral corner of the posterior gonopod sternite (LP8-1). Finally, muscle F6 originates halfway along the length of the BR8 pleurite and passes dorsomedially and slightly anteriorly to the posterolateral corner of the posterior gonopod sternite.

• Muscles originating from sternites and tracheal apodemes

Both gonopods include a muscle that originates from the sternite and inserts onto the coxae, neither of which correspond to any muscle in the walking legs. I1 originates along the lateral surface of the anterior gonopod sternite (LP7-2) and passes ventr omedially to its insertion at the anterolateral rim of the anterior gonopod coxa. J1 similarly originates along the lateral surface of the posterior gonopod sternite (LP8-1) but passes ventromedially to its insertion at the posterolateral rim of the posterior gonopod coxa.

The tracheal apodemes of each appendage pair, including the gonopods, are the origin site for numerous muscle fibers which variously converge onto insertion sites along the anterior and posterior rims of the left and right coxae. The origin sites of the muscle fibers are dispersed and result in frequent interdigitation of muscle fibers. We group these muscle fibers into four muscle pairs based on their insertion site and whether they are chiasmatic.

Muscles I2 and I3 insert onto the anterior rim of the anterior gonopod coxa (LP7-2). Similarly, J2 and J3 insert onto the anterior rim of the posterior gonopod coxa (LP8-1). Muscles I2 and J2 pass ventrally from the tracheal apodeme to the coxa of the same side, whereas I3 and J3 pass medioventrally from the tracheal apodeme and cross over to insert onto the opposite coxa.

Muscles I4 and I5 insert onto the posterior rim of the anterior gonopod coxa (LP7-2), with J2 and J3 inserting onto the posterior rim of the posterior gonopod coxa (LP8-1). I4 and J4 pass ventrally from the tracheal apodeme to the coxa of the same side, whereas I5 and J5 pass medioventrally from the tracheal apodeme and cross over to insert onto the opposite coxa.

• Muscles originating from coxae, prefemora, and femora

The coxa of the anterior gonopod (LP7-2) is the origin site for three muscles which insert onto the prefemur and femur. I6 originates from the anterodorsal corner of the anterior gonopod coxa and passes ventromedially to its insertion along the medial rim of the prefemur. I7 originates from an anterodorsal flange of the coxa and passes ventrolaterally to its insertion along the lateral rim of the femur. I8 originates from a similar posterodorsal flange of the coxa and passes ventrally to its insertion along the medial rim of the femur.

Three corresponding muscles originate from posterior gonopod coxa (LP8-1). J6 originates from the anterodorsal rim of the coxa, passing ventrally to insert along the anterior rim of the prefemur. J7 originates just medial to J6 and extends ventrally through the prefemur to insert at the lateral rim of the femur. J8 originates from a posterodorsal flange of the posterior gonopod coxa to pass ventrally through the prefemur and inserts at the medial rim of the femur.

An additional two muscles originate from the anterior gonopod femur, both passing through the postfemur and inserting onto the tibia. I9 originates from the lateral surface of the femur and passes ventromedially to its insertion at the posterior rim of the tibia. I10 also originates from the lateral surface of the femur, just anterior to I9, and passes medially to its insertion at the anterior rim of the tibia.

Finally, two muscles originate from the posterior gonopod femur, but neither insert onto the tibia. Instead, J9 passes anteriorly from its origin along the anterior surface of the femur to insert along the dorsal rim of the postfemur. J10 originates just ventral to J9 and also passes anteriorly but extends through the postfemur and tibia to insert onto the needle-shaped tarsus.

Polyzoniida: Hirudisomatidae: *Octoglena bivirgata* (Figs. S7-S8)

• Skeletal elements:

Each appendage pair in *Octoglena* is essentially similar in organization. As with *Siphonophora,* each leg pair and gonopod pair consists of a ventral sternite fused to paired tracheal apodemes, with the distal podomeres emerging ventrally from the sternite.

Viewed from the anterior, each sternite is a fully separate crescent-shaped sclerite along the ventral quarter of the body. It is a more or less vertical plate, forming the anterior edge of each appendage pair. Except where the coxae interrupt it on either side of the midline, the sternite's vertical plate curves posteroventrally, so that it meets the anterior edge of the succeeding sternite plate. Between the midline and lateral ends, the sternite is constricted to a narrow band to accommodate the coxae on its posterior side. From the midline of the sternite, an apodematic keel projects dorsally toward the center of the body. Unlike in *Siphonophora,* the tranversely ovoid gaps that accommodate the coxae are only enclosed on three sides – anterior, lateral, and medial – by the corresponding sternite. The posterior side of each coxa is instead in contact with the anterior edge of the succeeding sternite.

As in the walking legs, the gonopod tracheal apodemes in *Octoglena* are fused to the sternite. The tracheal apodemes are basally fused to external stigmata, which form at the anterolateral corners of the sternite. Within the body cavity, the tracheal apodeme extends dorsomedially as a large trunk. This trunk subsequently divides into a thick lateral branch which extends dorsally and slightly posteriorly, as well as an elongate medial branch.

The exception to this arrangement is the posterior gonopod sternite (LP8-1), in which the sternite is divided into three separate sclerites. The central portion is similar to that in the other appendage pairs, but the constricted band on either side of the middle plate tapers entirely to nothing. As a result, the two lateral plates and their tracheal apodemes each become a separate sclerite.

In the gonopod appendage pairs, the anterior and posterior gonopods are subequal in size. Both contain all the walking leg podomeres except the trochanter and claw. Both gonopods curve more or less ventromedially. The anterior gonopod (LP7-2) gradually curves anteriorly in its distal podomeres, but the

posterior gonopod (LP8-1) curves dramatically to the anterior. The anterior gonopod coxa (LP7-2) extends ventrally into a prominent lobe flattened along the anterior-posterior axis. As in *Siphonophora,* the terminal podomeres (both tarsi in *Octoglena*) are approximately conical. The posterior gonopod tarsus (LP8-1) is elongate and slots into a longitudinal groove in the anterior gonopod tarsus (LP7-2). The tip of the anterior gonopod tarsus curves laterally and clasps around the medial side of its coxa's ventral lobe.

Most podomeres form a full ring between the podomeres directly basal and distal to themselves, with the following exceptions. The posterior gonopod coxa (LP8-1) only halfway encloses the appendage, forming an anterior plate. The anterior gonopod prefemur (LP7-2) likewise encloses the appendage only partway, leaving the medial side open. For their part, the anterior gonopod coxa (LP7-2) and posterior gonopod prefemur (LP8-1) only enclose their respective appendages by a very narrow ring of cuticle.

• Extrinsic muscles inserting onto sternites and tracheal apodemes:

There are two paired longitudinal muscles linking successive tracheal apodemes, which are unmodified in the gonopod appendage pairs. They are identified as E1 and E2 between the anterior and posterior tracheal apodemes of BR7 (LP7-1 & LP7-2), as K1 and K2 between the gonopod tracheal apodemes (LP7-2 & LP8-1), and as F1 and F2 between the anterior and posterior tracheal apodemes of BR8 (LP8-1 & LP8-2). Whereas E1, K1, and F1 are oriented longitudinally with fibers that attach along both the lateral and medial branches of the tracheal apodemes, muscles E2, K2, and F2 are oriented obliquely such that they proceed posterolaterally from the medial branch of each tracheal apodeme to the lateral branch of each succeeding tracheal apodeme.

Three pairs of muscles originate from the BR7 and BR8 tergites and pass ventrally to the gonopod appendage pairs. E3 passes ventrally from its dorsal origin halfway along the length of the BR7 tergite to its insertion at the posterolateral corner of the anterior gonopod sternite (LP7-2). In the walking legs, the muscle corresponding to E3 additionally inserts onto the nearby anterolateral corner of the succeeding sternite, but there is no corresponding insertion site in the posterior gonopod sternite. Muscles E4 and F4 originate together just anterior to the halfway point along the length of the BR8 tergite, and

proceed anteroventrally to their insertion sites. E4 inserts onto the lateral branch of the anterior gonopod tracheal apodeme (LP7-2) while F4 inserts onto the posterolateral corner of the posterior gonopod sternite (LP8-1). Both E4 and F4 correspond to muscles in the walking legs.

An additional four pairs of muscles originate from the BR7 and BR8 pleurites and pass more or less medially to the lateral branches of the gonopod tracheal apodemes. Corresponding muscles insert onto the tracheal apodemes of the walking legs. Muscles E5 and F5 pass posteromedially in parallel to their insertions onto the tracheal apodemes of the anterior and posterior gonopods, such that E5 originates at the anterior rim of the BR7 pleurite and F5 originates halfway along the length of the same pleurite. Muscles E6 and F6 originate halfway along the length of the BR8 pleurite, with E6 passing anteromedially to its insertion on the anterior gonopod tracheal apodeme (LP7-2) and F6 passing roughly medially to its insertion on the posterior gonopod tracheal apodeme (LP8-1).

• Muscles originating from sternites and tracheal apodemes:

Each coxa receives a chiasmatic muscle pair that originates from the preceding appendage's tracheal apodeme. The E7 muscles originate from the tracheal apodemes of the BR7 anterior walking leg pair and pass ventromedially, crossing over each other to insert at the anterior edges of the anterior gonopod's (LP7-2) coxae. The K7 muscles are the corresponding muscle pair that originates from the anterior gonopod tracheal apodemes and insert onto the posterior gonopod coxae (LP8-1).

The K8 muscle pair originates medially along the anterior surface of the posterior gonopod sternite (LP8-1), passing anterolaterally to the posterior edges of the coxae. It lies ventral to K7 and anterior to J3. Muscle K8 is unique to the gonopod complex; there is no corresponding muscle in the walking legs.

Both gonopod appendage pairs contain a muscle pair with origin sites at the posterolateral corners of their respective sternites. Muscle I5 passes ventromedially from its origin to the posterior edge of the anterior gonopod coxa (LP7-2). Muscle J5 passes ventromedially from its origin to the posterior edge of the posterior gonopod prefemur (LP8-1), since the posterior gonopod coxa is an incomplete ring that only

spans the anterior half of the posterior gonopod. Neither I5 nor J5 correspond to any muscle in the walking legs.

Muscles I1, I2, and J1 originate from the medial branches of the gonopod tracheal apodemes. I1 and I2 originate from the anterior gonopod (LP7-2) tracheal apodeme, with I1 lying anterior to I2. Both muscles pass ventrally, with I2 inserting onto the posterior rim of the anterior gonopod prefemur and I1 inserting onto the posterior rim of the femur. J1 in the posterior gonopod corresponds to I1 in the anterior gonopod. It originates from the posterior gonopod (LP8-1) tracheal apodeme and inserts ventrally onto the femur.

Each gonopod contains two muscle pairs that originate medially from the sternite and insert onto the coxae. I3 and J3 originate from the dorsal process along the midline of the sternite ("sternite apodeme" of Manton, 1961), passing ventrolaterally to insert onto the anterior rim of their gonopods' resepctive coxae. Muscles I4 and J4 incorporate muscle fibers that originate along the sternite apodeme and along the dorsal surface of the sternite lamina along the ventral midline that separates the coxae. I4 and J4 pass laterally to insert onto the posterior rim of their gonopods' respective coxae.

• Muscles originating from coxae, prefemora, and femora:

Anterior and posterior gonopod coxae are the origin sites for two muscles which pass posteroventrally from their attachment sites on the anterior surfaces of the coxae and insert onto their respective femora. Muscles I6 and J6 insert onto the medial rims of their femora, whereas I7 and J7 insert onto the lateral rims of their femora.

Both gonopod prefemora are the origin sites for femoral muscles. I8 and J8 pass anteroventrally from their origins on the posterior surfaces of the prefemora and insert onto the posteromedial margins of their respective femora. J9 is an additional femoral muscle exclusive to the posterior gonopod (LP8-1). It passes medially from its origin on the anterolateral surface of the posterior gonopod prefemur to its insertion onto the medial rim of the posterior gonopod femur.

The remaining ten muscles intrinsic to the gonopods all originate from the femora. In the anterior gonopod, muscles I10 and I11 originate from the posterior surface of the femur and pass medially to insert onto posterior rims of the postfemur and tiba, respectively. The corresponding muscles in the posterior gonopod (J10 and J11) originate from the posterodorsal surface of the femur and pass anteriorly to insert onto the dorsomedial rims of the postfemur and tibia.

Finally, muscles I12, I13, and I14 all originate from the anterior surface of the femur and pass anteromedially to their insertions along the anterior rims of the postfemur, tibia, and tarsus, respectively. The corresponding muscles in the posterior gonopod (J12, J13, and J14) originate from the posterolateral surface of the femur, passing anteriorly to their insertions onto the lateral rims of the postfemur, tibia, and tarsus, respectively.

Callipodida: Tynommatidae: *Tynomma mutans* (Figs. S9-S10)

• Skeletal elements

The gonopod complex of Callipodida incorporates only the anterior appendage pair of BR7 (LP7-1). It comprises just three SE. A2 and A3 are fused into a single paired sclerite. The obvious external feature of this sclerite is the thick ventral extension of A3 which is the sperm-transferring branch of the gonopod. This extension terminally divides into lateral and posterior branches. The posterior branch flares out into a vertical lamella with a process emerging from its lateral surface. This process further branches into two further narrow processes. The seminal canal runs along the lateral side of A3 from its base, terminating at the tip of the ventral branch of the narrow processes.

A1 is a single central triangular sclerite hinged onto A3 via its lateral bases. The triangular shape of A1 and the position of this single central sclerite anterior to paired sclerites (A3) is presented as evidence that A1 is the sternite. Sternites of the walking legs in *Tynomma* share the triangular shape, albeit not as enlarged, as well as the position anterior to a pair of coxae.

The dorsally extending flanges of the paired sclerite are considered to be the tracheal apodemes (A2), fused onto the coxae (A3). This interpretation is supported by the hollow tube inside this flange. In fact, the hollowness extends ventrally along a plate bounding the lateral side of A3. Together, A2 and A3 form a concavity such that the ventral portion of this plate is actually exposed medially (part of A3).

• Extrinsic muscles

The *Tynomma* gonopod complex is motivated primarily by six pairs of extrinsic muscles. Two of these muscles, E1 and E2, originate from the tracheal apodeme of the preceding body ring (LP6-2). E1 runs ventrally from its origin to the anterodorsal edge of A1. Muscle E2 instead runs posterodorsally from their shared origin to the dorsal apex of A2.

Of the remaining four extrinsic muscles, all originate from the gonopod-bearing body ring (BR7). E3 originates from the dorsolateral corner of BR7, just behind the prophragma. From this origin E3 runs ventrally to the basal posterior surface of A3. E4 originates from the lateral surface of BR7 and runs anteromedially to the medial plate of A3, along its lateral wall. Muscle E5 originates from the ventromedial extremity of the pleurotergite (the medial ventral section of the BR7 is occupied by the gonopod complex). E5 runs dorsally from its origin to the dorsal apex of A2, passing just posterior to muscle E4 perpendicular to it. Finally, E6 originates from the succeeding tracheal apodeme (LP7-2) and runs anterodorsally to the basal posterior surface of A3, ventral to the insertion site of E3.

• Intrinsic and transverse muscles

There are two intrinsic muscle pairs and a single transverse muscle in *Tynomma.* The transverse muscle, T, attaches to the dorsolateral corners of A3. Muscle I1 is especially thick, with fanlike insertions all along the dorsolateral rims of A2 and A3. The muscle fibers of I1 converge anteroventrally onto the dorsal rim of A1. Finally, I2 runs transversely across the inside of A3 from its lateral surface to its medial surface. The attachment sites of I2 are near the base of the sperm-carrying ventral extension of A3. The function of I2 is unknown, since its attachment sites are apparently both on the same sclerite.

Chordeumatida: Conotylidae: *Conotyla* sp. (Figs. S11-S13)

• Summary

In *Conotyla* there are few separately moveable sclerites but numerous muscles. Of the millipedes we examined, *Conotyla* has by far the largest number of extrinsic muscles, with sixteen extrinsic muscles originating variously at the tracheal apodemes of the preceding (LP6-2) and following (LP8-1) leg pairs, the sternite of the following leg pair, the prophragmas of BR7 and BR8, and the lateral and dorsal walls of BR7. Half of these origin sites are on BR7. The large number of muscles with lateral origin sites suggests that *Conotyla* has the ability to rotate the entire gonopod complex around the millipede's longitudinal axis. This is in contrast to other eugnathans in which the extrinsic muscles are limited to extensors and retractors located to the anterior and posterior of the gonopod complex.

The entire gonopod complex is also unusually well integrated. Of the nine intrinsic muscles, four connect the tracheosternal sclerites of the anterior (LP7-1) and posterior (LP7-2) gonopods. This may be a functional constraint imposed by the skeletal simplicity of the chordeumatidan gonopod plan. With so few separately moving articulated sclerites, it is possible that much of the motion required for copulation is performed by the aforementioned extrinsic muscles as well as those intrinsic muscles that span the two gonopods.

There does not appear to be any transverse musculature (an apparent fiber in the *Conotyla* image is asymmetrical and connects the anterior tracheosternal sclerite to itself, so we have dismissed it).

In contrast to the more proximal sclerites, the two distal sclerites of the posterior gonopod (LP7-2) appear to have very few movement options. There is one thin muscle that spans the two sclerites, but we couldn't find any muscle connecting these two sclerites to the otherwise very well integrated proximal sclerites. This thin muscle appears to flex the more distal sclerite medially. The primary function of these two sclerites seems to be glandular, with almost all the internal space occupied by a large gland with a pore opening to a basal sclerite.

The *Conotyla* gonopod complex comprises six sclerites apparently representing eight skeletal elements, as well as twenty-six muscles.

• Skeletal elements

Of these six sclerites, two belong to the anterior gonopod (LP7-1) and four to the posterior gonopod (LP7-2). In both gonopods the tracheal apodemes remain well developed and are not extensively modified from the original walking leg. The anterior tracheal apodeme (A1) is partially hollow but without an external stigma, whereas the posterior tracheal apodeme (P1) is hollow throughout and retains its stigma. Therefore, the posterior tracheal apodeme likely functions as part of the tracheal system. The presence of a lateral pore to allow tracheal radiation provides additional corroborating evidence.

The paired tracheal apodemes of both gonopod pairs (A1 & P1) are ventrally fused to a medially connected sternite. In the anterior gonopod, this is reduced to a transverse bar (A2), whereas in the posterior gonopod the sternite also includes a deltoid plate that projects posteriorly from the transverse bar (P2). This sternal plate is positioned medially between the paired coxites of the posterior gonopod.

In the anterior gonopod, there is one paired sclerite distal to the tracheosternite, considered to be the coxite (A3). It extends ventrally from the sternite, which provides the coxite with a single condyle at its lateral base.

The posterior gonopod has three paired sclerites, each articulating in series. The proximalmost sclerite is considered the coxite (P3), followed by the prefemur (P4) and femur (P5). The posterolateral corners of the deltoid sternal plate (P2) function as the single condyle for each posterior coxite (P3). In contrast to the anterior coxite (A3), whose condyle is at its lateral base, the posterior coxite's condyle is at its medial base. The bulk of the posterior coxite projects ventrally and intertwines with the anterior coxite, with the anterior coxite enfolding the posterior coxite laterally. The articulation site between the posterior coxite and prefemur is at the coxite's lateral base and is circular. The inside of the coxite communicates with the hoemocoel via a narrow slitted constriction.

The postfemur (P4) and femur (P5) of the posterior gonopod are similar in construction to the walking leg podomeres. However, they arc dorsally rather than ventrally, and have very little internal musculature. Most of the volume of both sclerites and the basal portion of the coxite are occupied by a

continuous sac, probably a gland. However, it is unclear where this gland debouches. The trochanter is not apparent. The presence of a muscle connecting the prefemur and femur supports this interpretation, since the trochanter does not carry any muscle attachment points (Boxshall, 2004).

• Muscles

The twenty-six muscles include sixteen extrinsic and ten intrinsic muscles. Due to the large number of muscles, we have listed each individually for clarity. Seven extrinsic muscles insert onto the anterior gonopod (LP7-1, group E) and nine to the posterior gonopod (LP7-2, group F). Of the ten intrinsic muscles, four are intrinsic to the gonopod complex but extrinsic to each individual gonopod (group K), two are intrinsic to the anterior gonopod (group I), and four are intrinsic to the posterior gonopod (group J).

• Anterior gonopod (LP7-1) extrinsic muscles:

E1: Originates at the preceding tracheal apodeme (LP6-2) on its medial surface. Proceeds medioventrally, with the paired muscles crossing each other medially. Inserts at medial base of A3.

E2: Originates at ventral base of preceding tracheal apodeme (LP6-2), very near to its fused connection with its sternite. Origin is along the anteromedial surface of the apodeme and along its anterior crest. Proceeds anteriorly and inserts onto A1 along its posterior surface. The insertion is near the fused connection between A1 and A2. SE A1 has a lateral flange that acts as an insertion point for part of E2. There is also a creased ridge along the anterior surface of A1 that is roughly parallel to the lateral flange, but medial to it. E2 is a one of the thickest gonopod muscles.

E3: Originates at preceding tracheal apodeme (LP6-2) on its posterior and lateral surfaces. Proceeds anteriorly and inserts onto A1 along its anterolateral surface near its dorsal apex.

E4: Originates along the dorsolateral rim of the BR7 prophragma. The exact origin site is cut off from the 3D image, so it is unclear whether it inserts along the anterior or posterior surface of the prophragma. The muscle proceeds ventrally to its insertion along the dorsal apex A1. At its apex, A1 is

linear in cross-section, with a hollow posterolateral corner and proceeding as a solid sheet to an anteromedial corner, with a creased ridge on its anterolateral side. E4 inserts along the tip of this sheet and along the creased ridge.

E5: Originates along the interior surface of the BR7 prozonite, on its lateral side. Proceeds ventromedially to its insertion along the lateral side of A1. The insertion site is midway down the length of A1, just ventral to the insertion site of E2.

E6: Originates along the interior surface of the BR7 prozonite, near the ventromedial corner of the BR7 pleurotergal arch. Proceeds dorsally to its insertion along the posterolateral edge of A1. The E6 insertion sites is just posterior to the E3 insertion site.

E7: Originates along the interior surface of the BR7 metazonite, just posterior to the demarcation between prozonite and metazonite. The origin site is near the ventral edge of the pleurotergal arch. Muscle proceeds anteromedially to its insertion along the anterior surface of the lateral flange in A1.

• Posterior gonopod (LP7-2) extrinsic muscles

F1: Originates near the medial midline of the succeeding sternite (LP8-1), along its posterior surface. Proceeds dorsolaterally, with the paired muscles crossing over each other near the origin sites. Inserts along the posteromedial surface of P1. In particular, P1 in cross-section comprises a sheet-like plate extending laterally from its medial corner and turning posteriorly. This posterior corner contains the hollow tracheal pouch, which extends posteriorly and tapers off until it is no longer sclerotized. F1 inserts along the posteromedial surface of this hollow corner.

F2: Originates at the succeeding tracheal apodeme (LP8-1), along its anterolateral surface. The origin site is midway between the dorsal apex of the succeeding tracheal apodeme and its fusion point with its sternite. Muscle proceeds anteroventrally to its insertion onto the posteromedial surface of P1, just ventral to the origin site of F1.

F3: Muscle F3 consists of two subunits with different origin sites on BR8. F3a originates along the interior surface of the BR8 metazonize, just posterior to the demarcation between prozonite and

metazonite. F3b originates along the medial rim of the BR8 prophragma. The origins of both subunits are situated along the lateral side of the BR8 pleurotergal arch. F3a is longer and joins with F3b as it passes near the BR8 prophragma. Both subunits proceed anteriorly to their insertion along a creased fold at the posterior corner of P1. The creased fold runs dorsally from where P1 separates on its posterior brach.

F4: Originates along the anterior rim of the BR8 prophragma. The origin is on the dorsolateral side of the pleurotergal arch. Muscle proceeds anteroventrally to its insertion along the posterior surface of P1. The insertion point for F4 is between the creased fold that serves as the insertion for F3 (lateral to F4 insertion) and the hollow branch for P1 (medial to F4 insertion).

F5: Originates along the interior surface of the BR7 prozonite, just posterior to the prophragma. The origin site is on the lateral side of the pleurotergal arch. The muscle proceeds ventromedially to its insertion along the lateral surface of the ventral base of P1. This insertion site is just dorsal to the fusion point between P1 and P2.

F6: Originates along the interior surface of the BR7 prozonite, just anterior to the demarcation between prozonite and metazonite. The origin site is on the ventrolateral side of the pleurotergal arch. The muscle proceeds dorsally to the insertion along the lateral surface of P1. The insertion site is separated from the anterior surface of P1 by a dorsoventral ridge.

F7: Originates along the interior surface of the BR7 metazonite. The origin site is on the ventrolateral side of the pleurotergal arch. The muscle proceeds anterodorsally to its insertion along the lateral surface of P1. Like F6, its insertion is along and posterior to the crest at the anterolateral corner of P1. The insertion site of F7 is just dorsal to F6, reaching to the dorsal apex of P1.

F8: Originates along the interior surface of the BR7 metazonite. Although the actual origin site is cut off in the available 3D image, by extrapolating its path is appears to originate on the dorsolateral side of the BR7 pleurotergal arch, just posterior to the demarcation between prozonite and metazonite. The muscle proceeds ventromedially to its insertion along the dorsal surface of the posterior hollow tracheal branch in P1.

F9: Originates along the interior surface of the BR7 prozonite. Although the actual origin site is cut off in the available 3D image, by extrapolating its path it appears to originate on the dorsolateral side of the BR7 pleurotergal arch, near but posterior to the prophragma. The muscle proceeds posteroventrally to its insertion along the dorsalmedial surface of P1 at its dorsal apex.

• Gonopod complex intrinsic muscles

K1: The anterior attachment site is the posterior corner of A1 at the dorsal apex. Proceeds posteriorly across the dorsal apex of P1 before arcing ventrally to the posterior attachment site along the posterior corner of P1, just dorsal to the insertion site of F4.

K2: The anterior attachment site is along the posteriolateral corner of A1 ventral to the dorsal apex. Proceeds directly to its posterior attachment site along the anterior surface of P1. The posterior attachment site is just anterolateral to the lateral creased fold of P1.

K3: Originates along the anterior surface of P1, near its dorsal apex. The origin site is just medial to that of K2. Muscle K3 proceeds anteroventrally to its insertion along the posterior surface of A1, roughly midway from the base of A1 to its dorsal apex.

K4: Originates along the posteromedial surface of A1, just near its dorsal apex. The origin site is just ventral to that of E4. Muscle K4 proceeds ventromedially, with the paired muscles crossing each other near the insertion site. Insertion is near the medial centerline of P2 and just anterior to the triangular plate that extends posteriorly from the transverse bar of P2.

• Anterior gonopod intrinsic muscles

I1: Originates along the anterior surface of A1, just medial to the creased fold. Proceeds ventromedially past the transverse bar A2, with the transverse bar anterior to I1. The insertion of I1 is at the anteromedial base of A3 just lateral to the insertion of E1.

I2: Originates at the ventromedial extremity of the sheet-like portion of A1. Proceeds ventrally to its insertion at the posterolateral base of A3.

• Posterior gonopod instrinsic muscles

J1: Originates along the anterior surface of P1, just medial to the creased fold. Proceeds ventromedially past the transverse bar of P2, with the transverse bar anterior to J1. The insertion of J1 is at the anteromedial surface of P3.

J2: Originates along the posterior surface of P1, ventral to the origin sites of F1 and J3. Muscle J2 proceeds posteroventrally to its insertion along the posterior base of P3.

J3: Originates along the posterior surface of P1, dorsal to the origin site of J2 and anterior to that of F1. Muscle J3 proceeds ventromedially and the pair of muscles cross each other at the body's midline. The insertion point of J3 appears to be a tendon that extends to the posterior base of P3, just posterior to the insertion of J2.

J4: This is the only muscle intrinsic to the posterior gonopod which does not insert onto P3. It originates at the anterior base of P4 and proceeds laterally along the main axis of P5 to its insertion at the dorsal base of P5.

• A note on *Conotyla* muscle data

The muscle fibers of several muscles in the *Conotyla* specimen appear to have bunched up or collapsed across the length of the muscle. This is seen most prominently in extrinsic muscles F8 and F9. In both muscles, the fibers near the insertion site are bunched up, appearing like thick blobs. As these muscle are followed toward their origins, the visible portion of the majority of muscle fibers becomes a thin narrow line, with a flattened appearance. These thin collapsed muscle fibers offer little contrast against the background haemocoel, making our standard semi-automated segmentation process ineffective. The cause for these bunched and collapsed fibers is unknown, but could be related to the specimen's preservation history and its age.

Spirobolida: Rhinocricidae: *Eurhinocricus* sp. (Figs. S14-S15)

• Summary

The gonopod complex of Spirobolda consists of two pairs of appendages. In *Eurhinocricus,* the anterior gonopod (LP7-1) has the overall appearance of a more or less vertical plate. The posterior gonopod pair (LP7-2) consists of two slender appendages which fit snugly into sheath-like gaps in the anterior gonopod (this is why the anterior gonopod of Spirobolida is often called the "coleopod"). The close physical association between the gonopod appendage pairs belies the relative lack of skeletomuscular integration shown by skeletal and muscular networks. Both gonopod appendage pairs feature a mixture of extrinsic and intrinsic musculature, but the musculature connecting the two pairs is notably limited to a single muscle pair.

• Skeletal elements

The anterior gonopod (LP7-1) contains five SE which are well-integrated into a large plate, whereas the posterior gonopod (LP7-2) is much simpler with only two SE.

Among the five anterior gonopod SE, A2 alone makes up most of the anterior surface of this plate. A2 is roughly triangular and flat, except at its lateral dorsal corners which extend as a posterior tongue around the lateral base of the gonopod. The hollow rodlike tracheal apodemes, represented by A1, are fused to and project dorsally from these tonguelike plates.

The anterior gonopod's posterior surface is mostly made up of A3 and A4. Of the two, A4 is much smaller. It is a wedge-shaped sclerite along the gonopod's midline. At its base, A4 is fused to the paired A3 sclerites on either side via a flexible cuticle.

A3 is a comparatively complex sclerite, which may be best understood when conceptually subdivided into four subunits. On either side of A4, A3 spreads sheetlike laterally and somewhat anteriorly, forming the posterior wall of the anterior gonopod. This anterior slope creates a longitudinal concavity that the posterior gonopod fits into like a sheath. Dorsally from the posterior wall, A3 narrows

into a muscle apodeme (totally distinct from the tracheal apodeme, A1) which lies entirely inside the body cavity. On the lateral flank of the posterior wall, the A3 sheet spreads posteriorly to laterally enclose the posterior gonopod sheath, before wrapping around the lateral and anterior surfaces of the anterior gonopod. The resulting tubelike structure becomes the ventral base for A5. Both the posterior wall and the base of A5 extend ventrally (distally) into triangular sheets on the posterior and anterior surfaces of the gonopod, respectively. The two triangular sheets converge into a ventral edge which encloses A3 distally.

The final anterior gonopod SE, A5, emerges from A3 as mentioned above. It emerges from the tubelike flank of A3 whose cross-section is wider than long. Consequently, the cross-section of A5 is also wider than long, with A5 being somewhat flattened along the anterior-posterior axis. A5 extends ventrally and slightly medially. It is ventrally enclosed at its distal apex, which features a knoblike lateral projection.

The posterior gonopod (LP7-2) is much simpler in its organization. The tracheal apodeme, P1, is similar in appearance to A1. Both are long, rodlike, and hollow. P1 ventrally articulates with the lateral rim of P2, which is thin and elongate. As P2 extends ventrally, it also arcs gradually to the posterior. It is somewhat flattened at an angle oblique to the body axes. That is to say, its cross-section is longer along the millipede's anterolateral-posteromedial axis than it is along the anteromedial-posterolateral axis.

• Anterior gonopod extrinsic muscles

Among the five extrinsic muscles inserting onto the anterior gonopod (LP7-1), only E3 does not originate from the BR7 pleurotergite. Instead, it originates from the dorsal surfaces of both BR6 tracheal apodemes (LP6-1 & LP6-2). The muscle fibers of both E3 muscle subunits are trunked together as they pass dorsally to their insertion at the dorsal apex of A1.

Of the four muscles originating from BR7, three also insert onto A1. E1 originates from the ventrolateral corner of of the BR7 pleurotergite, roughly halfway along its length. It passes anterodorsally to the posterior surface of A1, near its dorsal apex. The origin site of E4 appears to be the dorsolateral corner of the pleurotergite, but it is cut off in our 3D image. From its origin, it passes ventromedially to its

insertion along the medial surface of A1 near the point of fusion between A1 and A2. Along its path to its insertion, E4 passes just medial to E1. Finally, E5 originates from the lateral pleurotergite along the anterior rim of the prophragma. It passes ventromedially while also arcing anteriorly and then posteriorly, arriving at its insertion along the lateral surface of A1 near where A1 and A2 fuse together. E5 passes just lateral to E3.

The remaining anterior gonopod extrinsic muscle, E2, inserts onto A3. It originates from the ventrolateral corner of the BR7 pleurotergite, just posterior to the E1 origin site. From here it runs anterodorsally before taking a remarkably sinuous path to its insertion. E2 passes dorsally and then arcs anteriorly in order to pass along the interior surface of the retracted gonopod sac membrane. Its insertion site is a transverse ridge near the dorsolateral corner of A3. This ridge emerges laterally from the base of the A3 dorsal apodeme and forms the posterolateral rim of A3.

Anterior gonopod intrinsic muscles

The anterior gonopod contains three intrinsic muscles. I1 originates from the medial surface A1, about midway along its length. It runs ventromedially, with the left and right I1 muscles converging at the midline and inserting at the dorsal end of A4. Muscle I2 originates from the anterior surface of the A3 dorsal apodeme and runs ventromedially, also converging along the midline. Specifically, the posterior surface of A2 bears and apodematic ridge along its midline, which is the insertion site for I2. Finally, the massive I3 muscle originates from the lateral tubelike region of A3, running ventrally to insert along the lateral and anterior basal rim of A5.

• Muscle spanning anterior and posterior gonopods

A single muscle, K, runs between the tracheal apodemes of the anterior and posterior gonopods. At its anterior end, K attaches to the posterior surface of A1 near its dorsal apex. K is very skinny and arcs posterolaterally and then posteromedially to pass laterally around E4. The posterior attachment site for muscle K is along the anterolateral surface of P1.

• Posterior gonopod extrinsic muscles

There are two extrinsic muscles that insert onto the posterior gonopod. F1 originates from the lateral side of the BR8 pleurotergite along the anterior surface of its prophragma. It runs medially and slightly anteriorly to the lateral surface of P1, near the ventral end of P1. F2 originates from the lateral end of the succeeding tracheal apodeme (LP8-1) along is dorsal surface. From here, it runs dorsolaterally along the posterior surface of the gonopod sac membrane. Its ultimate insertion is not visible in our 3D image, but by extrapolating its direction of travel we believe it inserts at the dorsal apex of P1.

• Posterior gonopod instrinsic muscles

There are two intrinsic muscles in the posterior gonopod, both originating from the tracheal apodeme (P1) and inserting at the base of P2. The origin sites of both muscles are cut off from our 3D image, but both run parallel to P1 toward their ventral insertions onto P2. It seems likely that both J1 and J2 originate at or near the dorsal apex of P1. Muscle J1 surrounds P1 on the lateral, posterior, and medial sides, whereas J2 occupies much of the space anterior to P1. J1 inserts at the posterior dorsal rim of P2 and muscle J2 inserts opposite it at the anterior dorsal rim of P2.

Spirostreptida: Cambalidea: Cambalidae: ?*Titsona* sp. (Figs. S16-S17)

• Summary

The *Titsona* gonopod complex is made up of anterior (LP7-1) and posterior (LP7-2) appendage pairs. Each gonopod pair is fairly well integrated by multiple intrinsic muscles. The gonopod complex as a whole is very loosely integrated by muscles, with only one intrinsic muscle connecting the anterior and posterior gonopod. The reduced muscular integration between anterior and posterior gonopod sclerites appears to be the result of increased skeletal integration between the two gonopods.

In particular, A3 of the anterior gonopod and P2 of the posterior gonopod are basally joined with a longitudinal semicircular rib. The longitudinal rib is bisected orthogonally by a transverse semicircular rib. These ribs are probably firm but flexible, similar to tentpoles. Like crossed tentpoles, the orthogonal intersection of the ribs provides stability without rigidity. The crossed orthogonal ribs cause the gonopod complex to move as a concerted unit while still allowing limited independent rotation of anterior and posterior gonopod pairs. The connective membranous integument uniting these “tentpoles” to sclerites A3 and P2 results in a continuous exterior concave space (gonocoel), simultaneously separating the anterior and posterior gonopods as well as the left and right sclerite pairs from each other. This gonocoel is strikingly cruciform in frontal section.

• Skeletal elements

The anterior gonopod (LP7-1) contains three distinct sclerites. A1 and A2 together comprise a wishbone-shaped single sclerite joined ventromedially along the millipede’s midline. The paired dorsolaterally extending prongs (A1) are the tracheal apodemes, and are hollow. Each tracheal apodeme has a subapical branch extending medially which serves as a muscle attachment site. The left and right A1 are medially fused to A2, which forms the ventromedial section of the shared sclerite. The anterior surface of A2 is exposed although its posterior surface faces the inside body cavity. In contrast, A1 is entirely within the body cavity. Based on its position, A2 is interpreted to be the LP7-1 sternite, demarcated from the tracheal apodemes (A1) at the band where the gonopod sac membrane attaches.

The remaining two anterior gonopod SE are both paired. A3 is a bulky sclerite and contains much of the volume of the gonopod complex. It has a pointed distal process at the ventral extremity of its anterior surface as well as a medial distal process at the ventral extremity of its posterior surface. The posterior process extends medially to P3 of the posterior gonopod (LP7-2), interlocking the two gonopod pairs. The sclerotized walls of A3 provide a complete ring, with a dorsal fenestra allowing communication between the anterior gonopod and the body cavity. A2 overlies the medial basal portion of the paired A3 sclerites on their anterior surfaces. This is consistent with the position of the leg pair sternites anterior to the coxa in *Titsona*. Due to the ringlike shape of A3 and its articulation with A2, we interpret A3 as the coxa of LP7-1. A curtain-like membrane extends dorsally from the posterior and medial rims of A3, linking it to the transverse and longitudinal "tentpoles", respectively.

A4 is distal to A3 and articulates with it by a socket on the lateral face of A3. Due to its position distal to A3, A4 may be homologous to the walking leg prefemur. The bulk of A4 extends posteriorly from A3, with a strongly sclerotized lateral wall parallel to a poorly sclerotized medial wall. A4 rotates primarily along a transverse axis.

The posterior gonopod pair (LP7-2) contains two paired sclerites. The basalmost of the two contains two fused SE, P1 and P2. The combined sclerite consists of a dorsoventrally oriented rod (P1) fused to the lateral side of a thin ring (P2). P1 has two branches that split near its dorsal apex, with the medial branch being dorsoventrally flattened into a plate. Basal to the point where it splits into two branches, P1 is hollow. Based on its rod shape and hollowness, we interpret P1 to be the tracheal apodeme of LP7-2.

P2 is a dorsoventrally narrow band. Although strongly sclerotized along its anterior and lateral surfaces, its posterior and medial surfaces are poorly sclerotized. The exterior surfaces of P2 are all exposed and its interior surfaces are all continuous with the body cavity. Distally, P2 articulates with sclerite P3. Based on its ring shape and articulation with P3, we interpret P2 to be the coxa of LP7-2. The fusion of the tracheal apodeme (P1) to the coxa (P2) in the posterior gonopod differs from the pattern seen in the anterior gonopod, in which the tracheal apodeme (A1) is fused to the central sternite (A2) and the

coxite (A3) is a free sclerite. No sternal residue was identified in the posterior gonopod. A curtain-like membrane extends dorsally from the anterior and medial rims of P2, linking it to the transverse and longitudinal “tentpoles”, respectively.

P3 is the distalmost sclerite of the posterior gonopod. Due to its position distal to P2, it may be homologous to the walking leg prefemur. P3 is most strongly sclerotized along its posterior surface, where it interlocks with the posteroventral process of A3. The remaining surfaces of P3 are poorly sclerotized, and it seems to be relatively flexible and amorphous.

• Muscles

There are nineteen gonopodal muscles in *Titsona*, divided between nine extrinsic muscles (groups E & F), nine intrinsic muscles (groups I & J), and one muscle passing between the anterior and posterior gonopod appendage pairs (group K). Among the extrinsic muscles, only three of the nine insert onto the anterior gonopod (LP7-1) with the other six inserting onto the posterior gonopod (LP7-2). Of the remaining nine intrinsic muscles, six are intrinsic to the anterior gonopod and three to the posterior gonopod.

• Anterior gonopod extrinsic muscles

E1: Originates from an apodematic flange extending dorsally from the anterior rim of the BR7 prophragma at its ventrolateral corner. Proceeds dorsally towards its insertion along the lateral surface of A1, at a ridge that runs transversely across the lateral edge of A1 near its dorsal apex. The muscle fibers proceed less than half the distance from insertion to origin; a tendon apparently spans the remaining distance to the origin.

E2: Originates along the posterior surface of the hollow dorsal branch of the preceding tracheal apodeme (LP6-2). Proceeds dorsally to its insertion along the anterior surface of A1, at its dorsal apex.

E3: Originates from several separated sites along the anterior rim of the BR7 prophragma, on its dorsolateral side. The muscle fibers proceed ventromedially, converging to their insertion along the edge of A1 at its dorsal apex. The insertion site is linear along the millipede's left-right axis.

• Posterior gonopod extrinsic muscles

F1: Originates along the interior surface of BR7, at the dorsolateral side. The origin site is about midway between the prophragma and the demarcation between prozonite and metazonite. The muscle proceeds ventromedially to its insertion at the dorsal apex of P1 and along its anterior surface just ventral to the apex.

F2: Originates along the anterior rim of the BR8 prophragma, on its dorsolateral side. Proceeds anteromedially and ventrally to its insertion along the posterior edge of the platelike medial branch of P1.

F3: Originates along the anterior surface and up to the dorsal apex of the succeeding tracheal apodeme (LP8-1). Proceeds anterodorsally to its insertion along the posterior surface of P1, on its thin dorsal branch.

F4: Originates along the anterior surface of the succeeding tracheal apodeme (LP8-1), just ventral to the origin site of F3. Muscle F4 proceeds anteriorly to its insertion site along the posterior surface of P1, just dorsal to the point where it fuses to P2.

F5: Originates along the interior surface of BR7, at its ventrolateral side. The origin site is about midway between the prophragma and the demarcation between prozonite and metazonite. The muscle proceeds dorsomedially to its insertion partially along the dorsal surface of P1 basal to the divergence of its dorsal and medial branches and partially along the ventral surface of the P1 medial branch near the branching point.

F6: Originates along the posterior rim of the BR7 prophragma, on its lateral side. Proceeds medially and slightly posteriorly to its insertion along the lateral surface of P2 near its posterior corner. There appears to be a short tendon or membrane connecting the medial termini of the F6 muscle fibers to P2.

• Gonopod complex intrinsic muscle

K: Originates along the posterior surface of A1, near the A1 dorsal apex. Proceeds posteroventrally to its insertion along the posterolateral surface of P1, approximately midway between its point of fusion with P2 and the divergence point of the P1 medial and dorsal branches.

• Anterior gonopod intrinsic muscles

I1: Originates along the anteroventral surface of A1, near its dorsal apex. Proceeds ventrally to its insertion along the posterior base of A3.

I2: Originates along the anterior surface of A1, ventral and lateral to the origin of I1. Muscle I2 proceeds ventrally, deep to I1. It inserts along the interior of A3 at its ventromedial edge. The insertion site is thickened and positioned between the anterior medial and posterior processes of A3, basal to both.

I3: Originates along the anteroventral surface of A1, ventral and medial to the origin of I1. Muscle I3 proceeds ventrally, deep to I1 and medial to I2. The insertion is along the medial base of A3.

I4: Originates along the ventral surface of the medial branch of A1. Proceeds ventrally, passing just anterior to the ventromedially angled basal part of A1. Inserts along the anterior base of A3.

I5: Originates on the interior surface of A3, along a ledge that extends posteriorly from the anterior base of A3. Muscle fibers converge ventrally to the insertion at the ventral base of A4. The insertion site is a horn-shaped process that extends dorsally from the medial corner of the A4 base.

I6: Originates along a ridge running ventrodorsally along the interior medial surface of A3. Proceeds ventrolaterally just posterior to I5. Inserts along the dorsal base of A4.

• Posterior gonopod intrinsic muscles

J1: Originates along the anteroventral surface of the P1 medial branch. Proceeds anteroventrally to its insertion at the anterolateral base of P3.

J2: Originates along the ventral surface of the P1 medial branch, posterior to the origin of J1 and medial to the origin of J3. Muscle J2 proceeds ventrally to its insertion at the anteromedial base of P3.

J3: Originates along the ventral surface of P1 on its medial branch and at the branching point between its medial and dorsal branches. Its origin site is lateral and posterior to that of J2. Muscle J3 proceeds ventrally to its insertion along the posterior base of P3.

Spirostreptida: Spirostreptidea: Harpagophoridae: *Phyllogonostreptus nigrolabiatus*

No new data were generated for Spirostreptidea. Instead, Wilson's (2005) thorough morphological study of *Phyllogonostreptus nigrolabiatus* (Newport, 1844) was used as the basis for the spirostreptidean SE and muscle networks. Additional information on the organization of SEs was sourced from Demange's work (1967). Table S3 provides the alphanumeric designations for each of the SEs and muscles in *Phyllogonostreptus* cross-referenced to the names given by Wilson (2002).

Julidia: Julidae: *Ommatoiulus avatar* (Figs. S18-S20)

• Summary

The gonopod complex of Julida is one of the most organizationally complex. In *Ommatoiulus,* we identified nine sclerites. It is difficult to immediately comprehend the overall form of the julidan gonopod complex due to it having several apical branches, many of which are united by a convoluted system of translucent membranes and non-sclerotized cuticle. The anterior gonopod (LP7-1) is the structurally simpler of the two appendage pairs, with only two sclerites divided into three SE. The A3 SE extends ventrally as the gonopod complex's anteriormost apical branch. In contrast, the posterior gonopod appendage pair (LP7-2) contains seven sclerites and eight SE. Of its three main apical branches, one is non-sclerotized. A bar-like longitudinal sclerite seems to form a non-muscular mechanical linkage between the anterior and posterior portions of the posterior gonopod pair.

• Skeletal elements

The anterior gonopod consists of two sclerites, both of which are paired with no medial connection to their opposite counterparts. The basalmost sclerite comprises a long posterodorsally arcing tracheal apodeme (A1) and a small platelike sternite (A2) with an exposed anterior surface. The identities of these two SE are strongly supported by the physical continuity of the hollow area inside A1 into a pitted depression on the external anterior face of A2. A prominent transverse ridge on the anterior surface of A2 is the membrane attachment site that demarcates the divide between sternite and tracheal apodeme.

A3 articulates against A2 and extends ventrally as the anteriormost apical branch in the gonopod complex. It is sheetlike with its medial and lateral margins folding posteriorly to partially enshroud the following apical branch (P2). Along the proximal lateral corner of A3, the sclerite thins to a membrane that extends posterior as a sheet to enclose the anterior gonopod laterally. At the posterior lateral corner of the anterior gonopod, this membrane sclerotizes into A4, a small plate that directly overlies the anterior surface of P2. Despite the close physical association of A4 and P2, we interpret A4 as being part of the anterior gonopod due to its continuous membranous connection to A3. This interpretation is strengthened

by the appearance of A4 as an additional layer of cuticle overlying P2 and its basal (dorsal) connection to P2 at the dorsolateral extremity of the gonopod sac membrane.

The posterior gonopod is comparatively more complex. The fused P1 and P2 SE together make up the anteriormost major sclerite in the posterior gonopod. The large, platelike lateral branch of the P1 (the tracheal apodeme) extends dorsolaterally from the fused area between P1 and P2. The P1 lateral plate apodeme arcs somewhat posteriorly toward its dorsal apex and carries a longitudinal ridge along its posterior surface. P1 also has a medial branch that extends dorsomedially from its ventral meeting point with the lateral branch. The P1 medial branch is fused ventrally to P2.

P2 is dorsally fused to both the lateral and medial branches of P1, and is thus approximately platelike near its proximal (dorsal) base. As it extends ventrally, P2 quickly tapers to a slender rodlike shape. This is the anteriormost of three apical branches in the posterior gonopod, and is surrounded on its anterior, lateral, and posterior sides by A3. The posterior quarter of this rod is enclosed by a thin membrane that was not captured in the segmentation process, so that in our figures P2 appears to show a rod with a longitudinal groove along its posterior surface. In fact, this “groove” is actually the posterior inner face of the sclerite making up the P2 rod’s anterior surface. The ventral fusion of P1 to P2 indicates that the latter is probably the posterior gonopod sternite. A pit that may represent the spiracle appears on the anterior surface of P2, and is overlain anteriorly by A4.

A complex array of sclerites occupy the space posterior to P1 and P2, along the midline of the posterior gonopod. Two paired sclerites, P3 and P4, both articulate along the posterior medial corner of P2. Of the two, P3 is ventral to P4 and extends ventrally as a crescent that arcs posteriorly. On each side, the P3 sclerite forms the rigid anterior part of a spherical reservoir for seminal fluid. P4 runs dorsomedially past the seminal fluid reservoir as a longitudinal bar. At its posterior end, it articulates with P5, a sclerite that extends ventrally from its articulation with P4.

The P5 sclerite forms a rigid anteriomedial wall for the proximal (dorsal) half of the solenomerite. The solenomerite is the posteromedial apical branch of the posterior gonopod and unlike the other apical branches it is distally non-sclerotized. Seminal fluid is carried ventrally from the seminal fluid reservoir to

the distal (ventral) tip of the solenomerite via a canal running longitudinally along the medial surface of the solenomerite.

Two more SE complete the posterior gonopod. Sclerite P6 is a small disc-shaped plate that lies posterior to P5 and articulates with its proximal (dorsal) end. The posterolateral edge of P6 articulates with the dorsomedial apex of the much larger P7 sclerite. P7 can be conceptualized as three subsections. The dorsomedial section forms a large apodematic plate inside the body cavity, which is the attachment site for two large intrinsic muscles. Toward the middle of P7, three platelike walls on the anterior, medial, and posterior sides converge to enclose a triangular lumen (the dorsomedial apodeme forms the posterior side of this lumen at its ventral end). Finally, the ventral end of P7 extends ventrally to form the posterolateral apical branch of the posterior gonopod.

• Anterior gonopod extrinsic muscles

The anterior gonopod receives two extrinsic muscle pairs. E1 is divided into two parts, with origin sites along the dorsal surfaces of the lateral branches in the preceding two tracheal apodemes (LP6-1 & LP6-2). The majority of E1 muscle fibers originate from the LP6-2 tracheal apodeme. From these origin sites, E1 runs dorsally, terminally curving posteriorly over the A1 plate to reach its insertion along the dorsal surface of A1. Muscle E2 originates from the dorsolateral corner of BR7, from an apodematic flange along the anterior surface of the prophragma. E2 curves anteriorly and ventromedially to reach its insertion site at the anterior surface of the A1 dorsal apex just posterior to the insertion of E1 and dorsal to the anterior attachment site of K2.

• Posterior gonopod extrinsic muscles

The posterior gonopod receives three extrinsic muscle pairs. F1 is a thin stringy muscle originating from BR7 along the interior rim of the dorsolateral prophragma, slightly dorsomedial to the E1 origin. From its origin, F1 runs ventrally before curving anteriorly to its insertion along the lateral rim of P1 near its dorsal apex. F2 originates from the dorsolateral corner of BR8 along the anterior surface of

the prophragma. It runs ventrally for a short distance before curving anteriorly to its insertion at the anterolateral edge of P1 near its ventral end. There is a bulge along the posterolateral edge of P1 to serve as an apodeme to receive F2. Finally, F3 originates from the dorsal surface of the succeeding tracheal apodeme (LP8-1). F3 runs dorsally and slightly anterolaterally to its insertion along the posterior surface of the P1 dorsal apex.

• Muscles running between gonopod pairs

There is a well-developed set of muscles connecting the gonopod tracheal apodemes (A1 & P1) to each other. Because A1 and P1 are shaped like large parallel plates and spaced close to each other along the anterior-posterior axis, all three of these muscle pairs are very thick. K1 is attached at the posterior surface of A1 at its dorsal apex and runs posteriorly to the anterior surface of P1 at its dorsal apex. K2 attaches to A1 midway along its length, just ventral to the K1 attachment site. From here, K2 runs posteroventrally to its attachment site at the ventral base of P1. Finally, K3 attaches to A1 at its ventral base, just ventral to the K2 attachment site. K3 runs dorsally and posterolaterally to its posterior attachment site along the anterior surface of P1, just lateral to the K2 attachment site.

• Muscles originating from the anterior gonopod tracheal apodeme

There is a single muscle intrinsic to the anterior gonopod. I1 originates along the posteromedial edge of A1 at the point where A1 curves posteriorly. It runs ventrally and slightly medially to its insertion at the posterior dorsal edge of A3. In addition to I1, there is a single transverse muscle, T, spanning the anteromedial edges of the left and right A1. Muscle T runs just anterior to I1.

• Posterior gonopod intrinsic muscles

Three intrinsic muscles connect the posterior gonopod sclerites to each other. Both J1 and J2 originate from the tracheal apodeme (P1) and insert onto P7. Muscle J1 originates from the posterior surface of P1 at its dorsal apex. From here, it runs ventrally to its insertion along the dorsal edge of the

plate forming the posterior wall of the P7 triangular lumen as well as along the dorsal edge of the P7 dorsomedial plate. J2 originates from the posterior surface of P1 at its ventral base. From here, J2 runs posteriorly to its insertion along the anterior surface of the P7 dorsomedial plate just ventral to the J1 insertion site. J1 and J2 run approximately perpendicular to each other.

One intrinsic muscle inserts onto P6, the small disc-shaped plate. J3 originates from the medial edge of P1 near its dorsal apex. It runs ventromedially to insert onto a membrane adjacent to anterodorsal edge of P6.

Stemmiulida: Stemmiulidae: ?*Stemmiulus* sp. (Figs. S21-S22)

• Skeletal elements

*Stemmiulus* has a single gonopod pair in the anterior position of BR7 (7-1) followed by a reduced leg pair in position 7-2. Because leg pair 7-2 is highly modified from the normal walking legs and sunken into a membranous pouch along with the gonopod we consider it as part of the gonopod complex for *Stemmiulus*.

The anterior gonopod (7-1) contains seven highly integrated SE with moderate intrinsic musculature. A1 and A2 are the paired, fused sternite and tracheal apodeme. A1 can be identified as the tracheal apodeme since it is internally hollow and the opening of the hollow is at a pit at the base of the tracheal apodeme where it fuses to A2. A1 is unusually robust for a tracheal apodeme, and expands dorsally despite being transversely flattened. A2 extends posteromedially as well as ventrally, forming a crescent that surrounds the more distal sclerites on their anterior, lateral, and posterior sides. The posteromedial branch is interpreted as part of the sternite since its posterior surface is exposed rather than inside the body cavity.

SE A3 forms the curved lateral walls of the basal part of the anterior gonopod. It is connected to A4 distally via a membrane. A4 is a fully enclosed subconical sclerite which tapers ventrally and is transversely flattened. The A4 sclerites run parallel to the sclerites A6 and bracket them laterally on either side.

A5 emerges from a dorsomedial extension of A3, and extends ventrally as a long, needlelike cone. A5 passes posteriorly to A7 and extends ventrally into a membranous sheath running along the posterior surface of A6.

A7 is a trapezoidal platelike sclerite that occupies the posterior basal wall of the anterior gonopod. The two A7 sclerites are joined at a medial suture. A7 is connected to the distal A6 via a membrane. A6 is a fully enclosed sclerite which occupies the medial distal portion of the anterior gonopod. The anterior surfaces of the paired A6 extend basally as long parallel lamellae, and are basally bracked by the anterior edges of A2. The posterior surface of A6 is dissected by an oblique slit running

from its basolateral corner to its distomedial corner. The lateral and medial edges of this slit are connected by the membrane which forms a cylindrical sheath for A5.

Appendage pair 7-2 consists of a medially fused tracheal apodeme and sternite with three distal leg podomeres. The musculature is minimal, with no intrinsic musculature. P1 can be identified as the tracheal apodeme since it is internally hollow and opens into a pit on the anterior surface of P2. P1 also lies entirely inside the body cavity whereas P2 is anteriorly exposed. In addition to the main dorsal branch, P1 also has a small process that extends ventrolaterally. P1 is functionally important as an insertion point for extrinsic muscles that serve the gonopod complex. This makes it clear that leg pair 7-2 is an integrated part of the gonopod complex. P2 forms an arch with a ventral process that medially separates the left and right P3 and P4 SE.

The remaining SE of the posteror gonopod appear to be the reduced remnant of a walking leg pair and lack any muscle attachments. P3 is reduced to a plate on the anterior side. P4 is distal to P3, but forms a complete ring. P5 is a small plate that forms a distal cap for the posterior gonopod.

• Muscles inserting onto tracheal apodemes

Tracheal apodemes are the main insertion site for extrinsic muscles in both the anterior and posterior gonopods. In the anterior gonopod, two extrinsic muscles insert onto A1. E2 originates from near the base of the preceding leg pair's tracheal apodeme (LP6-2) and passes dorsally to the anterior surface of the distal apex of A1. E3 originates from the ventrolateral surface of BR7. It passes dorsally and slightly anteriorly just posterior to the BR7 phragma and inserts onto the lateral surface of A1.

The posterior gonopod receives four extrinsic muscles, all inserting onto P1. F1 originates from the lateral side of the BR7 prophragma and passes ventromedially to its insertion at the ventrolateral process of P1. F2 originates from the lateral apex of the succeeding tracheal apodeme (LP9-1) and runs anteriorly to the dorsal branch of P1. F3 originates along the medial midline of the succeeding sternite (LP9-1) and takes a sinuous path dorsally, laterally, and anteriorly to the dorsal branch of P1. Muscle F4

originates from the dorsolateral corner of the BR8 prophragma and passes anteroventrally to insert at the dorsal branch of P1. Muscles F2, F3, and F4 all insert alongside each other on P1.

There is only one muscle that spans the anterior and posterior gonopods. K attaches along the posterior surface near the distal apex of A1 and passes posteroventrally to the distal apex of P1.

• Muscles inserting onto the anterior gonopod SE A2-A7

Although most of the muscles inserting onto the anterior gonopod SE are intrinsic, there is a single extrinsic muscle that inserts onto A6. Muscle E1 originates from the distal apex of the preceding tracheal apodeme (LP6-2). E1 is chiasmatic, with paired E1 muscles passing posteromedially from their origins and crossing medially at the midline. E1 inserts at dorsal base of the anterior plate of A6.

Of the five intrinsic muscles, only I1 originates from the tracheal apodeme (A1). It originates from the medial surface of A1 just posterior to the insertion of E2. From there, I1 it passes ventrally to insert at dorsal base of the anterior plate of A6, alongside E1.

In the remaining four intrinsic muscles, the functional polarity of attachment sites is not clear due to the integration of the SE. I2 attaches to the posterior surface of the anteroventral branch of A2 and passes dorsally to the dorsolateral corner of A7, just posterior to I1. Muscle I3 attaches to the dorsomedial corner of A4 and fans out medially along the medial surface of A6. Muscle I4 also attaches to the dorsomedial corner of A4, but passes dorsomedially to attach on either side of the suture attaching the left and right A7 SE to each other. Finally, I5 attaches basally along the dorsal end of A3 and passes ventrally to anterior surface of A4.

There is one transverse muscle between the left and right A2. It passes directly posterior to I2 and anterior to the crescent shaped posterior branch of A2.

Polydesmida: Polydesmidae: *Pseudopolydesmus serratus*

The gonopod skeletomusculature of Polydesmida has already been described in a previous work (Zahnle *et al.,* 2022). Table S3 provides the alphanumeric designations for each of the SEs and muscles in *Pseudopolydesmus* cross-referenced to the existing names listed in that work.

Overall, the gonopod of Polydesmida is among the simplest in terms of the numbers of morphemes and their relationships. The gonopod complex comprises a single appendage pair (LP7-1) with four SE and eight muscles. Four of the muscles are extrinsic and mostly insert onto the tracheal apodeme (A1). There are three intrinsic muscles that insert onto the two diverging sclerites A3 and A4, both of which articulate with A2. Finally, a transverse muscle connects the paired gonopods laterally.

*Anatomical Network Analysis*

Phylogenetic signal

For Blomberg's K tests on phylogenetic signal, P values of 0.05 or less were considered statistically significant. There was not a strong phylogenetic signal detected in the distribution of most network measurements (Table 4). Phylogenetic signal was detected in N for all network types (except in walking leg SE networks, which all shared an N value of 38), as well as in K for walking leg muscle networks. This indicates that the number of SEs and muscles in an appendage is strongly tied to ancestry. Heterogeneity of connections per node is statistically significant for walking leg SE networks, and a P value of just over 0.05 was recorded in walking leg muscle networks. In the gonopods, L is statistically significant among SE networks while D is significant among muscle networks.

For the remaining network measurements, we must assume that similarity due to more recent shared ancestry is not a major factor their values. Other factors, such as constraints in function or during development, most likely occupy a larger role in the overall organization of millipede appendages.

Network Measurement Mapping: Skeletal Elements

Overall, AnNA shows a major disparity between the skeletal organization of gonopods and walking legs. In general, the values of network measurements in the walking legs are notably bunched together compared with the gonopods, whose measurements tend to span a wider range of values (Fig. 6).

Among the gonopod networks, the colobognaths (configuration 1, cyan) have unusually high N, K, and L values due to their walking leg-like gonopods which retain many distal leg segments. Stemmiulida likewise retains some of the distal leg segments in the posterior appendage of its gonopod complex. The posterior gonopod of Julida has a complex system of sclerites, many of which lack muscle attachment sites. The values of K and L in walking legs are all higher than in the gonopods, with the exception of Polyzoniida. This is due to the chain-like series of connections between leg segments. The gonopod network of Polyzoniida actually has more links than the walking leg network because of the

fragmentation of its LP7-2 sternite and the reduction of some of its SEs from full rings to crescents, which contact more than two other SEs.

The density of connections, D, is much lower in the walking legs and the colobognath gonopods than in the eugnathan gonopods. Low D is another result of the chain-like organization of SEs in these appendages. Most SEs are connected to only two other SEs, severely reducing appendage SE complexity. There appears to be an inverse correlation between D on the one hand, and N and K on the other. Taxa with high N and K, such as Colobognatha, Julida, and Stemmiulida, also have low D values. Callipodida, which has the lowest number of SEs, also has by far the highest value for D, since its few SEs are very tightly integrated.

Parcellation among modules, P, roughly follows the same trends as N, K, and L. There is also a correlation between number of modules detected in a network using the spinglass algorithm and its value for P. The gonopod SE networks with just two or three modules (Polydesmida, Callipodida, Spirostreptidea) have the lowest P, whereas those with six or seven modules (Colobognatha, Julida) have the highest (Table 2). This trend is far less pronounced in the walking leg SE networks, which have between six and ten modules but consistent values for P regardless. This suggests that integrated modules in the gonopod are of more or less uniform size, without many disproportionately small modules.

The measurement of connective heterogeneity, H, presents a distinct perspective from the other network measurements. The gonopod complexes with only a single appendage pair (configuration 4, red) have extreme values of H at opposite ends of the scale. Whereas the handful of SEs in the Callipodida gonopod pair are tightly interconnected, those of Polydesmida are mixed between nodes connected to many neighbors and nodes connected to few neighbors. The gonopod complexes of Chordeumatida and Cambalidea also stand out for their high heterogeneity, highlighting the contrast between SEs with many neighbors and those with few neighbors.

Network Measurement Mapping: Muscles

The measurement values from muscle networks were much more comparable between gonopods and walking leg in comparison to the major disparity seen between gonopods and walking legs in the SE networks. Overall, the range of measurements from gonopod and walking leg networks was similar (Fig. 7). The largest range disparities were in the measurements of linkage density (D), average path length (L), and clustering coefficient (C). The ranges of both D and C are larger in the gonopod networks, whereas the range of L is larger in the walking leg networks.

The mapped values for N and K are broadly comparable between the muscle networks for gonopods and walking legs. Both colobognath taxa have above average values for N and K in both appendage types. In the walking legs, the highest N and K values are in the sister taxa Chordeumatida and Callipodida. The gonopod complex of Chordeumatida has both the highest N of any gonopod network and the highest K of any eugnath gonopod network. However, the values of both N and K are substantially reduced in the Callipodida gonopod compared with in its walking leg. With the exception of Callipodida, it seems like high N and K in the walking leg is associated with high N and K in the gonopod.

As in the SE gonopod networks, the value of D tends to be inversely related to the values of N and K in the muscle gonopod networks. Two taxa that stand out in exception to this trend are Chordeumatida and Stemmiulida. The former has the highest values for K and D of any taxon as well as the highest N of the eugnathans. This speaks to the remarkably high complexity of muscle organization in Chordeumatida. Both Callipodida and Julida have high values for D, despite relatively low values for N and K. Such high density in muscle connectivity is due to the low number of SEs (in Callipodida) or the low number of SEs which receive muscle attachments (in Julida). D in walking leg networks is restricted to a relatively narrow, low value range.

The average shortest path length, L, shows a marked departure from the trend in SE data. Among the SE networks, the value of L in the gonopods spanned a wide range while its was constrained to a narrow, albeit high, range in the walking legs. However, among the muscle networks the values of L in the gonopod are restricted to a low, narrow range with the walking legs having a much wider range of L.

This shows that the chain-like organization of the walking legs applies to varying degrees to the muscles. In taxa with well-developed distal leg musculature like Stemmiulida and the juliform millipedes (Julida, Spirobolida, Spirostreptidea, & Cambalidea), multiple muscles inserting onto the claw, tibia, and tarsus contribute to a chain-like network organization. In the gonopods the distalmost appendage segments tend to receive as few as one or two muscle insertions, even in colobognath gonopods.

The value of P is correlated with the number of modules identified using the spinglass algorithm. For both the gonopod networks and walking leg networks, networks with three or four modules have the lowest P values. These include the gonopod networks for Callipodida, Spirostreptidea, and Julida as well as the walking leg networks for Spirobolida, Polydesmida, and Julida. With eight modules, the gonopod of Polyzoniida stands out with the highest P.

As with the SE networks, the distribution of H shows a different, somewhat surprising perspective. Siphonophorida has one of the highest H values in both gonopod and walking leg networks, but while H in Polyzoniida walking legs is relatively high it is low in the Polyzoniida gonopods. Spirobolida has a high H among the gonopod networks, but the lowest among walking leg networks. Callipodida has a high H among the walking leg networks, but relatively low H among gonopod networks.

The average values for clustering coefficients of nodes, C, varies across the range of gonopod networks, but is restricted to a narrow range among walking leg networks. In general, millipede taxa with two pairs of gonopods (cyan, blue, and orange) have higher C than those with only one pair (red). This may be due to increased integration among muscles within each of the individual gonopod appendages. Stemmiulida provides an exception, with remarkably low node clustering even with two gonopod pairs.

## Discussion

### *Interpreting Homology in Millipede Gonopods*

Careful study and comparison of gonopod and walking leg skeletomusculature across the gonopod-bearing millipedes have yielded some novel homology insights, although the identities of many SEs and muscles remain unresolved. At one extreme, the relatively plesiomorphic condition of colobognath gonopods encourages comparison to the walking legs. Colobognath gonopods are known for evolutionary conservatism. Although it is common to use gonopod morphological traits to identify species in many helminthomorph taxa (Sierwald & Bond, 2007; Mwabvu *et al.,* 2013), the same is not true for colobognaths (Gardner, 1974; Shelley, 1995; 1997), with attempts to do so yielding mixed results (Brewer *et al.,* 2012; Shorter *et al.,* 2018). At the other extreme, most eugnath gonopods are so highly apomorphic that both morphological comparisons with walking legs and among gonopod complexes in different taxa yield only limited insights. Surprisingly, the clade comprising Chordeumatida and Callipodida appears to occupy a middle position, with gonopod sternites that retain more plesiomorphic features than those in its sister clade, which contains all other Eugnatha.

In both colobognath taxa studied (Siphonophorida & Polyzoniida), the SEs and muscles of the gonopods closely resemble those in the walking legs. This similarity is clearest when comparing the proximal morphemes in each appendage. In Siphonophorida the sternites and tracheal apodemes of the gonopods are essentially identical to those in the walking legs, with the apodemes forming distinctive plates spanning the anterior and posterior dorsal margins of the sternite (Fig. S5). Similarly, the gonopod sternites and tracheal apodemes of Polyzoniida closely resemble those of its own walking legs, albeit in slightly modified form with the posterior gonopod sternite (LP8-1) divided into one median and two lateral SEs (Fig. S7).

Compared with the most proximal morphemes, the distal morphemes of the colobognath gonopods are substantially modified. Whereas the walking legs each have a prominent trochanter forming a complete ring between the coxa and prefemur, the gonopods lack trochantera entirely. The coxal sacs that debouch on the ventral sides of the coxae (Manton, 1961) are also absent from the gonopod coxae.

The remaining leg podomeres – coxa, prefemur, femur, postfemur, tibia, and tarsus – are mostly intact but modified in shape. Both complexes are reoriented anteromedially compared to the ventrolaterally oriented walking legs and both feature a thickened, blunt-tipped anterior gonopod (LP7-2) which partially surrounds an elongate, needle-tipped posterior gonopod that extends anteriorly. The shapes of the gonopod sternites appear to be modified only enough to accommodate the reshaped coxae and prefemora.

There is also a marked divide between the proximal and distal muscles in the colobognath gonopod complexes. Whereas the extrinsic muscles all correspond to identical or nearly identical serial homologs in the walking legs, the intrinsic muscles are either modified in comparison to their walking legs homologs or lack walking leg serial homologs. Most extrinsic muscles inserting onto the sternites and tracheal apodemes of the gonopod complex have corresponding serial homologs in the walking legs of both Siphonophorida (muscles E1-5, F1-6, and K1-2; Fig. S6) and Polyzoniida (E1-7, F1-2, F4-6, K1-2, and K7; Fig. S8). The exception is muscle K8 in Polyzoniida, which connects the posterior gonopod sternite (LP8-1) to the anterior gonopod coxa (LP7-2) and may contribute to functional integration of the gonopod complex.

As in Colobognatha, the gonopods of the orders Callipodida and Chordeumatida retain a more plesiomorphic condition than those of the other eugnath orders. This is most immediately evident in comparing the morphologies of SEs in the walking legs and gonopod of Callipodida. In both, the sternite forms a triangular plate along the anterior of each appendage. In the gonopod of Callipodida (LP7-1), the tracheal apodemes seem to have fused with their respective coxae. The small, hook-shaped internal processes of the walking leg stigmata have been enlarged in the gonopod and posteroventrally as the pseudoflagellae (Fig. S9). Despite substantial transformation, the basalmost SEs are still recognizable in the callipodidan gonopod.

This trend also extends to the extrinsic gonopod muscles of Callipodida. All six extrinsic muscles in the gonopod are probably serial homologs of muscles in the walking legs. Several of the muscles are similar in size to their walking leg homologs, most notably E1 and E5. The insertions of E3, E4, and E6 have all moved from the tracheal apodemes in the walking legs to the coxae in the gonopods, possibly as

a consequence of the reduced size of the gonopod tracheal apodemes (Fig. S10). Nonetheless, the organization of extrinsic muscles is largely unaltered from the walking legs.

The same trend in plesiomorphic SEs is present in Chordeumatida. The sternites and tracheal apodemes of both appendage pairs in the chordeumatidan gonopod complex studied here (Fig. S11) closely resemble those of the walking legs. When comparing the anterior gonopod (LP7-1) and posterior gonopod (LP7-2) sternites to the walking leg sternite, all three feature transverse sternal bars anterior to their coxae. However, the sternal bar in the walking leg sternite extends ventrally as a triangular plate like that of Callipodida, whereas that of the posterior gonopod extends posteriorly as a medial plate that bears the condyles for its coxae. The anterior gonopod sternite consists exclusively of the transverse bar.

The posterior gonopod retains plesiomorphic features not shared by the anterior gonopod, including functional stigmata, medial branches of the tracheal apodemes (albeit reduced), and segmented prefemora and femora. The prefemora and femora of the posterior gonopod contain minimal musculature, instead serving as reservoirs for glands that debouch in the coxae (Shear, 2000).

Finally, the proximal muscles in Chordeumatida also strongly resemble those in the walking legs (Figs. S12-S13). The numerous extrinsic muscles that originate from the body rings (BR7-8) and insert onto the tracheal apodemes of the gonopod complex also appear in the corresponding anterior and posterior tracheal apodemes of the walking legs (E4-7 & F3-9). Muscles spanning the tracheal apodemes of successive appendage pairs are also similar. In the walking legs, two muscles connect each pair of tracheal apodemes, with one pair proceeding longitudinally between apodemes and a second pair proceeding posteroventrally to the base of the succeeding leg pair's apodeme. This pattern is loosely followed in the gonopod pairs. Between LP6-2 and the anterior gonopod (LP7-1) are the two typical pairs (E2-3), with an extra pair between the two gonopod pairs (K1-3) and only the longitudinal pair between the posterior gonopod (LP7-2) and LP8-1 (muscle F2).

All appendage pairs additionally have chiasmatic muscles passing from the apodemes to the succeeding sternite. The equivalent muscles originating from the anterior and posterior gonopod pairs are K4 and F2, respectively. E1 is the equivalent muscle originating anterior of the gonopod complex

(tracheal apodeme of LP6-2) but inserts onto the coxa (A3) of the anterior gonopod (LP7-1), skipping the sternite (A2). The muscle's insertion site seems to have migrated, perhaps due to functional specialization of the anterior gonopod pair.

*Comparative Morphological Insights: Paramorph Hypothesis Evaluated*

Zahnle *et al.* (2022, see fig. 8) proposed a paramorph hypothesis which laid out expectations for the evolution of gonopods across major taxa. According to this hypothesis, the developmental patterning of each trunk appendage type in Diplopoda is governed by a distinct set of interacting genes, called a character identity network (ChIN; Wagner, 2014). Each new type of appendage arises through genetic duplication, freeing the duplicate ChIN to gain new functions. Paramorphic body parts can thus be conceptualized as the morphological counterpart to paralogous genes.

Our study of morphology in the gonopods and walking legs across a broad selection of millipede taxa has produced evidence that is challenging to reconcile with the gonopod paramorph hypothesis. The challenges are: (1) there is little morphological evidence to suggest that closely related eugnaths share similar gonopods, (2) Colobognatha, Callipodida, and Chordeumatida all possess gonopod sternites, tracheal apodemes, and extrinsic muscles that are unmodified from the walking legs or have only minor modifications, and (3) the proximal elements in both gonopod pairs of Chordeumatida partially resemble the walking legs, but to different degrees.

The first challenge is difficult to address because of the lack of either subjective comparative similarities or strong measured phylogenetic signal in our data. Either eugnathan gonopods are so derived that only weak similarities remain, or we are forced to reject the hypothesis that eugnathan gonopods evolved once as an evolutionary novelty and subsequently evolved independently from walking legs.

To address the second challenge, our evidence suggests that the basal gonopod elements of the various millipede taxa are either excluded from or incompletely integrated to varying degrees into their respective gonopod ChINs. The plesiomorphic condition of the proximal elements colobognath, callipodidan, and chordeumatid gonopods could indicate that the ancestral gonopod ChINs only

encompassed the coxa, distal appendage SEs, and intrinsic muscles. As gonopod function evolved, minor modifications of the sternite, tracheal apodeme, and extrinsic muscles – such as those seen in Polyzoniida – gave way to more major modifications. The genes responsible for post-embryonic modification of the proximal appendage elements would become developmentally synchronous with the other postembryonic gonopodal modifications and may become developmentally integrated into the gonopod ChIN. On the molecular level, expansion of the region a ChIN regulates could result from variation in the diffusion distance of a regulatory gene that initiates developmental individualization of the gonopod complex (Wagner, 2014).

Unfortunately, this line of reasoning does little to resolve the question of whether gonopods arose convergently in Colobognatha and Eugnatha. Although colobognathan gonopods have highly plesiomorphic proximal elements, there is also substantial proximal plesiomorphy in gonopods of the Callipodida + Chordeumatida clade. The strongest evidence supporting separate origins for colobognathan and eugnathan gonopods is probably the absence of a gonopod pair at the anterior BR7 position, because all eugnathans at least possess one pair at this position. Conversely, only colobognathans possess a gonopod pair at the anterior BR8 position.

Finally, the variably apomorphic gonopod appendage pairs in Chordeumatida potentially provide insight into the evolutionary process that led to the functionally complex, integrated gonopod complexes of taxa such as Julida, Spirobolida, and Cambalidea. Even a cursory survey of the literature indicates that deeper taxonomic sampling of chordeumatidan gonopod morphology than that provided here would be desirable. In all four chordeumatidan suborders, gonopod complexes contain two gonopod pairs, of which either may be the sperm-transferring appendage. In addition to the gonopod, the leg pairs surrounding the gonopod complex (LP6-2, LP8-1 & LP8-2) are often reduced or modified to carry glands that open onto the coxae (Shear, 2000). In suborder Heterochordeumatidea, the distal walking leg SEs of LP8-1 are reduced or lost (Shear, 2000). Similar to the posterior gonopod, the LP8-1 prefemur and femur are modified with the postfemur, tibia, tarsus, and claw completely absent. The enlarged coxa continues to

fulfill its role as a glandular orifice. In suborder Chordeumatidea, LP8-1 can be highly modified with lobes and processes that cause it to resemble the posterior gonopod (Blower, 1985).

The reductions and modifications of LP8-1 in Heterochordeumatoidea and Chordeumatidea show a potential evolutionary path to integration of new appendage pairs into the gonopod complex (Shear, 2000). Leg pairs adjacent to the gonopods might be modified to adopt novel functions in copulation, such as glandular secretion. The resulting evolutionary transformation series from walking leg to gonopod might follow the following stages: (1) unmodified walking leg pair in proximity to gonopod complex; (2) modified walking leg pair with coxal glands for accessory copulatory function; (3) heavily modified walking leg pair with coxal glands and reduced distal segments; (4) gonopod in which the coxa is either responsible for sperm transfer or tightly integrated with function of sperm transferring gonopod.

The fact that such functional fluidity is only seen in the gonopods of Chordeumatida might be explained by the retention of sternite and tracheal apodeme shape in the Callipodida + Chordeumatida clade. By retaining low integration between SEs of the gonopod appendage pairs even as increased muscular integration enables coordinated function, the appendage pairs comprising the gonopod complex retain their evolutionary modularity. In contrast, the gonopods of other eugnaths (Juliformia, Polydesmida, Stemmiulida) have attained extensive integration of their SEs, so that the individual appendage pairs have lost their modularity.

*Phylogeny and Development Constrain Number of Morphemes and Links*

Blomberg's K test results on N for all networks, and in the walking leg muscle networks, suggests that the distribution of these network measurements is strongly influenced by evolutionary history (Table 4). In the gonopods of Eugnatha, this manifests as the gradual loss of SEs and muscles since the ancestral split between Eugnatha and Colobognatha. The high numbers of SEs in Julida and Stemmiulida are the exceptions to this trend. Both gonopod complexes are unique in their organization. In Julida, one or a few SEs splintered into many. The posterior appendage pair in the Stemmiulida gonopod complex seems to be a partially modified walking leg; perhaps the common ancestor of Stemmiulida and Polydesmida.

In addition to the phylogenetic signal in N and K, the muscle network organization may show signals of developmental constraints. The number of muscles in the gonopod complex is closely related to the number of muscles in the walking legs of the corresponding taxon. For a given taxon, N and K in the colobognath gonopods and walking legs are very close in value, as expected by their less modified gonopods. In the Eugnatha, every gonopod network has fewer muscles than the corresponding walking leg network. However, within Eugnatha, taxa with a higher N in the walking legs network also tend to have a higher N in the gonopod network. Although this relationship is not as clear in the values of K in the muscle networks, the K values for Chordeumatida are the highest in both the gonopod network and walking leg network.

These data suggest a developmental constraint on the number of muscles and shared muscle attachment sites in the gonopods. High values of N and K in the walking leg may be a developmental prerequisite for high values in the gonopod. In other words, the number of muscles in the gonopod does not exceed the number in the corresponding walking leg. Is it possible that each muscle in the gonopods is the developmental homolog of one of the walking leg muscles? In Polydesmida, at least, it is known that no differentiated muscles are discernible in the developing gonopod (Zahnle *et al.,* 2022). Perhaps nascent muscle tissues are able to retain their identities through this process. In insect metamorphosis, some muscle fibers undergo atrophy and remodeling while others are completely ablated (Hegstrom & Truman, 1996; Kuleesha *et al.,* 2016). It seems plausible that this developmental pathway also applies to millipede muscle fibers during gonopod development.

*Appendage Configuration Does Not Explain Network Measurements*

There are few discernible trends in the network measurements among gonopod networks sharing the same appendage configuration. This probably indicates that the functional differences in gonopods are deeper than just positional configuration. For example, the gonopod complexes of Polydesmida and Callipodida have markedly different organization despite both comprising a single appendage pair. Even in the closely related suborders of Spirostreptida, Spirostreptidea and Cambalidea, shared gonopod

configuration belies very different organization. The subequal, strongly integrated gonopod appendage pairs of Cambalidea contrast with the large lever of the anterior gonopod pair and reduced plate of the posterior pair in Spirostreptidea.

It is also possible that the fundamental functional changes seen throughout eugnath gonopod evolution have erased some aspects of the ancestral history in appendage organization. Each functional shift throughout gonopod macroevolutionary history probably alters the ancestral pattern of organization. If enough substantial alterations accrue, it may become difficult to recognize the ancestral pattern. This limitation in deciphering organizational shifts has been likened to a palimpsest, a reusable document that still contains traces of incompletely erased messages (Hallgrímsson *et al.,* 2009).

*Modularity Is Central to Function in Gonopods*

Among the network measurements used in our analyses, parcellation serves best as a proxy for modularity because it measures whether the modules that make up the network contain a similar number of nodes. Parcellation values in the gonopod networks are correlated with the number of modules detected. This is not true of the walking legs, at least in the SE networks. Parcellation increases when there are more modules but also when the modules are of approximately equal size. Adding more small modules to a network which is already dominated by one or a few much larger modules will not substantially alter the parcellation value.

The fact that gonopods with a larger number of detected modules also have larger parcellation values indicates that gonopod modules are roughly equal in size. That is, the gonopods are highly modular, especially in comparison to the walking legs. Because parcellation values are not explained by phylogenetic history (high P-values in Blomberg's K tests) or developmental constraints (no correlation between gonopod and walking leg networks), they are probably driven by the evolution of the gonopods to fulfill particular reproductive functions. Modularity is thought to enable the evolution of new functions by diminishing developmental, genetic, and functional interdependence among modules (Cheverud, 1996; Wagner, 1996).

*Limitations*

Each appendage type (gonopod, walking leg, telopod, *etc.*) represents a module at the evolutionary and developmental levels. Because integration and modularity can manifest at different hierarchical levels of organization (Klingenberg, 2014; Rasskin-Gutman & Esteve-Altava, 2014), it seems likely that we are missing important skeletomuscular information placing the modularity of these appendages in a broader organismal context. In particular, it would be useful to enumerate the complete trunk musculature in addition to the appendage musculature.

We believe that the order Chordeumatida represents fertile ground for future work on this topic. The four suborders within Chordeumatida differ substantially in the organization of their gonopods and notably feature two different gonopod appendage configurations among them (Shear, 2000). However, in this paper we only described the gonopod complex of *Conotyla,* a member of suborder Heterochordeumatidea. The phylogeny used for AnNA only has representatives of suborder Craspedosomatidea (Rodriguez *et al.,* 2018). Therefore, future work on the subject of gonopod macroevolution should at least include representation of multiple suborders within Chordeumatida.

One of the strengths of AnNA is the ability to discretize complicated morphological relationships into a quantitative model (Rasskin-Gutman & Esteve-Altava, 2014). However, this quantitative information is the product of a qualitative process of interpretation. In the preparation of this paper, our taxonomy of morphemes and the relationships between them underwent multiple iterations as we compared multiple appendages. Although we strived to apply our taxonomy consistently to produce comparable networks for each appendage and morpheme type, the potential subjectivity of these data should be kept in mind. Nonetheless, we believe that the broad signals derived from these data are worth interrogating.

## Conclusions

Our broad survey of the skeletomusculature of millipede gonopds has yielded both new insights into gonopod organization as well as new challenges to our understanding of it. Chief among these is the recognition that the proximal elements (sternite, tracheal apodemes, extrinsic muscles) of the gonopods in Colobognatha, Chordeumatida, and Callipodida undergo no change or only minor changes during gonopod development. Consequently, the paramorph hypothesis of gonopod novelty must be rejected or revised. If indeed gonopod novelty was the result of the duplication and subsequent sexual selection of the walking leg character identity network, it must initially have excluded the aforementioned proximal elements. Additionally, the paramorph hypothesis posits that the gonopods from more closely related millipedes will be morphological similar. However, the network measurements derived from anatomical network analysis fail to support this hypothesis, indicating at best an inconsistent phylogenetic signal. Further results from anatomical network analysis suggest that developmental processes and function in sexual selection are better at explaining gonopod organization than phylogenetic history.

References

Akkari, N., Enghoff, H., Metscher, B.D., 2015. A new dimension in documenting new species: High-detail imaging for myriapod taxonomy and first 3D cybertype of a new millipede species (Diplopoda, Julida, Julidae). PLOS ONE e0135243.

Arnold, P., Esteve-Altava, B., Fischer, M.S., 2017. Musculoskeletal networks reveal topological disparity in mammalian neck evolution. BMC Evolutionary Biology 17, 251.

Attems, C.M.T., 1926. Progoneata. In: Kükenthal, W.G. (Ed.), Handbuch der Zoologie. Vierter Band. Erste Hälfte. De Gruyter, Berlin, pp. 7–238.

Blower, J.G., 1985. Millipedes. Synopses of the British Fauna, n.s. 35, 1–242.

Boxshall, G.A., 2004. The evolution of arthropod limbs. Biological Reviews 79, 253–300.

Brewer, M.S., Spruill, C.L., Rao, N.S., Bond, J.E., 2012. Phylogenetics of the millipede genus *Brachycybe* Wood, 1864 (Diplopoda: Platydesmida: Andrognathidae): Patterns of deep evolutionary history and recent speciation. Molecular Phylogenetics and Evolution 64, 232–242.

Brölemann, H.W., 1935. Myriapodes Diplopodes (Chilognathes I). Faune de France 29, 1–368.

Cheverud, J.M., 1996. Developmental integration and the evolution of pleiotropy. American Zoologist 36, 44–50.

Demange, J.-M., 1964. Les appendices postêrieures (9e paire) du diplosegment gonopodial (VIIe) des Spirostreptoidea (Myriapodes Diplopodes). Bulletin du Muséum National d'Histoire Naturelle, 2e Série 36, 191–210.

Demange, J.-M., 1967. Recherches sur la segmentation du tronc des Chilopodes et des Diplopodes Chilognathes (Myriapodes). Mémoires du Muséum National d'Histoire Naturelle, n.s. 44, 1–188.

Demange, J.-M., 1972. Contribution a la connaissance du developpement postembryonnaire de *Pachybolus ligulatus* (Voges). Biologia Gabonica 8, 127–161.

Drago, L., Fusco, G., Garollo, E., Minelli, A., 2011. Structural aspects of leg-to-gonopod metamorphosis in male helminthomorph millipedes (Diplopoda). Frontiers in Zoology 8, 1–16.

Esteve-Altava, B., Molnar, J.L., Johnston, P., Hutchinson, J.R., Diogo, R., 2018. Anatomical network analysis of the musculoskeletal system reveals integration loss and parcellation boost during the fins-to-limbs transition. Evolution 72, 601–618.

Gardner, M.R., 1974. Revision of the millipede family Andrognathidae in the Nearctic region. Memoirs of the Pacific Coast Entomological Society 5, 1–61.

Hallgrímsson, B., Jamniczky, H., Young, N.M., Rolian, C., Parsons, T.E., Boughner, J.C., Marcucio, R.S., 2009. Deciphering the palimpsest: Studying the relationship between morphological integration and phenotypic covariation. Evolutionary Biology 36, 355–376.

Hegstrom, C.D., Truman, J.W., 1996. Steroid control of muscle remodeling during metamorphosis in *Manduca sexta*. Journal of Neurobiology 29, 535–550.

Hilken, G., Sombke, A., Müller, C.H.G., Rosenberg, J., 2015. Diplopoda, tracheal system. In: Minelli, A. (Ed.), The Myriapoda Volume 2. Brill, Leiden, pp. 129–152.

Hoffman, R.L., 1979. Classification of the Diplopoda. Muséum d'Histoire Naturelle de Genève, Geneva.

Jiang, X., Shear, W.A., Hennen, D.A., Chen, H., Xie, Z., 2019. One hundred million years of stasis: *Siphonophora hui* sp. nov., the first Mesozoic sucking millipede (Diplopoda: Siphonophorida) from mid-Cretaceous Burmese amber. Cretaceous Research 97, 34–39.

Klingenberg, C.P., 2014. Studying morphological integration and modularity at multiple levels: concepts and analysis. Philosophical Transactions of the Royal Society B: Biological Sciences 369.

Koch, M., 2015. Diplopoda, general morphology. In: Minelli, A. (Ed.), The Myriapoda Volume 2. Brill, Leiden, pp. 7–67.

Kuleesha, Y., Puah, W.C., Wasser, M., 2016. A model of muscle atrophy based on live microscopy of muscle remodelling in *Drosophila* metamorphosis. Royal Society Open Science 3, 150517.

Liu, W., Rühr, P.T., Wesener, T., 2017. A look with μCT technology into a treasure trove of fossils: The first two fossils of the millipede order Siphoniulida discovered in Cretaceous Burmese amber (Myriapoda, Diplopoda). Cretaceous Research 74, 100–108.

Manton, S.M., 1954. The evolution of arthropodan locomotory mechanisms. Part 4. The structure, habits and evolution of the Diplopoda. Journal of the Linnean Society of London, Zoology 42, 299–368.

Manton, S.M., 1956. The evolution of arthropodan locomotory mechanisms. Part 5. The structure, habits and evolution of the Pselaphognatha (Diplopoda). Journal of the Linnean Society of London, Zoology 43, 153–187.

Manton, S.M., 1958. The evolution of arthropodan locomotory mechanisms. Part 6. Habits and evolution of the Lysiopetaloidea [Diplopoda], some principles of leg design in Diplopoda and Chilopoda, and limb structure of Diplopoda. Journal of the Linnean Society of London, Zoology 43, 487–556.

Manton, S.M., 1961. The evolution of arthropodan locomotory mechanisms. Part 7. Functional requirements and body design in Colobognatha (Diplopoda), together with a comparative account of diplopod burrowing techniques, trunk musculature and segmentation. Journal of the Linnean Society of London, Zoology 44, 383–462.

Molnar, J., Esteve-Altava, B., Rolian, C., Diogo, R., 2017. Comparison of musculoskeletal networks of the primate forelimb. Scientific Reports 7, 10520.

Moritz, L., Wesener, T., 2019. The first known fossils of the Platydesmida—An extant American genus in Cretaceous amber from Myanmar (Diplopoda: Platydesmida: Andrognathidae). Organisms Diversity & Evolution 19, 423–433.

Moritz, L., Wesener, T., 2021. Electrocambalidae fam. nov., a new family of Cambalidea from Cretaceous Burmese amber (Diplopoda, Spirostreptida). European Journal of Taxonomy 755, 22–46.

Münkemüller, T., Lavergne, S., Bzeznik, B., Dray, S., Jombart, T., Schiffers, K., Thuiller, W., 2012. How to measure and test phylogenetic signal. Methods in Ecology and Evolution 3, 743–756.

Mwabvu, T., Lamb, J., Slotow, R., Hamer, M., Barraclough, D., 2013. Is millipede taxonomy based on gonopod morphology too inclusive? Observations on genetic variation and cryptic speciation in

*Bicoxidens flavicollis* (Diplopoda: Spirostreptida: Spirostreptidae). African Invertebrates 54, 349–356.

Ostachuk, A., 2019. What is it like to be a crab? A complex network analysis of eucaridan evolution. Evolutionary Biology 46, 179–206.

Ostachuk, A., 2021. A network analysis of crab metamorphosis and the hypothesis of development as a process of unfolding of an intensive complexity. Scientific Reports 11, 9551.

Paradis, E., Claude, J., Strimmer, K., 2004. APE: Analyses of Phylogenetics and Evolution in R language. Bioinformatics 20, 289–290.

Petit, G., 1973. Étude morphologique et expérimentale de la métamorphose d'un appendice ambulatoire en gonopode chez le diplopode *Polydesmus angustus* Latz. Annales d'Embryologie et de Morphogenèse 6, 137–149.

Petit, G., 1976. Developpements compares des appendices copulateurs (gonopodes) chez *Polydesmus angustus* Latzel et *Brachydesmus superus* Latzel (Diplopodes : Polydesmidae). International Journal of Insect Morphology and Embryology 5, 261–272.

Rasskin-Gutman, D., Esteve-Altava, B., 2014. Connecting the dots: Anatomical Network Analysis in morphological EvoDevo. Biological Theory 9, 178–193.

Remane, A., 1952. Die Grundlagen des natürlichen Systems, der vergleichenden Anatomie und der Phylogenetik. Geest & Portig, Leipzig.

Revell, L.J., 2012. phytools: an R package for phylogenetic comparative biology (and other things). Methods in Ecology and Evolution 3, 217–223.

Richter, S., Wirkner, C.S., 2014. A research program for Evolutionary Morphology. Journal of Zoological Systematics and Evolutionary Research 52, 338–350.

Rodriguez, J., Jones, T.H., Sierwald, P., Marek, P.E., Shear, W.A., Brewer, M.S., Kocot, K.M., Bond, J.E., 2018. Step-wise evolution of complex chemical defenses in millipedes: a phylogenomic approach. Scientific Reports 8, 3209.

Shear, W.A., 2000. On the milliped family Heterochordeumatidae, with comments on the higher classification of the order Chordeumatida (Diplopoda). Invertebrate Taxonomy 14, 363–376.

Shear, W.A., Edgecombe, G.D., 2010. The geological record and phylogeny of the Myriapoda. Arthropod Structure & Development, Fossil Record and Phylogeny of the Arthropoda 39, 174–190.

Shelley, R.M., 1995. The milliped family Hirudisomatidae in the New World (Polyzoniida). Brimleyana 23, 103–143.

Shelley, R.M., 1997. The milliped family Polyzoniidae in North America, with a classification of the global fauna (Diplopoda Polyzoniida). Arthropoda Selecta 6, 3–34.

Shorter, P.L., Hennen, D.A., Marek, P.E., 2018. Cryptic diversity in *Andrognathus corticarius* Cope, 1869 and description of a new *Andrognathus* species from New Mexico (Diplopoda, Platydesmida, Andrognathidae). ZooKeys 786, 19–41.

Sierwald, P., Bond, J.E., 2007. Current status of the myriapod class Diplopoda (Millipedes): Taxonomic diversity and phylogeny. Annual Review of Entomology 52, 401–420.

Sierwald, P., Spelda, J., 2023. MilliBase. Accessed at https://www.millibase.org on 2023-09-02.

Stoev, P., Moritz, L., Wesener, T., 2019. Dwarfs under dinosaur legs: A new millipede of the order Callipodida (Diplopoda) from Cretaceous amber of Burma. ZooKeys 841, 79–96.

Verhoeff, K.W., 1928. Klassen und Ordnungen des Tierreichs, Band 5, Abteilung II, Buch 2: Klasse Diplopoda. Akademische Verlagsgesellschaft, Leipzig.

Wagner, G.P., 1996. Homologues, natural kinds and the evolution of modularity. American Zoologist 36, 36–43.

Wagner, G.P., 2014. Homology, Genes, and Evolutionary Innovation. Princeton University Press, Princeton, New Jersey.

Wesener, T., Moritz, L., 2018. Checklist of the Myriapoda in Cretaceous Burmese amber and a correction of the Myriapoda identified by Zhang (2017). Check List 14, 1131–1140.

Wilson, H.M., 2002. Muscular anatomy of the millipede *Phyllogonostreptus nigrolabiatus* (Diplopoda: Spirostreptida) and its bearing on the millipede “thorax.” Journal of Morphology 251, 256–275.

Young, B.A., 1993. On the necessity of an archetypal concept in morphology: with special reference to the concepts of “structure” and “homology.” Biology and Philosophy 8, 225–248.

Zahnle, X.J., Ma, M., Bond, J.E., 2022. Skeletomuscular atlas and deep homology of a metamorphosing genitalic appendage in a flat-backed millipede (Polydesmida: Polydesmidae: Pseudopolydesmus). Insect Systematics and Diversity 6(4), 1-15.

**Table 1.** Descriptive identification of morphemes according to Young (1993) and examples of its implementation in this paper.

| Spatial proximity | Material composition | Examples |
|---|---|---|
| Disjointed | Intrinsically identified | A muscle and a skeletal element that are not in contact with each other |
| Disjointed | Extrinsically identified | Two muscles that are not in contact with each other; two skeletal elements that are not in contact with each other |
| Adjoining | Intrinsically identified | A muscle and a skeletal element that are in contact at the muscle's attachment site onto the skeletal element |
| Adjoining | Extrinsically identified | Two muscles in contact at a shared attachment site (extrinsically identified by not sharing their other attachment sites); two skeletal elements fused together into a single sclerite (extrinsically identified by their distinct evolutionary histories) |

**Table 2.** List of skeletal element networks constructed for Anatomical Network Analysis, as well as the network measurements calculated from them. N = number of nodes; K = number of edges (links); D = average edge density per node; C = average clustering coefficient per node; L = average shortest path length between two nodes; H = heterogeneity between number of edges per node; M = number of modules detected; P = parcellation of network among its constituent modules.

| Taxon | Genus | Appendage | Node Type | N | K | D | C | L | H | M | P |
|---|---|---|---|---|---|---|---|---|---|---|---|
| Siphonophorida | *Siphonophora* | Gonopod | Skeletal Element | 28 | 27 | 0.071 | 0 | 5.36 | 0.507 | 6 | 0.827 |
| Polyzoniida | *Octoglena* | Gonopod | Skeletal Element | 32 | 39 | 0.079 | 0.103 | 4.74 | 0.625 | 7 | 0.854 |
| Callipodida | *Tynomma* | Gonopod | Skeletal Element | 10 | 14 | 0.7 | 0.767 | 1.3 | 0.299 | 2 | 0.48 |
| Chordeumatida | *Conotyla* | Gonopod | Skeletal Element | 14 | 16 | 0.176 | 0.174 | 2.68 | 0.776 | 4 | 0.735 |
| Spirobolida | *Eurhinocricus* | Gonopod | Skeletal Element | 12 | 13 | 0.197 | 0 | 2.36 | 0.617 | 4 | 0.736 |
| Cambalidea | ?*Titsona* | Gonopod | Skeletal Element | 13 | 14 | 0.179 | 0.038 | 2.47 | 0.705 | 5 | 0.793 |
| Spirostreptidea | *Phyllogonostreptus* | Gonopod | Skeletal Element | 11 | 14 | 0.255 | 0.37 | 2.27 | 0.538 | 3 | 0.628 |
| Julida | *Ommatoiulus* | Gonopod | Skeletal Element | 22 | 32 | 0.139 | 0.201 | 2.81 | 0.55 | 7 | 0.847 |
| Stemmiulida | *Stemmiulus* | Gonopod | Skeletal Element | 23 | 30 | 0.119 | 0.162 | 3.08 | 0.641 | 5 | 0.764 |
| Polydesmida | *Pseudopolydesmus* | Gonopod | Skeletal Element | 18 | 18 | 0.25 | 0.133 | 2 | 0.866 | 2 | 0.494 |
| Siphonophorida | *Siphonophora* | Walking Leg | Skeletal Element | 38 | 43 | 0.061 | 0.286 | 6.29 | 0.38 | 10 | 0.896 |
| Polyzoniida | *Polyzonium* | Walking Leg | Skeletal Element | 38 | 39 | 0.055 | 0.025 | 6.91 | 0.531 | 6 | 0.821 |
| Callipodida | *Callipus* | Walking Leg | Skeletal Element | 38 | 40 | 0.057 | 0.043 | 6.81 | 0.479 | 6 | 0.83 |
| Chordeumatida | *Nanogona* | Walking Leg | Skeletal Element | 38 | 40 | 0.057 | 0.043 | 6.81 | 0.479 | 7 | 0.846 |
| Spirobolida | *Spirobolus* | Walking Leg | Skeletal Element | 38 | 45 | 0.064 | 0.192 | 5.67 | 0.567 | 10 | 0.893 |
| Cambalidea | ?*Titsona* | Walking Leg | Skeletal Element | 38 | 41 | 0.058 | 0.057 | 6.73 | 0.544 | 6 | 0.827 |
| Spirostreptidea | *Plusioporus* | Walking Leg | Skeletal Element | 38 | 41 | 0.058 | 0. 057 | 6.73 | 0.544 | 6 | 0.827 |
| Julida | *Ommatoiulus* | Walking Leg | Skeletal Element | 38 | 41 | 0.058 | 0. 057 | 6.73 | 0.544 | 6 | 0.828 |
| Stemmiulida | *Stemmiulus* | Walking Leg | Skeletal Element | 38 | 40 | 0.057 | 0.043 | 6.81 | 0.479 | 6 | 0.83 |
| Polydesmida | *Polydesmus* | Walking Leg | Skeletal Element | 38 | 41 | 0.058 | 0.175 | 6.29 | 0.438 | 9 | 0.881 |

**Table 3.** List of muscle networks constructed for Anatomical Network Analysis, as well as the network measurements calculated from them. N = number of nodes; K = number of edges (links); D = average edge density per node; C = average clustering coefficient per node; L = average shortest path length between two nodes; H = heterogeneity between number of edges per node; M = number of modules detected; P = parcellation of network among its constituent modules.

| Taxon | Genus | Appendage | Node Type | N | K | D | C | L | H | M | P |
|---|---|---|---|---|---|---|---|---|---|---|---|
| Siphonophorida | *Siphonophora* | Gonopod | Muscle | 66 | 379 | 0.177 | 0.784 | 2.49 | 0.468 | 4 | 0.743 |
| Polyzoniida | *Octoglena* | Gonopod | Muscle | 84 | 437 | 0.125 | 0.721 | 2.68 | 0.265 | 8 | 0.868 |
| Callipodida | *Tynomma* | Gonopod | Muscle | 38 | 124 | 0.363 | 0.667 | 1.7 | 0.304 | 3 | 0.659 |
| Chordeumatida | *Conotyla* | Gonopod | Muscle | 52 | 510 | 0.385 | 0.736 | 1.75 | 0.34 | 4 | 0.737 |
| Spirobolida | *Eurhinocricus* | Gonopod | Muscle | 30 | 119 | 0.274 | 0.77 | 2.17 | 0.467 | 5 | 0.784 |
| Cambalidea | ?*Titsona* | Gonopod | Muscle | 38 | 188 | 0.267 | 0.822 | 2.15 | 0.358 | 5 | 0.773 |
| Spirostreptidea | *Phyllogonostreptus* | Gonopod | Muscle | 22 | 60 | 0.26 | 0.682 | 2.31 | 0.27 | 3 | 0.661 |
| Julida | *Ommatoiulus* | Gonopod | Muscle | 27 | 129 | 0.368 | 0.825 | 1.83 | 0.255 | 3 | 0.623 |
| Stemmiulida | *Stemmiulus* | Gonopod | Muscle | 27 | 58 | 0.165 | 0.483 | 2.94 | 0.386 | 5 | 0.784 |
| Polydesmida | *Pseudopolydesmus* | Gonopod | Muscle | 30 | 66 | 0.314 | 0.613 | 1.91 | 0.282 | 4 | 0.747 |
| Siphonophorida | *Siphonophora* | Walking Leg | Muscle | 90 | 426 | 0.106 | 0.651 | 4.24 | 0.505 | 5 | 0.793 |
| Polyzoniida | *Polyzonium* | Walking Leg | Muscle | 92 | 413 | 0.099 | 0.594 | 3.31 | 0.416 | 8 | 0.855 |
| Callipodida | *Callipus* | Walking Leg | Muscle | 98 | 470 | 0.099 | 0.623 | 3.2 | 0.523 | 7 | 0.84 |
| Chordeumatida | *Nanogona* | Walking Leg | Muscle | 108 | 556 | 0.096 | 0.665 | 3.12 | 0.446 | 7 | 0.856 |
| Spirobolida | *Spirobolus* | Walking Leg | Muscle | 52 | 114 | 0.175 | 0.613 | 4.79 | 0.215 | 4 | 0.749 |
| Cambalidea | ?*Titsona* | Walking Leg | Muscle | 68 | 225 | 0.099 | 0.624 | 4.64 | 0.378 | 7 | 0.849 |
| Spirostreptidea | *Plusioporus* | Walking Leg | Muscle | 64 | 179 | 0.089 | 0.67 | 5.88 | 0.254 | 6 | 0.833 |
| Julida | *Ommatoiulus* | Walking Leg | Muscle | 48 | 98 | 0.178 | 0.631 | 4.62 | 0.279 | 4 | 0.743 |
| Stemmiulida | *Stemmiulus* | Walking Leg | Muscle | 82 | 316 | 0.095 | 0.634 | 4.72 | 0.446 | 10 | 0.879 |
| Polydesmida | *Polydesmus* | Walking Leg | Muscle | 80 | 312 | 0.2 | 0.689 | 2.82 | 0.434 | 4 | 0.734 |

**Table 4.** Results from Blomberg's K tests. Network measurements listed in left column, with appendage type/network type combinations listed in header row. Statistically significant P values marked with an asterisk.

| | **Gonopod SE** | | **Walking Leg SE** | | **Gonopod Muscle** | | **Leg Muscle** | |
|---|---|---|---|---|---|---|---|---|
| | **K** | **P** | **K** | **P** | **K** | **P** | **K** | **P** |
| **N** | **1.46611** | **0.005*** | - | - | **1.64334** | **0.0037*** | **1.36097** | **0.0077*** |
| **K** | 1.1291 | 0.0682 | 0.939716 | 0.3072 | 1.14167 | 0.0775 | **1.41229** | **0.0044*** |
| **D** | 0.922183 | 0.336 | 0.939716 | 0.3075 | **1.25333** | **0.0243*** | 0.898406 | 0.3583 |
| **C** | - | - | 0.970301 | 0.2265 | 0.906257 | 0.3858 | 0.790863 | 0.7076 |
| **L** | **1.61485** | **0.0107*** | 0.889437 | 0.4499 | 1.0668 | 0.108 | 1.08392 | 0.0921 |
| **H** | 0.764008 | 0.7819 | **1.70736** | **0.0002*** | 0.802449 | 0.6746 | 1.15989 | 0.0584 |
| **P** | 0.893185 | 0.382 | 1.08117 | 0.1032 | 0.882418 | 0.4157 | 0.868219 | 0.4386 |

A

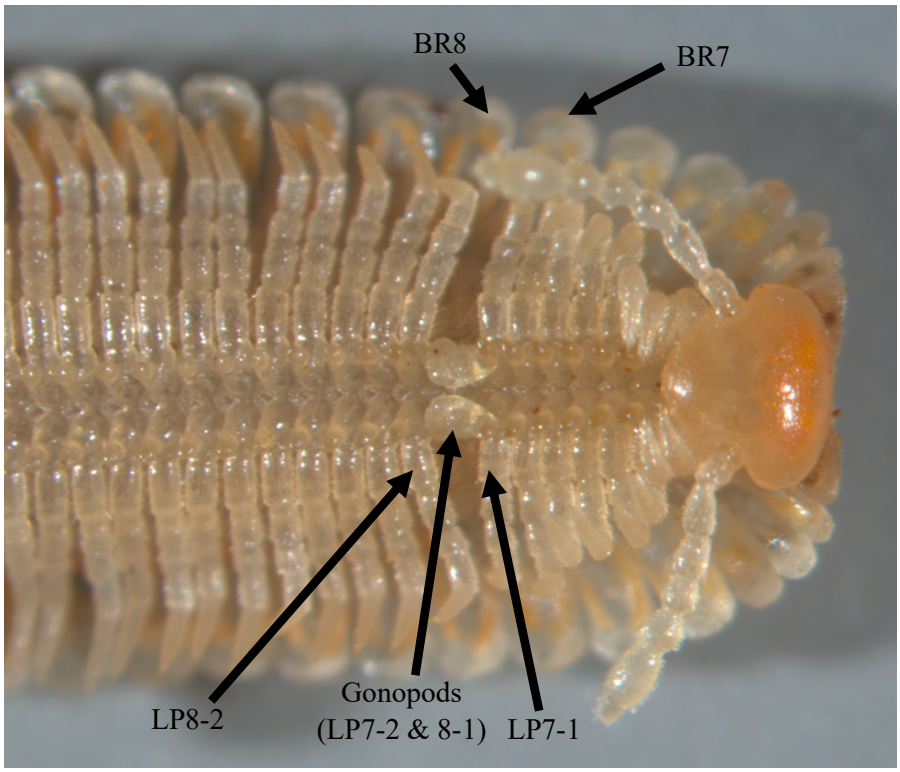


B

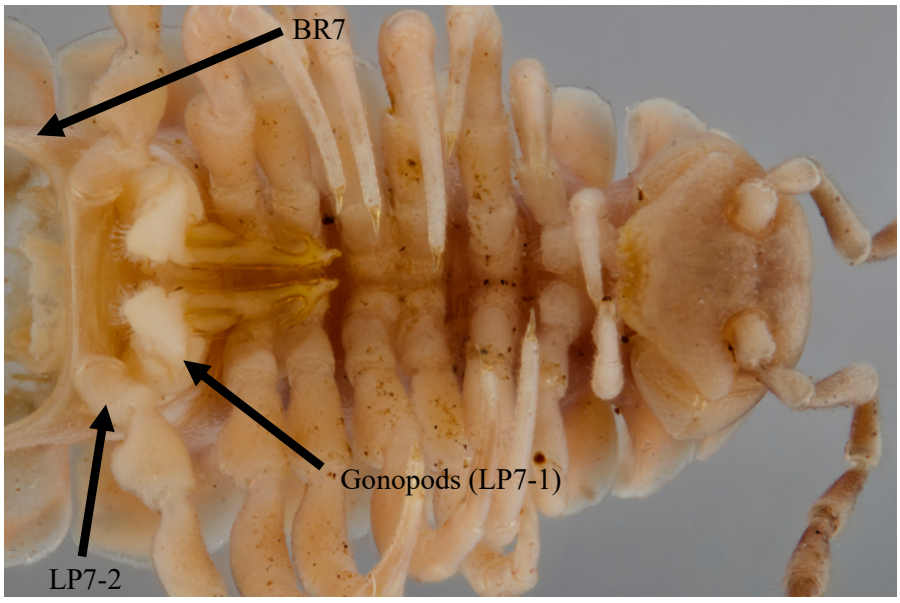


**Figure 1.** Examples of millipede gonopods *in situ*. A: Typical colobognathan gonopods in the species *Brachycybe producta* Loomis, 1936, spanning the seventh and eighth body rings. B: Relatively simple eugnathan gonopods in the species *Pseudopolydesmus canadensis* (Newport, 1844). The single gonopod pair is located at LP7-1, with a fully functional walking leg pair at the following position. Abbreviations: BR: body ring, LP: leg pair. Numerical designations explained in main text. Image in Fig. 1B provided by Stephanie Ware.

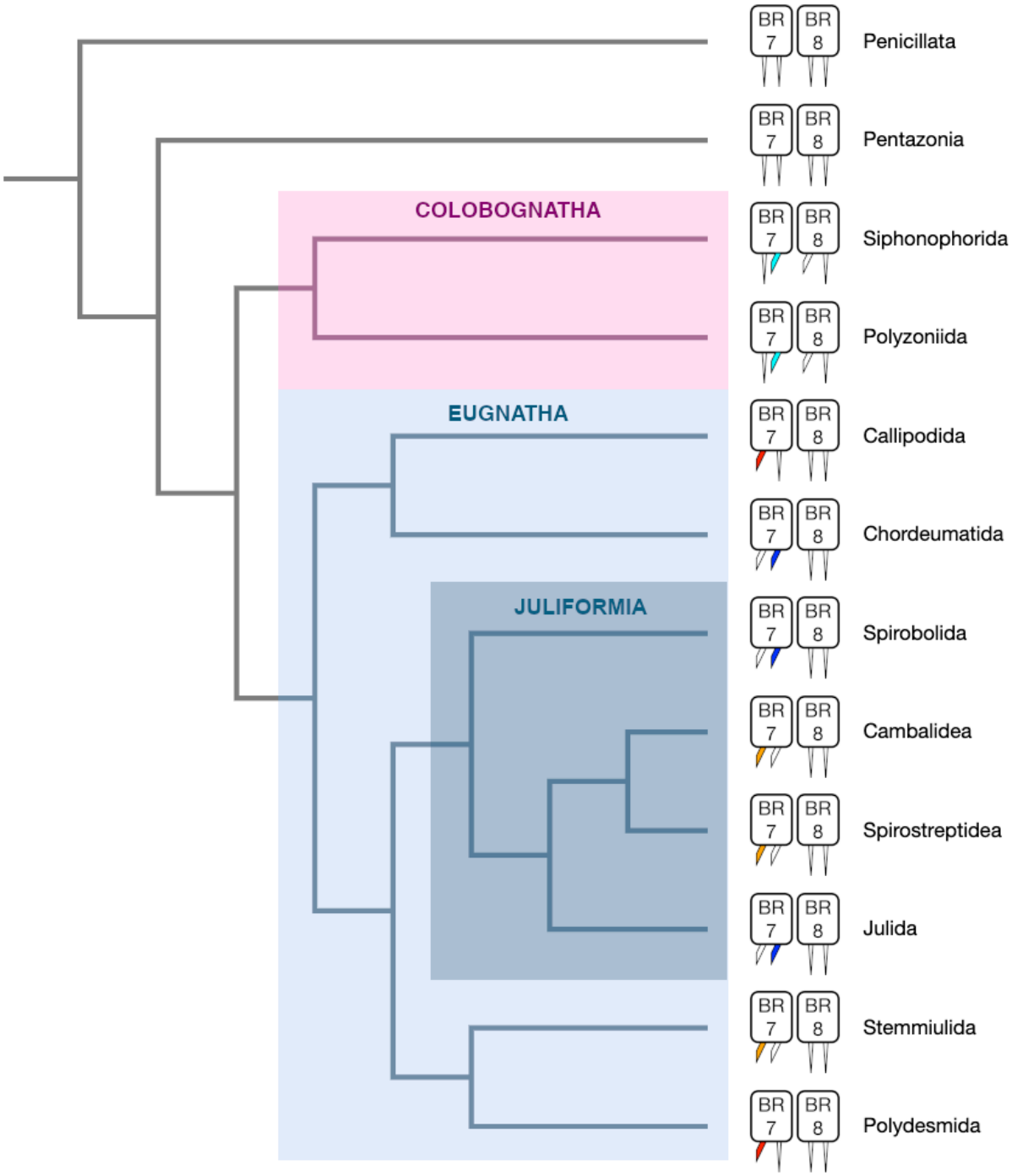


**Figure 2.** Phylogeny of millipedes (Diplopoda) and phylogenetic distribution of gonopod configurations across the class. Sperm-transferring gonopods are colored according to gonopod configuration. Configuration 1: cyan; configuration 2: dark blue; configuration 3: orange; configuration 4: orange. Penicillata and Pentazonia lack gonopods.

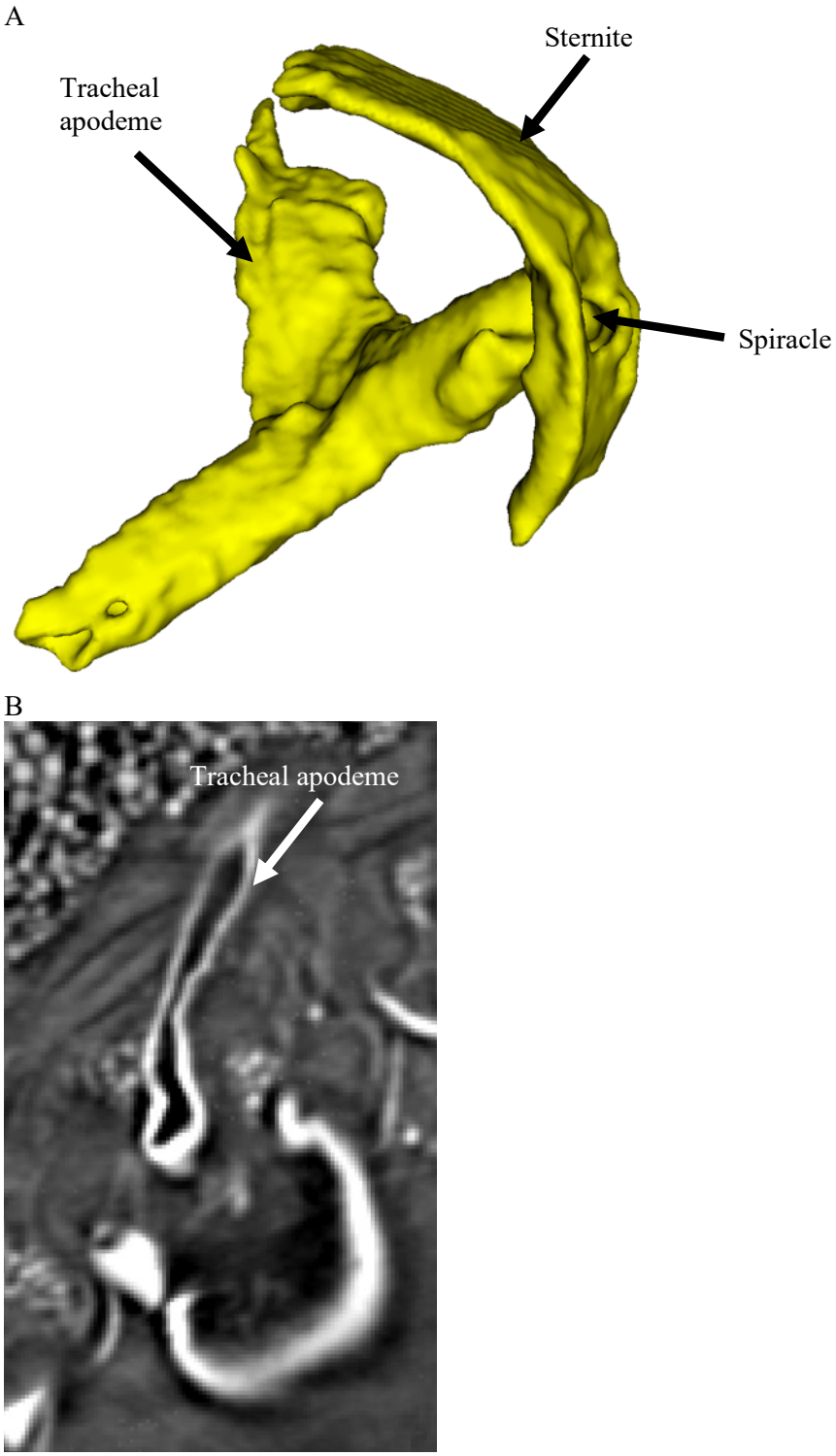


**Figure 3.** Illustration of typical sternite and tracheal apodeme. Images taken from the posterior gonopod pair (LP8-1) of the *Octoglena bivirgata* 3D image and segmentation. A: sternite and tracheal apodeme, showing spiracle where both skeletal elements are fused together. B: parasagittal section through *O. bivirgata* showing hollow tracheal apodeme.

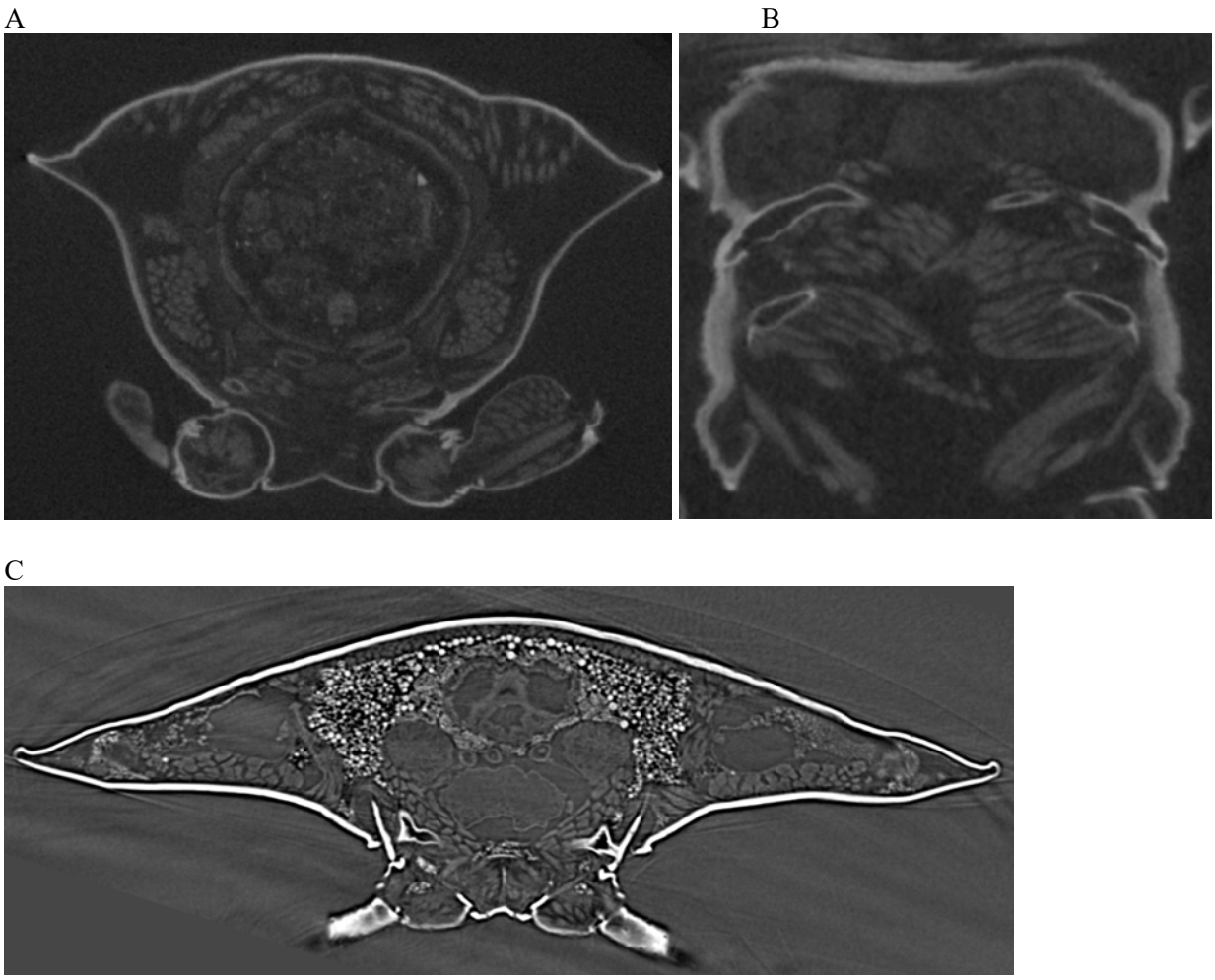


**Figure 4.** Illustrations of definitions for exceptional skeletal elements. A: cross-section of body ring in *Pseudopolydesmus serratus* (order Polydesmida), showing sternite in blue and pleurotergite in red; B: ventral view of body ring in *P. serratus,* showing anterior sternite in light blue and posterior sternite in dark blue; C: cross-section of the body ring in *Octoglena bivirgata* (order Polyzoniida), showing sternite in blue and pleurotergite in red.

A

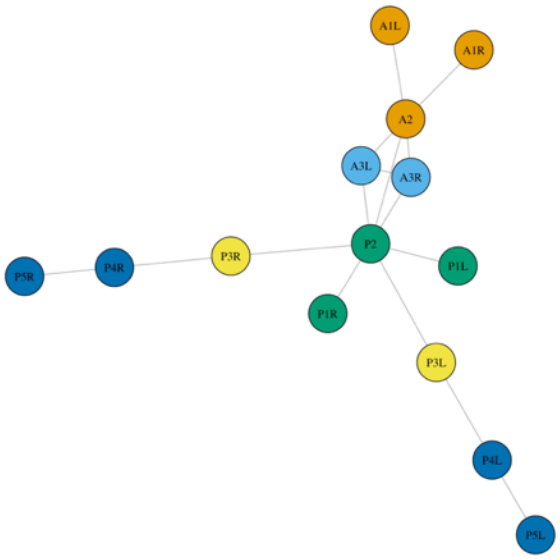


B

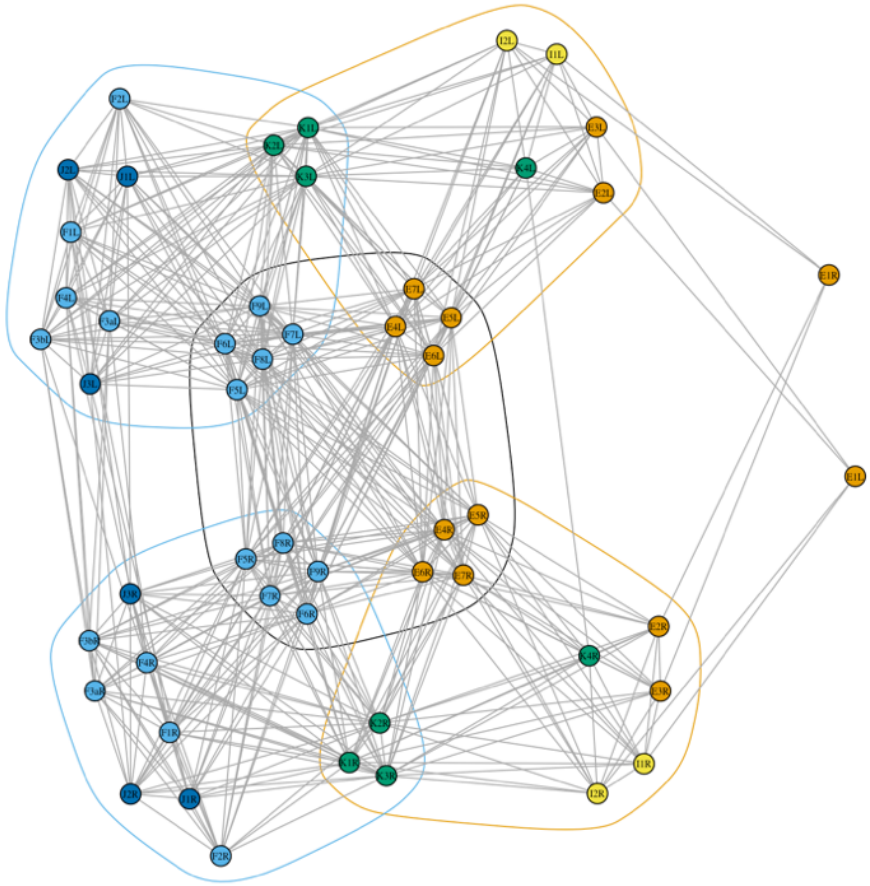

**Figure 5.** Examples of the two types of networks constructed for anatomical network analysis. The networks shown here model gonopod anatomy of *Conotyla* sp. (order Chordeumatida). A: skeletal element network; B: muscle network.

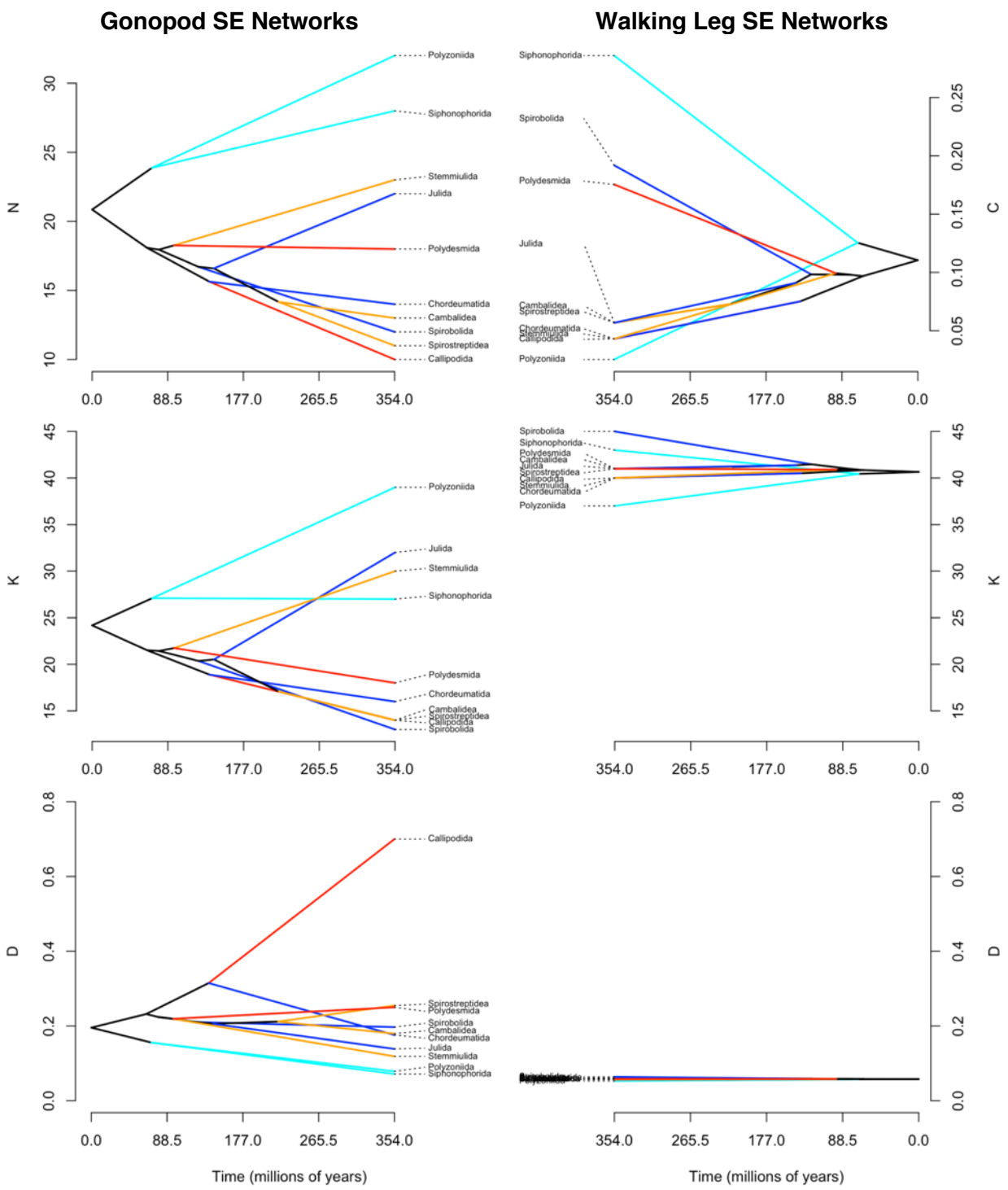


**Figure 6 (continued below).**

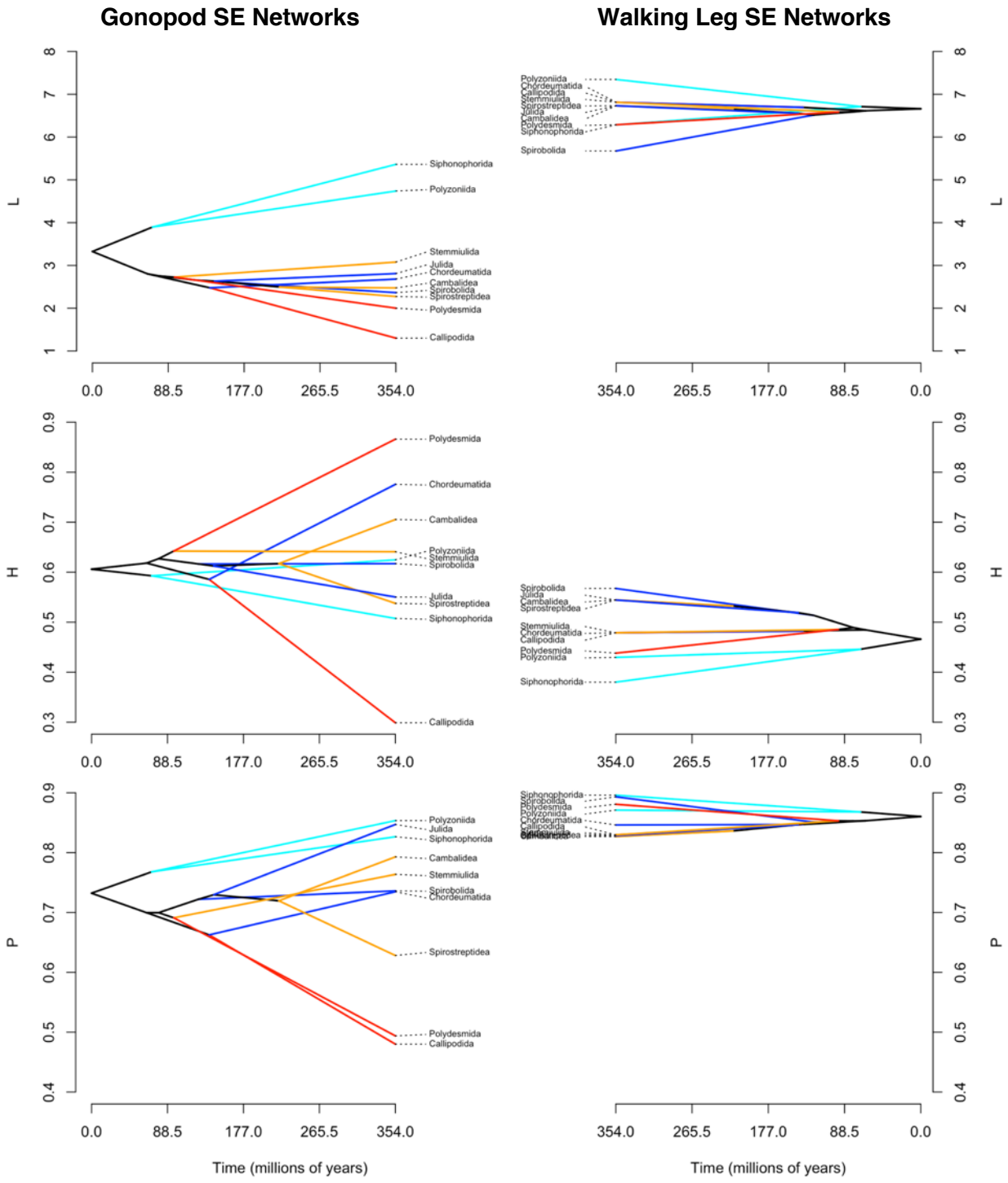


**Figure 6.** Phenograms of skeletal element network measurements. Tip colors represent gonopod appendage configurations. Cyan: gonopods at LP7-2 & LP8-1 with sperm transfer at LP7-2; Blue: gonopods at LP7-1 & LP7-2 with sperm transfer at LP7-2; Orange: gonopods at LP7-1 & LP7-2 with sperm transfer at LP7-1; Red: gonopods and sperm transfer at LP7-1.

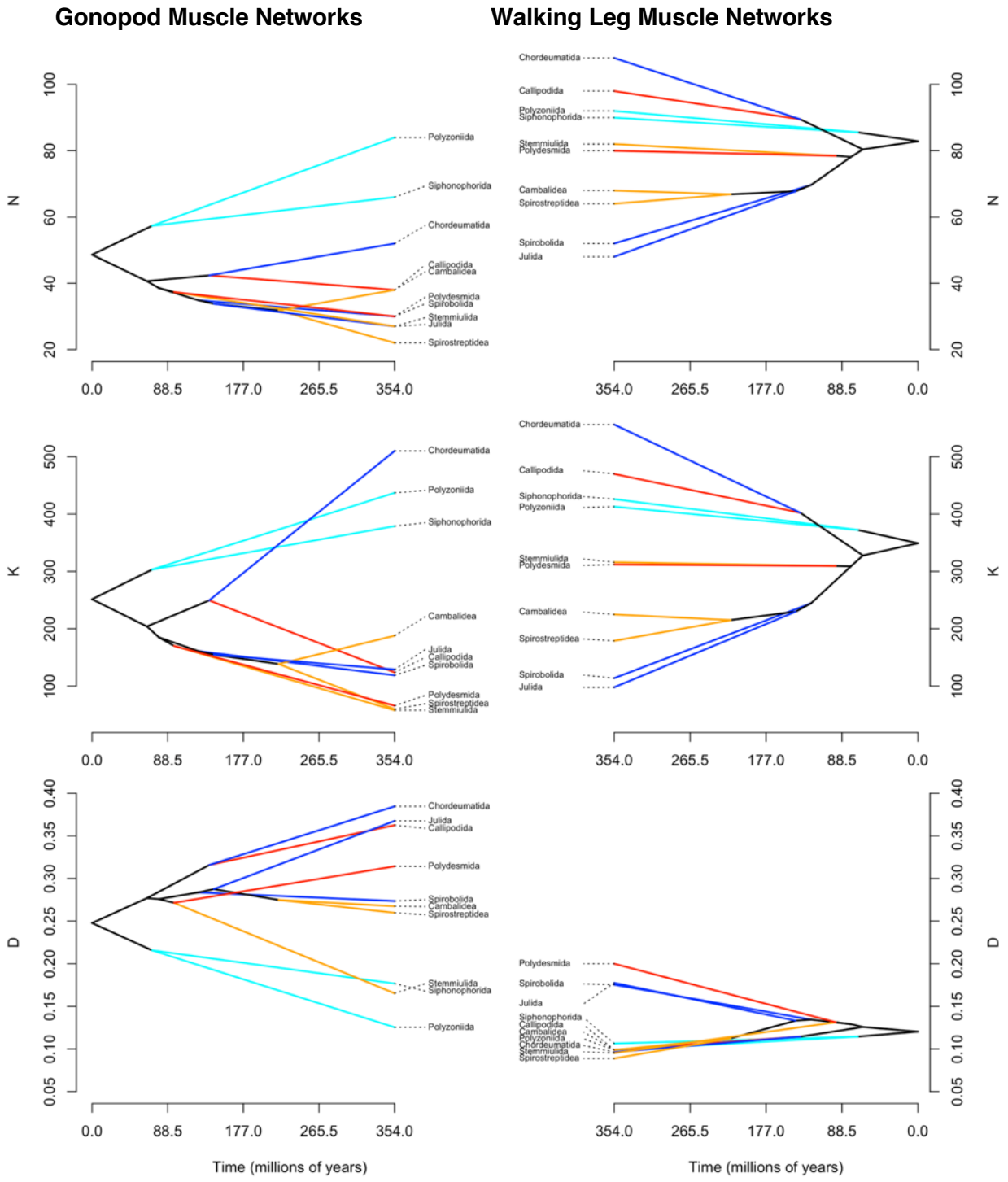


**Figure 7 (continued below).**

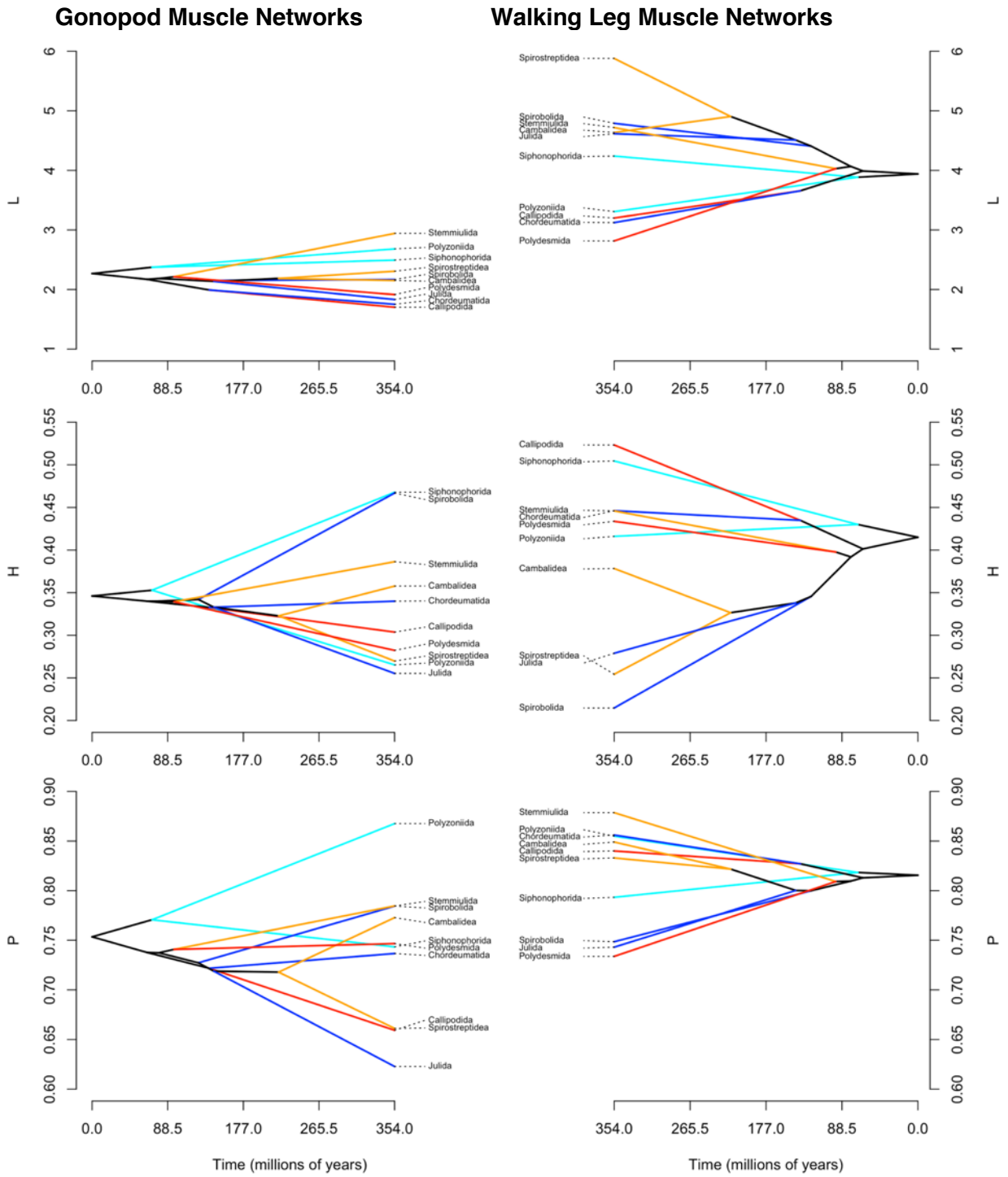


**Figure 7 (continued below).**

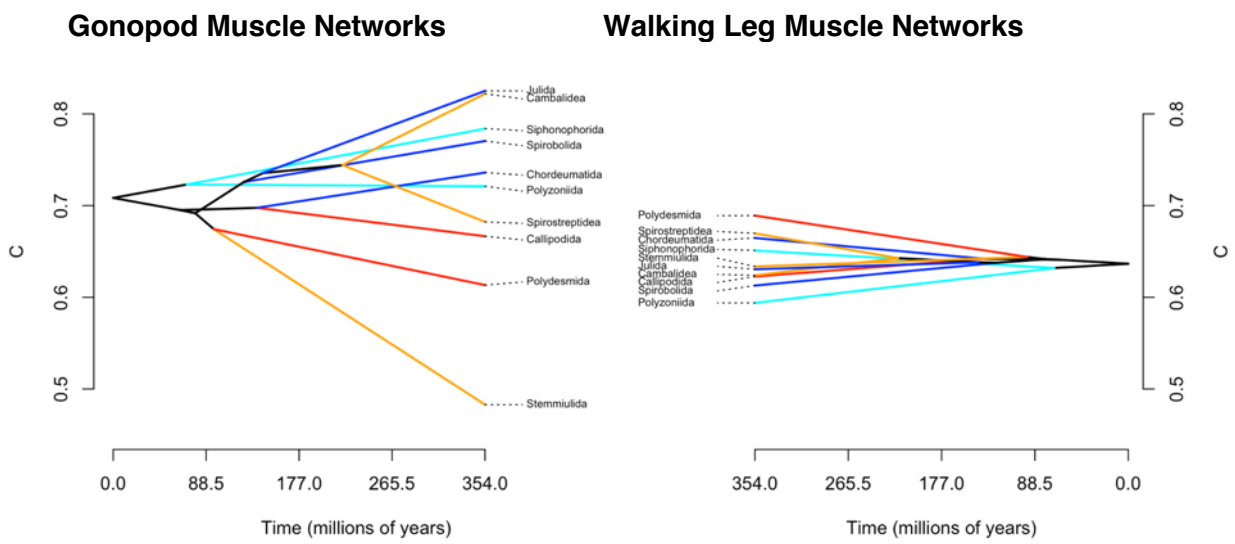


**Figure 7.** Phenograms of muscle network measurements. Tip colors represent gonopod appendage configurations. Cyan: gonopods at LP7-2 & LP8-1 with sperm transfer at LP7-2; Blue: gonopods at LP7-1 & LP7-2 with sperm transfer at LP7-2; Orange: gonopods at LP7-1 & LP7-2 with sperm transfer at LP7-1; Red: gonopods and sperm transfer at LP7-1.

**Table S1.** List of taxa, specimens, and literature data used in descriptive morphology.

| Taxon | Appendage Type | Species Source | Data Source |
|---|---|---|---|
| Siphonophorida | Gonopod | *Siphonophora* sp. | New 3D data from UCD specimen |
| | Walking Legs | *Siphonophora hartii* | Manton (1961) supported by 3D data from UCD specimen |
| Polyzoniida | Gonopod | *Octoglena bivirgata* | New 3D data from BMEA103394 |
| | Walking Legs | *Polyzonium germanicum* | Manton (1961) supported by 3D data from BMEA103394 |
| Callipodida | Gonopod | *Tynomma mutans* | New 3D data from BMEA102732 |
| | Walking Legs | *Callipus foetidissimus* | Manton (1958) supported by 3D data from BMEA102732 |
| Chordeumatida | Gonopod | *Conotyla* sp. | New 3D data from UCD specimen |
| | Walking Legs | *Nanogona polydesmoides* | Manton (1958) supported by 3D data from UCD specimen |
| Spirobolida | Gonopod | *Eurhinocricus* sp. | New 3D data from FMMC3783 |
| | Walking Legs | *Spirobolus* sp. | Manton (1958; 1961) |
| Cambalidea | Gonopod | ?*Titsona* sp. | New 3D data from BMEA102595 |
| | Walking Legs | ?*Titsona* sp. | New 3D data from BMEA102595 supported by Manton (1958) |
| Spirostreptidea | Gonopod | *Phyllogonostreptus nigrolabiatus* | Wilson (2002) supported by Demange (1967) |
| | Walking Legs | *Phyllogonostreptus nigrolabiatus* | Wilson (2002) |
| Julida | Gonopod | *Ommatoiulus avatar* | 3D data from holotype (Akkari *et al.,* 2015) |
| | Walking Legs | *Ommatoiulus sabulosus* | Manton (1958) |
| Stemmiulida | Gonopod | *Stemmiulus* sp. | New 3D data from UCD specimen |
| | Walking Legs | *Stemmiulus* sp. | New 3D data from UCD specimen |
| Polydesmida | Gonopod | *Pseudopolydesmus serratus* | Zahnle *et al.* (2022) |
| | Walking Legs | *Polydesmus angustus* | Manton (1954; 1958) supported by Zahnle *et al.* (2022) |

**Table S2.** List of SE and muscle labels in *Phyllogonostreptus nigrolabiatus* gonopod, as used in this paper. Names of SEs and muscles are listed according to Wilson (2002).

| **SE label** | **SE name (Wilson, 2002)** |
|---|---|
| A1 | apodeme arm |
| A2 | sternite |
| A3 | coxa |
| A4 | telopodite |
| A5 | apodeme base |
| A6 | coxal flange (paracoxite of Demange, 1967) |
| | |
| **Muscle label** | **Muscle name (Wilson, 2002)** |
| E1 | Apodeme-tergal muscle (*gp2*) |
| E2 | Ventral coxa-tergite 6 muscle (*gp6*) |
| E3 | Dorsal coxa-tergite 6 muscle (*gp7*) |
| F1 | Apodeme-posterior gonopod muscle (*gp9*) |
| F2 | Posterior gonopod-tergite 8 muscle (*gp10*) |
| K1 | Leg 9-gonopod apodeme muscle (*gp8*) |
| K2 | Leg 9-pleurotergite muscle (*gp10*) |
| I1 | Medial apodeme-coxa muscle (*gp1*) |
| I2 | Posterior apodeme-coxa muscle (*gp3*) |
| I3 | Lateral apodeme-coxa muscle (*gp4*) |
| I4 | Intrinsic coxal muscle (*gp5*) |

**Table S3.** List of SE and muscle labels in *Pseudopolydesmus serratus* gonopod, as used in this paper. Names of SEs and muscles are listed according to Zahnle *et al.* (2022).

| **SE label** | **SE name (Zahnle *et al,* 2022)** |
|---|---|
| A1 | tracheal apodeme |
| A2 | coxa |
| A3 | prefemur |
| A4 | cannula |
| | |
| **Muscle label** | **Muscle name (Zahnle *et al,* 2022)** |
| E1 | *protractor coxae anterior* |
| E2 | *retractor coxae inferus* (inserts onto tracheal apodeme A1) |
| E3 | *retractor coxae superus* (inserts onto coxa A2) |
| E4 | *protractor coxae posterior* |
| I1 | *levator prefemoris* |
| I2 | *depressor brevis prefemoris* |
| I3 | *adductor cornui* |
| T | *intercoxae* |

**Gonopod SE networks**

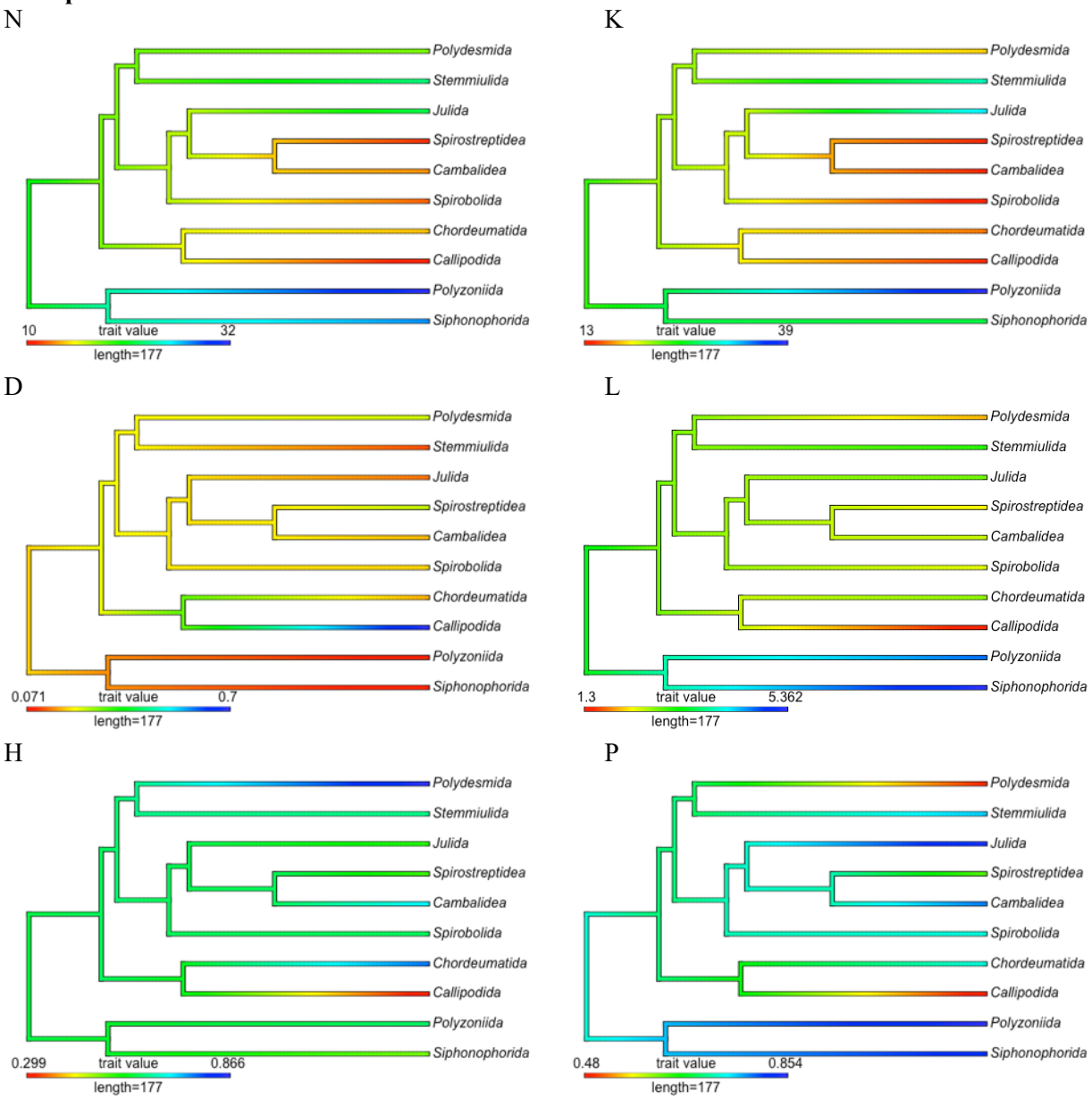


**Figure S1.** Ancestral character mapping for measurements derived from gonopod skeletal element networks.

**Walking leg SE networks**

K

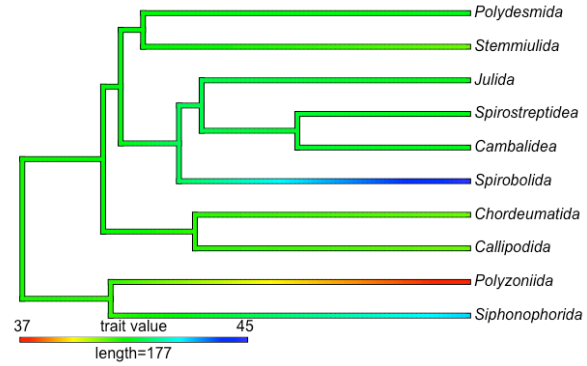


D

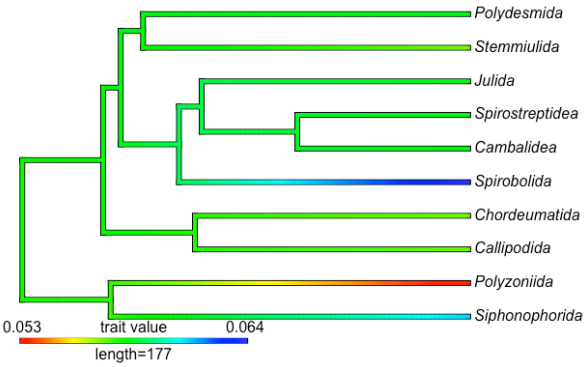


L

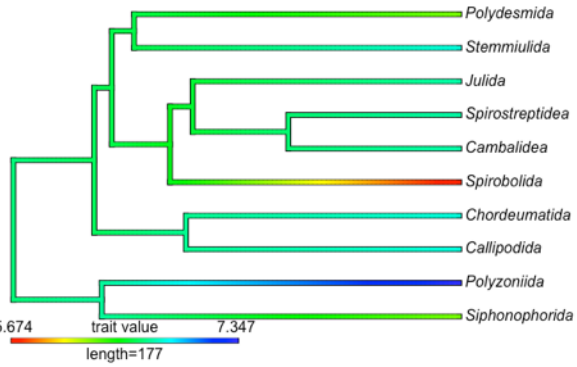


H

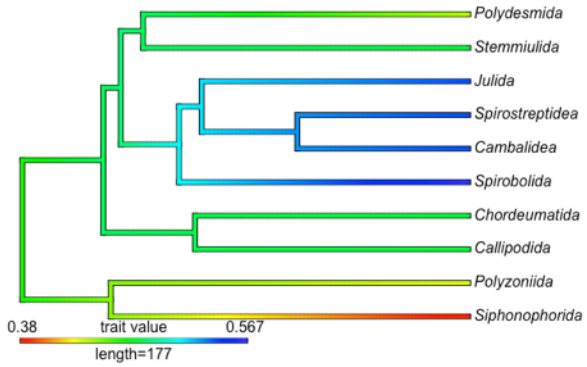


P

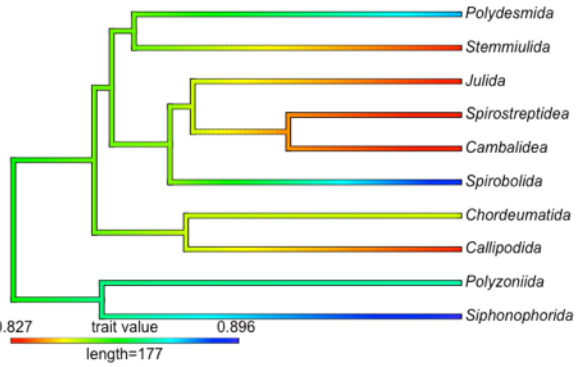


**Figure S2.** Ancestral character mapping for measurements derived from walking leg skeletal element networks.

**Gonopod muscle networks**

N

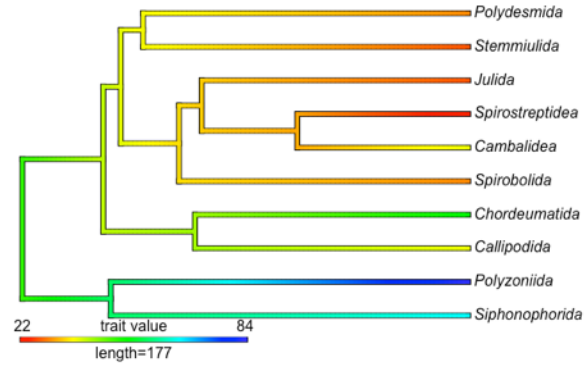


K

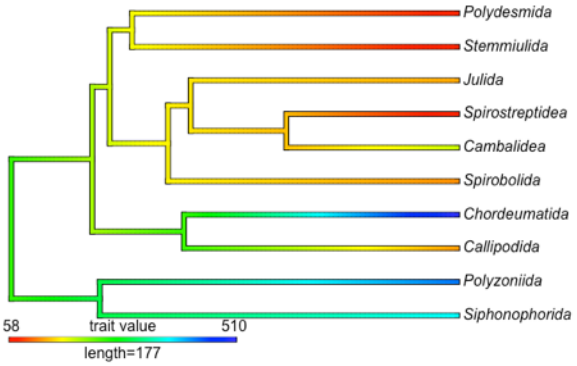


D

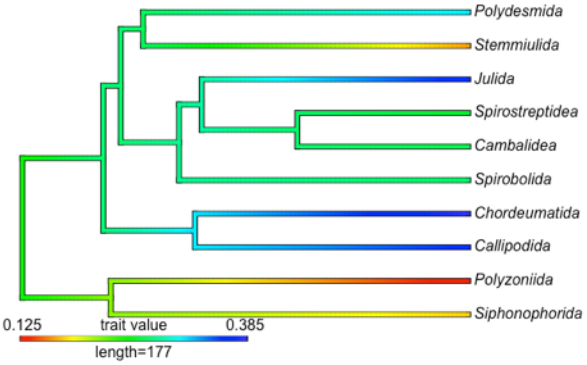


L

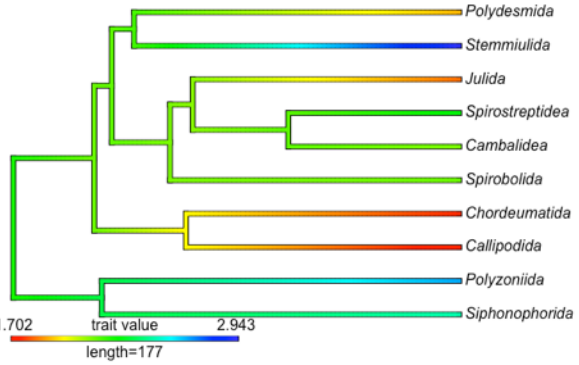


H

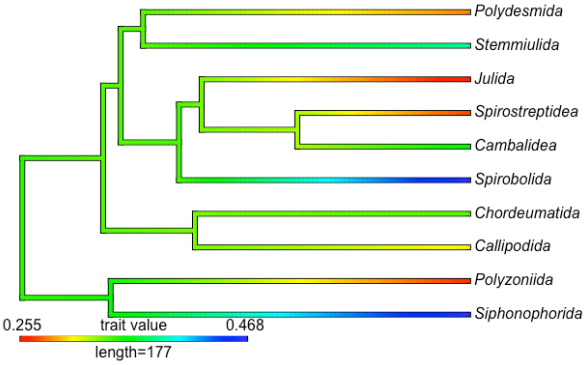


P

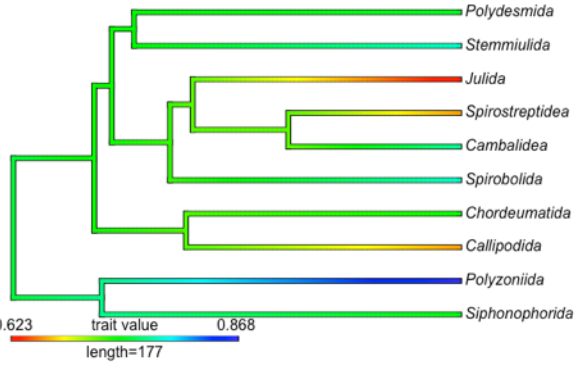


**Figure S3 (continued below).**

C

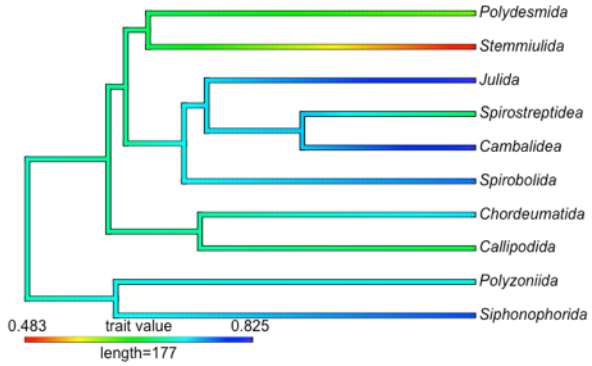


**Figure S3.** Ancestral character mapping for measurements derived from gonopod muscle networks.

**Walking leg muscle networks**

N

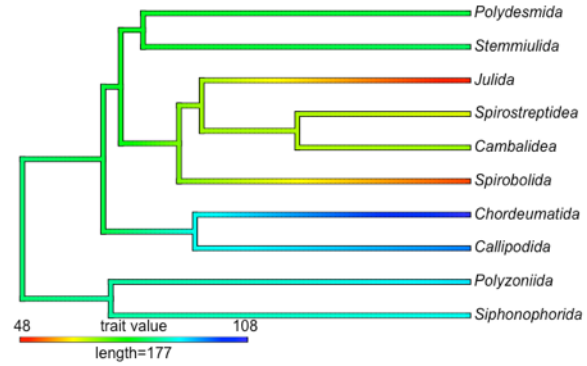


K

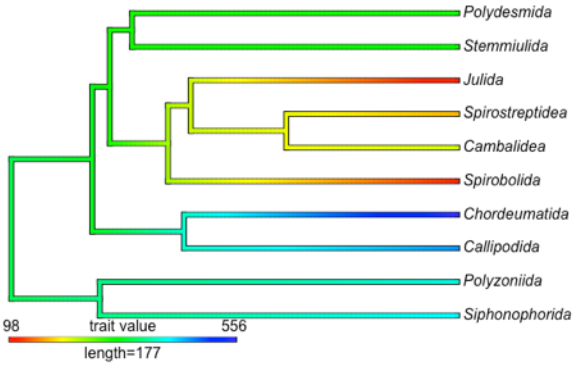


D

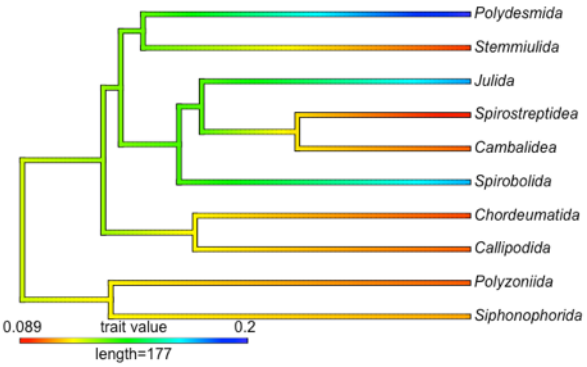


L

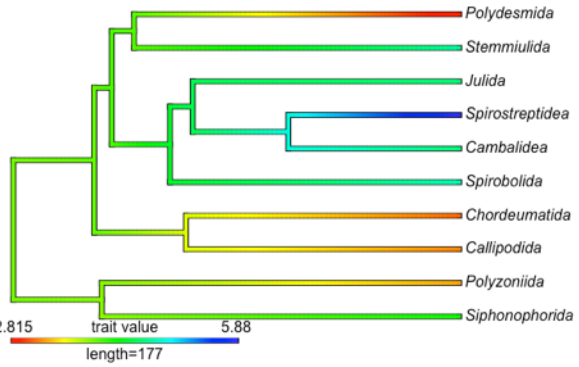


H

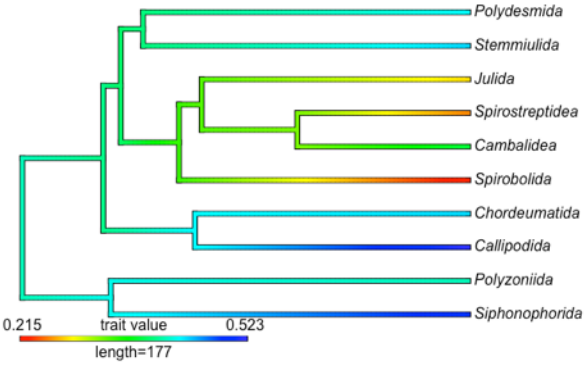


P

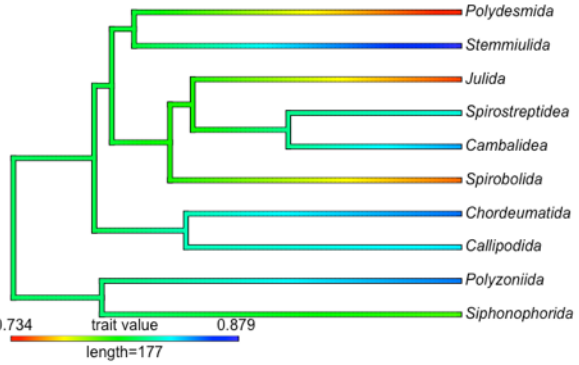


**Figure S4 (continued below).**

C

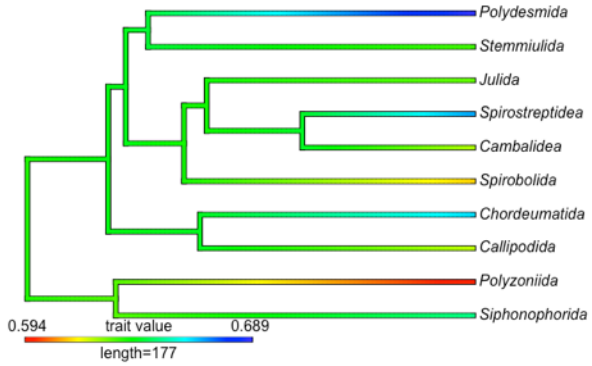


**Figure S4.** Ancestral character mapping for measurements derived from walking leg muscle networks.

A

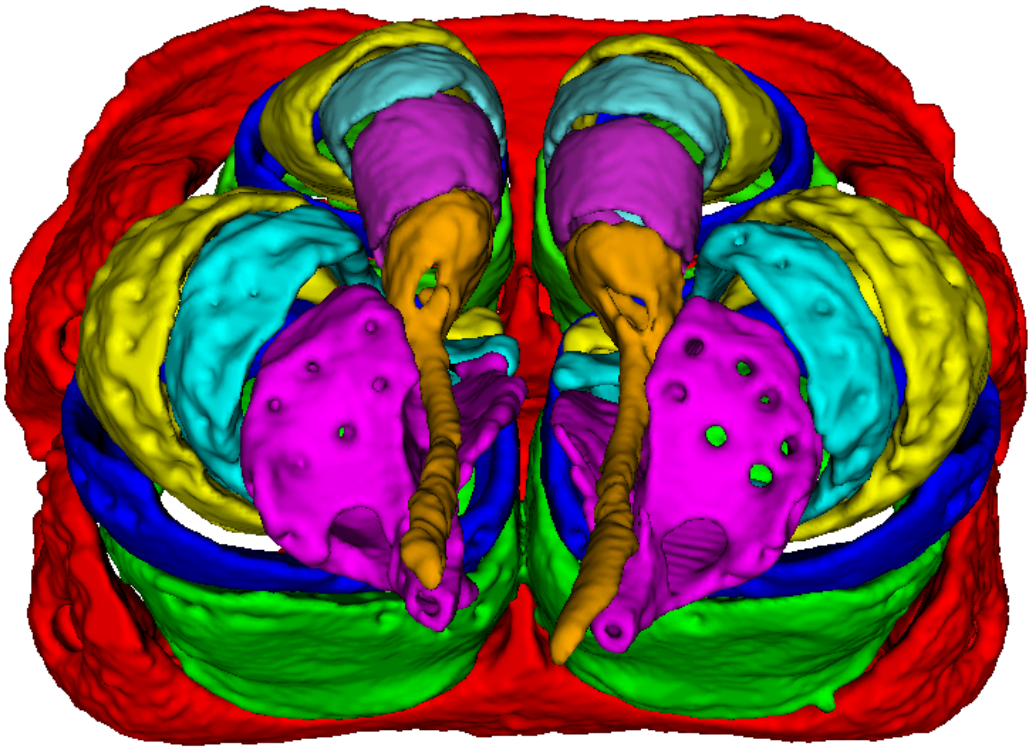

B

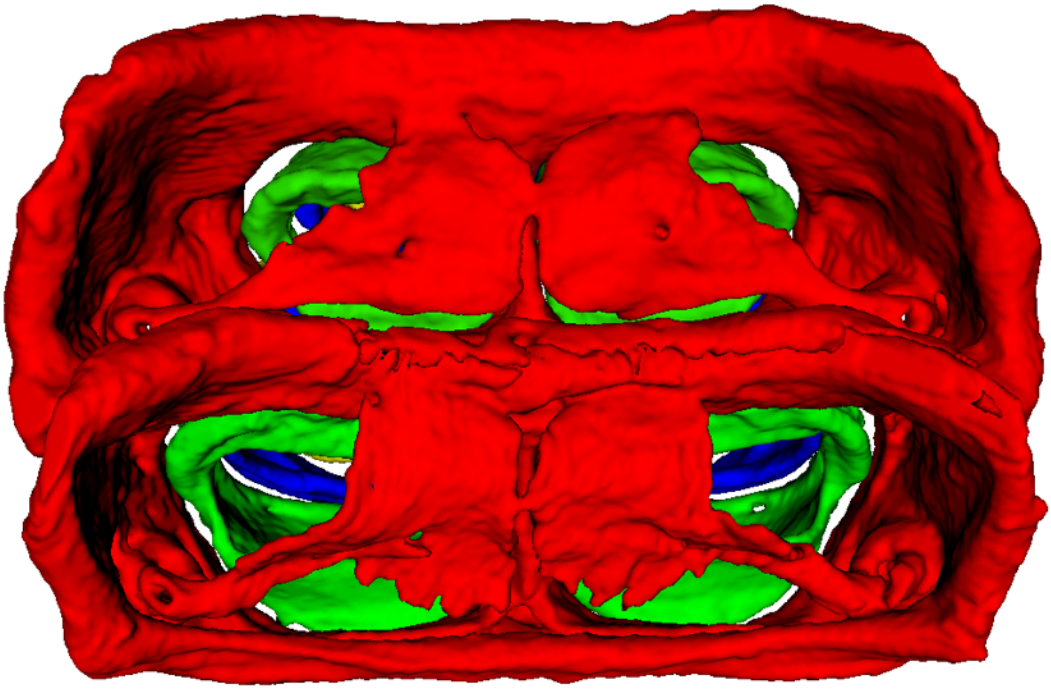

**Figure S5.** *Siphonophora* sp. gonopod skeletal elements. A: ventral view; B: dorsal (internal) view.

A

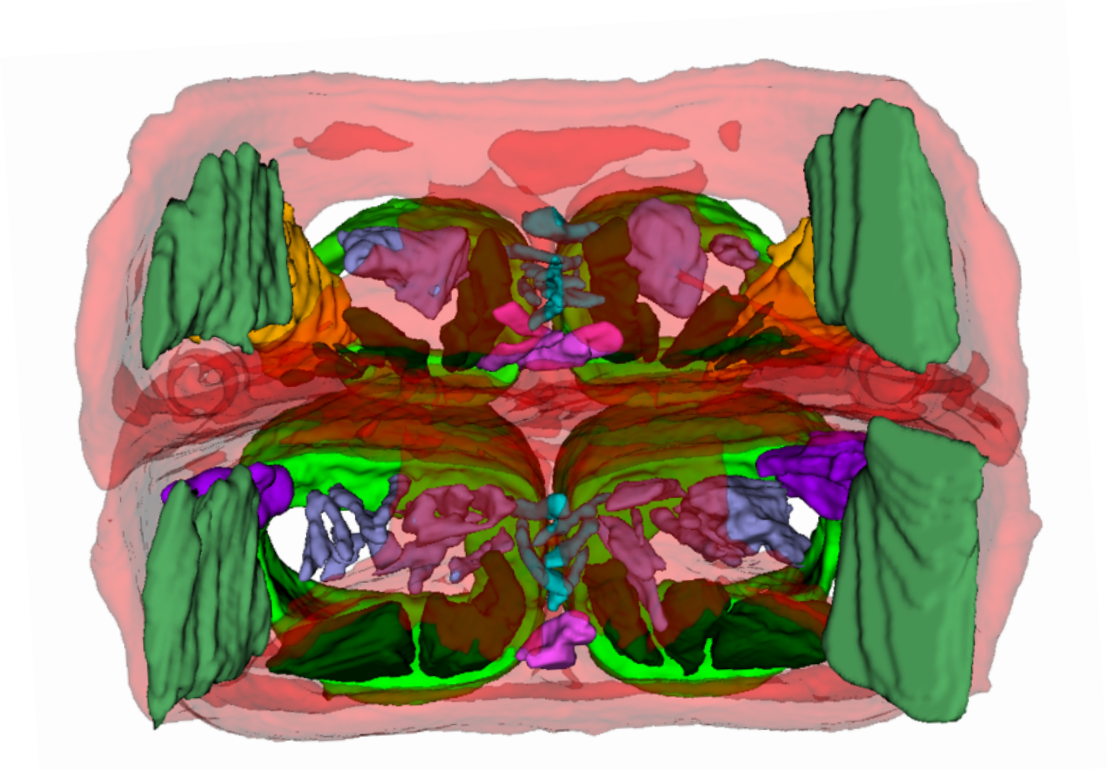

B

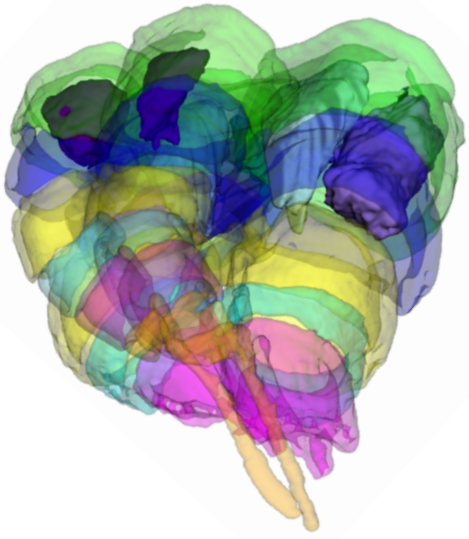

**Figure S6.** *Siphonophora* sp. gonopod muscles visible through translucent skeletal elements. A: dorsal (internal) view; B: lateral view.

A

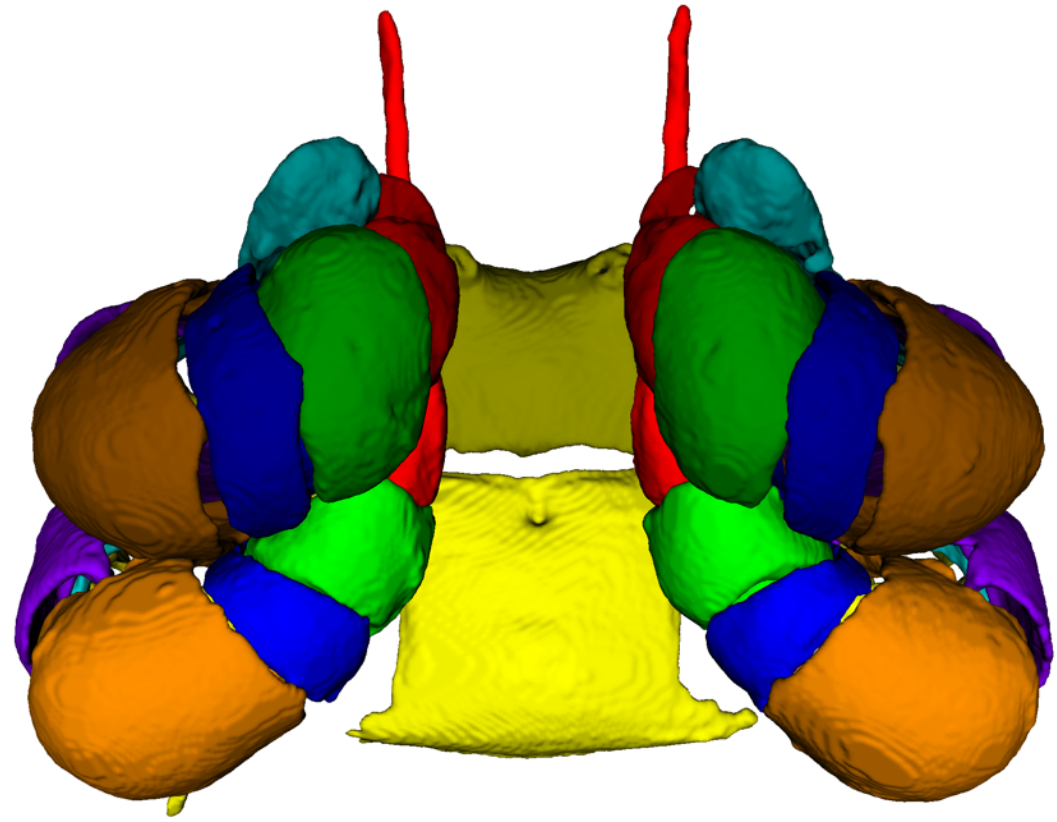

B

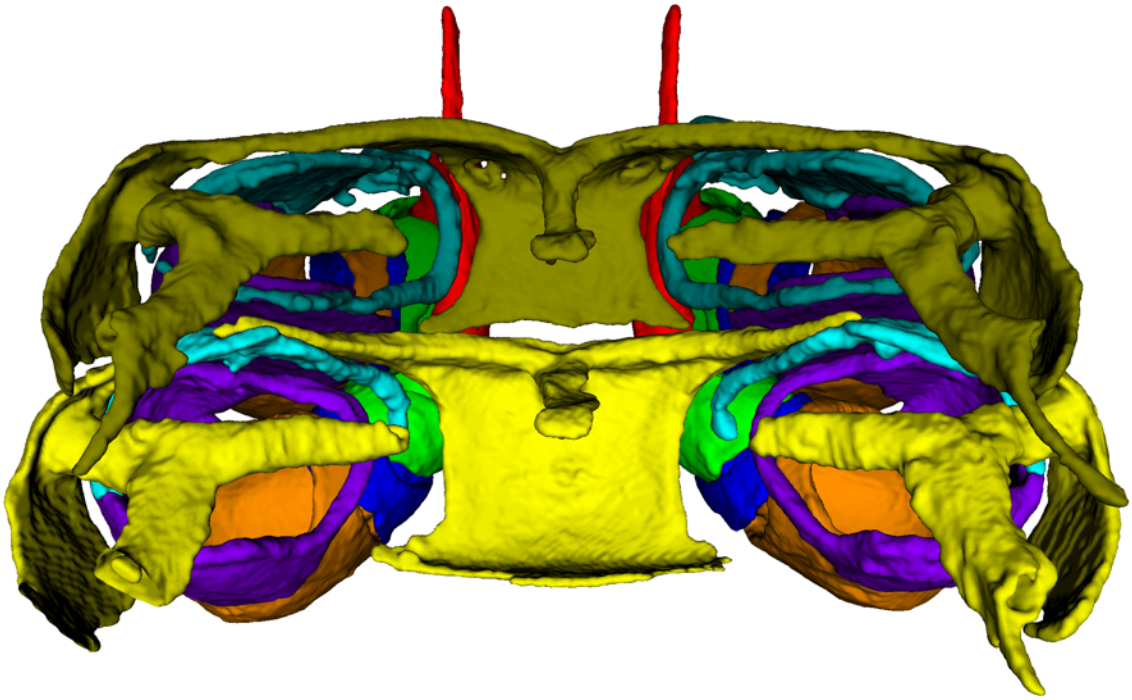

**Figure S7.** *Octoglena bivirgata* gonopod skeletal elements. A: ventral view; B: dorsal (internal) view.

A

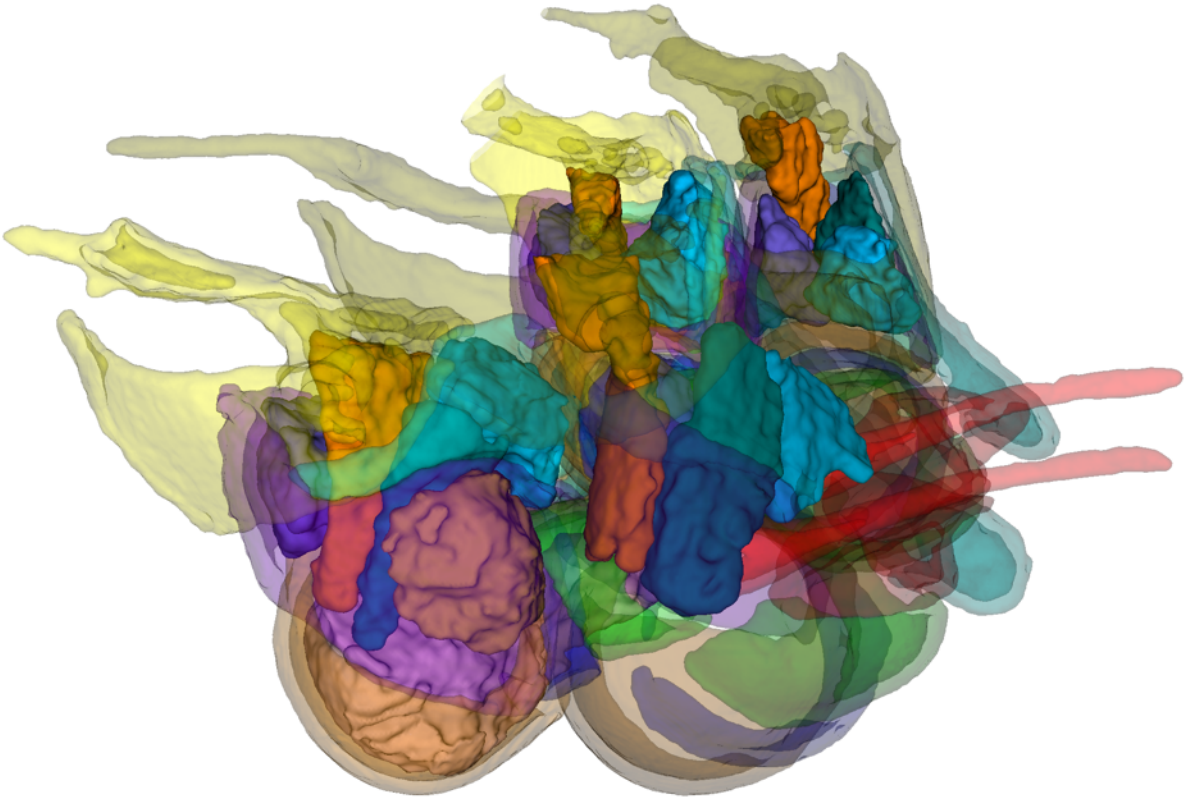

B

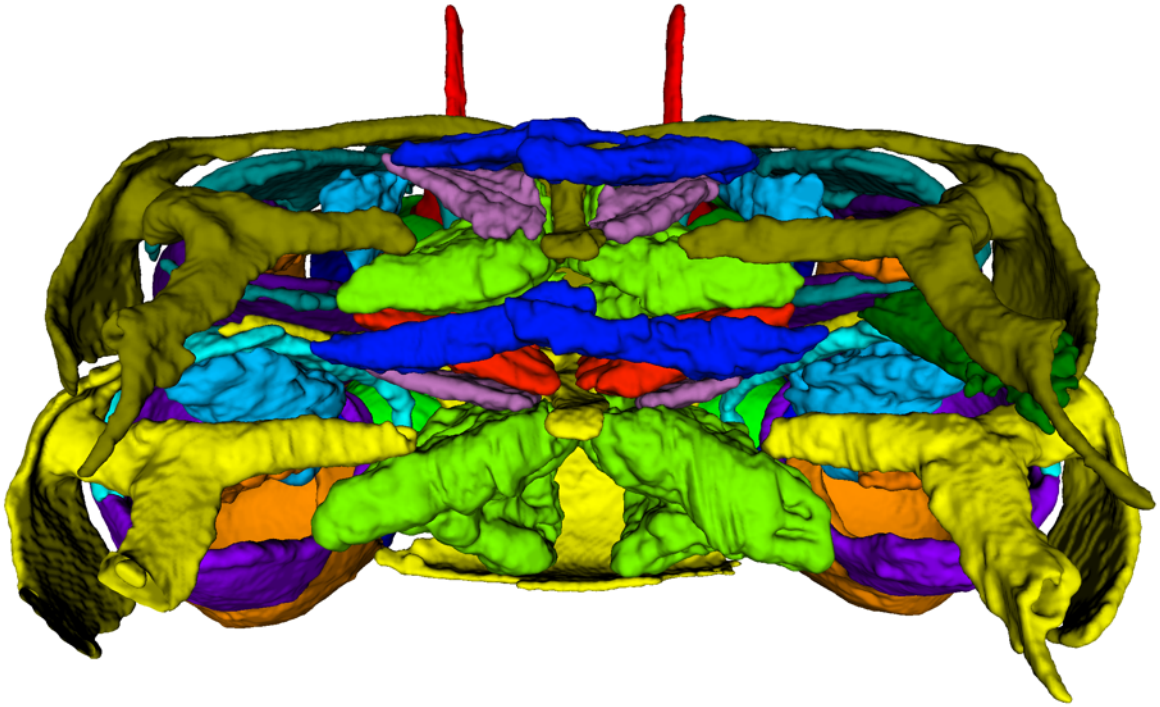

**Figure S8.** *Octoglena bivirgata* gonopod muscles. A: lateral view with translucent SE; B: dorsal (internal) view.

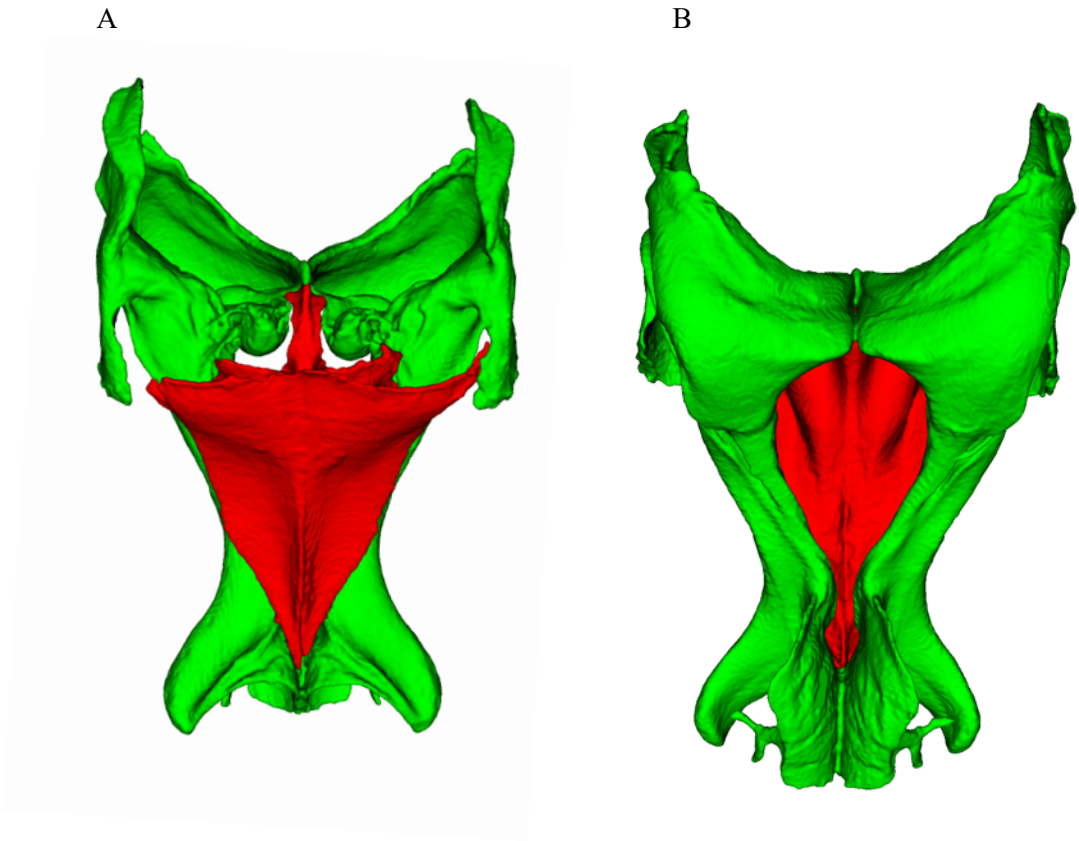


**Figure S9.** *Tynomma* gonopod skeletal elements. A: anterior view; B: posterior view.

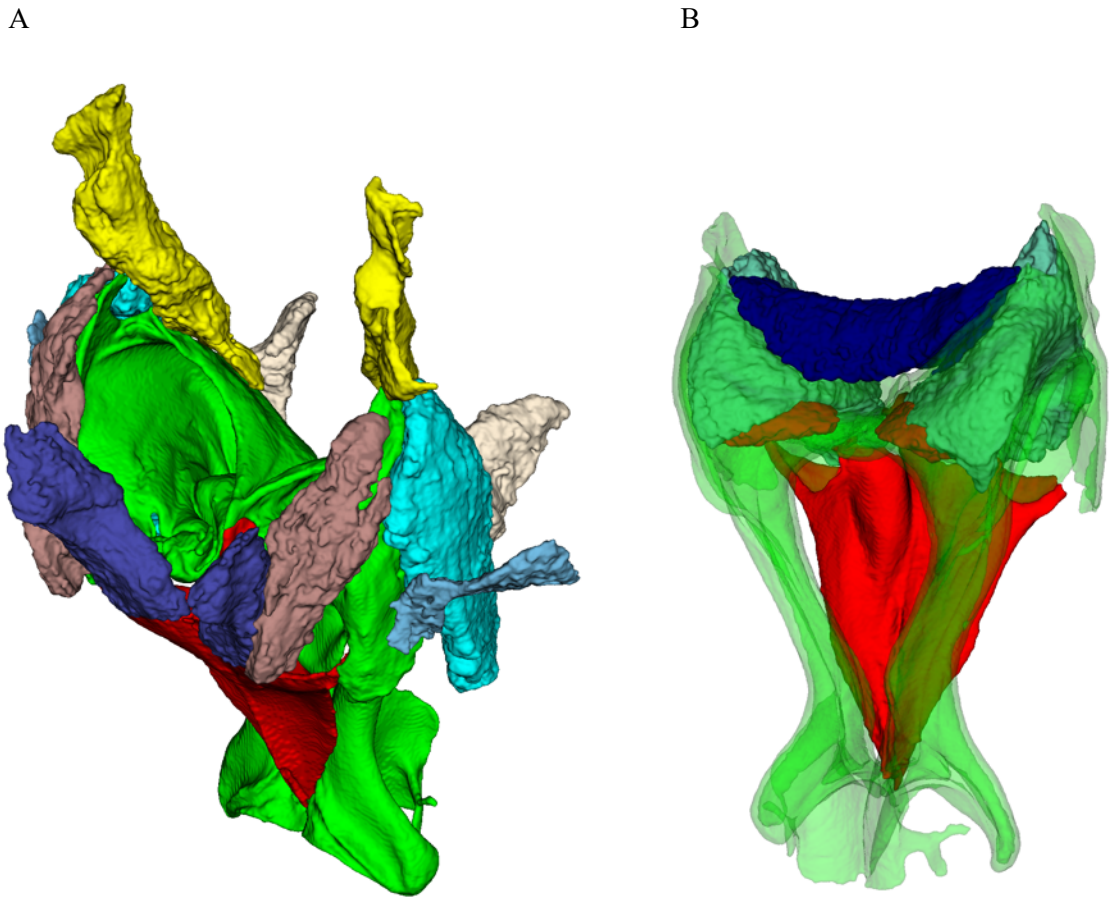


**Figure S10.** *Tynomma* gonopod muscles. A: anterolateral view highlighting extrinsic muscles; B: posterior view with translucent A2 and A3, highlighting intrinsic and transverse muscles.

A

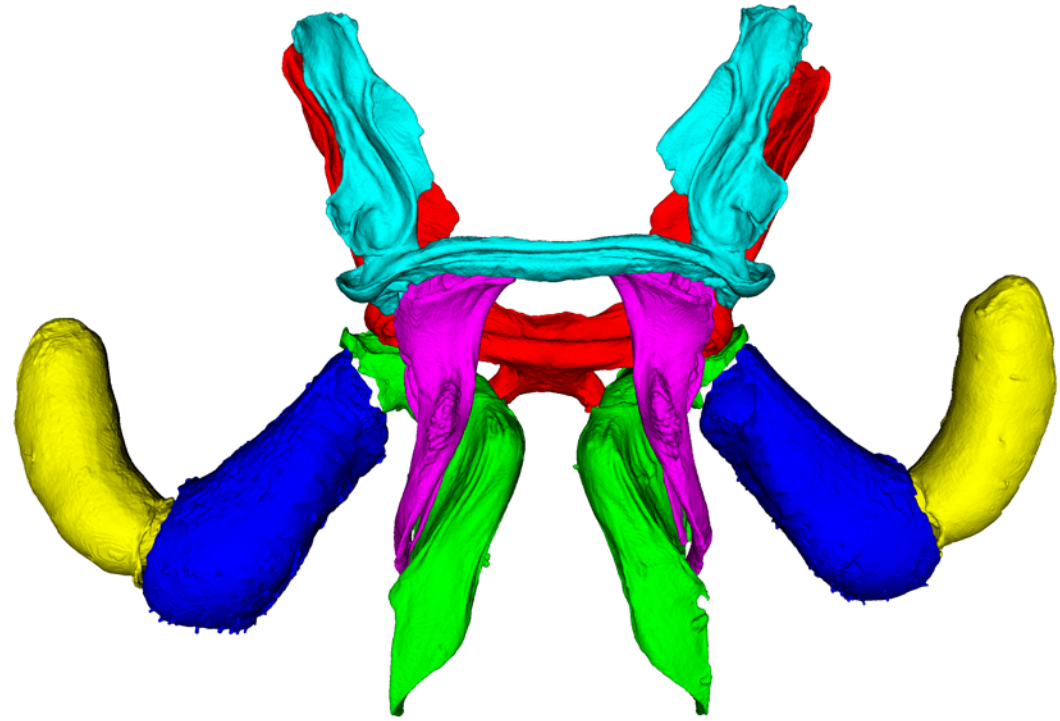

B

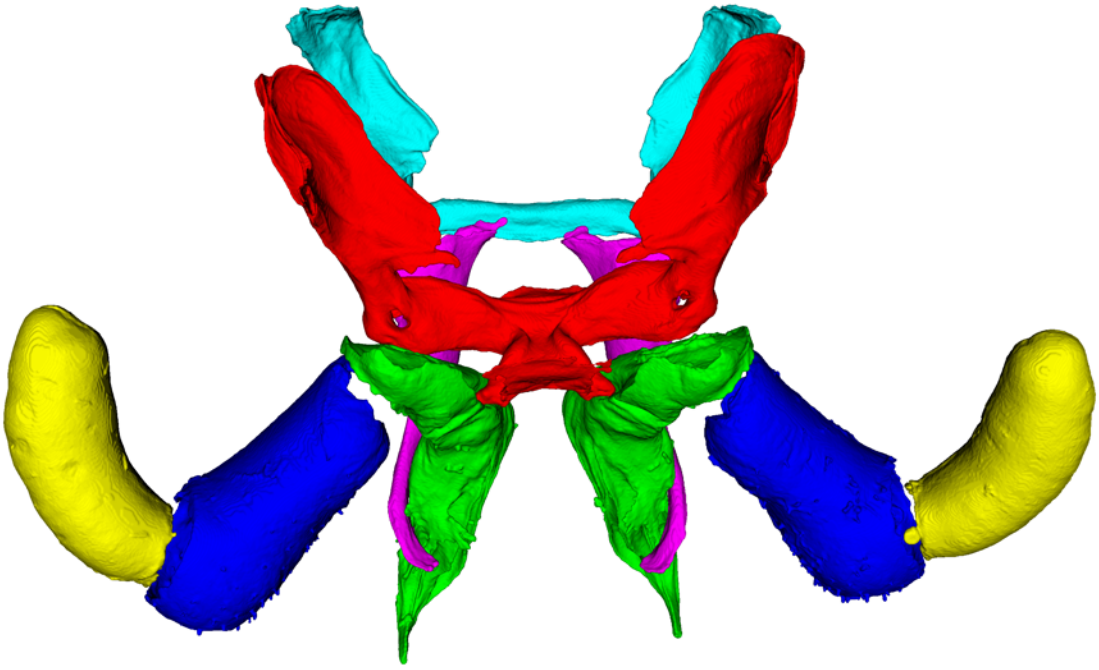

**Figure S11.** *Conotyla* sp. gonopod skeletal elements. A: anterior view; B: posterior view.

A

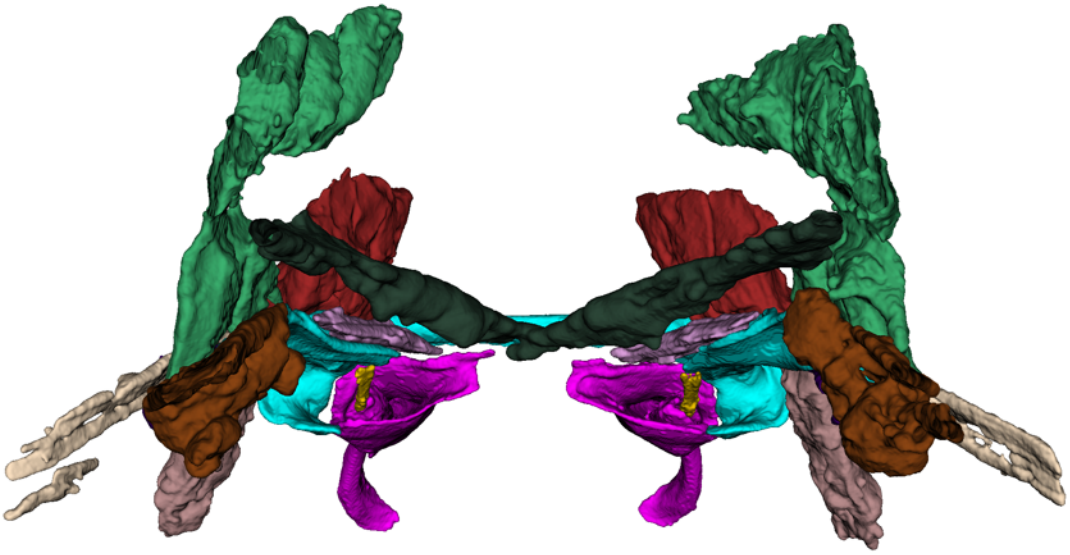

B

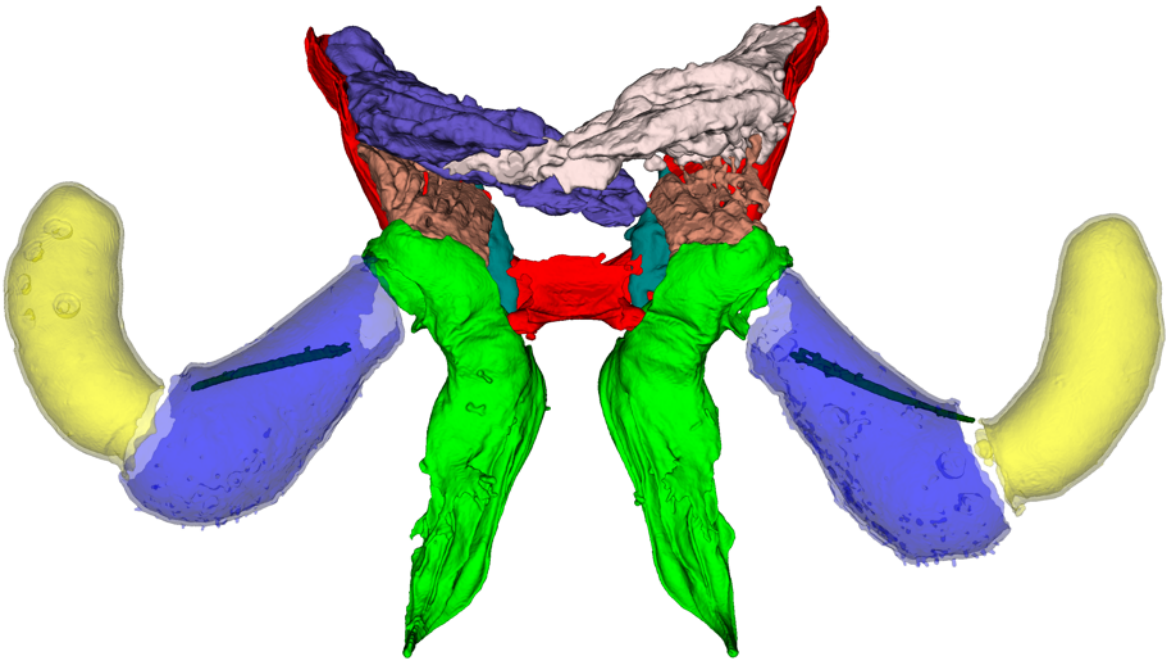

**Figure S12.** *Conotyla* sp. gonopod muscles. A: dorsal (internal) view of the anterior gonopod pair (LP7-1). B: posterior view of the posterior gonopod pair, with P4 and P5 translucent to show J4 muscle.

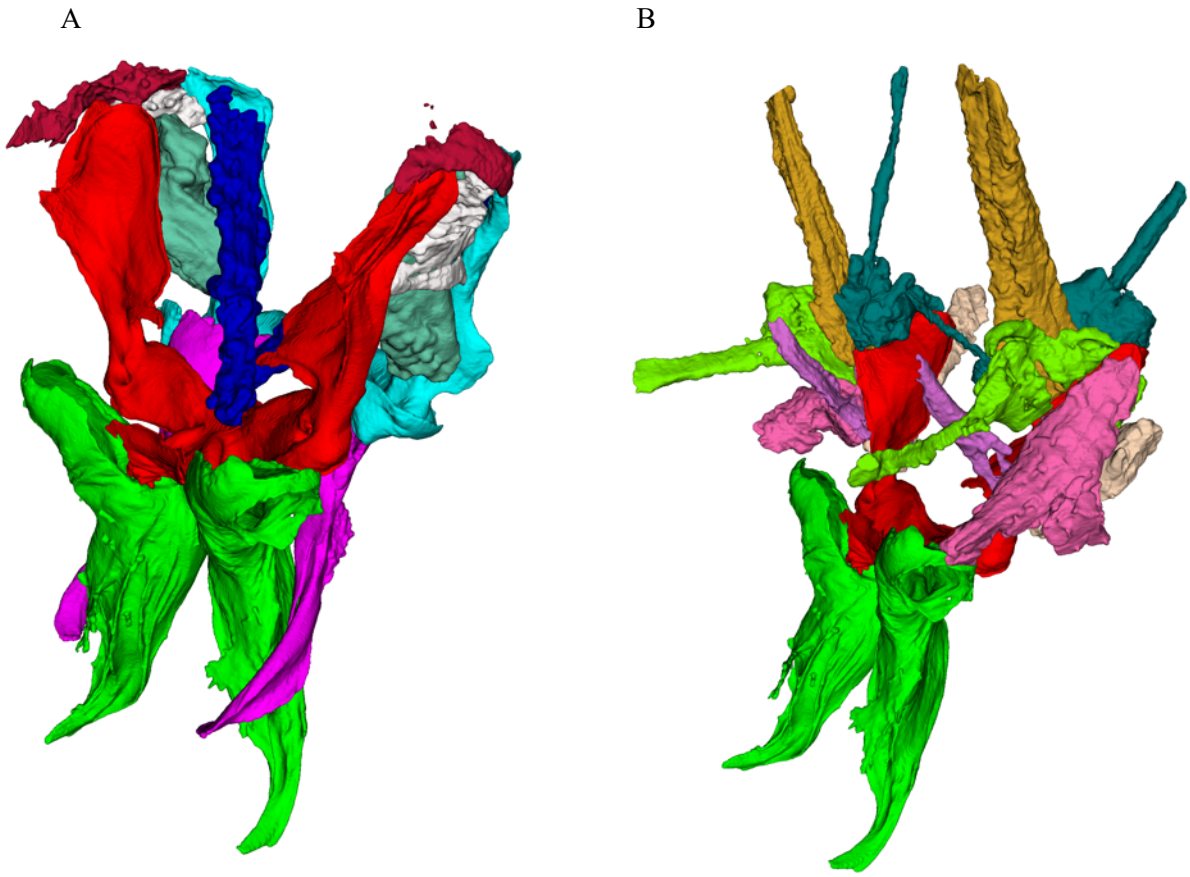


**Figure S13.** *Conotyla* sp. gonopod muscles in posterolateral view. A: Both gonopod pairs. B: posterior gonopod pair only, highlighting posterior gonopod extrinsic muscles.

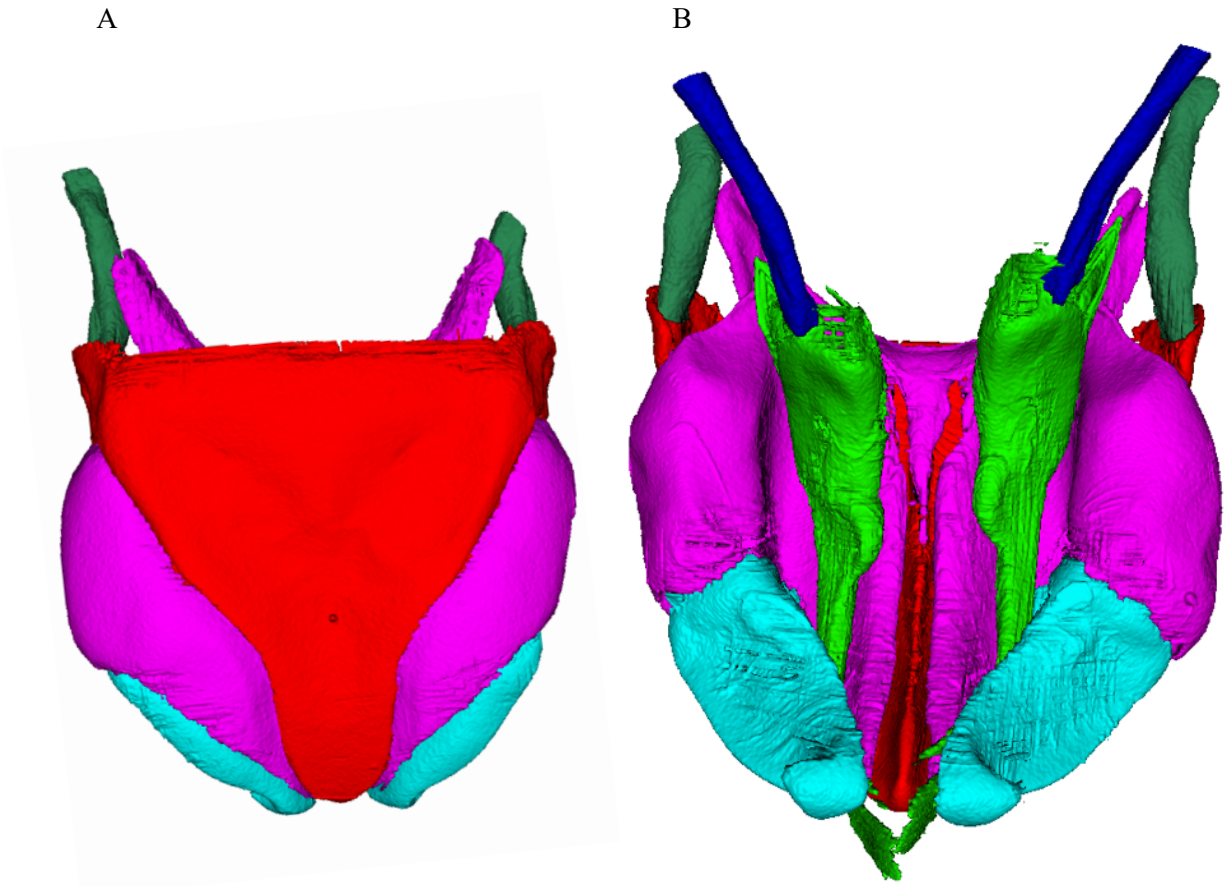


**Figure S14.** *Eurhinocricus* sp. gonopod skeletal elements. A: anterior view of anterior gonopod only; B: posterior view with both gonopod appendage pairs.

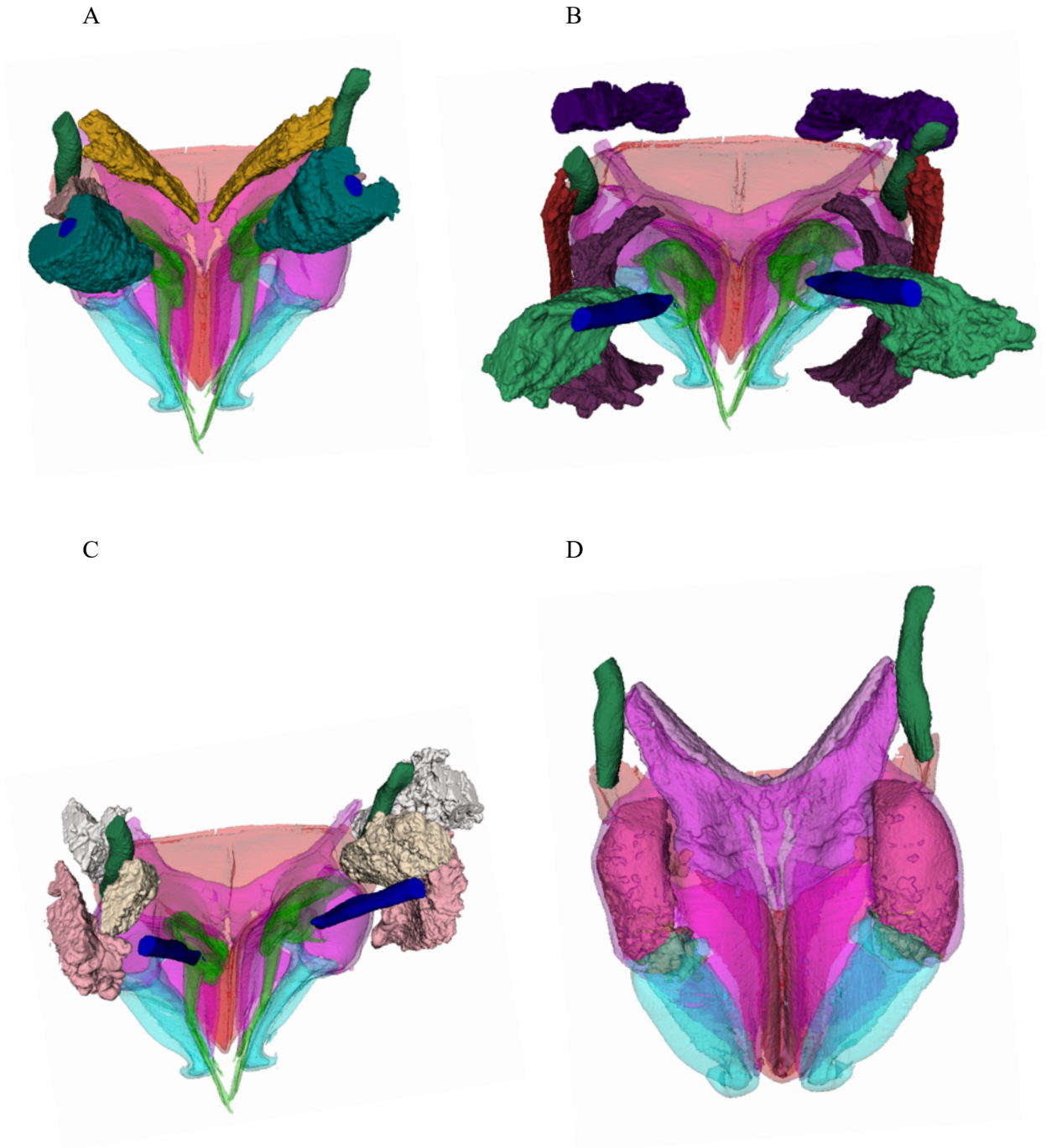


**Figure S15.** *Eurhinocricus* sp. gonopod muscles, posterior view with successive muscles removed from A to D. Fig. S11D highlights intrinsic muscles through transclucent SE.

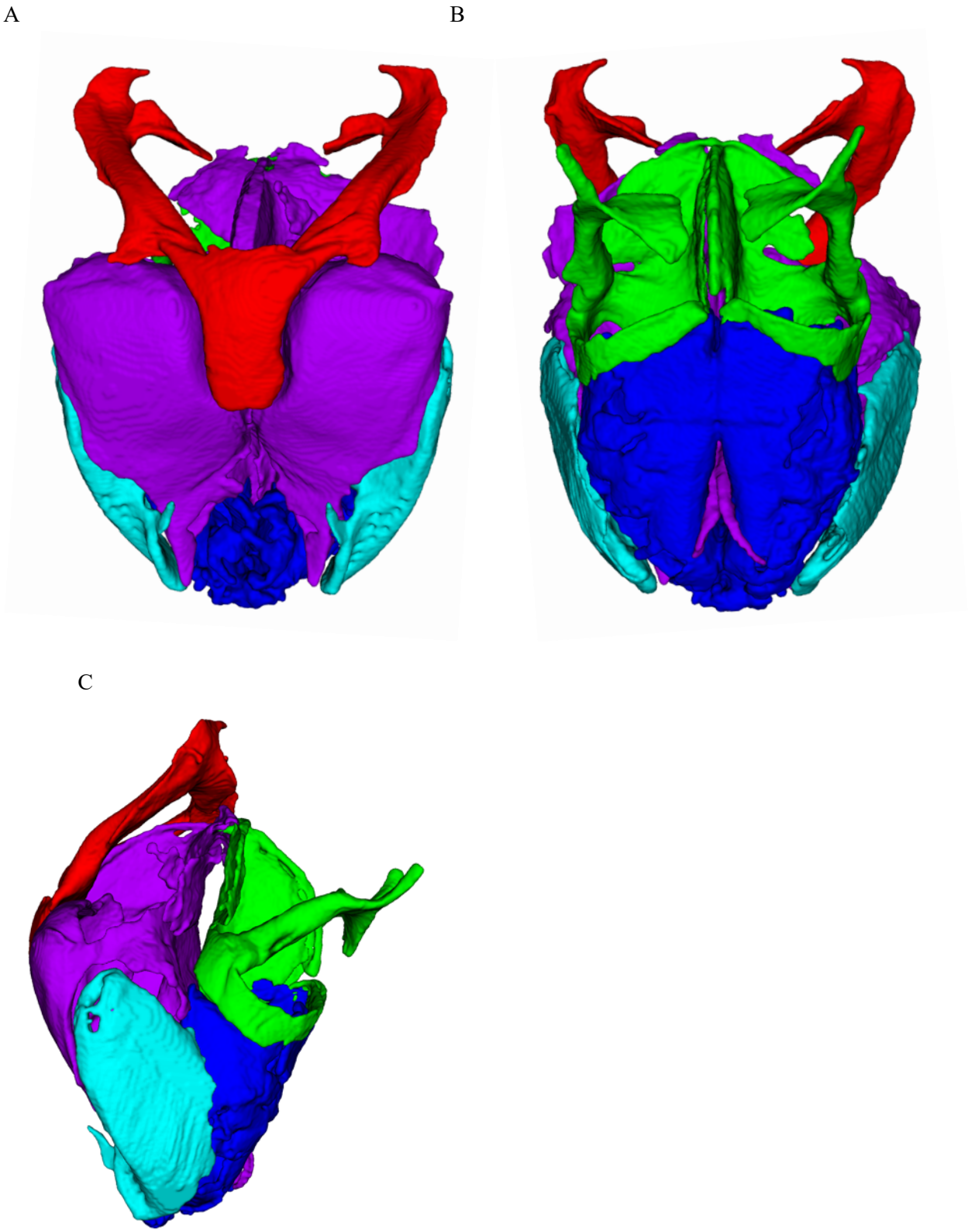


**Figure S16.** ?*Titsona* sp. gonopod skeletal elements. A: anterior view; B: posterior view; C: lateral view.

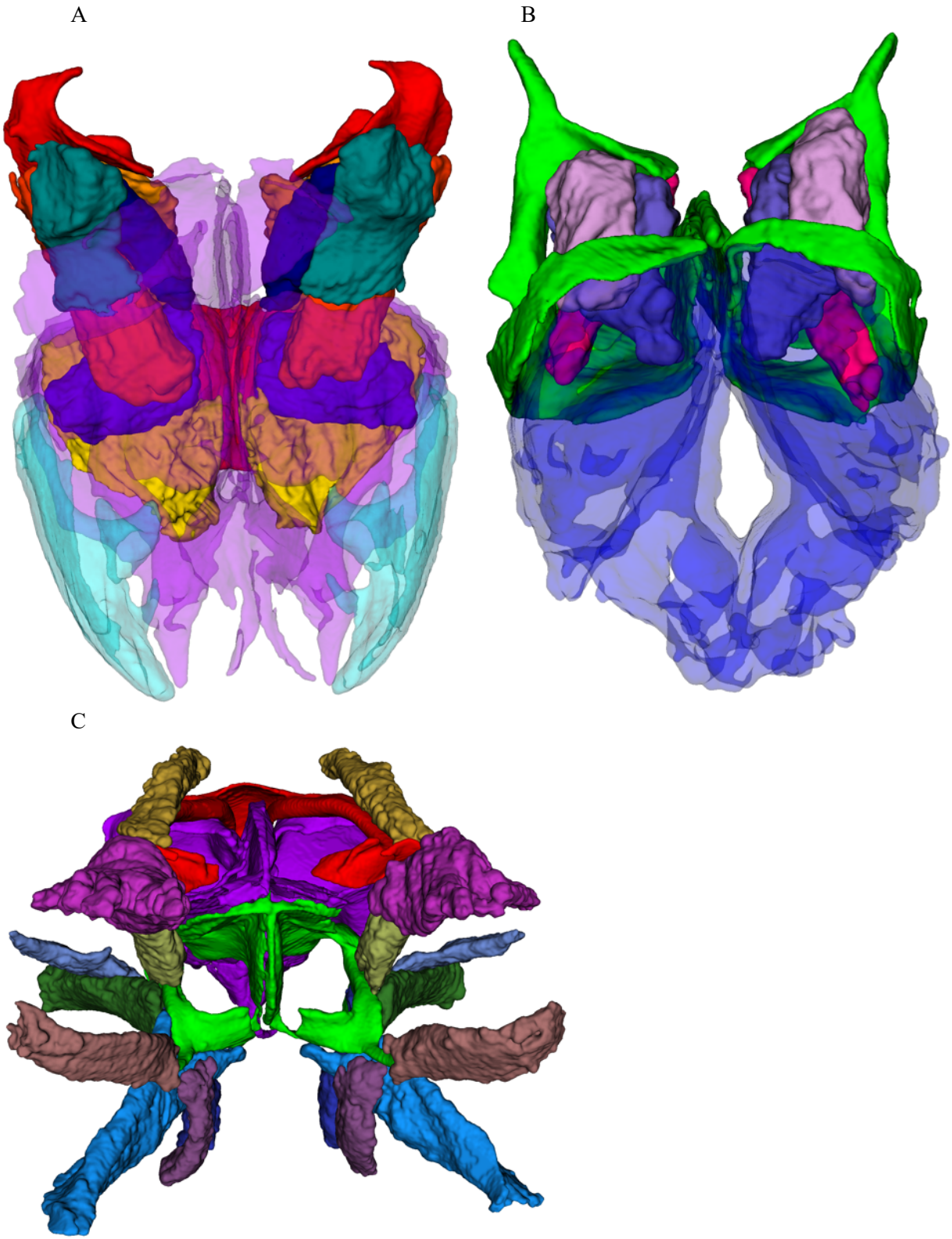


**Figure S17.** ?*Titsona* sp. gonopod muscles. A: anterior view of anterior gonopod only, with distal sclerites translucent; B: posterior view of posterior gonopod only, with distal sclerites translucent. C: dorsal (internal) view highlighting extrinsic muscles and cruciform gonocoel.

A

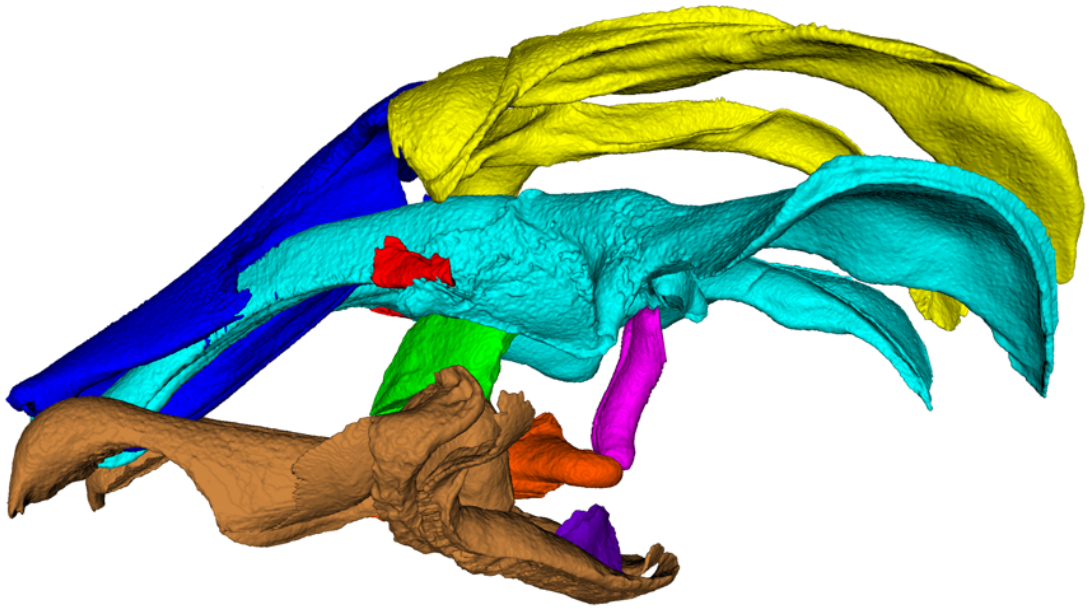

B

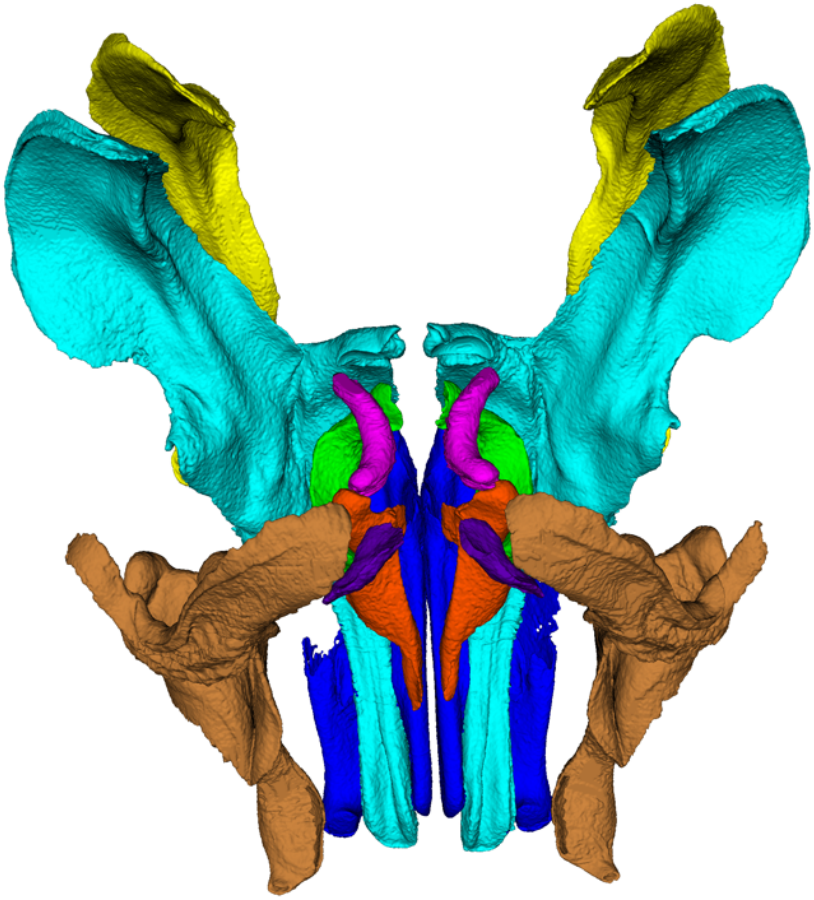

**Figure S18.** *Ommatoiulus avatar* gonopod skeletal elements. A: lateral view; B: posterior view.

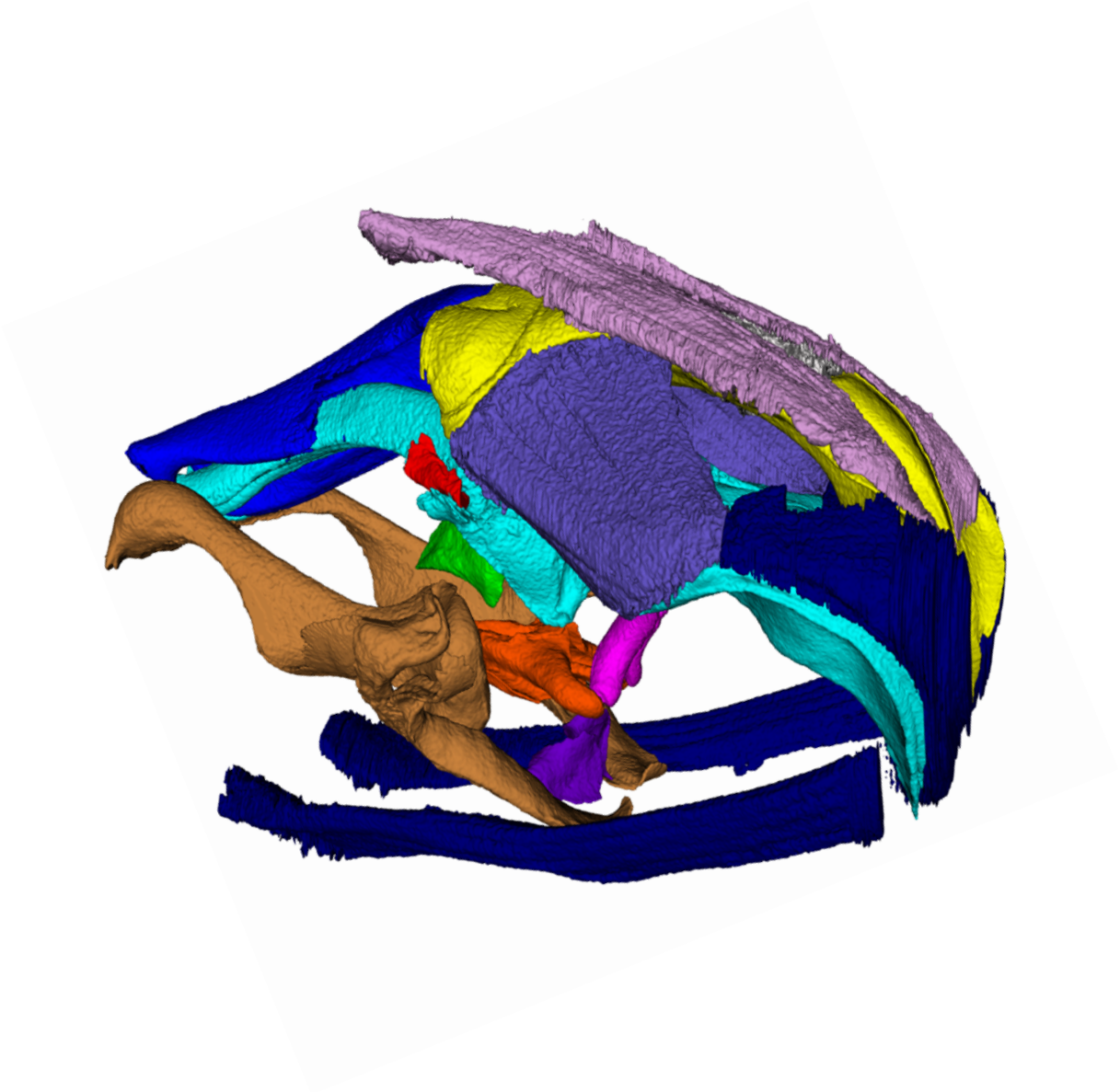

**Figure S19.** *Ommatoiulus avatar* gonopod muscles from a lateral view.

A

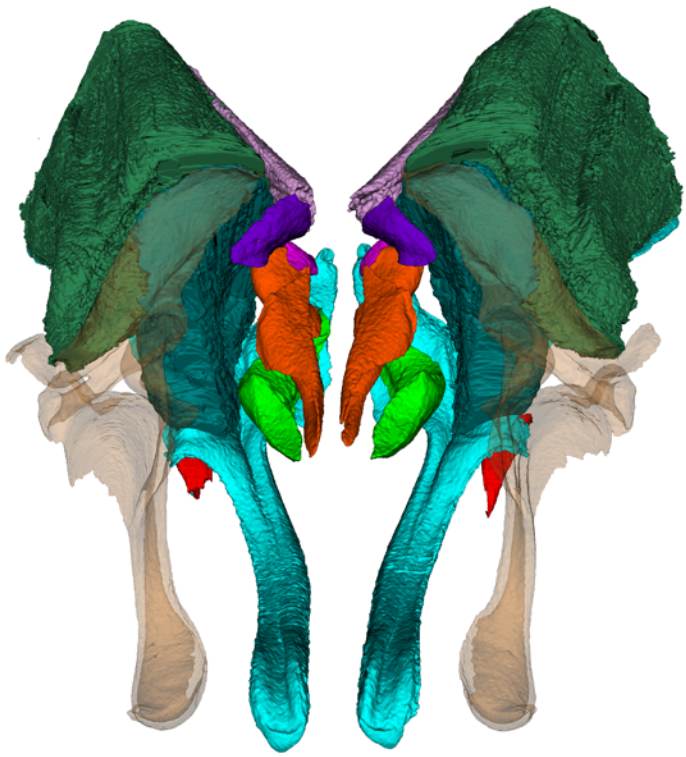

B

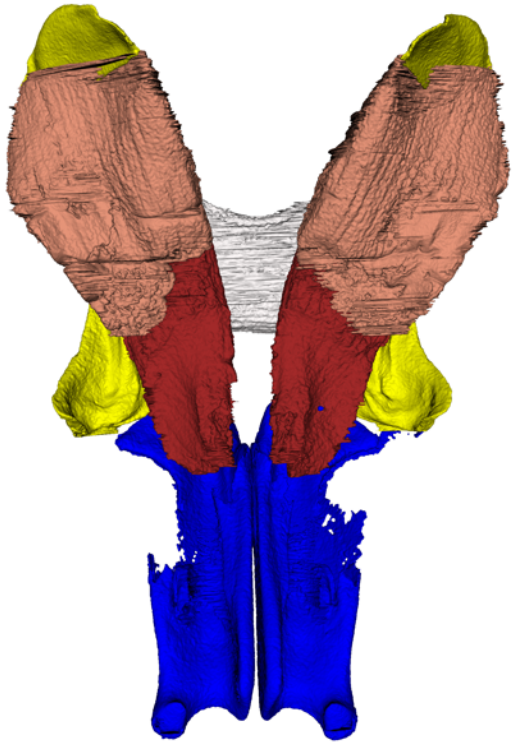

**Figure S20.** *Ommatoiulus avatar* gonopod muscles. A: posterior view with both gonopod appendage pairs, with P7 translucent highlighting posterior gonopod intrinsic muscles; B: posterior view with anterior gonopod only, highlighting anterior gonopod intrinsic muscles.

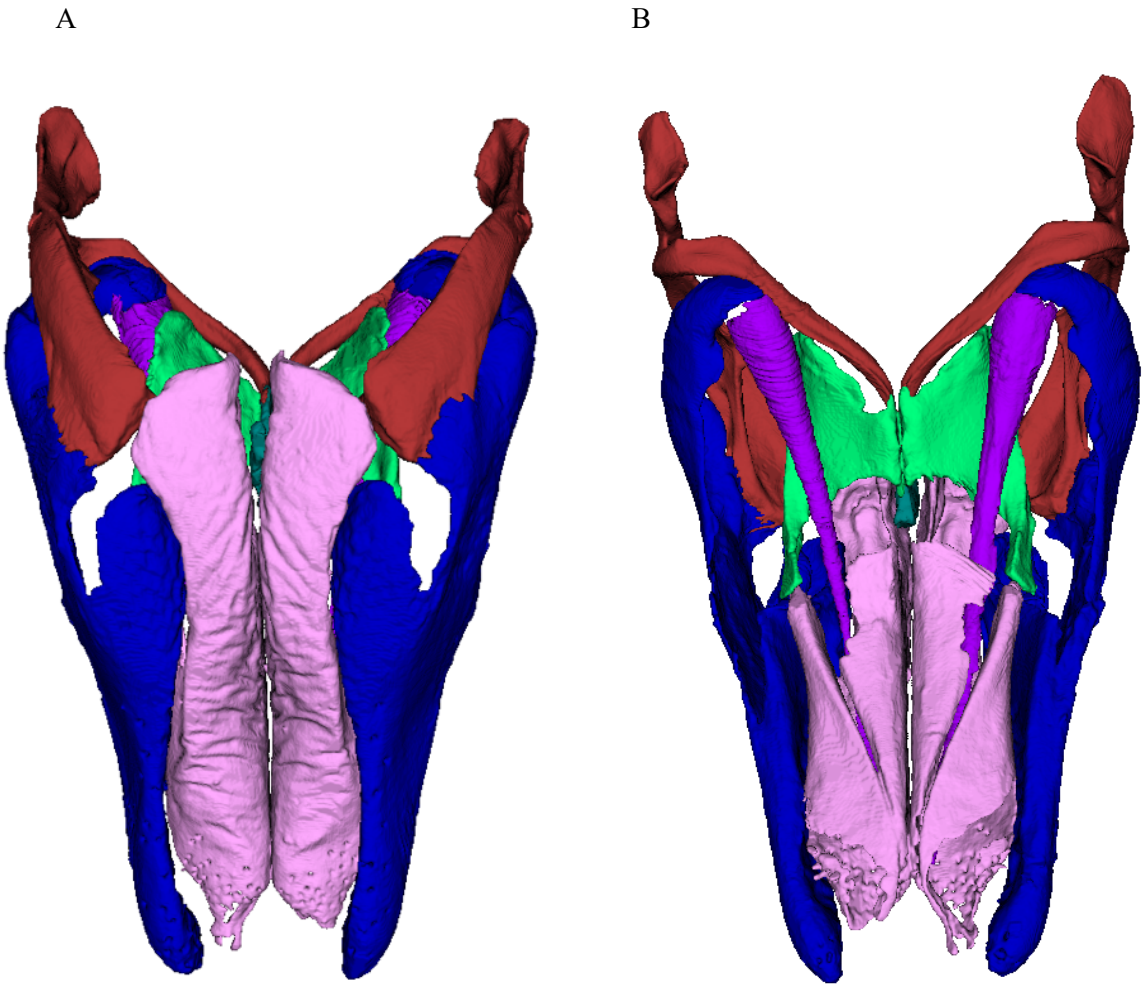


**Figure S21.** ?*Stemmiulus* sp. anterior gonopod appendageg pair (LP7-1) skeletal elements. A: anterior view; B: posterior view.

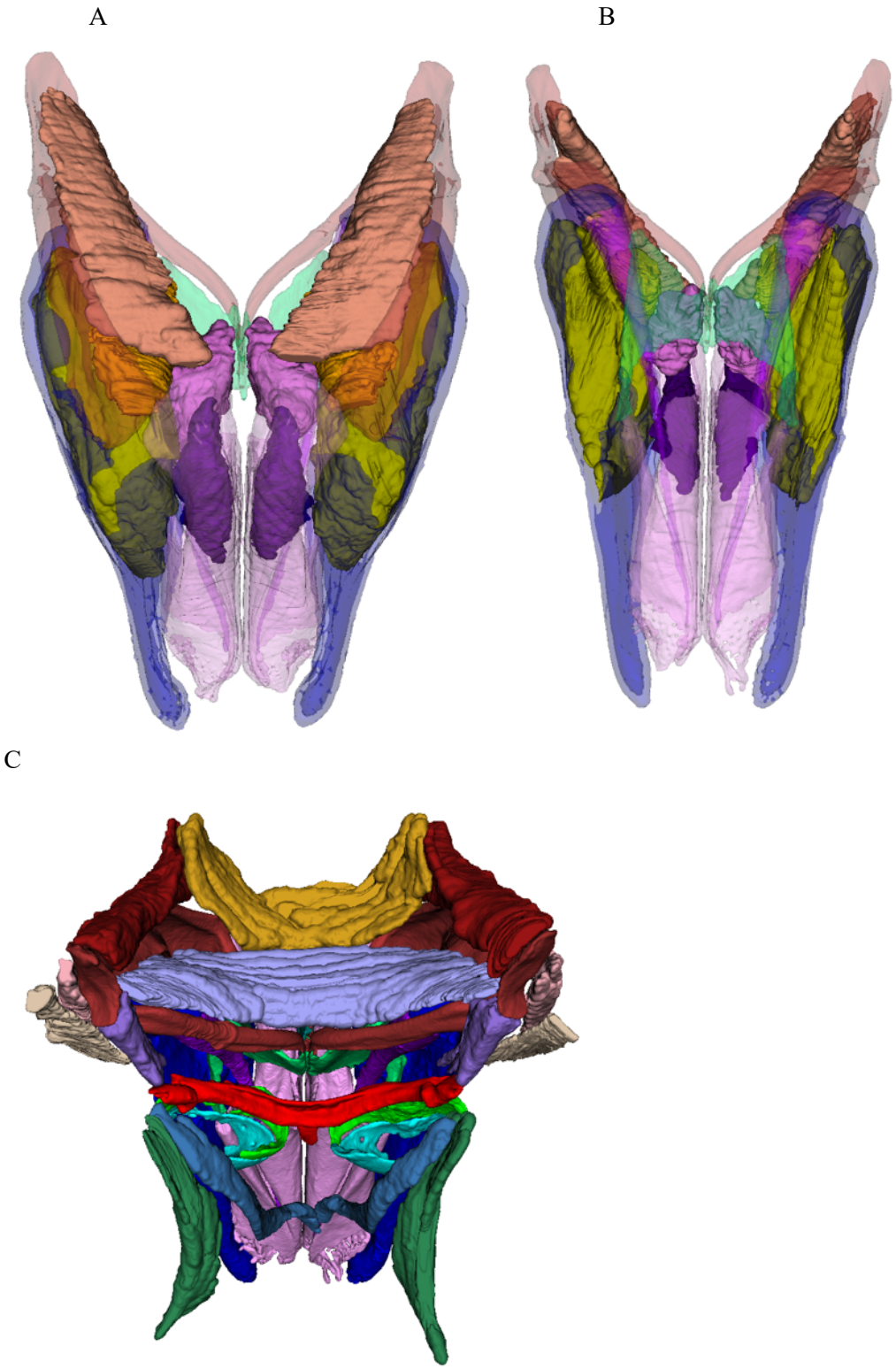


**Figure S22.** ?*Stemmiulus* sp. gonopod muscles. A: anterior view of anterior gonopod pair only (LP7-1) with translucent SE highlighting initrinsic muscles; B: same, from posterior view; C: complete gonopod complex (including reduced LP7-2 appendage) from posterior view, highlighting extrinsic muscles.